# Glial Cell Reactivity in Mouse Models Reflecting

Different Aspects of Alzheimer's Disease

Dissertation of the
Graduate School of Systemic Neurosciences of the
Ludwig-Maximilians-University Munich

Submitted by Mona Gwendolyn Behrendt

Glial Cell Reactivity in Mouse Models Reflecting

Different Aspects of Alzheimer's Disease

Dissertation of the
Graduate School of Systemic Neurosciences of the
Ludwig-Maximilians-University Munich

Submitted by Mona Gwendolyn Behrendt

Munich, September 2011

Supervisor: Dr. Leda Dimou

Second expert appraiser: Prof. Dr. Magdalena Götz

Date of oral defense: 12.1.12

Für meine Eltern

Table of Content

Abbreviations

Aβ	Amyloid-β-peptide
AD	Alzheimer's disease
ADP	Adenosine diphosphate
ALDH1L1	Aldehyde dehydrogenase 1 family, member L1
AMPA	α-amino-3-hydroxy-5-methyl-4-isoxazolepropionic acid
APC	Adenomatous polyposis coli
APH1	Anterior pharynx defective 1
APOE	Apolipoprotein E
APP	Amyloid precursor protein
APS	Ammonium persulfate
ATP	Adenosine triphosphate
BACE	β-side cleaving enzyme
BBB	Blood brain barrier
BrdU	5-Bromo-2′-Deoxy-Uridine
BSA	Bovine serum albumin
CAG	Chondroitin sulfate gylcosaminoglycan
CAM	Calcium/calmodulin-dependend kinase
CC	Corpus callosum
Cdk	Cycline dependent kinase
CK	Calcium/ calmodulin- dependent protein kinase II Promotor
CNPase	2`3`-cyclic nucleotide 3`-phosphodiesterase

CNS	Central nervous system
DR6	Death receptor 6
COX-2	Cyclooxigenase-2
CSPG	Chondroitin sulphate proteoglycans
DAPI	4′,6-Diamidino-2-phenylindol
DSD-1	Dermatan sulfate-dependent proteoglycan-1
E	Embryonic day
ECM	Extracellular matrix
EBSS	Earle`s Balanced Salt Solution
EDTA	Ethylenediamine-tetraacetic acid
EGF	Epidermal growth factor
EGFR	EGF receptor
ET-1	Endothelin-1
fAβ	Fibrillar Aβ
FAST	Functional Assessment Staging of Alzheimer's Disease
FGF	Basic fibroblast growth factor
FGFR	FGF receptor
GABA	Gamma-aminobutyric acid
GDS	Global Deterorientation Scale
GFAP	Glial fibrillary acidic protein
GFP	Green flourescent protein
G1	Gap 1 phase
GLAST	Astrocyte-specific glutamate transporter 1
Glt1	Excitatory amino acid transporter 2

GM	Grey matter
G protein	Guanine nucleotide-binding protein
GS	Glutamine synthetase
GSTpi	pi form of Glutathione-S-Transferase
HBSS	Hank's Balanced Salt Solution
Iba 1	Monocytic cell specific ionic binding
IGF-1	Insulin-like Growth Factor I
IL	Interleukin
JAK	Janus activated kinase
JNK	c-Jun N-terminal kinase
LPS	Liposccharide-binding protein
LTP	Long-term potentiation
MAG	Myelin assocuated glycoprotein
MCAO	Middle cerebral artery occlusion
MBP	Myelin basic protein
mdl	Major dense line
MFG	Mid frontal gyrus
MMP9	Metalloproteinase 9
NCSTN (APH2)	Nicastrin
NG2	Chondroitin sulfate proteoglycan
NMDA	N-Methyl-D-aspartate
NO	Nitic oxide
OPC	Oligodendrocyte precursor cell
p	Postnatal day

PBS	Phosphate buffered saline
PDGFR-α	Platelet-derived growth factor receptor-α
PDGF	Platelet-derived growth factor
PDL	Poly-L-Lysine
PEN2	Presenilin enhancer 2
PFA	Paraformaldehyd
PHF	Paired helical filament
PLP	Proteolipid protein 1
PNS	Peripheral nervous system
PSEN1	Presenilin 1
PSEN2	Presenilin 2
PVDF	Polyvinylidenfluorid
RMS	Rostral migratory stream
S100b	S100 calcium binding protein b
SDS	Sodium dodecyl sulfate
SEZ	Subependymal zone of the lateral ventricle
SHH	Sonic hedgehog
SM	Sensory-motor cortex
STAT	Signal transducers and activators of transcription
STG	Superior Temporal Gyrus
TetO	Tet-Operon
TGA	Transforming growth factor
TNC	Tenascin C
TNFα	Tumor necrosis factor alpha

TTA	Transactivator domain
UDP	Uridine diphosphate
UTP	Uridine triphosphate
WM	White matter

Figures

Tables

1   Summary

Human Alzheimer's disease (AD) is a chronic neurodegenerative disease with progressive neuronal loss, extracellular plaque deposition and intraneuronal tangle formation. Another hallmark commonly observed in AD patients is loss of myelin as well as focal demyelination in the plaque core areas.

Here, I set out to examine the glial cell reactivity in mouse models of AD in order to determine similarities and differences to invasive injuries. One important rationale for this comparison is the recent discovery of glial cells with stem cell properties after invasive injury. Therefore, the aim of this work was to determine if these cells also appear in non-invasive injuries. I analyzed astrocytes as these cells are commonly involved in the brain's reaction toward injury. In addition, I analyzed cells of the oligodendrocyte lineage to detect possible myelin repair mechanisms in response to AD pathology.

Under certain lesion conditions such as stab wound lesion, a great number of astrocytes up-regulate different markers known to be present in astroglial stem cells, resume proliferation and regain stem cell properties *in vitro*, since they give rise to self-renewing, multipotent neurospheres. Investigation of the astrocytes in APPPS1 mice, which by the age of six weeks exhibit progressive plaque deposition of human AD, revealed a strong reaction toward plaque deposition as detected by the expression of different markers characteristic of reactive astrocytes. In addition, a subset of these cells increased in proliferation, however, in contrast to stab wound lesion only a small number of astrocytes proliferated. When testing the neurosphere forming capacity of reactive glial cells of the cortical grey matter, it was significantly decreased in APPPS1 mice compared to the acutely injured brain. To understand if the decreased neurosphere forming capacity was due to the lack of neuronal loss, another mouse line, the CK/p25 mice, with pronounced inducible neuronal cell death, intraneuronal Aβ and tau pathology was used. Surprisingly, despite a strong astrogliosis neurosphere forming capacity was nearly absent in cells isolated from the cerebral cortex of this mouse line. Interestingly, reactive astrocytes also hardly proliferated *in vivo*, in line with the lack of neurosphere forming capacity.

To unravel the molecular mechanisms mediating the differences in astrocyte proliferation and stem cell generation observed in the different lesion paradigms, intracellular signalling cascades involved in astrocyte proliferation such as phospho-cJun and Olig2 were analyzed. Phospho-cJun expression was observed in a small subset of astrocytes upon stab wound and most prominently in CK/p25 mice, whereas it was nearly absent in APPPS1 mice. In contrast to that Olig2 expression was most prominently elevated in stab wounded animals and APPPS1 mice, whereas it was only mildly increased in CK/p25 mice. This suggests that both, phospho-cJun expression as well as Olig2 expression must be present to mediate proliferation of astrocytes upon stab wound injury.

To understand which signals allow up-regulation of both phospho-cJun and Olig2 in the invasive brain injury paradigm, I examined the blood brain barrier integrity. First, I investigated if blood-derived immune cells would enter the brain in APPPS1 and CK/p25 mice as it is known that after stab wound many of these cells invade. Also in APPPS1 as well as CK/p25 mice few immune cells entered the brain indicating that the blood brain barrier is permissive for some of these cells. However, analysis of the blood brain barrier integrity in APPPS1 and CK/p25 mice revealed that it is closed for molecules over a size of 3000 dalton. Therefore, signals from the blood may be present upon stab wound injury and absent in AD-related mouse models, as they can enter the brain in the former and may trigger astrocyte proliferation and stem cell dedifferentiation.

Another hallmark commonly observed in AD patients is loss of myelin. To understand if this pathology is also reflected in APPPS1 mice, I analyzed the amount and integrity of myelin in APPPS1 mice. Plaque deposition was sufficient to induce focal demyelination in plaque core areas of cortical grey and white matter in these mice, similar the observations obtained from AD patients. Myelin protein amounts per axon were significantly decreased in APPPS1 mice at six months of age and reached control levels again at nine months of age. Additionally, an increase in myelin aberrations was detected in APPPS1 mice at six months of age, while thereafter the number of aberrations remained stable until nine months of age. The increase in myelin aberrations was accompanied by a transient increase in the number of cells of the

oligodendrocyte lineage already six months of age. Furthermore, these cells displayed an increased proliferation, which persisted up to eleven months of age. In addition, an elevated differentiation into mature oligodendrocytes in the cortical grey and white matter was observed in APPPS1 mice. Therefore, myelin is a vulnerable target upon chronic amyloid plaque deposition in mice and it appears that myelin repair mechanisms such as e.g. remyelination are induced in response to this pathology.

When human brain tissue of patients with AD was examined, a decreased number of cells belonging to the oligodendrocyte lineage was present in different brain regions compared to normal, aged patients. These results indicate that in human AD pathology myelin repair mechanisms seem to be not as efficient as in mice.

2   Introduction

For a long time it was believed that after brain lesion the adult central nervous system (CNS) does not have any capacity for repair and neurons are only generated embryonically. However, in 1969 it was discovered that the adult brain retains the ability to generate new neurons from neural stem cells in at least two zones of neurogenesis, namely the subependymal zone of the lateral ventricle and the subgranular layer of the hippocampus[1,2]. About thirty years later, these adult neural stem cells were found to be, surprisingly, of glial cell origin[3-6]. Furthermore, other glial cells residing in non-neurogenic brain parenchyma were discovered to represent more than a sole supportive structure, rather being actively involved in multiple brain functions. In addition, different glial cell types such as astroglia and NG2+ glia have been frequently implicated in the brain's reaction toward injury. This reaction harbours beneficial as well as detrimental features, which influence the regenerative capacity of the injured brain. Until today, most of the common brain diseases accompanied with neuronal loss, like e.g. Alzheimer's disease, cannot be cured. However, the growing knowledge on glial cells and especially their reaction toward different types of injury will help us to develop new therapeutic strategies.

2.1   Structural Elements of the Central Nervous System

It is only about 200 years ago that Schwann and Schleiden put forward the cell theory in 1838. In their theory they proposed that there exists a general principle of construction for all organisms, which is the composition of basic units, named cells[7-9]. Their theory was further refined by Rudolf Virchow, a German medical doctor and biologist in 1855, who added the idea that every cell arises from another cell[10]. Only one year later he also discovered the existence of a connective substance, which embeds the nervous elements. As this connective substance appeared different from other organs he named it "neuroglia" [11,12]. However, Virchow was not the first to discover glial cells,

since Müller had described the "müllerglia" of the retina already in 1851[13]. In the beginning of the 1860s Otto Deiter identified stellate cells in cortical grey and white matter. Shortly after, Michael von Lenhossek put forward the expression "astrocyte" for this cell type[14,15] and Andrietzen finally distinguished protoplasmic grey matter astrocytes from fibrous white matter astrocytes in 1893[16]. The famous neurobiologist Ramón y Cajal also had great impact on the discovery of the other glial cell types, by reporting the existence of an additional 3rd class of neuroglia (reviewed by[12]). Around the 1920s this third class of glia was shown to contain both, "oligodendroglia" and "microglia" by Pío del Río Hortega, a spanish physician and anatomist[17,18]. Later, Penfield further confirmed the existence of oligodendrocytes[19]. Recent studies revealed that oligodendrocytes comprise a cell lineage, which includes oligodendrocyte progenitors in the adult brain which were originally described as beta astrocytes by H. Reiners in 1982[20]. William Stallcup could further identify these cells by using an antibody directed against the chondroitin sulfate proteoglycan (NG2) protein[21,22]. As these NG2+ cells exhibit features associated with progenitor cells abut also establish synaptic contacts to neurons they are currently recognized as a separate class of glia[23,24].

The discovery of glial cells took place during a time of conflict between the "reticularists and the neuronists", who had different theories on how the brain is organized. Camillo Golgi held the reticularistic view, believing that nerves are structured in a syncytium-like continuum. On the contrary, Ramón y Cajal, stated the "neuron doctrine", which was based on the cell theory. He could demonstrate that the nervous system consists of individual cells, which he called "neurons". Soon after, neurons were assumed to be the only substrate for brain function, while glia cells remained as a sole supportive element (reviewed by[25]). Recently, this view has been challenged by the discovery of important roles of glial cells in brain function and neurogenesis.

2.2   Glial Cells as Stem Cells in the Central Nervous System

Recent reseach discovered that glial cells display stem cell functions in the developing embryo and in the adult central nervous system (CNS).

2.2.1   Radial Glia- Neural Stem Cells in Development

An important step in CNS development is the formation of the three germlayers during gastrulation, which takes place in mice at around embryonic day (E) 6.5, the endoderm, mesoderm and ectoderm. After induction of the dorsally located ectodermal neural plate, neurulation starts at around E8-8.5. During that process a part of the neuroectoderm thickens, unfurls and results in the closure of the neural tube along the rostro-caudal axis. The tube is fully established at E9.5-E10[26]. It consist of a single layer of neuroepithelial cells, which already generate the first neurons[27] (Figure 2- 1). Finally, at E9-10 neurogenesis starts with the appearance of radial glia cells, which function both as neuronal progenitors[28,29] as well as a scaffold used by migrating neurons[30,31]. The transition of the neuroepithelial cells into radial glia cells is characterized by the progressive downregulation of most epithelial features[32], and also by gaining astroglial properties[33,34]. Radial glia therefore contain many features of astroglial cells. Furthermore, they are polarized cells, with one primary cilium-bearing apical domain that contacts the fluid of the ventricle, and a basal domain that contacts the meninges, basal lamina and blood vessels[5]. Asymmetric cell division of radial glia cells leads to the generation of neurons and intermediate progenitors[35]. The intermediate progenitors may further differentiate into neurons and macroglial cells (astrocytes and oligodendrocytes) even though it is still debated if these cell types arise from the same or different intermediate progenitors. At the end of neurogenesis, radial glia possibly differentiate into ependymal or astroglial cells[36] (Figure 2-1).

The previous view of a complete developmental switch from neurogenesis to gliogenesis[37] was recently re-defined, since some precursor cells are restricted to produce either neurons or glia as early as E9.5[29,34,38]. Only a subpopulation of radial glia cells gives rise to more than one cell type[29,34,39,40]. The presence of neural stem cells in adulthood can be explained by the maintainance of these multipotent radial glia cells in specific niches[5].

2.2.2 Adult Neural Stem Cells

Adult neural stem cells which retain the expression of characteristic molecules reminiscent of radial glia cells, reside in the sugranular zone of the hippocampal dentate gyrus and along the lateral ventricle in the subependymal zone (SEZ)[6]. In the mouse, neurogenesis occurs most prominently in the SEZ[5]. Here, slow-proliferating astroglia-like stem cells, also refered to as type B cells, generate neuroblasts (type A cells) and oligodendrocyte progenitors after passing through an intermediate state of fast proliferating precursors (transit-amplifying precursors, type C cells)[6]. The neuroblasts in the SEZ migrate through the rostral migratory stream (RMS) to the olfactory bulb, where they integrate as mostly GABA ergic (GABA; gamma-aminobutyric acid) and dopaminergic but also glutamatergic interneurons[6,41]. Adult neural stem cells of the SEZ are intercalated into the ependymal layer with their apical side contacting the ventricle via a single cilium, while their basal side is associated with blood vessels in the brain parenchyma[42,43] (Figure 2- 1).

Adult neural stem cells are situated in a certain "niche", whose microenvironment enables self-renewal and the generation of progeny[42-45]. Components that specify this niche include e.g. the presence of membrane bound molecules and a special extracellular matrix (ECM). The proximity to the special ECM structure present in the vicinity of blood vessels, capillaries and underneath the meninges, may be important for type B cell maintainance[46]. However, also the cilium, through which stem cells contact the ventricle has great impact on their ability to function as stem cells[42]. One important ECM component present in the postnatal and adult neural stem cell niche is a chondroitin sulfate proteoglycan, the dermatan sulfate-dependent proteoglycan-1 (DSD-1). Interestingly, growth factors have binding sites in defined chondroitin sulfate motifs. Growth factors also contribute to the stem cell niche and are involved in neuronal progenitor proliferation[47,48]. Another relevant ECM molecule, tenascin C (TNC), is also highly expressed within the SEZ throughout postnatal and adult life, contributing to the niche by e.g. modulating growth factor signalling[49,50]. But what defines a neural stem cell?

These cells have the ability to **self-renew** and the potential to give rise to cells of all lineages (**multipotency**). To identify stem cells the **neurosphere assay** has been developed as an *in vitro* readout. After isolation from the

SEZ, cells are kept as a single cell suspension in growth factor (epidermal growth factor (EGF) and fibroblast growth factor (FGF)) containing medium. After a few days in culture, certain cells start to proliferate and generate floating clonal neurospheres. These neurospheres are passagable for a long period of time, which underlines the capacity of the isolated cells to self-renew. Upon plating onto coated cover slips and withdrawal of growth factors, neurospheres can be differentiated into neurons, astrocytes and oligodendrocytes thus proving multipotency[51-53].

In conclusion, the specialized microenvironment in the SEZ allows the generation of new neurons throughout adulthood. However, when adult SEZ tissue is transplanted into the striatum only glial cell types are generated[54]. These data suggest that the environment outside the neurogenic niches is less supportive for neurogenesis. Interestingly, upon stroke injury, neuroblasts become re-rerouted toward the damaged lesion side, thereby overcoming this anti-neurogenic environment[55,56]. Ablation of these neuroblasts results in an increased infarct volume and exacerbated post-ischemic sensory-motor deficits[57]. Also in another lesion paradigm where cortico-spinal neurons degenerate neuroblasts are recruited to the neocortex. These progressively differentiate into mature pyramidal neurons, with some even projecting into the spinal cord[58]. These results indicate that the microenvironment in some injury conditions apparently has the ability to support neurogenesis.
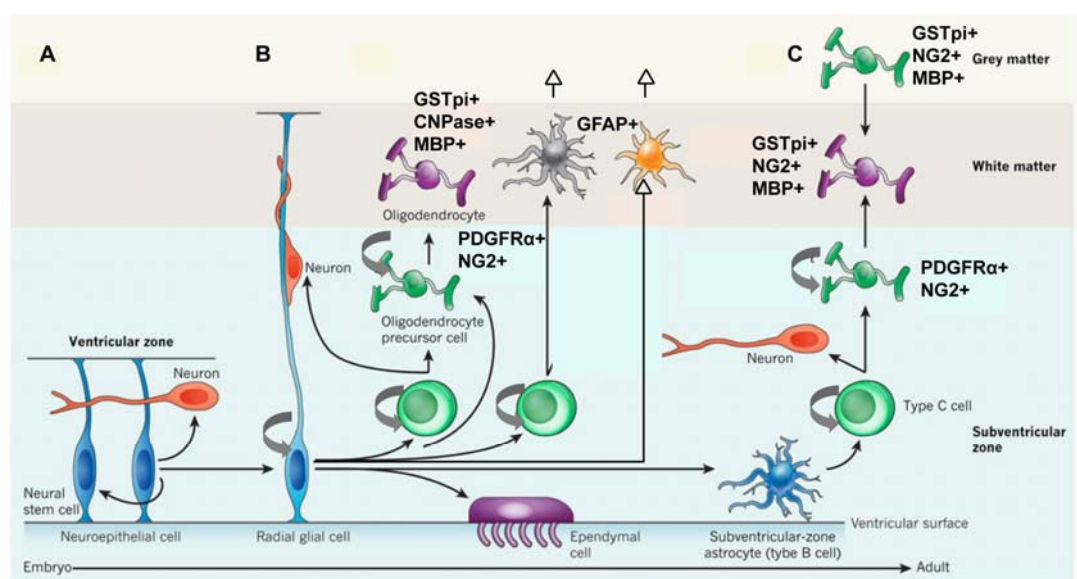
Figure 2- 1. Neuro/Gliogenesis from the Embryo to the Adult.

The progression from the embryo to the adult is shown from left to right (A to C). Black and grey arrows indicate self-renewal and/or differentiation from one cell type to another. Markers of macroglia and their precursors are listed. (A) Self-renewing neuroepithelial cells line the ventricles throughout the neuraxis at the stages of neural tube closure. These cells may generate some neurons. Neuroepithelial cells are transformed into radial glial cells as neurogenesis begins. (B) Radial glia generate either neurons directly or via intermediate progenitor cells and oligodendrocyte precursor cells, which in turn produce neurons and oligodendrocytes, respectively. Radial glia can also become astrocytes, as well as producing intermediate progenitors that expand in number before producing astrocytes. Protoplasmic astrocytes and fibrous astrocytes might arise from common or independent progenitors. Radial glia also produce ependymal cells. (C) In adults, oligodendrocytes are produced by two independent pathways: type B cells in the cortical subventricular zone produce transit-amplifying cells (known as type C cells), which in turn produce OPCs as well as neurons. The OPCs subsequently generate oligodendrocytes, and OPCs that are already resident in the grey matter also produce oligodendrocytes. Furthermore, type C cells generate neuroblasts. GFAP, glial fibrillary acidic protein; GSTpi, pi form of the Glutathione-S-Transferase; NG2, chondroitin sulfate proteoglycan; MBP, myelin basic protein; PDGFR-α, platelet-derived growth-factor receptor-α. All green cells are intermediate progenitors, with type C cells being a subset of these, and all blue cells are neural stem cells (even though each blue cell is a different type) modifed from[36].

2.3   Glial Cells in the Adult Brain

Recent research of the adult human brain discovered that glia cells are approximately as abundant as neurons[59]. However, the ratio differs enormously between regions. For example in the neocortex there are about 27.9 billion glia compared to 21.4 billion neurons[59,60]. This results in a glia to neuron ratio of 1.3 glia to one neuron[59,60]. In the adult human brain about 75% of all glia are oligodendrocytes, 20% astrocytes and 5% microglia[61].

Most interestingly, the total number of glial cells (glia is greek and means "glue") in the brain increases with evolution[62,63]. In accordance with that for example in the flat worm *Caenorhabditis elegans* the ratio of neurons to astrocytes is six to one. In higher developed animals such as rodents only three neurons per one astrocyte are present[64,65].

2.3.1 Astroctyes

Soon after birth, radial glia cells retract their processes and differentiate into astrocytes or ependymal cells[36,66,67]. Radial glia can either transform directly into astrocyte progenitors or generate them via a basal progenitor stage[36,68]. Some astrocytes in the grey matter of the ventro-lateral forebrain and spinal cord are also generated from embryonic NG2+ cells[69,70]. After astrocyte specification, astrocyte precursors migrate to their final destinations, such as e.g. the adult grey matter.

Adult grey matter astrocytes of the cerebral cortex are referred to as **proto-plasmic** astrocytes (Figure 2- 2A). They are characterized by many fine branching processes appearing in a globoid distribution, which envelop synapses[71]. Astrocytes populate the grey matter in an essentially non-overlapping manner, yet, they form gap junctions at the distal tips of their processes with neighbouring astrocytes[72-74]. In rodents, a single astrocyte contacts several hundred dendrites and envelopes up to 100`000 synapses[75]. Most synapses therefore consist of three elements, namely the astroglial perisynaptic process, the presynaptic neuronal terminal and the postsynaptic neuronal membrane, which led to the expression "tripartite synapse"[76]. The astrocyte's ensheathment of synapses guarantees proper synaptic function by maintaining ion concentration, pH, water and transmitter homeostasis. As astrocytes express different ion channels[74] and transporters they are "somewhat excitable". Changes in intracellular Ca^{2+} concentrations[74] are of importance for astrocyte-neuron and astrocyte-astrocyte communication[77]. Long range signaling between astrocytes is achieved by Ca^{2+} waves, which propagate via gap junctions[78,79]. Synaptically active gliotransmitters released by astrocytes, such as e.g. glutamate, adenosine triphosphate (ATP), γ-aminobutyric acid (GABA), tumor necrosis factor α (TNFα), shown to influence neuronal and synaptic physiology[76,77,80,81]. Besides the role of astrocytes in synaptic transmission, they also participate in synapse maturation and maintenance[82-84]. Another important function of astrocytes is removal of glutamate from the synaptic cleft via the glutamate-glutamine cycle. Glutamate is the most important excitatory transmitter in the CNS, however, if present in excess, it triggers excitotoxic neuronal death[85]. Glutamate is taken

up from the synaptic cleft via astrocytic transporters such as the excitatory amino acid transporter 2 (also known as GLT1) and the astrocyte-specific glutamate transporter 1 (GLAST)[74]. Within the astrocytes, glutamate is catalyzed by the glutamine synthetase (GS) into the non-toxic glutamine and recycled back to neurons.

As astrocytes contact the basement membrane at the blood vessels via a specialized process called astrocyte endfoot, they exert an additional function in regulating blood flow (Figure 2- 2B). They produce and release vasoactive substances, which alter the blood vessel's diameter[86] according to changes in neuronal activity[87].

Astrocytes furthermore participate in the formation of the blood brain barrier (BBB), which is a diffusion barrier that separates the brain extracellular lumen from the blood. It limits the influx to the brain parenchyma based on molecular size and polarity[88,89]. At the cellular level, endothelial cells ensheath the capillaries forming tight junctions between them (Figure 2- 2C). These cells are then surrounded by a basal lamina, perivascular pericytes and astrocyte endfeet[88-90].

In addition to the above described functions, astrocytes are also metabolically coupled to neurons e.g. by the brain glycogen metabolism. Glycogen is stored in glycogen granules mostly in astrocytes[71]. The glycolysis transforms glycogen into lactate, which then serves as an energy substrate for neurons[91].

In summary, astrocytes are important for balancing the brain's extracellular homeostasis. In addition, they regulate the metabolic support for neurons by e.g. adjusting the blood flow. Therefore, astrocytes are a prerequisite for proper brain function under physiological conditions. Also after brain injury, it is of importance to re-establish brain homeostasis.
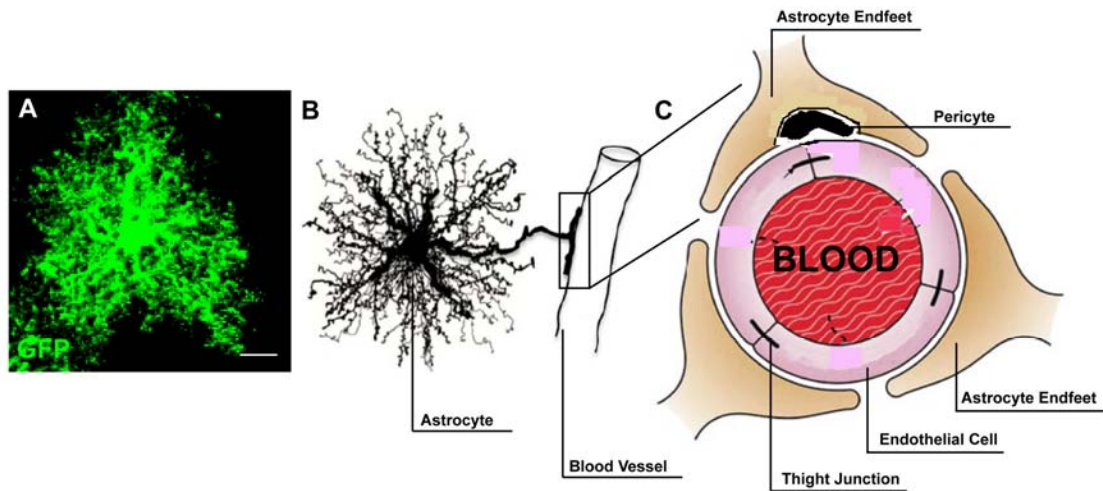
Figure 2- 2. Schematic Overview of Astrocytes and the Blood Brain Barrier.

(A) is a representative picture of a protoplasmic astrocyte. GFP was a staining performed in the GLAST::CreERT2 x CAGGFP, which is almost exclusively expressed by astrocytes. (B) depicts a schematic overview of the astrocyte's contact to a blood vessel. (C) is an overview on the composition of cells contributing to the blood brain barrier. Endothelial cells ensheath the blood vessel and form tight junctions between them. Also pericytes are located at blood vessels. Astrocyte endfeeth surround the endothelial cells, building an additional barrier. Scale bar: 10 µm. Modified from[71,90].

2.3.1.1   Subsets of Astrocytes

The increasing knowledge of the diversity and complexity of astrocyte functions argues for a heterogenic cell population. Astroglia can be distinguished by their morphology, localisation, and the expression molecules such as e.g. intermediate filaments. The latter constitute together with actin filaments and microtubules, the cytoskeleton, which e.g. mediates dynamic scaffold and structures the cytoplasm of a cell[92].

The already mentioned, **protoplasmic** astrocytes of the cortical grey matter express markers such as the calcium binding protein S100b, the glutamate transporters GLAST, GLT1 and GS. Furthermore, they are characterized by the presence of glycogen granules. Both features are commonly shared with other astroglial subtypes. The so called **fibrous** astrocytes reside in the corti-

cal white matter. They display an elongated morphology with many long fiber-like processes, which envelop the nodes of Ranvier[71]. Besides their localisation, they can be distinguished from protoplasmic astrocytes by the additional expression of the glial fibrillary acidic protein (GFAP). Furthermore, they have overlapping domains, contrary to protoplasmic astrocytes, and may exert mostly supportive functions[71]. Most interestingly, also the **adult astroglia-like stem cells** are considered an astrocyte subtype, as they express common astroglial markers such as e.g. S100b, GLAST, GS and GLT1[42,93] (for details see table 2- 1) and also exhibit the presence of glycogen granules. However, they also retain the expression of immature glia markers (**radial glia**) such as e.g. vimentin, nestin, DSD-1 and TNC[40,42]. Both, the adult neural stem cells as well as parenchymal astrocytes contact the blood vessels trough their basal domain. However, the apical domain of SEZ stem cells contacts the lateral ventricle, while parenchymal astrocytes ensheath synapses.

In conclusion, adult protoplasmic and fibrous astrocytes share hallmarks with the astroglia-like neural stem cells. However, the most striking discrepancy between radial glia and adult neural stem cells compared to adult cortical astrocytes is the neurogenic and proliferative capacity, which is lacking in the latter[94]. Interestingly, this changes upon injury, where astrocytes become reactive and gain some aspects of radial glia and neural stem cells. In the adult brain parenchyma, however, also other glial cell types such as the cells of the oligodendrocyte lineage reside.

Antigene/ Feature	Neuroepithelial Cell	Radial Glia	Adult Neural Stem Cell	Fibrous Astrocyte	Protoplasmic Astrocyte	Reactive Astrocyte upon Acute Injury
Glycogen Granules	−	+	+	+	+	+
GLAST	−	+	+	+	+	+
s100b	−	+	+	+	+	+
GS	−	+	+	+	+	+
GLT1	−	+	+	+	+	+
Nestin	+	+	+	−	−	+
GFAP	−	+ (e.g. in primates) / − (not in rodents)	+	+	−	+
TNC	−	+	+	−	−	+
DSD-1	−	+	+	−	−	+

Table 2- 1. Marker Expression of Astrocyte Subtypes.

The table depicts the marker expression of different astroglial subtypes as well as neuroepithelial cells. DSD1 - dermatan sulfate-dependent proteoglycan-1, GFAP- Glial fibrillary acidic protein, GLAST - astrocyte-specific glutamate transporter 1, GLT1 - excitatory amino acid transporter 2, GS - glutamine synthetase, s100b – calcium binding protein, TNC - tenascin C. Modified from[29,95].

2.3.2 Oligodendrocyte Lineage

During development three waves of **oligodendrocyte progenitor cells** (OPC) are generated. First, OPCs appear in the ventral forebrain at E12.5, and then also migrate into the telencephalon, entering the cerebral cortex at E16. However, most of these cells are eliminated at postnatal stages. The second wave starts in the lateral and/or caudal parts of the ganglionic eminences around E15. After birth, OPCs are generated in the cortex and in the neurogenic niches[6,96].

OPCs are stellate cells and can be identified by both: the earliest expressed platelet-derived growth factor alpha receptor (PDGFRα), and the chondroitin sulfate proteoglycan NG2 (NG2), which is up-regulated once progenitors leave their germinal zone[97-101]. The mammalian NG2 protein (also termed CSPG-4) is a single transmembrane spanning protein and could be classified as a member of the neurexin protein family, which are cell adhesion molecules that are involved in the mediation of neuronal contacts at the synapse. However, the NG2 protein could also exert functions of a proteoglycan, since its chondroitin sulfate gylcosaminoglycan (CAG) chains are linked to the extracellular domain[102]. Different interaction partners may be relevant for the function of NG2+ cells at synapses and early myelination of axons but they are not fully understood until today. Furthermore, the NG2 protein is possibly involved in cell polarization and migration[102]. Antibodies directed against the NG2 protein are commonly used to identify OPCs in the developing and adult CNS (Figure 2- 3). In the adult, an OPC subset retains the ability to differentiate into mature oligodendrocytes, while down-regulating NG2 expression[103-105]. **Mature oligodendrocytes** can be visualized by their expression of the pi form of the Glutathione-S-Transferase (GSTpi)[106] (Figure 2- 3). Signals from electrically active axons regulate the up-regulation of myelin-associated proteins such as e.g. the proteolipid protein (PLP), the myelin basic protein (MBP) or the myelin-associated glycoprotein (MAG) in mature oligodendrocytes, resulting in lineage progression into **myelinating oligodendrocytes**[107]. Signalling also occurs from the oligodendrocyte to the neurons, since oligodendrocytes e.g. produce growth factors and induce axonal organization[108-112].

The basic helix loop helix transcription factor Olig2, a transcriptional repressor, is expressed throughout the oligodendrocyte lineage (Figure 2- 3). It exerts important functions in the specification and differentiation of oligodendrocytes[113-115]. Interestingly, Olig2 is up-regulated in different injury paradigms[116].
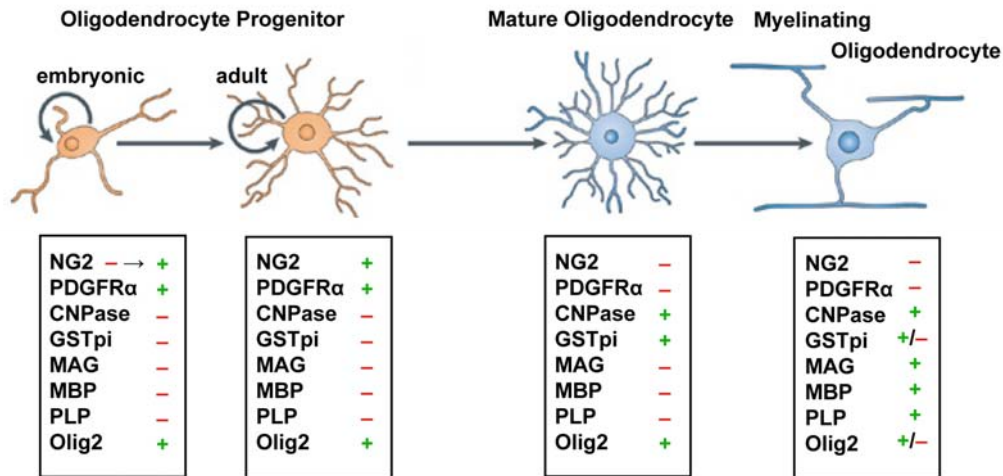
Figure 2- 3. Oligodendrocyte Lineage and their Specific Expression of Markers.

Shematic pictures of cells of the cells belonging to the oligodendrocyte lineage. In the boxes below relevant marker for the specific cell types are listed. The green plus shows the presence of the depicted marker and the red minus its absence. CNPase - 2`3`-cyclic nucleotide 3`-phosphodiesterase, GSTpi - Glutathione-S-Transferase, MAG - myelin-associated glycoprotein, MBP - myelin basic protein, NG2 - Chondroitin sulfate proteoglycan, PDGFRα - platelet-derived growth factor alpha receptor , PLP - proteolipid protein. Modified from[117].

2.3.2.1   Features of NG2-Glia

After myelination during development has occurred, NG2-positive cells still ubiquitously populate the adult cerebral cortex comprising 5-8% of all cells[118,119]. They exhibit a complex stellate morphology extending many finely branched processes[120]. Almost all NG2 cells co-express PDGFRα and Olig2, as well as Sox 10, whereas only a small subset additionally expresses astrocytic markers such as the glutamine synthetase (GS)[102,121].
NG2+ cells have the capacity to divide, while maintaining their multiple-branched processes[122]. Therefore, they constitute the majority of the proliferating cell population outside the neurogenic niches in the adult mouse brain[103,105,122,123]. Also in the adult human brain, NG2 as well as Olig2 is expressed by the vast majority of cycling cells, located throughout the cortex[124]. The biological significance of the quiescent non-proliferating NG2+ cell population still remains to be determined.

In contrast, the mitotically active oligodendrocyte progenitor cells are known to contribute to the generation of new oligodendrocytes during adulthood[103,105,123]. In addition, fate mapping analysis of Olig2+ cells revealed that some of these cells retain the ability to <u>differentiate</u> from an oligondendrocyte progenitor into myelinating oligodendrocytes in the rodent cortical white matter. In contrast, only a small proportion of Olig2+ oligodendrocyte progenitor cells in the cortical grey matter differentiates into mature oligodendrocytes[103,105,125].

Apart from their differentiation along the oligodendrocyte lineage in the adult brain, there is also evidence indicating <u>some degree of lineage plasticity</u> of NG2+ cells. Upon transplantation of fetally-derived OPCs into the adult glial-depleted brain or shiverer mice (hypomyelinated mice) they can generate astrocytes and myelinating oligodendrocytes. Notably, adult-derived transplanted OPCs give only rise to cells of the oligodendrocyte lineage[126,127]. In line with these data, fate mapping analysis of embryonic NG2+ cells revealed a production of astrocytes in the grey matter of the ventral forebrain and spinal cord in addition to the generation of cells of the oligodendrocyte lineage. In contrast, adult fate mapped NG2+ cells generate only cells of the oligodendrocyte lineage[69,70,128,129]. This suggests that NG2+ cells are intrinsically potent to generate astrocytes, but this ability is lost at adult stages. At early postnatal stages, NG2-positive cells *in vitro* could still generate astrocytes and mature, action potential-propagating neurons, suggesting that they not yet lost their multipotency[130]. Along this line, production of few neurons from adult NG2+ or PDGFRα+ oligodendrocyte progenitors has been observed also *in vivo*[131,132], suggesting that indeed some extent of neurogenesis may be mediated by NG2-positive cells. However, these data are still a matter of debate, since fate mapping of other mouse lines such as NG2-EYFP knockin (EYFP, enhanced yellow flourescent protein) or Olig2::CreER[TM] mice did not reveal neurogenesis originating from these Olig2+ or NG2+ cells[105,121,133].

Another exciting feature of NG2+ cells is that most NG2-positive progenitors establish intimate contact to neuronal synapses and the nodes of Ranvier[134-137]. Upon glutamate release by neurons, NG2+ cells generate an inward current mediated by a postsynaptic-like structure present on the glial membrane,

which contains α-amino-3-hydroxy-5-methyl-4-isoxazolepropionic acid (AMPA) receptors[136,138,139]. This led to the idea of a <u>neuron-NG2 glia synapse</u> and to the expression "synantocytes" for NG2+ glia[136]. In addition, NG2+ cells in the corpus callosum express functional N-Methyl-D-aspartate (NMDA) receptors[140]. Besides glutamate, additional evidence for an evoked GABA(A) receptor current in response to interneuronal GABA release exists for NG2+ cells (Lin and Bergles, 2004). Therefore, NG2-positive glia can be distinguished according to their expression of different voltage-depended ion channels in both, the cortical grey and white matter, which results in different physiological properties. Strikingly, the generation of depolarization-induced immature spikes of a subpopulation of white matter NG2+ cells in the adult rat has been reported[141]. Yet, the consequences of the neurotransmitter re-lated excitability of NG2+ cells is not well known. It is suggested that e.g. ac-tivation via AMPA receptors may be involved in inhibiting proliferation and lineage progression in development[142], while NMDA receptor mediated glu-tamate inputs on NG2+ cells may play a role in cell migration[143]. Whether all the above described synaptic features of NG2+ glial cells are transient or if they are a heterogenic cell population, where specific subpopulations exert different functions is still under debate. For example it has been shown that during the process of remyelination of a demyelinated area, axon-oligodendrocyte progenitor synapses are formed only transiently. When the progenitors differentiated into mature oligodendrocytes, these synapses where lost[144,145]. Given all these facts, NG2+ cells exhibit features of both, progenitor cells, but also cells with synaptic contacts to neurons[23,24,117].

2.3.2.2   Myelinating Oligodendrocytes

One important function of myelinating oligodendrocytes is myelin formation, which occurs in the central nervous system. Myelin enables rapid electrical conductance in neurons by electrically insulating the axons[146,147]. Upon mye-lination, axon potentials are restricted to spaced intervals spared from myelin, referred to as "nodes of Ranvier" [148,149]. Within the nodes of Ranvier, voltage-gated sodium channels cluster on the axonal membrane which allow fast sal-

tatory generation and conductance of action potentials[148,150,151]. In addition to the myelin acting as an insulator, different myelin proteins were shown to trophically support the axon, as upon loss of certain myelin proteins, axons can undergo degeneration[152,153]. Therefore, many cognitive and motor functions depend on myelin formation.

One oligodendrocyte is able to myelinate up to 50 axon segments, the so called "internodes" [147]. Myelin consists of numerous wrappings of the oligodendrocytic bilayered plasma membrane around the axon. Up to now, 342 proteins have been associated with CNS myelin[147]. In general, it can be subdivided into **compact** and **non-compact** myelin, with axonal internodes mostly consisting of the compact form of myelin (Figure 2- 4A,B,C). Ultrastructurally, compact myelin is characterized by alternating circular dark (major dense-line (MDL)) and lighter lines around an axon (intraperiod line (IPL)) (Figure 2- 4B). In areas of compact myelin, cytoplasm is mostly excluded, allowing tight stacking of plasmamembranes around the axon[154]. The most abundant proteins in the compact myelin are the PLP together with its smaller splice form DM20 as well as the MBP, which comprise to about 30-45 % and 22-35 % of the total myelin amounts, respectively[147,155,156] (Figure 2-4B`). MBP is so far the only myelin protein necessary for myelin formation. Accordingly, the shiverer mouse mutant, which lacks most of the gene encoding for MBP, has only thin myelin (hypomyelination)[157-159]. MBP has been implicated in e.g. signalling and cytoskeletal interactions[160-162]. On the contrary, the presence of the very hydrophobic transmembrane protein PLP is dispensable for myelin formation, since knockout mice still form myelin. However in the knockout mice, myelin stability decreases with age and additionally axons develop defects such as axonal spheroids[163].Other functions of the PLP protein include a role in oligodendrocyte survival[153,154,163].

The second component of CNS myelin is the non-compact myelin, which is not as densely packed as the compacted form so that intracellular cytoplasm and cytoskeletal assemblies still occur. Regions where non-compacted myelin can be found in the CNS include myelin wrappings next to the axons (abaxonal) and myelin wrappings away from the axon (adaxonal) (Figure 2-4A`,A``,B) and the segments near the nodes[154]. For example, the enzyme 2`3`-cyclic nucleotide 3`-phosphodiesterase (CNPase) is located in the cyto-

plasm of non-compacted myelin (Figure 2- 4C). It constitutes approximately 4-15 % of the total myelin amount. The physiological function of the phosphodiester hydrolysis of 2',3'-cyclic nucleotides to 2'-nucleotides, which is catalyzed by the CNPase, is still not known[154]. Yet, this enzyme has an important function in mediating axonal survival, since loss of the CNPase1 gene results in neurodegeneration[152]. Also the myelin-associated glycoprotein (MAG) is expressed in the non-compacted myelin (Figure 2- 4B``). It is enriched in the innermost non-compacted myelin membrane, which is directly apposed to the axonal membrane[164,165]. MAG accounts for 0.1-1% of the total myelin amount and is a type I transmembrane glycoprotein. It has been implicated in axon-myelin stabilization[166] and has been speculated to inhibit axonal regeneration after injury[167,168].

Importantly, the number of wrappings of the oligodendrocytes membranes depends on the diameter of the axon: the thicker the axon diameter, the thicker is the myelin[169]. This is usually determined by the so called g-ratio, which is the ratio between the diameter of the axon and the outer diameter of the myelinated fiber[170]. The age of the maximum of myelination, where the rate of myelin formation is greatest, is around postnatal day 20[156,171].
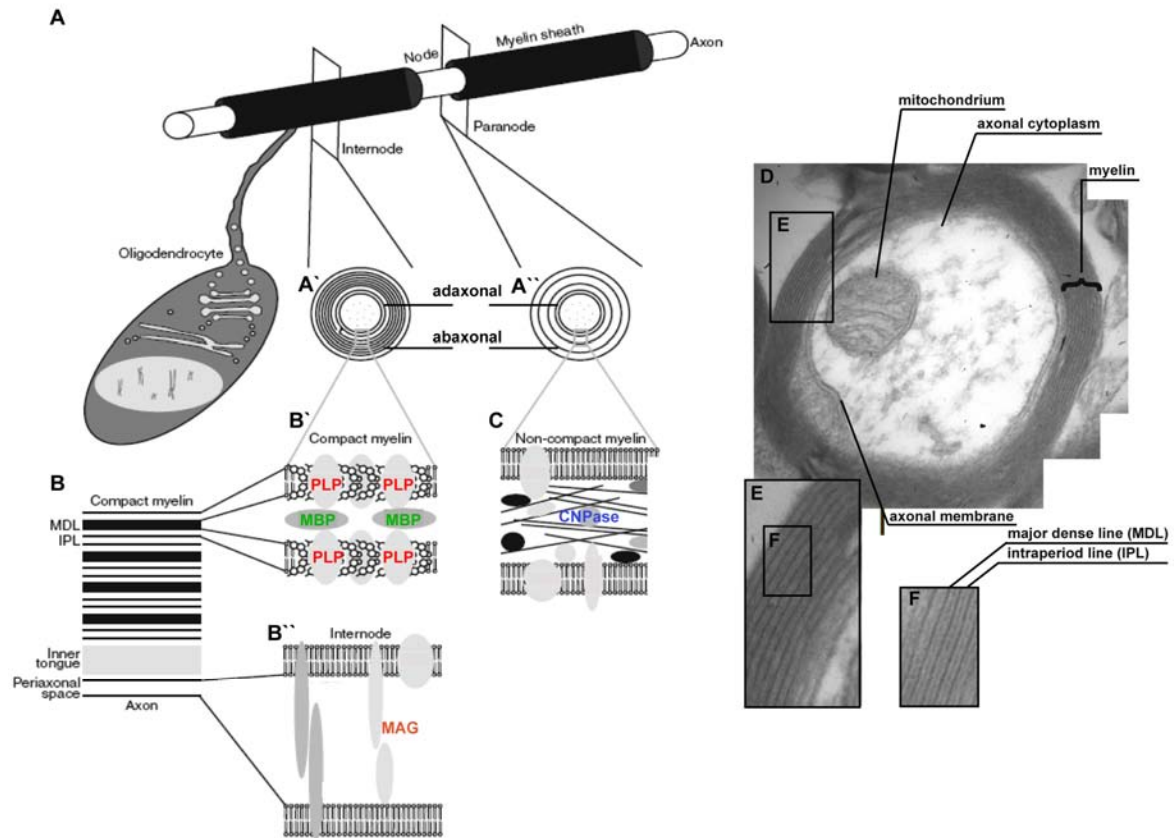
Figure 2- 4. Myelin Structure.

(A) shows a schematic overview of an axon myelinated by an oligodendrocyte. Cross-sections in internodal (A`), and paranodal (A``) segments. In (B) an overview of the structure of compacted myelin is depicted. (B`) is a blow up of the internodal compact myelin and its protein components PLP – proteolipid protein and MBP – myelin basic protein. (B``) is a magnification of the inner most myelin sheath, which is directly apposed to the axon. (C) represents structural components of non-compact myelin such as CNPase - 2`3`-cyclic nucleotide 3`-phosphodiesterase. Picture was modified from[147]. Representative Electron Photograph of a Myelinated Axon. (D) is a representative picture of a myelinated axon. (E) is the magnification of the myelin sheaths of the myelinating oligodendrocyte. (F) shows a further enlargement, where one can distiguish between the major dense line (MDL) and the interperiod line (IPL).

2.3.3 Microglia

In contrast to astrocytes and oligodendrocytes, microglial cells emerge from the mesoderm and populate the cerebral cortex at around E10–E19 in ro-

dents[172-174,175,176]. In the adult rodent CNS, they comprise more than 10% of all cells. In the healthy condition they are considered to be „surveillant microglia". They are referred to as "ramified cells" that have small cell somata and extend radial, non-overlapping processes[177], which are constantly moving while sensing the environment[178,179]. Furthemore, a small number of microglial cells seems to actively divide, which may contribute to their maintainance in the CNS[180]. Upon injury also bone marrow-derived cells can infiltrate from the blood into the brain and adopt a microglial identity. Therefore, it is still under debate if these cells may also contribute to the microglial maintainance in the healthy brain[172,181]. Invasion of such bone marrow-derived cells was already observed, however other studies could not corroborate these observations[182,183,180]. Thus, the precise mechanisms of microglial cells maintainance in the adult brain remain to be elucidated. One important function of microglia is their ability to rapidly respond to changes in the environment such as brain injury.

2.4   Glial Cells and their Reaction towards Injury

Glial cells of the CNS provide structural and functional support for neurons under physiological conditions. In addition, glial cells also react toward brain injury. As observed in the peripheral wound repair, scar formation also takes place in the either mechanically or pathologically injured brain. The process of scar formation is evolving from glial cells with time at the lesion side[184,185]. The glial scar mainly consists of astrocytes, however, after severe lesion with open meninges, it also includes other cell types such as myelin debris, infiltrating blood-borne immune cells, fibroblasts, pericytes, endothelial cells, microglia and NG2+ cells[184,186-188]. Such a severe lesion paradigm, where glial scar formation take place, is represented by the acute stab wound injury, where the cortical grey matter is acutely cut with a knife as well as experimental stroke, where the middle cerebral artery is occluded (MCAO). In the former, the cut leads to a transient edema with necrotic and apoptotic cells death. Furthermore, opening of the meningitis results in invasion of blood-derived cells[189]. In the latter, the blood flow falls to less than 20 % at the ves-

sel which is occluded[190,191]. As a result, glucose and oxygen delivery are disrupted, also causing neuronal and glial cell death via multiple processes such as excitotoxicity, acidotoxicity, ionic imbalance, oxidative and nitrative stress, inflammation, peri-infarct depolarisation and apoptosis[192]. The penumbral tissue next to the core area is less affected, since it gains perfusion from adjacent vessels with the blood flow being reduced to 20-40 % [191]. Here, cell death occurs in a slower progressive manner via inflammation and apoptosis[192].

Glial scar formation is mostly considered to be beneficial in the initial phase after brain injury, as it seals the lesion side and restores the brain's homeostasis by, amongst other things, initiating angiogenesis[187,193]. However, the same tissue additionally is considered an obstacle for axonal growth in the long run and is therefore also implicated in disturbing recovery[185].
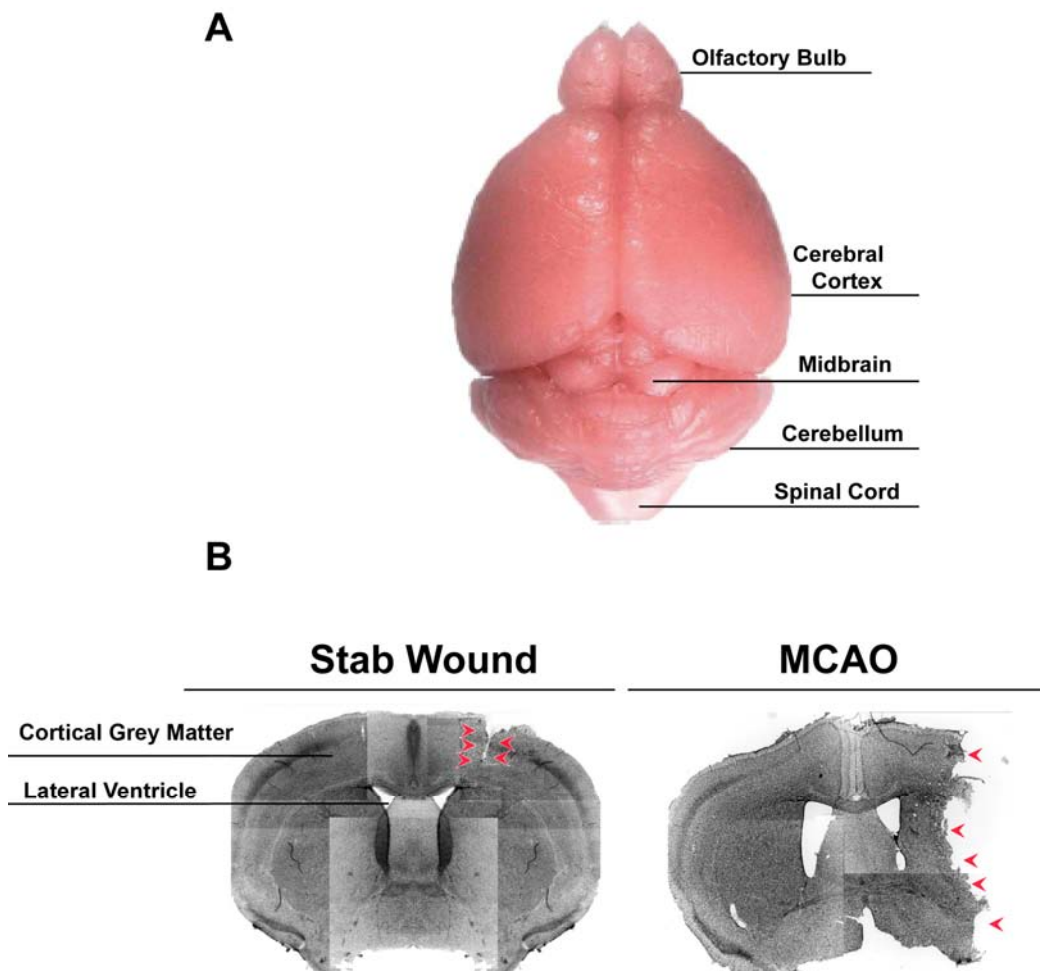
Figure 2- 5. Mouse Models of Acute Brain Injury.

(A) is a representative picture of a mouse brain. (B) demonstrates coronal DAPI stained sec-
tiones, where the lesion area of a stab wound lesion and an MCAO (middle cerebral artery
occlusion) model for stroke are indicated with the red arrowheads. Modified from[194,195].

Immediately after injury, glial cells first undergo morphological and functional
changes. This leads e.g. to an increase of the de novo synthesis of soluble
factors such as growth factors, cytokines and proteases[95]. In accordance to
these differences also the extracellular matrix (ECM) changes[196,197], which
may strengthen the tissue and promote wound contraction[184,185,198]. The se-
verity of the glial cell reaction is correlated to the severity of the injury and
must not always include glial scar formation, which is most prominent in large
invasive injuries such as e.g. stab wound lesion described above[187]. In gen-
eral upon injury, microglial cells are considered as one of the first cell type
located at the CNS injury side. Interestingly NG2+ cells react similarly fast
since proliferation of both cell types is increased as early as three days after
injury at the lesion side[103]. In contrast, reactivity of astrocytes is delayed with
e.g. their increased proliferation occuring at seven days post injury[184].

2.4.1 Reactive Astrocytes

Given the potential of astroglial cells to act as stem cells in two neurogenic
niches such as the SEZ and the sugranular layer of the dentate gyrus of the
hippocampus, it is of special interest to determine their reaction towards in-
jury also in non-neurogenic zones such as the cortical grey matter.
Reactive astrogliosis is a well known feature upon brain injury where astro-
cytes become reactive. Depending on the duration, severity and type of in-
jury, the features of this phenomenon vary. The most striking event where
astroglia take part is glial scar formation, which seems to be restricted to
large invasive injuries. The glial scar is not only comprised of astrocytes but
may also include e.g. fibromeningeal cells[188], other glia (e.g. NG2+ glia) and
dense collagen extracellular matrix. The astrocytes present in the glial scar
include astrocytes, which were present before injury as well as the astrocytes

generated by proliferation after the lesion. Interestingly, protoplasmic astrocytes present in the glial scar now display overlapping regions contrary to their physiological non-overlapping distribution[199,200]. It has to be considered that the astrocyte's reaction toward injury exerts both detrimental and beneficial effects. Along this line, glial scar formation inhibits axonal regeneration, due to the enrichment in chondroitin sulphate proteoglycans (CSPGs) in the ECM, which are also released by astrocytes[186]. Other detrimental effects include e.g. the possible release of neurotoxic levels of glutamate[201], reactive oxygen species[202] or cytokines from astrocytes upon injury. The latter may worsen the inflammatory response, since *in vivo* antagonization of a cytokine signalling pathway (the NFkB pathway) in astrocytes promotes neuronal resistance to injury[203,204]. Pro-apoptotic molecules may diffuse via gap junctions into surrounding brain areas, thereby triggering further brain damage[201]. Strikingly, deletion of reactive astrocytes (GFAP/vimentin double knockout or GFAP ablationed mice) results in improved synaptic and post-traumatic regeneration[205,206].

This view has been challenged by the fact that reactive astrocytes also protect the brain tissue in many ways. Ablation of reactive astrocytes simultaneously increases the infarct volume as seen e.g. upon MCAO[207]. This indicates that astrocyte reactivity may exert different effects switching from initially positive to negative ones[95]. The glial scar additionally prevents inflammatory cells and other cells from entering the intact parts of the brain[199,205,208]. Consequently, ablation of proliferating astrocytes after injury results in an increase in inflammation and lesion volume as well as insufficient BBB repair[205,208]. Astrocytes additionally protect e.g. against oxidative stress[209,210] and take-up potentially excitotoxic glutamate[211]. Furthermore, they metabolically support neurons upon brain lesion[212]. Beyond that, astrocytes are capable of releasing pro- and anti-inflammatory molecules, thereby contributing to the brain's immune response[213,214].

Other prominent characteristics of astrocyte reactivity after injury include astrocytic hyperthrophy, up-regulation of intermediary filaments (Figure 2- 6) and eventual proliferation[187]. Moreover, extracellular matrix molecules such as the glycoprotein tenascin C (TNC) and the DSD-1 chondroitin sulfate epi-

tope (detected by the 473HD antibody) are released by reactive astrocytes upon acute brain lesion[48,95,215,216].

Most interestingly, upon acute brain injury a subset of reactive astrocytes regains the ability to proliferate, the most striking feature of embryonic and adult neural stem cells[103,216,217]. On the contrary, in the healthy cortical grey matter astrocytes rarely divide[217]. In terms of a time course of the reaction it is known that e.g. after acute stab wound injury, protoplasmic astrocytes first become hyperthrophic and up-regulate GFAP and/or nestin expression. At this early time point, astrocytes also up-regulate and secrete extracellular matrix proteins such as TNC and DSD-1. At later time points (7 days after injury) about 55 % of the total astrocyte cell pool resumes proliferation[95,103]. Could all astrocytes proliferate in a sufficiently large injury condition or is it a specific subset of astrocytes exhibiting a greater potential? So far these questions still need to be elucidated.
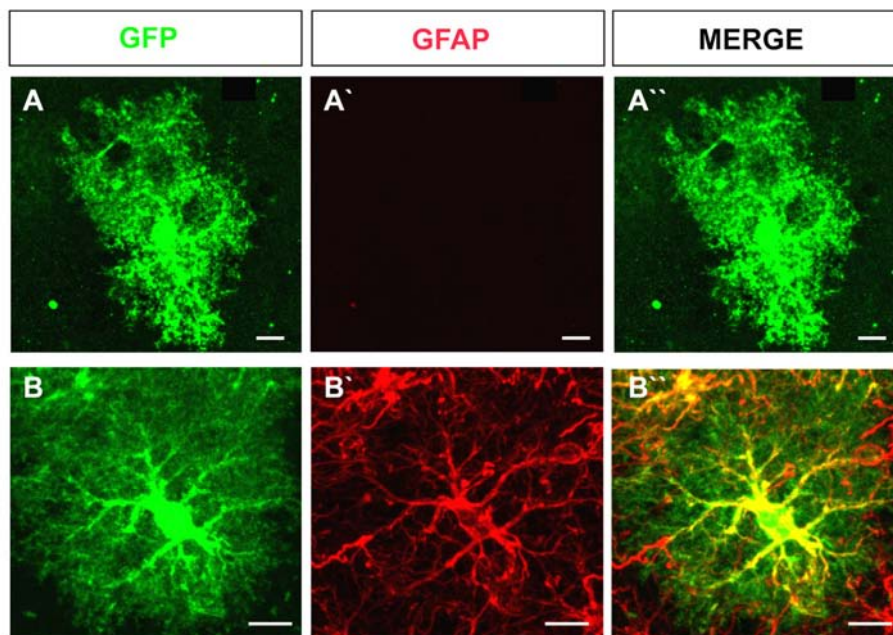
Figure 2- 6. Reactive Astrocyte.

Representative picture of an astrocyte in the healthy brain in (A) and a hyperthrophic, reactive astrocyte, that up-regulated expression of the intermediate filament GFAP in (B). GFP is a staining performed in the GLAST::CreERT2 x CAGGFP, which is almost exclusively expressed by astrocytes. Notably, GFAP expression only co-localizes to the main fibers of the whole astrocyte. Scale bar: 10µm.

Another striking feature of protoplasmic reactive astrocytes after acute injury is that they exhibit the <u>potential to generate multipotent neurospheres</u> *in vitro*, a hallmark of neural stem cells[216-218]. Furthermore, upon injury distinct subsets of reactive astrocytes in the cortical grey matter re-express markers reminiscent of stem cells (see table 2- 1). A further prove for their potential after acute injury is the astrocyte's ability to adopt a neuronal fate e.g. upon forced expression of a neurogenic transcription factor[116].

In summary, the astrocyte's reaction can exert beneficial as well as detrimental effects. Furthemore, protoplasmic astrocytes de-differentiate upon acute brain injuries, acquiring features of neural stem cells. However, if astrocytes would have an equivalent stem cells potential also upon AD pathology has not been investigated so far.

2.4.2 The Reaction of NG2+ Glia toward Injury

Apart from their contribution to the glial scar, the NG2+ glia, also react toward injury. Upon e.g. acute stab wound injury or demyelinating injury, NG2+ glia become hypertrophic, up-regulate the expression of the NG2 protein and resume proliferation[103,116,219-221] (Figure 2- 7). Consequently, three to five days after e.g. acute brain injury NG2+ cells increase in number at the lesion side. Furthermore, the newly formed glial scar contains high levels of NG2+ cells, which also includes NG2-expressing macrophages and pericytes[188]. With time, NG2 protein expression then gradually declines[222,223]. Up-regulation of the NG2 protein putatively inhibits axonal regeneration[222], since the NG2 core protein induces growth cone collapse and inhibits axonal growth *in vitro*[224,225]. Accordingly, axonal growth within the glial scar increases in mice treated with an anti-NG2 antibody[226]. However, after spinal cord injury, NG2 null mutant mice show no difference in axonal regeneration compared to wildtype mice[227]. Along this line, in a co-culture of hippocampal neurons with NG2+ cells, neurite tips actively establish contacts to NG2+ glia. In addition, neurons co-cultured with NG2+ glia extend longer axons than in co-culture with fibroblasts[228]. Therefore, it is still under debate, if the NG2 protein exerts

beneficial or detrimental functions in terms of axonal regeneration within the glial scar.

Another feature of the reaction of NG2+ cells toward injury is their capacity to transdifferentiate under certain conditions. After acute cryolesion or demyelination in aged animals, NG2+ cells generate astrocytes[229,230]. In contrast to these findings, in other lesion paradigms, such as stab wound lesion, NG2+ cells fail to generate astrocytes[105,231]. This suggests that NG2+ cells may re-acquire their embryonic ability to generate astrocytes after specific types of brain injury. Interestingly, the ability to transdifferentiate upon demyelination is gained in aged animals, which would be of particular interest for sporadic Alzheimer's disease[230].

In addition to their possible abilities to transdifferentiate, NG2+ cells are frequently implicated in the process of remyelination upon e.g. demyelinating diseases where "myelin sheaths are lost from around axons" [170]. Demyelination leads to a redistribution of the axonal sodium channels from the node of Ranvier along the nude axon[232] resulting in non-saltatory and therefore slower conduction of action potentials. At places of remyelination saltatory condution is functionally re-acquired[233]. Yet, the remyelinated myelin usually is thinner than the original one[234,235]. NG2+ OPCs likely are the major cell population responsible for remyelination, as only little evidence indicates an involvement of mature opligodendrocytes in this process[170]. Proliferating NG2+ cells are observed around the demyelinated area before they possibly differentiate further into myelinating oligodendrocytes[236-238]. For demyelination occurring in the white matter, stem cells of the adult SVZ[239,145,240] or their progenitor cells in the RMS were discovered to represent additional sources for myelin repair[241,242 241,242].

In conclusion, NG2+ cells take part in the glial scar formation after large invasive injury. Furthermore, they proliferate after lesion and are likely involved in myelin repair after demyelination. However, so far little is known about the reactivity of NG2+ cells in response to chronic lesion paradigms such as Alzheimer's disease.
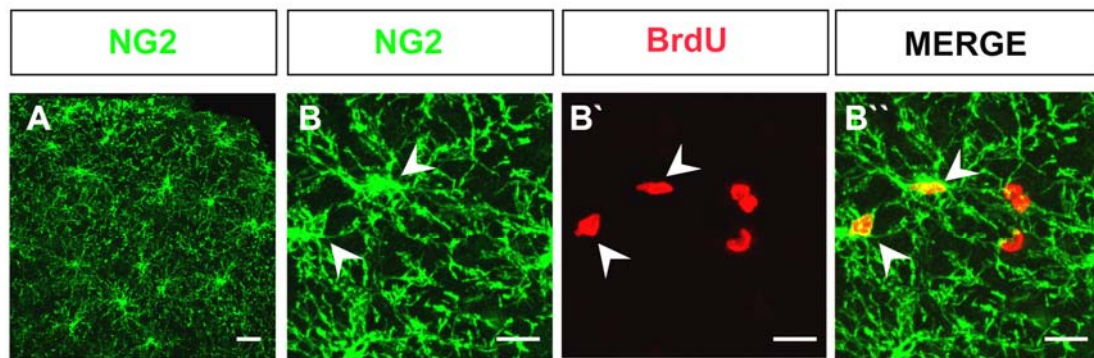
Figure 2- 7. NG2+ Cells in the Healthy and Lesioned Brain.

(A) represents NG2-positive cells populating the healthy cortical grey matter. (B) is a representative and magnified picture of NG2+ cells after lesion (here plaque deposition). 5-Bromo-2′-Deoxy-Uridine (BrdU) was applied to the drinking water for two weeks and incooperates into the DNA upon S-phase of the cell cycle. Therefore, B` and B`` indicate a previously proliferating NG2+ cell. Scale bar: 20µm.

2.4.3 The Reaction of Microglia toward Brain Injury

When a surveillant, ramified microglia senses stimuli such as damaged or apoptotic cells upon injury, it changes into a "reactive" state. For example, upon traumatic brain injury, ATP is released from dying cells which triggers via the purinoceptor $P2Y_{12}$ the extension of microglial processes. Microglia then rapidly migrate from toward the injury[243,244]. In addition to elevated expression of purinergic receptors also induced nitric oxide (NO)-synthase activity is correlated with an increased microglial activity[245-247]. Activated microglia produce numerous pro- and anti-inflammatory cytokines, growth factors and neurotrophins[177]. Upon mild injuries, the conversion from a ramified morphology into a "hyper-ramified" morphology is induced, which indicates the beginning of hyperthrophy. If the brain injury is more severe, hyper-ramified microglia enlarge their soma while retracting and shortening their processes so that they overt an amoeboid-like shape (see Figure 2- 8). In this stage of microglial activation, an increase in number via proliferation and/or recruitment from the blood is often observed[245]. In addition, the expression of several antigenes such as myeloid cell markers becomes elevated[177]. However,

in this reactive stage only little phagocytosis takes place[248]. Upon strong acti-
vation such as axotomy, microglia acquire the ability to phagocytose debris
such as degraded cells or myelin sheaths[249]. Furthermore, in such a condi-
tion they may also produce reactive oxygen and nitrogen species and may
express molecules related to T-cell activation (Figure 2- 8)[177,249].

Microglia exert important functions in the early brain reaction toward injury as
well as in the inflammatory response and it should be noted that the specific
microglial reaction also depends on the specific injury paradigm.
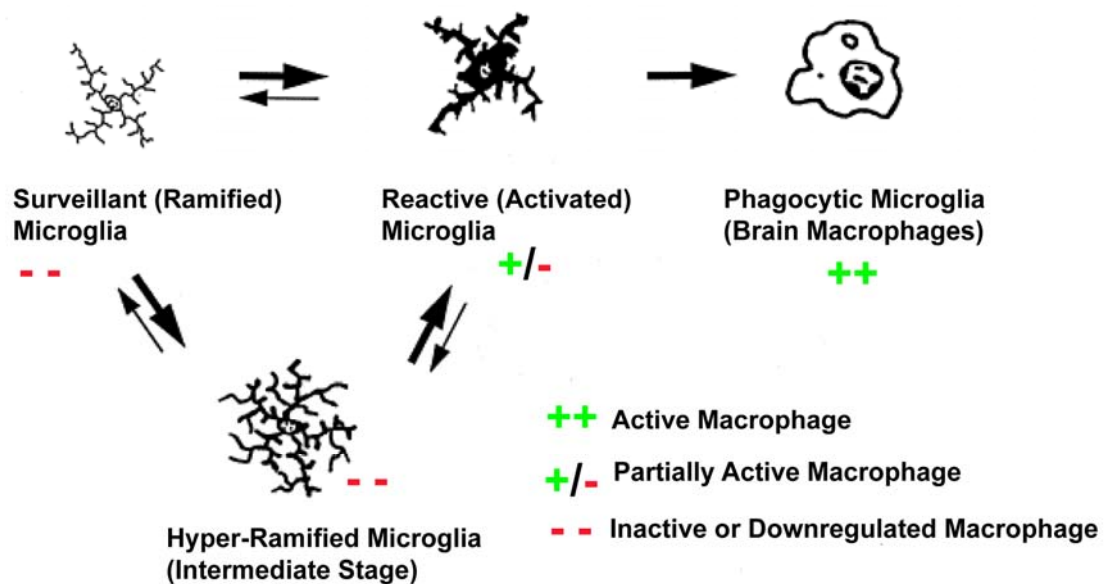
Figure 2- 8. Stages of Microglial Activation.

In response to injury microglial cells become reactive, by passing through an immediate
stage. Phagocytic activity is little in reactive microglia, while in severe injuries they addition-
ally gain phagocytic properties. Modified from[250-252].

2.5   Alzheimer's Disease – a Chronic Lesion Paradigm

Neurodegenerative diseases occur in an **acute** or **chronic** manner. In **acute**
lesions such as stroke, different types of neurons and glial cells in a restricted
brain area are injured and consequently lost in a short period of time. On the
contrary, in a **chronic** injury, degeneration takes place over a time period of
several years either selectively affecting a specific neuronal type as in Park-

inson's disease or acting more widespread as observed in Alzheimer's disease (AD)[253] .

2.5.1 Epidemiology

AD is a pathology responsible for 70-80 % of all dementia cases worldwide among people over 65 years of age[254]. Unfortunately, the incidence of AD doubles with every five years increase in age. Thus, the risk to get AD is around 0.6 % at the age of 65 to 69 and 8.4 % at the age of 85 years and older[255,256]. Especially, in highly developed countries where life expectancy is increased, this may lead to severe social and economic problems. For example, in the USA 4.5 million residents suffered from AD in 2000 [257] and it has been predicted that in 2050 the number of AD patients will be as high as 13.2 million in the USA[258].

Two forms of AD can be distinguished: the familial form and the sporadic form. The onset of the disease in the familial cases takes place at an age of 20-40 years as a consequence of mutations in certain genes (5-10 % of all AD cases; [259]). The sporadic form of AD affects patients later in life, at the age of 60 to 70 years[259]. For this AD form, age is considered a major risk factor[260]. In addition, the inheritance of the ε4 allele of the apoE4 transporter is another established risk factor. About 40-80 % of the sporadic AD patients are carriers of at least one allele[261,262]. The APOE4 allele increases the risk by three times in heterozygous and 15 times in homozygous carriers[263].

2.5.2 Clinical Presentation

AD is a disease that causes impairments in memory, thinking and behavior. The progression of AD is defined by different stages initially described by Dr. Barry Reisberg as the Global Deterorientation Scale (GDS), which characterizes seven stages[264,265]. A modified stage system, the Functional Assessment Staging of AD (FAST), measures more specifically the progression of mental decline[266-268]. In general, staging is based on the theory of retrogenesis, which claims that "degenerative mechanisms reverse the order of acquisition in normal development" (see table 2- 2), meaning that patients pro-

gressively loose the latest acquired memories first and afterwards the early childhood memories[269]. In general, the progression of AD occurs over many years and is difficult to predict.

2.5.3 Pathology

In 1907 the physician Alois Alzheimer[270] discovered the presence of extracellular amyloid plaques and the accumulation of intraneuronal neurofibrillary tangles in brain tissue of patients, who suffered from the disease that later was named after him.

Stage	*GDS*	*FAST Characteristics*
1	No cognitive decline	No functional decrement manifests
2	Very mild cognitive decline	Complains of forgetting location of objects; Subjective work difficulties.
3	Mild cognitive decline	Decreased functioning in demanding employment setting evident to co-workers; Difficulty in travelling to new locations.
4	Moderate cognitive decline	Decreased ability to perform complex tasks such as planning dinner for guests, or handling finances
5	Moderately severe cognitive decline	Requires assistance in choosing proper clothing; may require help to bath properly.
6	Severe cognitive decline	(a) Difficulty putting on clothing properly (b) Requires assistance bathing (c) Inability to handle mechanics of toileting (d) Urinary incontinence (e) Fecal incontinence
7	**Very severe cognitive decline**	**(a) Ability to speak limited to one to five words** **(b) All intelligible vocabulary lost** **(c) All motoric abilities lost** **(d) Stupor** **(e) Coma**

Table 2- 2. Decline in Human Alzheimer's Disease. Modified from[268].

2.5.3.1   Amyloid Plaques

Amyloid plaques are found in all AD cases. Per definition they are spherical extracellular deposits in the brain parenchyma, predominantly composed of the amyloid-β-peptide (Aβ). Initial patches of plaques are seen in the basal neocortex, while with time plaques spread into adjacent neocortical areas and the hippocampus[271]. How is the Aβ peptide produced? It turned out that Aβ is produced via a sequential proteolytic cleavage of an amyloid precursor protein (APP)[272,273]. The APP protein, which is encoded by a gene located on chromosome 21, is a type I transmembrane protein[272]. It is ubiquitously expressed[272] and is localised at the plasma membrane, trans-Golgi network, endoplasmatic reticulum, endosomal, lysosomal as well as mitochondrial membranes. In neurons, its functions range from roles in synaptogenesis, neurite outgrowth and cell adhesion[274-276]. Interestingly, APP expression is elevated during neuronal differentiation[277] as well as after brain injury[278].

Initially, the APP ectodomain (extracellular side) is shedded by a membrane-anchored protease, called β-secretase[279,280]. The remaining APP-stub is then proteolyzed by the γ-secretase complex, an aspartyl-protease[281]. It regulates the intramembranous cleavage within the APP transmembrane domain to finally release the Aβ peptides of different length (Aβ39-Aβ43)[282]. The γ-secretase is composed of 4 different proteins. Most important are the proteins presenilin 1 (PS1) and/or presenilin 2 (PS2), which harbour the active side of the γ-secretase[283]. The amino acid sequence of the Aβ peptide may differ due to the variability of the intramembranous cleavage. Aβ40 is the peptide predominantly present in the healthy condition, while Aβ42 is generated to a lesser extent. Upon AD, the Aβ40/Aβ42 ratio is shifted in favour of Aβ42, which is more hydrophobic, prone to form oligomers or aggregate into fibrils[284].

In AD three major Aβ deposits are present, namely vascular deposits and parenchymal diffuse or focal plaques. While diffuse plaques have a size of around 50 µm to several 100 µm, focal plaques show dense and spherical accumulations of the Aβ peptides and usually have a size of about 10-50 µm[285]. The latter may lead to neurite breakage and loss of spine[286]. Furthermore, glial cells react prominently toward focal plaques[287] and sparsely toward diffuse ones[288,289].

2.5.3.2   Tangles

The second hallmark of AD is the presence of intraneuronal neurofibrillary tangles[270]. Contrary to the progression of the amyloid plaques, neurofibrillary tangles first appear in a small region of the entorhinal cortex. Also subcortical nuclei, in particular the nucleus basalis of Meynert, which harbours acetylcholine efferent fibers connecting it to the cortex[290] and the locus coeruleus, that projects via noradrenergic efferences to the cortex[291] are affected early in the disease progression. With time neurofibrillary tangles spread over the limbic system to neurons in the higher neocortex[292].

But what are tangles? They consist of non-soluble hyperphosphorylated tau. Under physiological conditions tau is a highly-soluble protein[293,294], which is associated with axonal and also neuronal microtubules and is involved in the stabilization and assembly of them[294,295]. Its function is regulated by its degree of phosphorylation[293,296]. Upon AD, tau becomes aberrantly phosphorylated by e.g. the cycline-dependent kinase 5 (Cdk5), which leads to a detachment of tau from the microtubules, and results in their disruption[296,297]. Tau then assembles into paired helical filaments[298]. As the microtubuli disintegrate, the axonal transport system collapses[299], thereby contributing to neuronal cell death[300].

2.5.3.3   Synapse and Neuron Loss

Apart from extracellular plaque deposition and tangle formation, also neuronal and synaptic losses are part of human AD pathology. Continuing neuronal loss also accounts for brain atrophy and dysfunction[301,302]. Interestingly, neuronal loss takes place focally e.g. in layer II of the entorhinal cortex[303], the CA1 region of the hippocampus[304] and the superior temporal gyrus[305]. Even though neurons die, loss of synapses is most indicative for the intellectual deficit in AD[306-309]. Notably, neuronal as well as synapse loss but also tau pathology are additionally linked to the clinico-pathologic relationship of other dementias[310] and are therefore not solely indicative for AD.

Up to now, several theories on how AD progresses are discussed in the field of AD research. One of the leading hypotheses is the Aβ cascade hypothesis, which will be discussed below.

2.5.3.4   Aβ Cascade Hypothesis

Some familial AD cases carrying mutations in APP (about 36 mutations known) and all familial AD-patients with mutations in PS1 (about 180 mutations known) or PS2 (about 20 mutations known) display elevated production of Aβ42[284,311,312]. In these patients either Aβ42 levels are increased or the Aβ40/Aβ42 ratio is shifted in favour of Aβ42[313,314]. This imbalance of Aβ generation and the enzymatically mediated Aβ clearance (e.g. by the insulin-degrading enzyme)[315] is believed to be the major cause of plaque deposition, leading to dementia with tangle pathology[316]. Recent findings led to modifications of the hypothesis. First, plaque load of patients does not correlate with memory loss and second because robust plaque deposition has been detected also in non-demented individuals[309,317-319,320]. Third and most striking, a strong correlation between the presence of small soluble Aβ oligomers and cognitive decline was observed[321,322]. Therefore it is now believed that rather the small soluble Aβ oligomers may be the detrimental molecular component causing AD pathology with plaques serving as a potential reservoir[312]. However, one should keep in mind that many other hypotheses on how AD develops are discussed and each of them consequently leads to a different therapeutic strategy. One problem in studying AD could be due to the fact that so far no mouse model resembles the complete human AD pathology but rather reflect selected features[323]. However, this at the same time is an advantage since isolated aspects and consequences of the very complex pathology can be investigated independently. Therefore, I chose to examine on two of the known mouse models, namely the APPPS1 and CK/p25 mice reflecting distinct aspects of AD pathology observed in patients.

2.5.4 APPPS1- A Mouse Model with Plaque Deposition

The APPPS1 mouse line expresses two mutations known to be a cause of familial AD under the postnatally active neuronal minigene promoter Thy1[324]. It carries the so called "swedish double-mutation" of the APP protein at position 670 and 671 (KM670/671NL), which results in a switch from lysine to asparagine and methionin to leucine, respectively[325]. In humans this double-

mutation leads to AD onset between 45 and 61 years of age and continues for approximately seven years. In addition, the APPPS1 mouse line expresses a leucin to prolin point mutation in the PS1 gene, which is the most aggressive familial human AD mutation identified so far, the disease onset is around 24 years of age leading to death at the age of about 35. This PS1 mutation leads to an strong increase in the Aβ42 amount, while Aβ40 and Aβ38 levels decrease[326,327].

Transgenic human APP expression in APPPS1 mice exceeds endogenous APP expression by approximately three times. The ratio of Aβ40/Aβ42 in the double-mutated APPPS1 mice changes from 1 to 1.6 prior to plaque deposition to 1 to 5 in mice with plaques. APPPS1 mice display neocortical extracellular plaque deposition already apparent at three months of age, spreading later throughout the brain (Figure 2- 9). The initial plaques are small and dense. With age, amyloid plaque deposition progresses, resulting in an increase of both, plaque size and number. The highest rate of new plaque formation is detectable between four and five months of age (Figure 2- 9)[328]. At eight months of age, four types of plaques can be distinguished:

1) Vascular amyloid (rare and restricted to the large pial vessels)

2) Small, dense core plaques

3) Larger plaques with a dense core and a large halo of diffuse amyloid, and

4) Plaques with a dense core surrounded by a defined corona of diffuse amyloid[324]. The latter represents the plaque type mostly seen in human AD. In the vicinity of the plaques, dystrophic synaptic boutons, hyperphosphorylated tau-positive neuritic structures, an increase of microglial cell numbers and the presence of reactive astrocytes are observed. Furthermore, these mice exhibit cognitive defects[324], emphasizing the model's value of reflecting several important aspects of AD pathology.

In conclusion, APPPS1 mice exhibit progressive amyloid plaque deposition pathology but lack obvious neuronal death. Furthermore, tau pathology is restricted to areas around plaques and no tangle formation within neuronal cell bodies is detectable[324,329]. Therefore, this mouse model is suitable to study plaque-related glial reactions. Nevertheless, to gain insight into the glial cell reaction upon neuronal death and tangle pathology, I utilized an addi-

tional mouse model the CK/p25 mice, which is described in the following section.
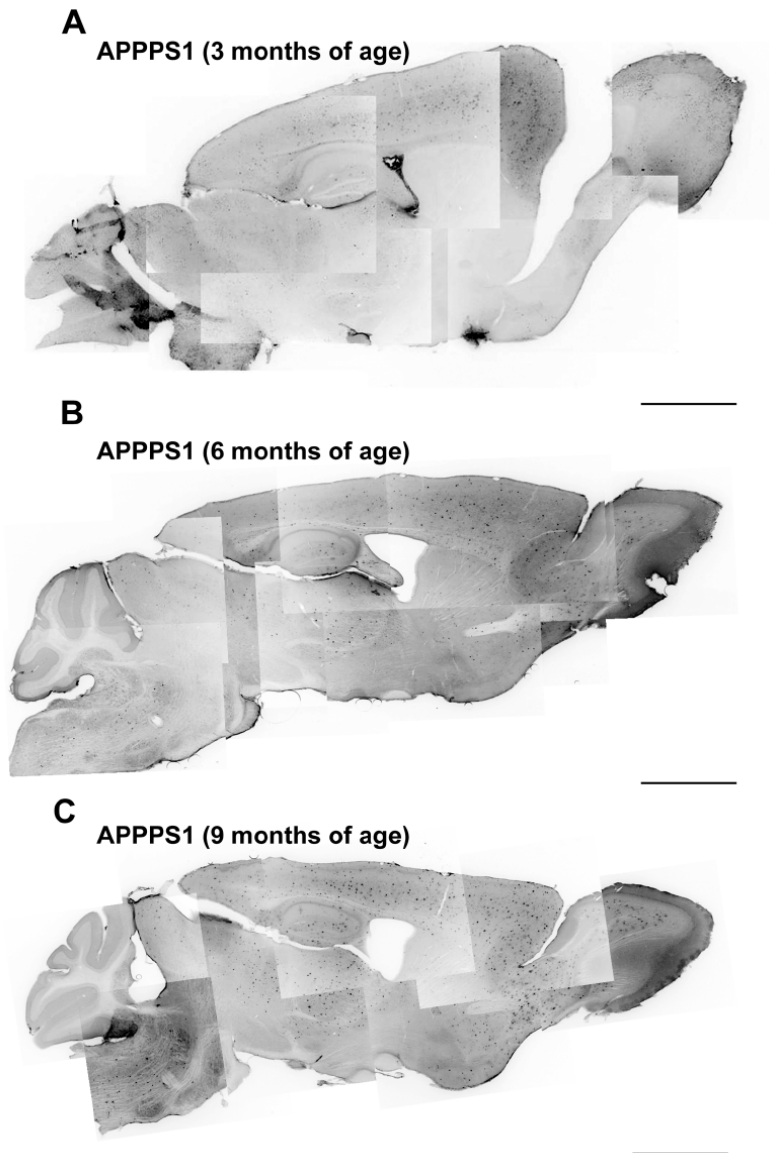
Figure 2- 9. Plaque Load at different Ages of APPPS1 Mice.

Pictures (A-C) show sagital sections of APPPS1 mice at (A) 3, (B) 6 and (C) 9 months of age. The sections were immuno-stained with the 6E10 antibody, detecting human APP and Aβ. The plaque burden constantly increases with age, including more brain regions, while mostly sparing the cerebellum. Scale bar: 200µm.

2.5.5 CK/p25- A Mouse Model with Neuronal Loss

The CK/p25 mouse line inducibly overexpresses human green flourescent protein (GFP)-tagged p25 (p25) under the control of the calcium/calmodulin-dependent protein kinase II (CK) promotor, which restricts the transgene expression to neurons of the forebrain[330,331]. The p25 peptide is physiologically generated from the p35 peptide via a calpain cleavage taking place upon e.g. oxidative stress or presence of the Aβ peptide[332-334]. Both, p25 and p35 are regulatory subunits of the cycline dependent kinase 5 (Cdk5)[335], with the subunit p25 leading to a longer lasting activation of Cdk5. Furthermore, the subunit p25 alters the Cdk5 substrate specificity and shifts its localisation from membrane-associated to nuclear and/or cytoplasmic. Upon regulatory subunit binding, the protein serine-threonine kinase Cdk5 becomes active and phosphorylates substrates on their serine and threonine residues[336]. As one of its targets includes the tau protein, Cdk5 was originally identified as the major tau kinase[337,338]. Upon human AD, p25 expression levels as well as Cdk5 activity are increased[339-341] and associated with apoptotic cell death[333,340].

The CK/p25 mouse line expresses p25 in neurons using the doxycycline-dependend Tet-OFF system (p25-TetOperon (TetO))[331,342]. After crossing these mice to mice expressing the transactivator domain (TTA) under control of the neuronal calcium/calmodulin-dependend kinase (CK) II promoter, withdrawal of doxycycline results in ectopic expression of p25 in neurons of the cerebral cortex (Figure 2- 10).
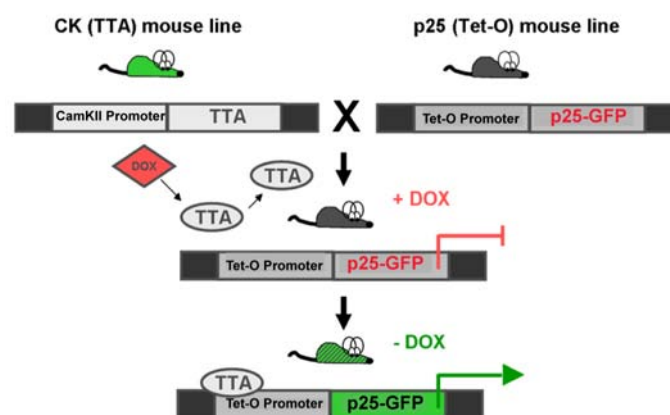
Figure 2- 10. CK/p25 Mouse Model.

CKp25 mice are generated via crossing the CK mice harbouring the transactivator domain (TTA) to the p25 mice, which expresses the p25 behind the Tet-Operon (Tet-O) promoter. Upon doxycycline (Dox) withdrawal, p25 becomes expressed specifically in CamKII-positive neurons in double-transgenic mice. Modified from[330].

As the p25 protein is fused to GFP (Figure 2- 10), staining for GFP confirms the expression of p25 in mature NeuN-positive neurons of double-transgenic mice 5 weeks after doxycycline withdrawal (Figure 2- 11A,B). At 2 weeks after doxycycline withdrawal, already apoptotic neurons are detectable, consistent with the described apoptotic death of these neurons (Figure 2-11C,D)[331]. At the same time point, the cortical thickness is slightly reduced compared to control mice. At 5 weeks of doxycycline withdrawal the cerebral cortex of CK/p25 mice is obviously reduced compared to control animals (Figure 2- 11E). According to the literature, expression of p25 in CK/p25 mice for five weeks leads to progressive apoptotic cell death with a brain weight reduction of 15-20 %. After transgene expression for eight or twelve weeks the bitransgenic mice exhibit a 25 % or 40 % decrease in the cortical neuronal density, respectively. In addition, hyperphosphorylation of tau can be detected in CK/p25 mice[331]. In addition, this transgenic mouse line exhibits intraneuronal accumulation of Aβ and the development of cognitive defects are present in this mouse line[342,343]. Consequently, within a few weeks of p25 expression, massive neuronal death and GFAP activation is observed in this mice[331,342]. CK/p25 mice therefore represent a valuable mouse model reflecting some features commonly observed upon human AD pathology.
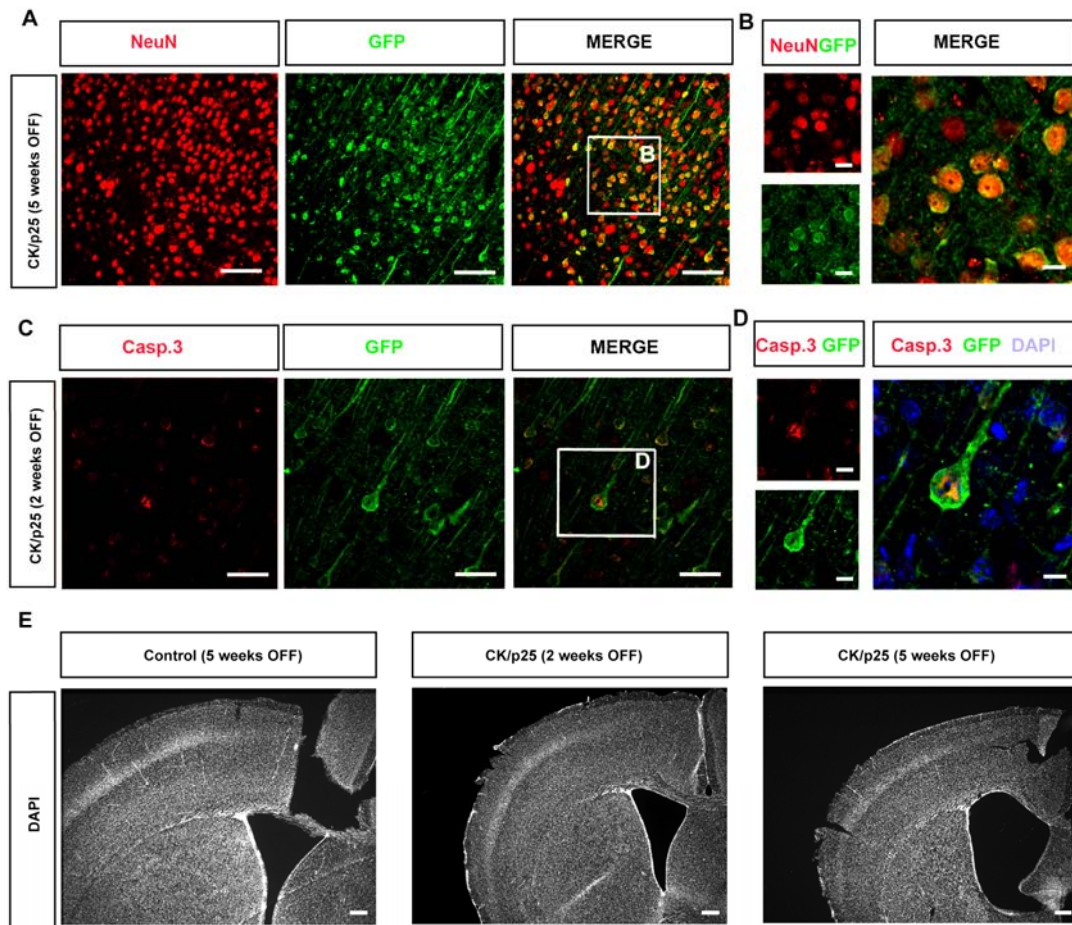
Figure 2- 11. Phenotype of CKp25 Mice upon Different Durations of Doxycycline Withdrawal.

As confirmation of the funtional mouse line, (A, B) show a staining for GFP, which detects p25 expression co-localising with NeuN-positive neurons. Staining for activated caspase 3 (Casp. 3) in (C), (D) shows an overlay of Casp.3 in a GFP labelled neuron. In (E) overview pictures of DAPI stained brain sections of control, CK/p25 2 weeks OFF and CK/p25 5 weeks OFF treated animals at an equivalent Bregma level are presented. The cortical thickness is reduced and the ventricular size is enlarged specifically 5 weeks OFF treated CK/p25 animals. Scale bar indicates 50 μm in (E) and 20 μm in (A-D).

2.6   Glial Cells in Alzheimer's Disease Pathology

2.6.1   Astrocytes

Upon Alzheimer's diesease astrocytes become reactive and are mostly associated with focal plaques[324,344-346]. Astrocytes densely surround the plaques with their processes, thereby forming a barrier between plaque and brain tissue[71,347]. Astrocytes in the vicinity of plaques also become hyperthrophic, while those located away from them were also shown to undergo atrophy[348]. In addition to these features upon AD, astrocytes overt altered gap junctional coupling and Ca-signaling, which may impair neuronal function[349]. Also the expression of glutamate transporters of astrocytes declines with increasing AD stage. This may additionally elevate the vulnerability of neurons toward excitotoxicity[211,350,351]. Importantly, changes in synaptic plasticity appear to be worsened by astrocyte atrophy[352].

Upon AD pathology, some endogenous degradation of amyloid plaques takes place. *In vivo* imaging revealed that although most of the plaques seem to be relatively stable within a couple of months, a few of them decrease in size with time[353]. Similarly, analysis of human AD patient tissue shows that the most advanced AD cases (measured by Braak staging) have a slightly reduced plaque frequency than cases of a previous stage[354]. Strikingly, astrocytes are not only attracted by Aβ42[355] but also are capable to take it up, accumulate it and degrade it *in vitro*[355-357]. Astrocytes that have taken up Aβ, may exert metabolic disturbances as well as a production of hydrogen peroxide, an oxidative stressor[358]. Some plaques may derive from the death and subsequent lyses of Aβ overloaded astrocytes[357].

In addition to the accumulation of Aβ, the expression of the Aβ-degrading enzyme neprilysin is induced in reactive astrocytes in mice, which exert extracellular plaque deposition[359,360]. However, neprilysin seems to be soley efficient for proteolytical degradation of soluble Aβ. The metalloproteinase 9 (MMP9), which is additionally produced and released by astrocytes located in the vicinity of extracellular plaques, represents a more efficient enzyme to reduce the plaque burden formed by aggregated amyloid fibrils (fAβ)[361].

As the inheritance of the ε4 allele of the apoE4 transporter is a major risk factor for sporadic AD, it is important to note that within the central nervous system, APOE is highest expressed by astrocytes and microglia[362]. Upon aging, expression levels of APOE are increased in astrocytes[103,363]. Similarly, upon AD pathology APOE co-localizes with astrocytes as well as plaques and tangles[364]. Furthermore, the expression of the apolipoprotein E in astrocytes seems to be crucial for their ability to accumulate Aβ, since in astrocytes where APOE is knocked out, this ability is lost[365]. According the the Aβ hypothesis AD is caused by an imbalance of Aβ clearance and Aβ production. Therefore, astrocytes may have a crucial contribution to the development of AD since APOE dysfunction is involved in the clearance of Aβ by astrocytes. Summarizing, astrocyte atrophy, altered Ca-signalling or other AD-related disturbances may additionally account for the emergence of the pathology.

3.6.2 Oligodendrocytes

Myelination of the frontal lobe white matter proceeds until mid-age in healthy humans and then declines progressively. On the contrary, grey matter structures are linearly lost in normal ageing[366]. Furthermore, myelin maintenance may comprise a continuous myelin turnover[105]. Thus aging, the major risk factor of developing sporadic AD, is accompanied with increases in myelin aberrations[369,370] and myelin breakdown[371,372], which is exacerbated upon AD pathology[371-373]. In addition to the formation of plaques and tangles as well as focal neuronal degeneration, loss of myelin is additionally observed in human AD patients. The white matter is reduced in size and the expression of myelin proteins in the corpus callosum (CC) and frontal cortex white matter is lowered[367,363]. In addition, loss of oligodendrocytes in the white matter has been reported[368]. Also grey matter structures express less myelin proteins and show diminished levels of grey matter lipids[369]. Myelin loss and exacerbated myelin breackdown upon AD may lead to a failure of action potential conductance and trophic axonal support having a great impact in the progression of cognitive impairment. In the healthy brain, NG2+ cells comprise a cell source for myelin repair as observed in different pathologies such as multiple sclero-

sis. Their reaction and reparative potential upon AD pathology remains to be elucidated[170].

3.6.3 Microglia

Aβ is also a potent activator of microglial reactivity, resulting in an increased secretion of diverse molecules such as inflammatory cytokines, activated complement proteins, proteases and reactive oxygen species[374,375]. Microglia are closely associated with amyloid plaques and increase in number in a proportional manner[376,377]. Upon appearance of newly formed plaques, microglia rapidly extend their processes and migrate toward them within 1-2 days[378,379]. Furthermore, they become activated, hyperthroph and exhibit a "proinflammatory phenotype" [370]. Similar to astrocytes, microglia are able to engulf fAβ. After phagocytosis has occurred, Aβ is found in endosome-like cellular compartments[381,38]. Whether the up-taken fAβ is actually degraded within the microglia is still debated. There is evidence that activated microglia in culture are able to degrade internalized fAβ[383], while other studies suggest only little degradation[384,385].

In a study conducted in 1989 in human patients with plaque deposition that had undergone a stroke, infiltrating macrophages into the brain had a greater capability to remove the amyloid. This finding indicates that invading macrophages may harbour a greater potential to phagocytose amyloid than the resident microglia present in the brain[380,386]. Also in mouse models of AD pathology, infiltrated blood-derived microglia are able to phagocytose fAβ and are associated with about 20 % of all plaques in the brain[378,387,388]. Although ablation of resident microglia from the brain does not affect the plaque size, soluble Aβ40 and Aβ42 fractions are increased in this experiment. Overall, this study reinforced the idea that resident microglia in the AD brain may be not efficiently degrading amyloid[389]. Therefore, how efficient the degradation of Aβ by resident microglia in an AD environment is remains debated. Also the role and potential of blood-derived immune cells needs to be elucidated in more detail. Interestingly, at later stages of AD pathology in human and mouse models, blood brain barrier breakdown may facilitate the entry of these cells into the brain[380,390,391].

Phagocytic functions of resident microglia may be impaired due to the pro-inflammatory environment in AD pathology[392,393]. For example pro-inflammatory molecules such as the liposccharide-binding protein (LPS) inhibit the fAβ up-take of microglia *in vitro*[371]. On the contrary, treatment of AD mice with anti-inflammatory drugs results in an reduced plaque burden[394,395]. Microglia also have a role in degrading soluble amyloid[396], as they secrete the insulin-degrading enzyme with one of its substrates being soluble amyloid[397].

In conclusion, glial cells are also reacting toward AD, however the pathology is different from invasive injuries. Therefore, glial cells may exert very distinct functions and abilities compared to other injuries.

2.7   Therapeutical Strategies

Until now, no cure exists for AD. Rather therapies aim to improve a patient's live. Thinking about the increasingly ageing society intensive care for AD patients is accompanied by enormous social costs. Development of new therapeutic approaches may contribute to improve a patient's life quality and reduce this social burden.

New therapeutics aim to decrease the production of Aβ, since according to the Aβ hypothesis, Aβ and/or its oligomers are the toxic component that initiates AD pathology. However, few clinical trials were executed so far and their outcome remains to be elucidated[372].

The so called "cell-based therapies" may also represent a new alternative therapeutic strategy in neurodegenerative diseases. Here, the aim is to replace lost neurons as well as glial cells by cell transplantation into the affected brain areas. In this regard e.g. embryonic stem cells or induced pluripotent stem cells from for example fibroblasts could comprise interesting cell sources. However, so far no stem cell therapy approach has proven to be beneficial enough to be suitable for routine use[241,376]. One concern is that the AD pathology may spread into the grafted cells as it has been shown in Parkinson's disease. When fetal nerve cells from the donor midbrain were transplanted into the striatum of patients with Parkinson's disease these cells

could survive[373]. Long-term surviving patients first benefited from the transplantation, but at later stages the transplanted cells developed Lewy pathology reminiscent of Parkinson's disease or dementia with Lewy bodies after 11-16 years[373]. Such a spread of pathology from host to donor cells in Parkinson's disease was also observed by two other studies, further underlining the possibility of such a spread of pathology into transplanted cells also upon AD[374,375]. In addition, the suitability of cell transplantations into the brains of AD patients may also be questionable since the pathology occurs in a widespread manner.

Interestingly, glial cells respond to AD pathology and in principle they can exert both, beneficial and detrimental effects. Most importantly, glial cells such as astroglia or oligodendrocytes may essentially contribute to the development and/or progression of AD pathology. Understanding of the glial cell reactivity may therefore help to elucidate new therapeutic strategies, by e.g. promoting positive and reducing detrimental effects.

2.8   Aims of the Study

The main objective of this thesis is to better understand reactive gliosis upon AD pathology.

As a first aim, I investigated the reaction and potential of reactive astrocytes in mouse models reflecting different aspects of human AD pathology. This was prompted by the recent discovery of a subset of astrocytes developing stem cell potential upon invasive injury. I therefore set out to determine to which extent this reaction also occurs in AD mouse models.

Since upon human AD myelin diminutions are commonly observed and may also contribute to the progression of the disease, I set out to determine whether this feature is reflected in a mouse model with progressive plaque deposition. If so, the aim was to investigate the glial reactivity to determine possible attempts for remyelination. Toward this end I analyzed how cells of the oligodendrocyte lineage, and especially of the NG2+ progenitors, as a potential source for remyelination, react toward plaque deposition.

3   Results

3.1   Reactive Gliosis

Glial cells react toward injury and in this regard astrocytes are of special interest because they harbour a great regenerative potential as upon acute lesion these cells are able to acquire a stem cell potential by forming self-renewing multipotent neurospheres[217]. The great ability of these cells is further underlined by the fact, that astrocytes can adopt a neuronal fate e.g. upon forced expression of neurogenic factors *in vitro*[376-378] and *in vivo* after acute brain lesion[116]. Additionally, astrocytes exert inflammatory responses in concert with microglia, which represent the "immune cells" of the brain. Yet, reactive astrogliosis may differ in its characteristics, according to the duration, severity and type of injury. The most striking feature of astrocyte reactivity is the formation of the glial scar. Other prominent features include astrocytic hyperthrophy, up-regulation of intermediary filaments and extracellular matrix molecules as well as eventual proliferation[48,95,187,215,216]. To carefully determine the severity of astrogliosis in APPPS1 mice all these parameters were investigated and compared to an acute lesion paradigm such as stab wound injury.

3.1.1   Hypertrophy and Up-regulation of Intermediate Filaments in APPPS1 Mice

To understand the astroglial cell reaction over time upon amyloid plaque deposition, I monitored the amyloid plaques with the anti-amyloid beta (Aβ) antibody directed against the amino acids 1 to 14 at the N-terminus of this protein; it therefore detects human Aβ (Fig. 3- 1A,B). Along with plaque deposition, reactive astrocytes were monitored by immunostaining of the intermediate filament GFAP, which has been shown to be up-regulated once protoplasmic astrocytes in the cortical grey matter become reactive[95]. The majority of the GFAP-positive astrocytes were located in the vicinity of

plaques in the 3 months old APPPS1 mice (Fig. 3- 1B). On the contrary, control mice exerted only subpially located or blood vessel-associated GFAP+ cells (Fig. 3- 1B). Between 6 and 11 months of age, GFAP+ astrocytes spread throughout the cerebral cortex of APPPS1 mice covering all layers (Fig. 3- 1B). Plaques accordingly further increased in density and volume as it has been described[328] until at least 11 months of age. Several of the early as well as the later reacting astrocytes in the APPPS1 mice were also hypertrophic (Fig. 3- 1C).

The majority of GFAP-positive reactive astrocytes additionally acquired immunoreactivity of the intermediate filament nestin, which was also observed after acute stab wound injury (Fig. 3- 2). Nestin is expressed by embryonic neuroepithelial and radial glial cells and may hence be indicative of a possible dedifferentiating response of astrocytes toward chronic and acute lesion paradigms (as observed after stab wound injury; Fig. 3- 2).

Thus, astrocyte reactivity, studied by GFAP and nestin immunoreactivity started in association and further increased in parallel with the plaque pathology in APPPS1 mice (Fig. 3- 1; 3- 2).
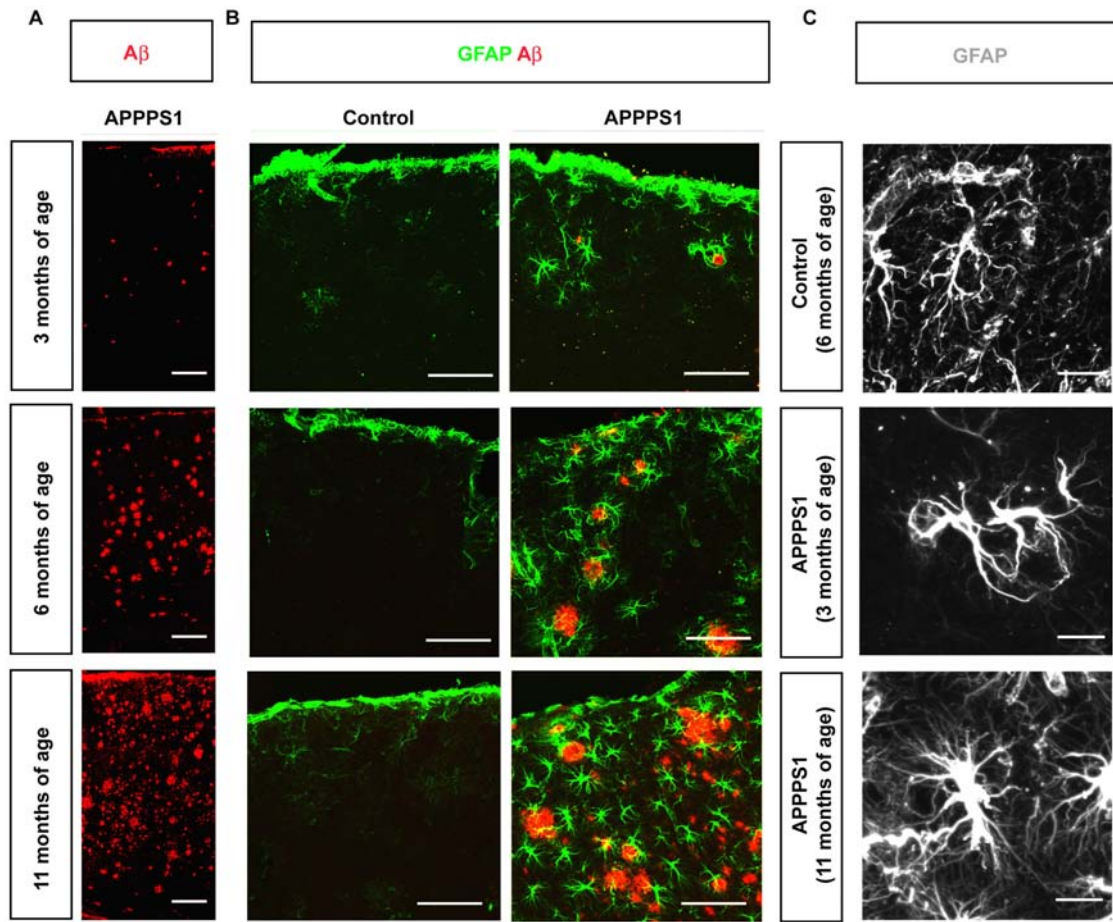
Figure 3- 1. Plaque Deposition and Astrocyte Reactivity in APPPS1 Mice.

(A) depicts the plaque load at different ages in APPPS1 mice. (B) shows the up-regulation of GFAP upon amyloidosis according to increasing plaque deposition with increasing age while in control animals only subpial and blood vessel-associated GFAP-positive astrocytes were observed. (C) shows magnifications of single astrocytes in control and APPPS1 mice at different ages. Scalebar: 100 μm in (A,B) and 20 μm in (C).
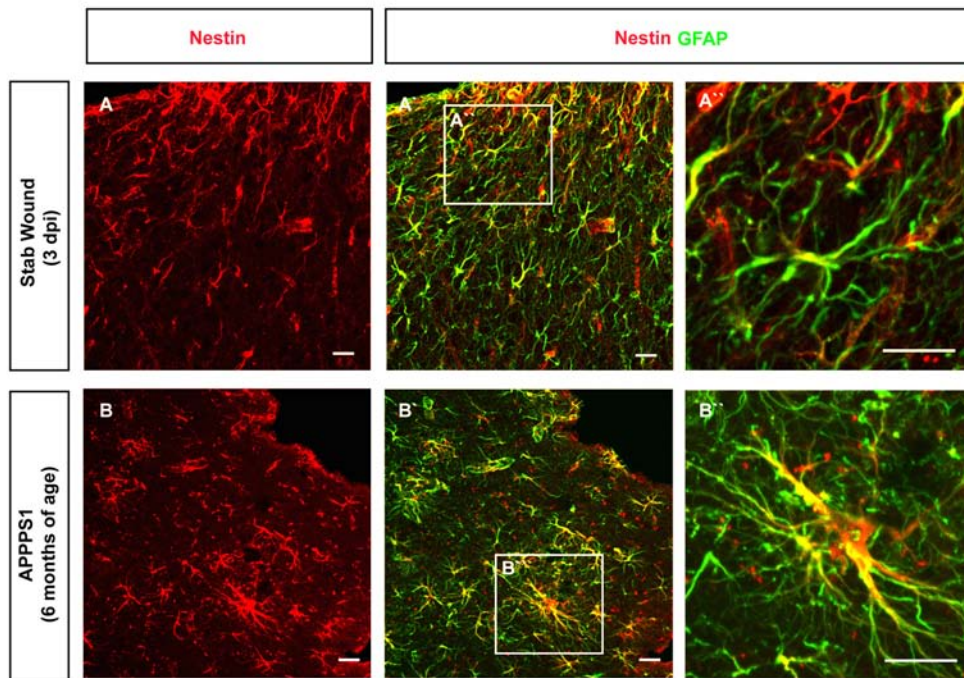
Figure 3- 2. Nestin Immunoreactivity of Reactive Astrocytes.

GFAP-positive reactive astrocytes in 6 months old APPPS1 mice acquire nestin immunore-activity. Scale bar: 20 μm.

3.1.2 Up-regulation of Extracellular Matrix Proteins

In the healthy brain, the extracellular matrix molecules tenascin C (TNC) and DSD-1, are highest expressed in the neurogenic niches and can be secreted by astrocytes. Thus, these proteins may be localized intracellularly or at the membrane. After acute lesion, reactive astrocytes up-regulate and secrete these extracellular matrix molecules[95,187,216]. To study if these molecules would also be up-regulated in the APPPS1 mice, the expression of the gly-coprotein TNC and the proteoglycan DSD-1 were investigated.

For staining for the DSD-1 protein the antibody detecting the 473HD epitope was utilized. The 473HD epitope was detected at high levels extracellularly close to the acute stab wound, whereas its expression was low in the healthy brain parenchyma (Fig. 3- 3A,B). In addition, GFAP+ astrocytes showed an increase in membrane associated DSD-1 protein expression compared to

controls (Fig. 3- 3A`,B`). Also upon chronic amyloidosis DSD-1 protein expression was elevated in comparison to control levels but it was still lower compared to acute stab wound condition (Fig. 3- 3A-C).

On the other hand, TNC expression was increased extracellularly as well as intracellularly within GFAP-positive astrocytes in stab wound and APPPS1 mice compared to controls (Fig. 3- 3D-F).

In conclusion, astrocytes became strongly reactive upon chronic amyloidosis. The up-regulation of extracellular matrix proteins as well as intermediate filaments, normally only expressed at low levels or in few cells in the healthy cortical grey matter but present at higher levels in the adult stem cells niche and stem cells, is indicative for the degree of dedifferentiation of reactive astrocytes in this lesion paradigm[95]. The data imply a similar severity (or degree of dedifferentiation) of reactive astrogliosis in the acute stab wound lesion in comparison to the APPPS1 mice.
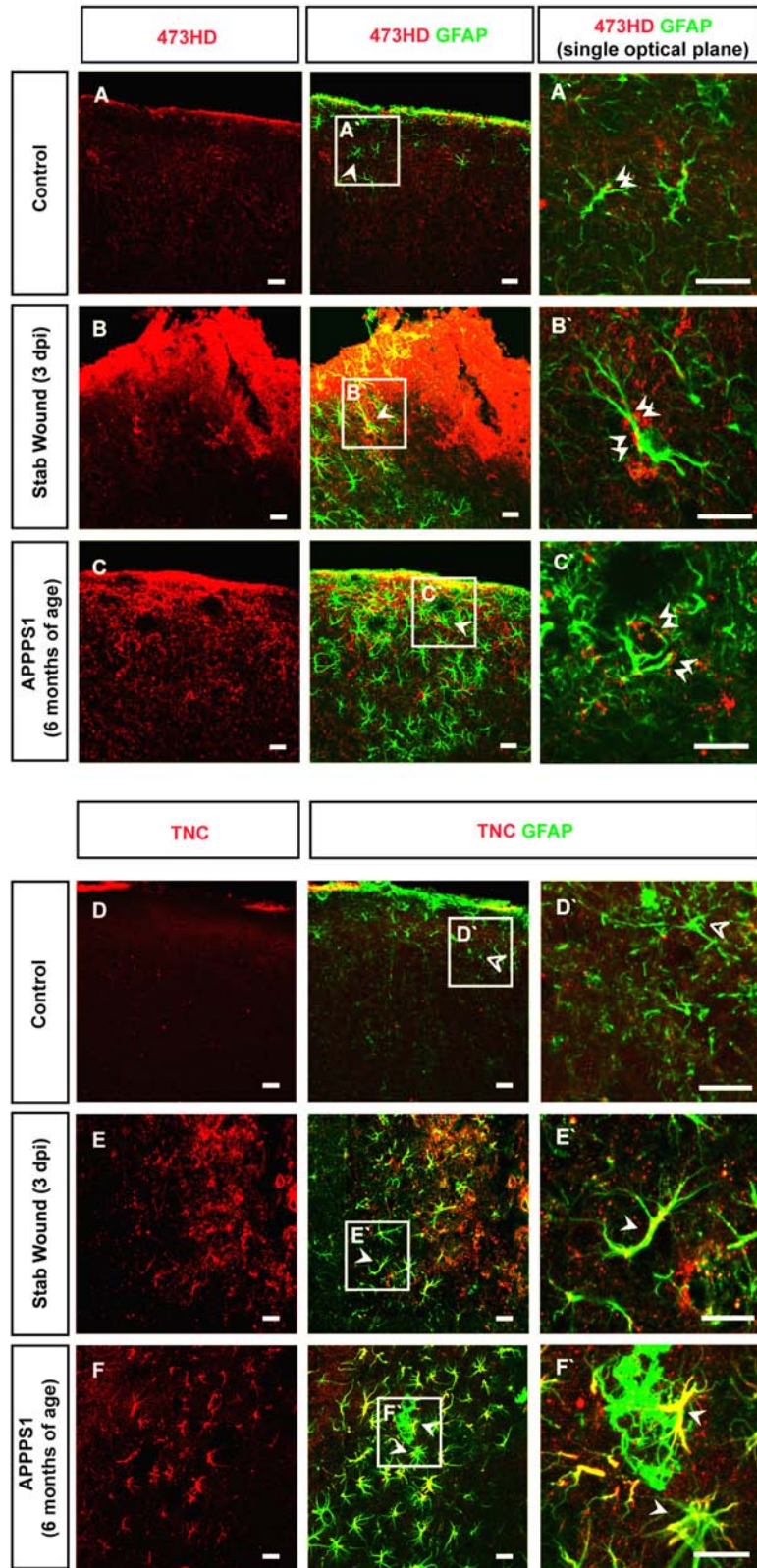
Figure 3- 3. Expression of the 473HD Epitope and TNC after Stab Wound and Chronic Amy-
loidosis

Depicted are representative pictures for immunostainings of the extracellular epitope 473HD and GFAP-positive astrocytes in healthy (control; A), stab wounded (three days post lesion (3 dpi); B) and 6 months old APPPS1 mice (C), as well as higher magnifications of the indicated inlays in (A`,B`,C`). The white arrowheads point toward membrane associated DSD-1 protein expression. In (D-F) pictures of TNC immunostainings in healthy control (D), stab wounded (3 days post lesion; E) and 6 months old APPPS1 mice (F) are shown. Additionally, higher magnifications of the equivalent immunostaining were added in (D`,E`,F`). The white arrowheads point towards double-positive cells, while the dark arrowhead shows a single positive cell. Scale bar: 20 µm.

3.1.3 Increased Proliferation upon Chronic Plaque Deposition

The severity of the reactive gliosis is supposed to gradually change according to the severity of the insult. Along this line, astrocyte proliferation is a feature occurring after large invasive injury[187]. After acute stab wound injury about 50 % of the astrocytes resume proliferation[103,217]. To investigate the degree of proliferation upon chronic amyloid plaque deposition, I applied 5-Bromo-2′-Deoxy-Uridine (BrdU) -a thymidin analogue that incorporates into the DNA during cell division- for 2 weeks to the drinking water of APPPS1 and age-matched control mice. First, I investigated the time course of proliferation by analyzing animals at 3, 6, and 11 months of age. Interestingly in control mice, proliferation significantly decreased with age, while in APPPS1 mice it increased from 3 to 6 months of age and then remained on a similarly elevated level. In comparison to control animals proliferation was markedly increased in APPPS1 mice from the age of 3 months on (Fig. 3- 4C). Of note, BrdU+ cells in 3 months old APPPS1 mice mostly accumulated in the vicinity of plaques (data not shown). However at 6 months of age, BrdU+ cells were also observed apart from plaques. Also at this time point proliferation was observed around plaques, stained with the 6E10 antibody detecting both human Aβ and APP, but also in plaque-free areas (Fig. 3- 4A,B).
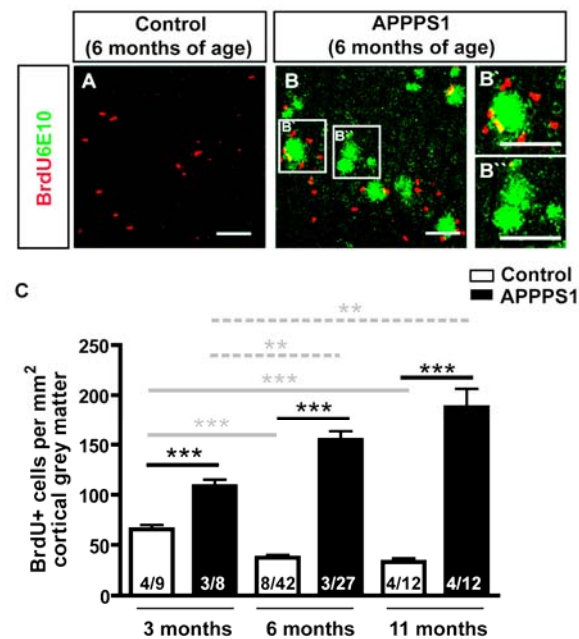
Figure 3- 4. Proliferation in the Cerebral Cortex Grey Matter of APPPS1 Mice.

(A,B) depict representative pictures of control and APPPS1 mice stained for BrdU and 6E10 at 6 months of age. BrdU-positive cells at 6 months of age accumulated often but not necessarily around plaques as shown in (B`,B``). (C) shows the quantitative analysis of BrdU+ cells per mm^2 cortical grey matter at different ages. The proliferation in APPPS1 mice was significantly increased from 3 months of age on. The numbers within the column indicate the number of animals as well as the number of slices quantified (n of animals/n of slices). Data are presented as mean per slices ±SEM. Scale bar: 50 µm.

To conclude, proliferation was already increased at 3 months of age. The most prominent elevation of BrdU+ cells in APPPS1 mice was detected at 6 months of age and remained on a stable level afterwards. However, different glial cell types may start dividing upon chronic amyloidosis. Therefore, I co-labelled BrdU-positive cells with different markers, namely S100b and/or GFAP, Iba1, and NG2 for the visualization of astrocytes, microglia and oligodendrocyte progenitors, respectively (Fig. 3- 5).

Expectedly in control mice, the percentage of proliferating NG2+ cells was greatest, while only few astrocytes and microglia contributed to the total BrdU pool. On the contrary, microglia represented the major cell type proliferating

around the plaques at 3 months of age in APPPS1 mice. At this time point, the percentage of NG2+ progenitors among the total number of BrdU+ cells was already markedly decreased compared to control animals. At 6 months of age, the proliferative response of glial cells largely reflected the observations obtained from 3 months old animals (around the plaques. Interestingly, the percentage of astrocytes was similarly low between 6 months old control and APPPS1 animals (Fig. 3- 5A,B,C,E). It became clear that the cell populations that are proliferating are very distinct in the cortical grey matter in the healthy versus the chronic amyloidosis condition.

To investigate if the decreased percentages of marker-positive cells over the BrdU population would also affect the total number of the proliferating cells in the APPPS1 mice, I quantified the number of Marker/BrdU double-positive cells per mm^2 cortical grey matter. Since upon chronic amyloidosis mice proliferation is most prominently increased at 6 months of age, I performed the quantification at this time point. Surprisingly, despite the decreased percentage of NG2+ glia over the BrdU population, the total number of NG2+BrdU+ cells was significantly increased (Fig. 3- 5D). In addition, even though the number of dividing astrocytes increased significantly in the APPPS1 mouse, the total amount of these cells was rather low (Controls had 1.3±0.3 S100bGFAP+/BrdU+ cells per mm^2, while APPPS1 had 3.1±0.5). Accordingly, they constituted only to a small fraction of 2.5 % of the total BrdU pool in 6 months old APPPS1 mice (Fig. 3- 5D,E), respectively. Thus, despite the fact that astrocytes became reactive, which was proven by the increased expression of GFAP, nestin, 473HD and TNC, their proliferative response was limited. This is very different to what has been observed in the acute stab wound injury, since proliferation of astrocytes remarkably increased in this lesion paradigm[103].

In accordance with the high percentage of microglia over the BrdU pool, also their total number was elevated in APPPS1 mice (Iba1/BrdU double-positive per mm^2), while in the healthy cortical grey matter microglial cells rarely divided (Fig. 3- 5D,E).
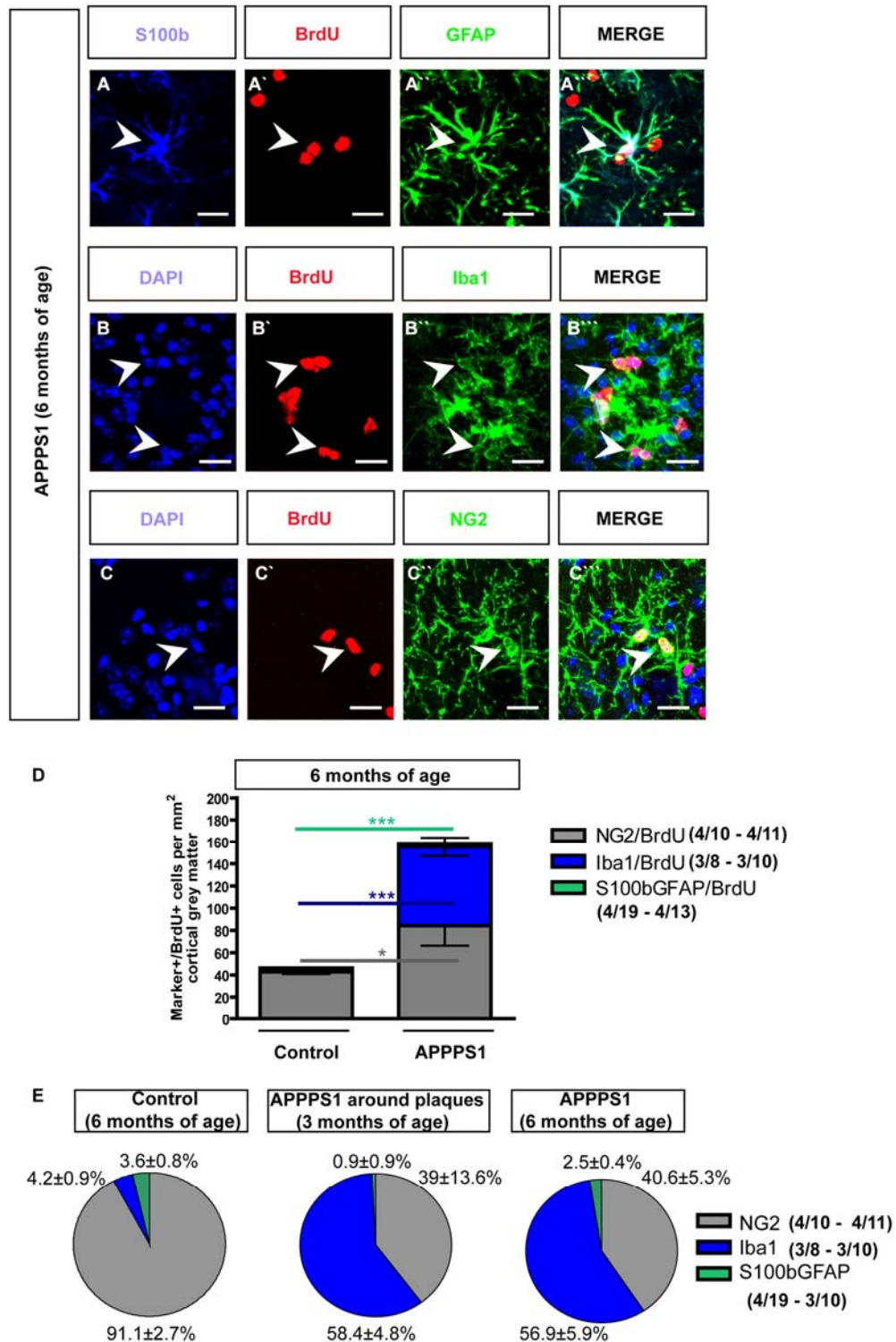
Figure 3- 5. Proliferation of Glial Cells in APPPS1 Mice.

(A) is an example of a BrdU+ astrocyte (S100b+ and GFAP+), while (B) depicts an accumu-
lation of proliferating Iba1+ microglia, (C) is an example of dividing NG2+ cells. (D) The total
number of proliferating cell types was quantified in 6 months old animals per mm^2 cortical
grey matter by double-staining of BrdU-positive cells with NG2 for oligodendrocyte progeni-
tors, Iba1 for microglia and S100b and/or GFAP for labelling astrocytes. (E) Subdivision of

the cell types that proliferate in control and APPPS1 mice at the age of 3 and 6 months. NG2+/BrdU+, Iba1+/BrdU+ and S100b and/or GFAP+/BrdU+ cells were quantified as the percentage of marker-positive cells over the proliferating BrdU+ pool. The numbers behind the markers indicate the number of animals as well as the number of slices quantified (n of animals/n of slices) for controls – APPPS1 6 months of age. Data are presented as mean per slices ±SEM. For APPPS1 3 months of age in (E) the data are presented as mean per plaques (3/10 for NG2 staining; 5/73 for Iba1 staining and 3/19 for S100bGFAP staining) ±SEM. Scale bar: 20µm.

3.1.4 Neurosphere Forming Capacity of the Cortical Grey Matter in APPPS1

Upon acute stab wound and focal laser lesion, some reactive glial cells have the potential to generate self-renewing, multipotent neurospheres *in vitro*. Interestingly, in acute stab wound lesion, reactive astrocytes were identified as the cell population responsible for neurosphere formation[95,216,217]. Since I observed a strong reaction of glial cells in chronic amyloidosis as well as a small but significant increase in astrocyte proliferation, I aimed to examine the potential of these reactive glial cells to generate self-renewing, multipotent neurospheres.

For this experiment, I dissected cortical grey matter tissue from APPPS1 and wild type control mice and compared it to grey matter tissue from wild type control mice which had undergone stab wound injury 3 days before. The data from the stab wounded animals were obtained in collaboration with Dr. Swetlana Sirko. As a further positive control, I isolated cells from the adult subependymal zone (SEZ), one of the neurogenic zones of the adult brain, where neurosphere formation has first been discovered[51].

From all tissue samples I plated an equal number of cells per well at clonal density (5 cells/µl) and quantified the number of primary neurospheres formed after 14 days in culture. As expected, most neurospheres had formed from SEZ tissue (Fig. 3- 6A, B). In addition, neurospheres did not form from the tissue of the intact and healthy cerebral cortex of young and aged healthy control mice. In further agreement with previous data, neurospheres formed from the stab wounded cerebral grey matter (Fig. 3- 6B). In line with the notion, that the adult SEZ contains many neural stem cells the number of SEZ

neurospheres was 10 times (10 x) higher compared to the stab wound. Significantly fewer primary neurospheres were generated from the cortical grey matter of APPPS1 mice, which were older than 6 months of age. 2 out of 9 cultures of cells from the cerebral cortex of APPPS1 mice did not generate any neurospheres. To test for multipotency of the primary neuropheres, these were plated and differentiated for 7 to 10 days. Some of the neurospheres (33%, 5 out of 15), which had formed, were multipotent and generated neurons, astrocytes and oligodendrocyte progenitors (Fig. 3- 6C), while the others remained glial.

3.1.5 Self-Renewal of Neurospheres

Since neurospheres obtained from the APPPS1 mice were multipotent also their ability to self-renew was investigated. This was achieved by splitting and subsequent seeding at a clonal density of 5 cells per µl. The secondary neurospheres were compared to secondary spheres obtained from acute stab wound lesion and SEZ tissue. Secondary neurospheres were counted 7 days after splitting. The number of secondary neurospheres increased in comparison to the primary neurosphere formation in all conditions. This is consistent with the idea of enrichment for self-renewing cells after passaging. Most secondary neurospheres were generated from the SEZ cells. Interestingly, APPPS1 mice generated significantly fewer secondary neurospheres compared to both, SEZ tissue and acute stab wound. Thus, the capacity of neurosphere self-renewal of cells from the cerebral cortex of APPPS1 mice is reduced compared to the acute lesion (Fig. 3- 6B).

3.1.6 Neurosphere Formation after Acute Stroke

As neurospheres were formed from the stab wounded cortical grey matter[217], I wanted to determine, whether neurosphere formation would also take place after another acute lesion paradigm such as MCAO (middle cerebral artery occlusion). These experiments were performed in collaboration with Dr. Martin Dichgans, Dr. Christophe Heinrich and Steffen Tiedt. The MCA was occluded by a filament for 1 or 2 hours and tissue was collected 3 days after the

surgery. Interestingly, the formation of primary neurospheres in this model was well comparable to the stab wound injury model. A similar number of neurospheres as observed upon acute stab wound formed within 14 days in culture (Fig. 3- 6B).
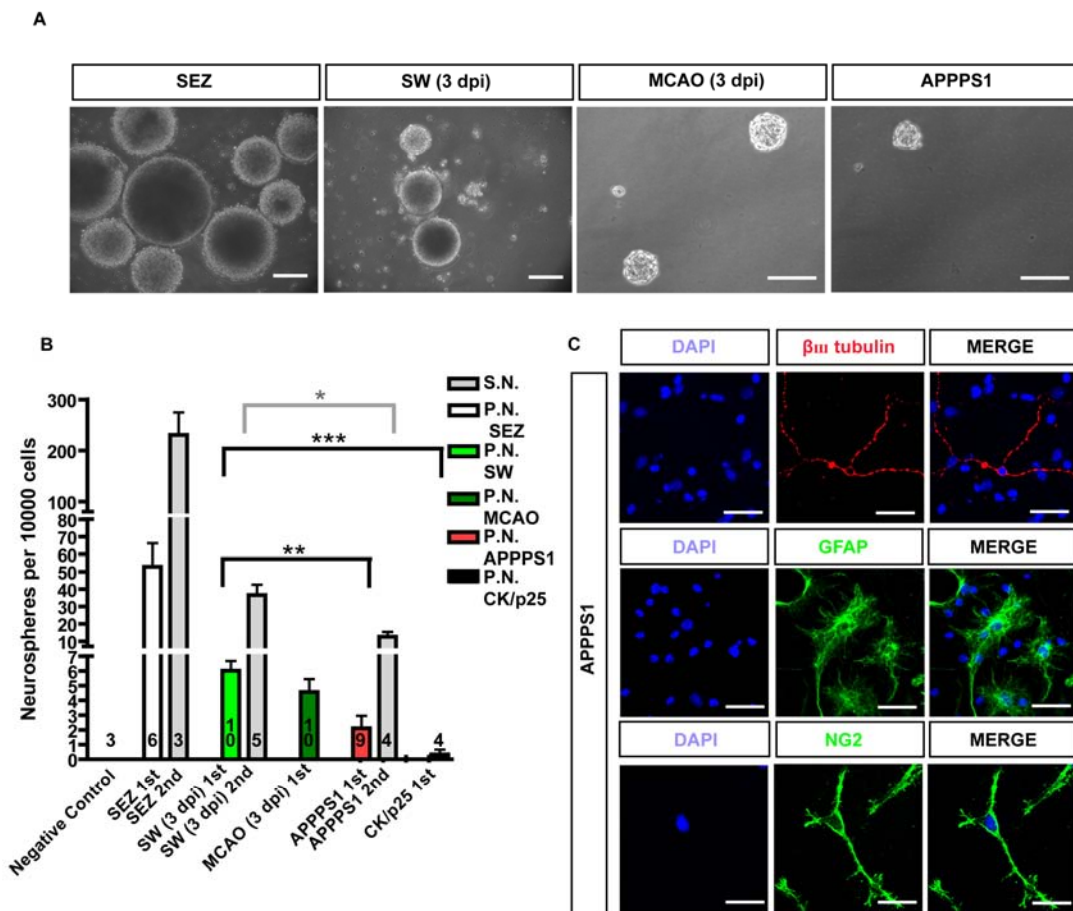
Figure 3- 6. Generation of Neurospheres.

(A) shows representative pictures of neurospheres from different lesion paradigms such as stab wound, MCAO and APPPS1 mice, including SEZ as a positive control. (B) the cloured bars are the quantification of primary neurospheres (P.N.) per 10000 plated cells. Neurosphere formation is significantly decreased upon chronic amyloidosis compared to acute stab wound. The quantification of secondary neurospheres (S.N.) is shown with the grey bars for the acute stab wound lesion, APPPS1 mice and SEZ as a positive control. Secondary neurospheres were generated at a higher rate than primary neurospheres in all conditions. The secondary neurosphere formation was decreased in APPPS1 mice compared to stab wound lesion (C) representative pictures of differentiated primary neurospheres of APPPS1 mice. βIIItubulin was used to detect neuronal, GFAP for astrocytes and NG2 for oligodendroglial progenitor cells. The number of the cultures analyzed are indicated within

the columns. Data are presented as mean per culture ±SEM. Scale bar: 50 μm in (A) and 20 μm in (C).

3.1.7 p25 Over Expressing Mice Exhibit Massive Neurodegeneration

One reason for the decreased neurosphere forming capacity of APPPS1 mice could be the virtual absence of neuronal cell death in APPPS1 mice [329]. In contrast, profound cell death has been observed after both, stab wound and stroke injury[189,379,380]. To investigate the possible effect of this, I examined a mouse model of amyloidosis which additionally overts profound cell death and tau pathology. I used the CK/p25 mouse model, which inducibly expresses p25 in neurons using the doxycycline-dependend Tet-OFF system. Ectopic p25 expression results in profound neuronal loss, up-regulation of GFAP in astrocytes, tau pathology and intraneuronal accumulation of amyloid (Fig. 2- 11 in introduction)[331,342].

To confirm neuronal loss, I stained brain slices from control animals, and from CK/p25 mice which expressed p25 for a period of 2 or 5 weeks. Already in 2 weeks OFF doxycycline treated animals a slight reduction in the cortical thickness could be detected. The profound reduction in NeuN-immunopositive neurons was observed in 5 weeks OFF treated CK/p25 mice (Fig. 3- 7A). Neuronal loss affected all layers including the upper layers of the cerebral cortex, where Cux1-positive neurons were reduced (Fig. 3- 7B-E).
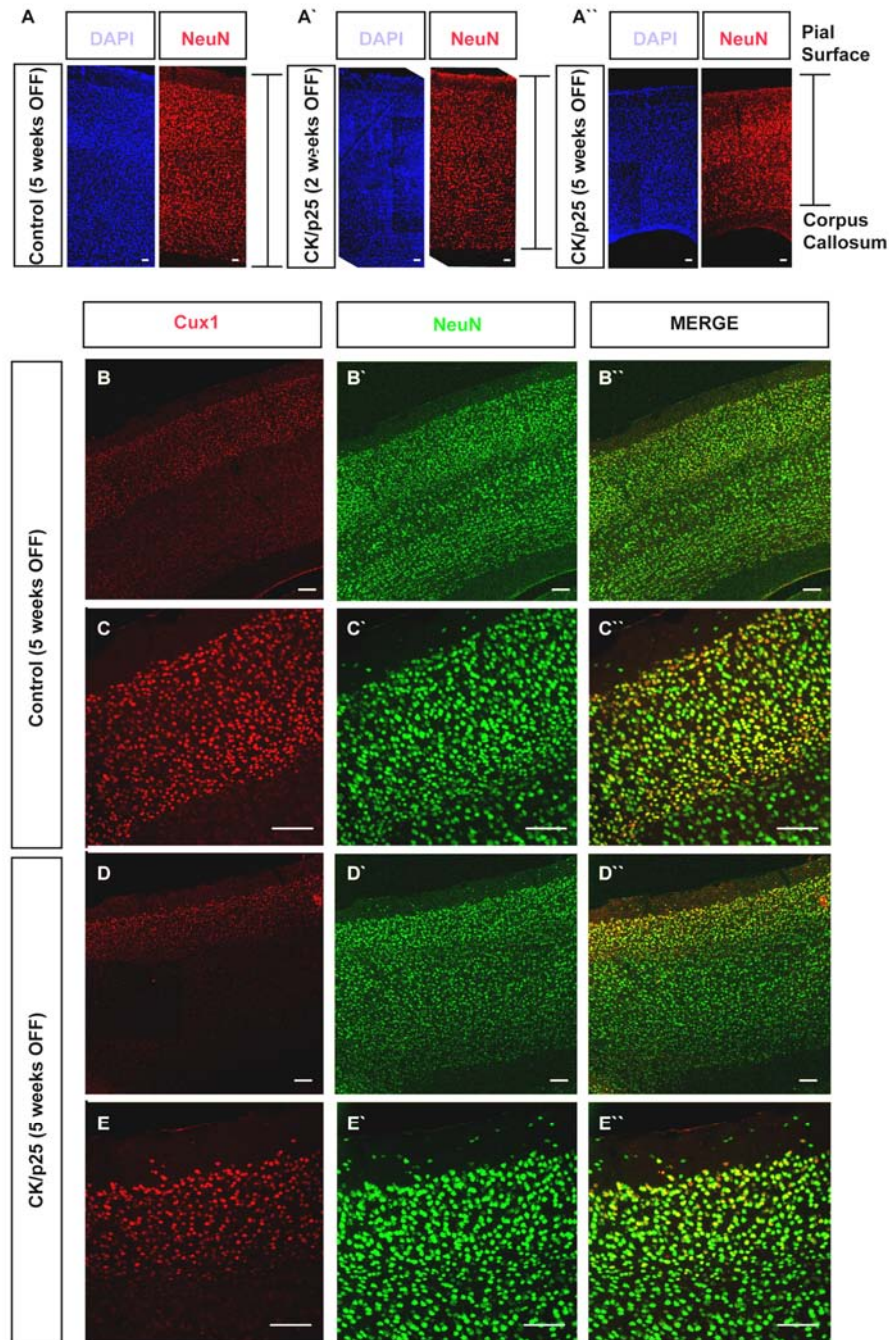
Figure 3- 7. Phenotype of CK/p25 Mice upon different Durations of Doxycycline Withdrawal.

In (A) overview pictures of DAPI and the according NeuN stained brain sections of control, CK/p25 2 weeks OFF and CK/p25 5 weeks OFF treated animals at an equivalent Bregma level are presented. The cortical thickness is reduced in 5 weeks OFF treated CK/p25 animals. (B-E) are representative pictures of Cux1-positive neurons double-labelled with NeuN in control (B,C) and CK/p25 mice 5 weeks OFF doxycycline (D,E). (C,E) are the corresponding higher magnifications of (B,C). Scale bar: 20 µm.

3.1.8 Reactive Gliosis in CK/p25 mice

To investigate the time course of reactive astrogliosis along with neuronal loss in CK/p25 mice, I stained brain sections with 2 and 5 weeks of p25 expression for the intermediate filament marker GFAP. Notably in control animals, which were equally treated with doxycycline, few GFAP astrocytes could be detected mostly located at the pial surface. These cells extended long and fine processes (Fig. 3- 8A). On the contrary, in CK/p25 mice GFAP up-regulation and astrocyte hypertrophy was already detected after p25 expression for 2 weeks (2 weeks OFF doxycycline treatment) not only at the pial surface but also in most layers of the cerebral cortex grey matter (only sparring a band between layer 3 and 5; Fig. 3- 8A). CK/p25 mice 5 weeks OFF doxycycline showed a greater spread of the GFAP+ astrocytes (Fig. 3-8A). In addition, the degree of astrocyte hypertrophy increased compared to animals with p25 expression for 2 weeks (Fig. 3- 8A). Of note, also microglia became hyperthroph, which was already apparent 2 weeks after doxycycline withdrawal. Furthermore, they obviously increased in number after 5 weeks of p25 expression in double-transgenic mice (Fig. 3- 8B).

To further characterize the reactive astrogliosis in CK/p25 mice, I examined the intermediate filament nestin as an additional intracellular marker for reactive astrocytes. Nestin was already shown to be up-regulated upon stab wound as well as in APPPS1 mice. Also upon neuronal loss, the majority of GFAP-positive astrocytes acquired nestin immunoreactivity (Fig. 3- 9A). Investigation of the extracellular matrix markers TNC and 473HD (Fig. 3-9B,C), showed an up-regulation similar to the observations obtained from stab wounded and APPPS1 mice (Fig. 3- 3).

To conclude, astrocytes became similarly reactive in CK/p25 mice. As observed in acute stab wound and APPPS1 mice, astrocytes became hyperthroph and up-regulated markers characteristic for reactive astrocytes such as GFAP, nestin, TNC and 473HD. Also microglia became hyperthroph and increased dramatically in number.
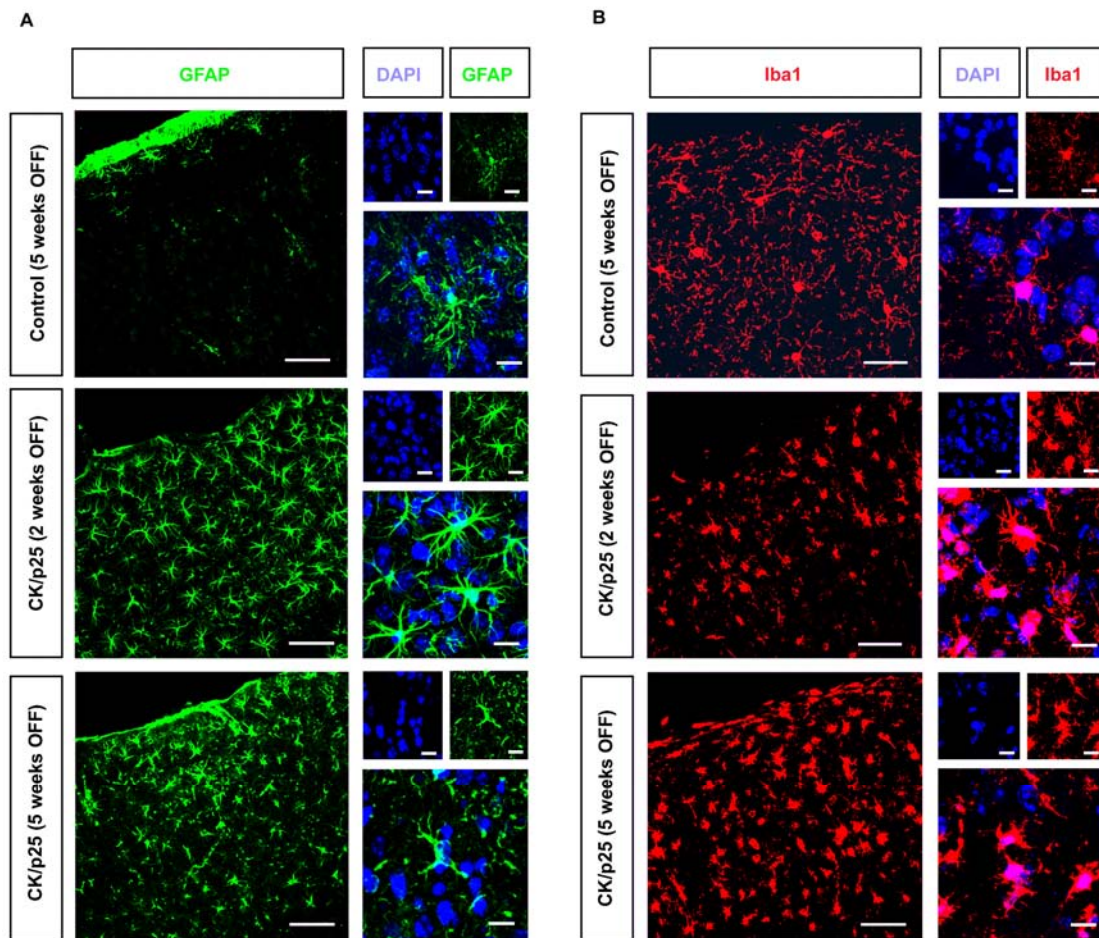
Figure 3- 8. Astroglial and Microglial Hyperthrophy and Reactivity in CK/p25 Mice

In (A) representative pictures of GFAP-positive astrocytes in control animals and CK/p25 mice 2 and 5 weeks OFF doxycycline are depicted. In control animals, which were also raised on doxycycline, only non-hyperthroph subpial and blood vessel-associated astrocytes were labelled by GFAP. Up-regulation of GFAP is already apparent in 2 weeks OFF CK/p25 mice. Astrogliosis worsens in 5 weeks OFF treated animals. Higher magnifications addition-ally confirmed the astrocytic hyperthrophy in the double-transgenic mice. (B) depicts micro-glial cells stained with Iba1. Microglial cells became hyperthroph and increase in number after doxycycline withdrawal of 2 and 5 weeks. Scale bar indicates 50 µm in the overviews and 10 µm in the higher magnifications.
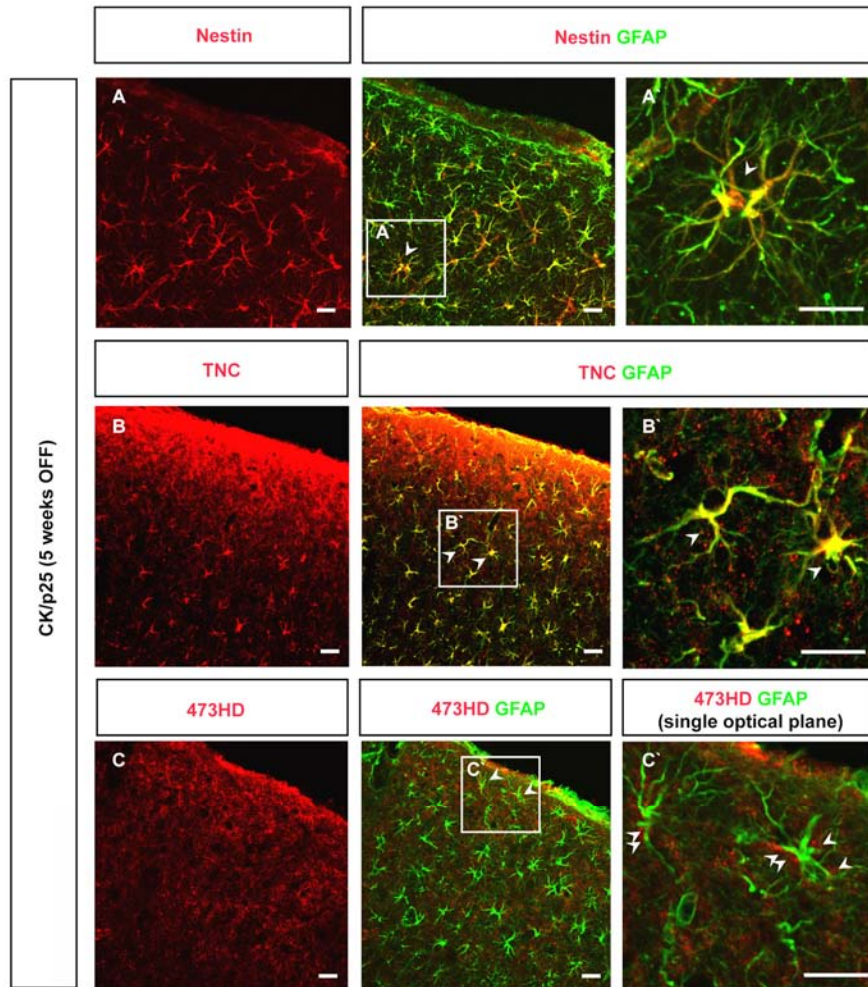
Figure 3- 9. Up-regulation of Nestin, TNC and 473HD upon Massive Neuronal Death.

Reactive astrocytes labelled with GFAP were co-localized with different markers characteristic for reactive astrocytes. A significant number of GFAP+ cells co-expresses nestin. The extracellular matrix epitope TNC is additionally up-regulated extracellularly in CK/p25 mice after 5 weeks with doxycycline withdrawal. Also the 473HD epitope expression is elevated in these mice. Scale bar: 20 μm.

3.1.9 Lack of Neurosphere Formation upon Neuronal Loss

When CK/p25 mice were utilized for the neurosphere assay, strikingly, even fewer primary neurospheres than detected in APPPS1 mice formed from the cerebral cortex of CK/p25 mice 5 weeks after doxycycline withdrawal

(0.3±0.3 neurospheres/10000 cells). This suggested that neuronal cell death cannot be the trigger for neurosphere-forming reactive glial cells.

According to what has been stated before[187], reactive astrogliosis can differ profoundly between different lesion paradigms such as acute and chronic lesion. Therefore, whereas the lesioned area of acutely injured mouse models overts a stem cell capacity of a subset of cells, this ability is not present as pronounced upon chronic plaque deposition and neuronal loss despite prominent astrogliosis. Also upon heavy neuronal death, which was similarly accompanied with severe reactive gliosis, cells of the cortical grey matter showed an even further decreased ability to form neurospheres *in vitro* (Fig. 3- 6). What might determine the different capacities of astroglia in the different mouse models and injury paradigms tested? One possibility is that astrocyte proliferation may correlate to the neurosphere forming capacity, since stab wound injury as well as MCAO are accompanied by a high rate of proliferation of these cells and generate most neurospheres. In comparison, in APPPS1 mice neurosphere formation as well as astrocyte proliferation was decreased. Therefore, the question arises if astrocytes proliferate in CK/p25 mice.

3.1.10   Proliferation of Glial Cells in CK/p25 Mice

To further evaluate the severity of reactive gliosis I examined the proliferation of glial cells by applying BrdU for 1 week via the drinking water. Control and CK/p25 mice were examined at 1 and 5 weeks after doxycyline withdrawal. Proliferation was most remarkebly increased after 2 weeks of p25 expression and the elevation was still observed after 5 weeks of doxycycline withdrawal (Fig. 3- 10A,B). Notably, in CK/p25 mice after 2 weeks of doxycycline withdrawal some animals showed greater proliferation, while others showed much less indicating some heterogeneous phenotype at this early time point.

To investigate in more detail which cell types would resume proliferation in CK/p25 mice, I examined the proliferation of reactive astrocytes by co-staining the BrdU-positive cells with the astrocyte specific markers S100b and/or GFAP (Fig. 3- 11A-C). Surprisingly, despite the profound neuronal cell

death, astrocyte proliferation was only tendencially increased at 2 and 5 weeks without doxycycline. Control animals had 1±0.4 BrdU+/S100b and/or GFAP+ cells per mm^2 which constituted 1.3±0.4 % of the entire pool of BrdU-labelled cells. In CK/p25 mice 2 weeks after doxycycline withdrawal the total number of BrdU/S100b- and/or GFAP was 2.7±0.7 double-positive cells per mm^2 and hence not significantly different. At this time point astrocytes still constituted only a similarly small proportion amongst all proliferating cells as in the control (1.2±0.5 %). Thereafter, after 5 weeks of doxycycline withdrawal astrocyte proliferation did not further increase in CK/p25 mice (1.7±0.6 double-positive cells per mm^2 constituting to 0.9±0.3 % of the total BrdU pool). These results demonstrate that the proliferative response of reactive astrocytes remained minor compared to acute invasive injury models and even diminished in regard to APPPS1 mice, which had a significant increase in th number of proliferating astrocytes in the cortical grey matter (Fig. 3- 11A-C).

Given the hyperthrophy of microglia already present in 2 weeks OFF treated CK/p25 mice and the increased number in 5 weeks OFF treated CK/p25 mice as described in Fig. 3- 8B, I examined microglia and their proliferative response to p25 over expression. Profound proliferation with an enormous increase in the number of BrdU-incorporating Iba1+ cells could be observed in both 2 and 5 weeks after doxycycline withdrawal in CK/p25 mice. Thus, microglia are activated in this injury model. Similarly to the APPPS1 mice microglia comprised the majority of proliferating cells thereby contributing most to the overall increase in proliferating cells after p25 overexpression (Fig. 3- 11A-C). When investigating the proliferation of NG2+ glia, interestingly, no changes in the proliferation of NG2-positive cells were observed upon p25 induction causing heavy neuronal loss compared to control animals (Fig. 3- 11B,C).
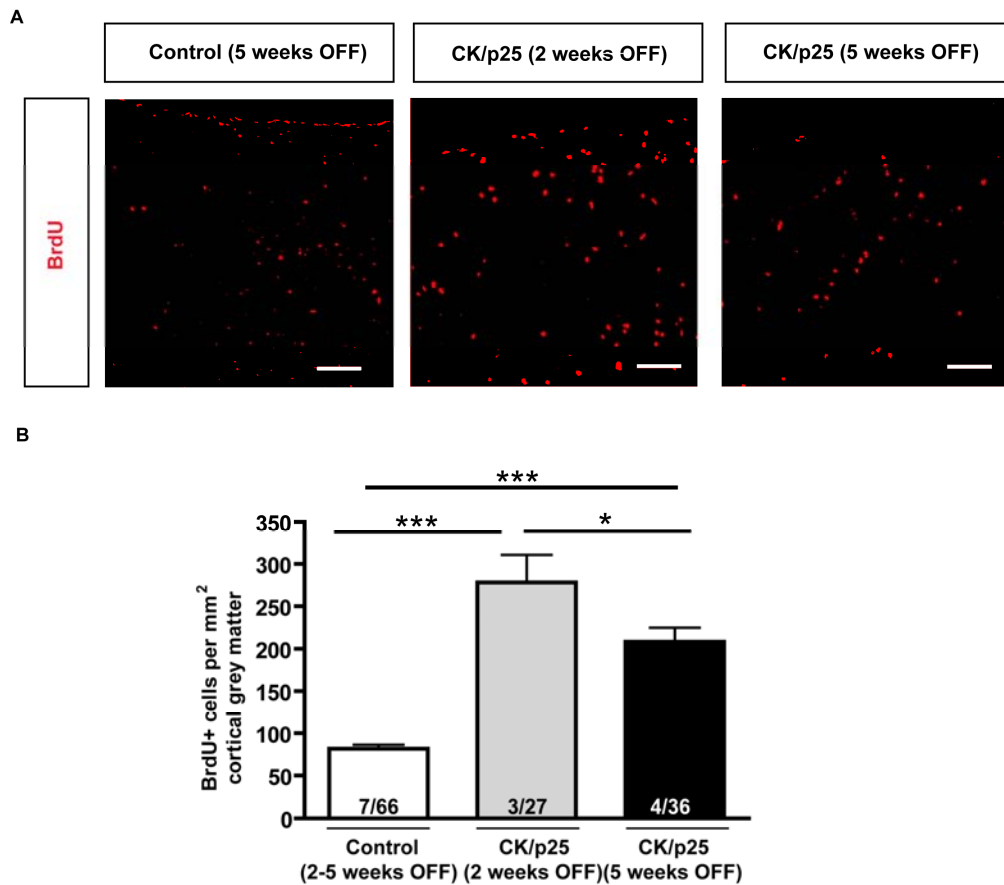
Figure 3- 10. Proliferation in CK/p25 Mice.

(A) shows representative pictures of BrdU-positive cells in the cortical grey matter. The quantification of BrdU+ cells per mm^2 is depicted in (B). Proliferation is significantly increased after 5 weeks of doxycycline withdrawal in CK/p25 mice. The numbers within the columns indicate the number of animals as well as the number of slices quantified (n of animals/n of slices). Data are presented as mean per slices ±SEM. Scale bar: 50μm.
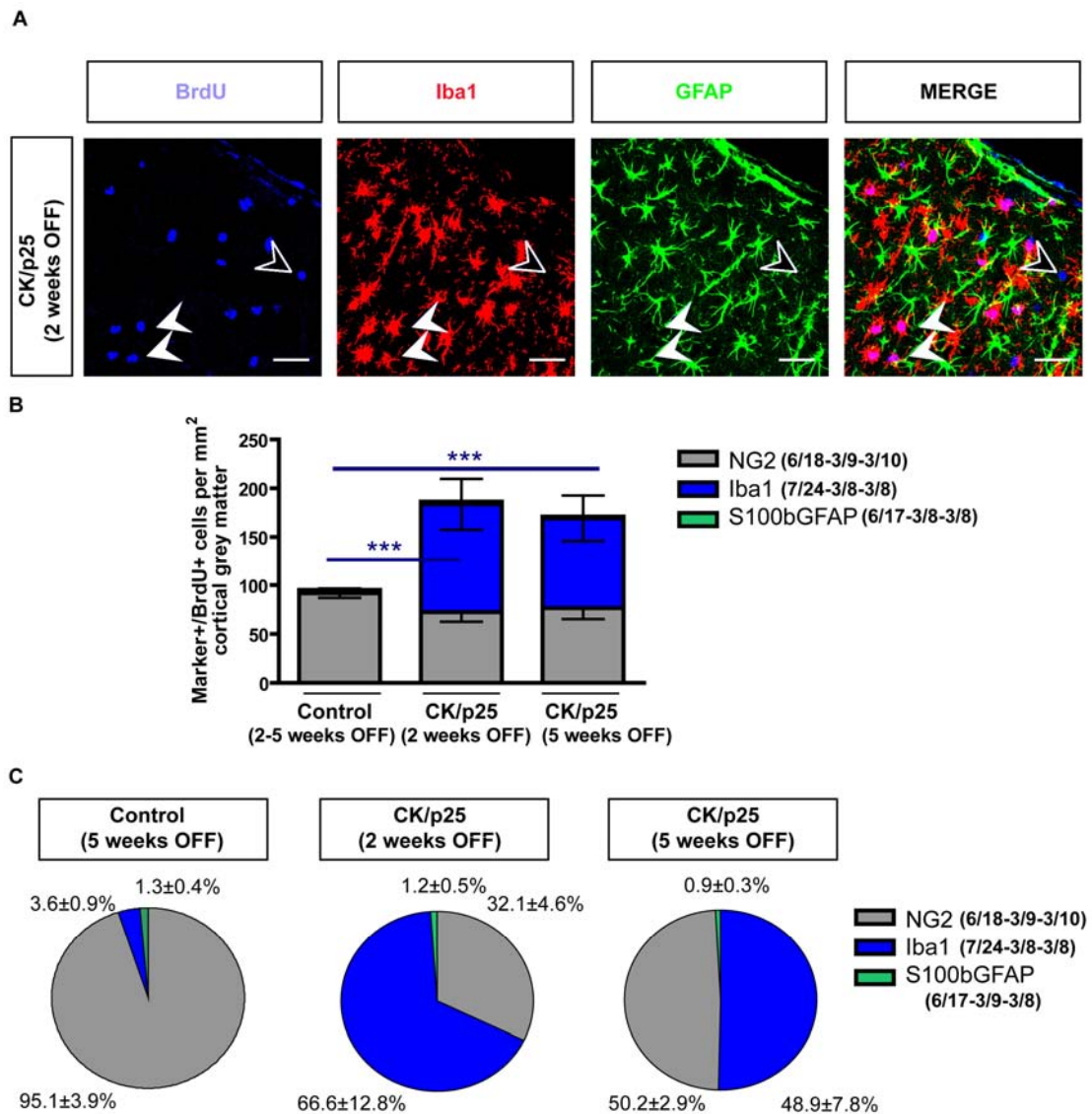
Figure 3- 11. Proliferative Cell Types in CK/p25 Mice.

Representative pictures of (A) BrdU+ Marker-negative cell the prominent overlay of BrdU and Iba1+ microglial cells in 2 weeks OFF treated CK/p25 mice. White arrowheads point toward BrdU+/Iba1+ cells while the dark arrowhead indicates a single potitive cell. (B) shows the total numbers of BrdU/Marker double-positive cells per mm^2 cortical grey matter, while (C) depicts the according percentages of marker+ cells over the total BrdU pool. The numbers behind the markers indicate the number of animals as well as the number of slices quantified (n of animals/n of slices) for controls - CK/p25 2 weeks OFF - CK/p25 5 weeks OFF. Data are presented as mean per slices ±SEM. Scale bar: 20µm.

In conclusion, in contrast to stab wounded and APPPS1 mice, astrocyte proliferation is not significantly increased in CK/p25 mice, which may also account for nearly absent capacity of the lesioned cortical grey matter to form neurospheres *in vitro*.

But what determines the amount of astrocyte proliferation in the different injury paradigms? One explanation is that signalling cascades that trigger astrocyte proliferation may be present in the stab wounded as well as (to a lesser extend) in the APPPS1 mice, which are absent in the CK/p25 mice. One such candidate is expression of the phosphorylated form of the immediate early gene cJun (pcJun), which has been shown to mediate astrocyte proliferation upon demyelination[381].

3.1.11 pcJun and pJNK Expression of Reactive Astrocytes in Different Lesion Paradigms

To investigate if pcJun is expressed by reactive astrocytes in the lesion paradigms that, I co-stained pcJun with GFAP and/or S100b to label reactive as well as non-reactive astrocytes. Quantification of the number of pcJun/S100bGFAP double-positive cells per mm^2 cortical grey matter revealed that their number is tendencially elevated upon stab wound and significantly increased upon neuronal loss (CK/p25) compared to non-lesioned control animals. Upon chronic plaque deposition in the APPPS1 mice, pcJun expression was equally low as control levels (Fig. 3- 12A-H). However, the percentage of pcJun-positive astrocytes in regard to all labelled astrocytes showed that only a small proportion of about 2 % (1.7±0.5 % in stab wounded and 1.8±0.3 % in CK/p25 mice) expresses it (Fig. 3- 12I).

These results were further evaluated by a staining for an upstream regulator. Since the phosphorylated form of the c-Jun N-terminal kinase (pJNK) was previously shown to phosphorylate cJun, an additional staining for pJNK was performed. Interestingly, pJNK was absent in control animals, but it was expressed by reactive GFAP-positive astrocytes upon stab wound or in CK/p25 mice. On the contrary, pJNK expression was concentrated in plaque areas in APPPS1 mice, and only few processes of GFAP+ astrocytes in the vicinity of

plaques were stained (Fig. 3- 13A-D). Therefore, this observation was in line with the expression of pcJun in very few astrocytes in the respective lesion paradigms.
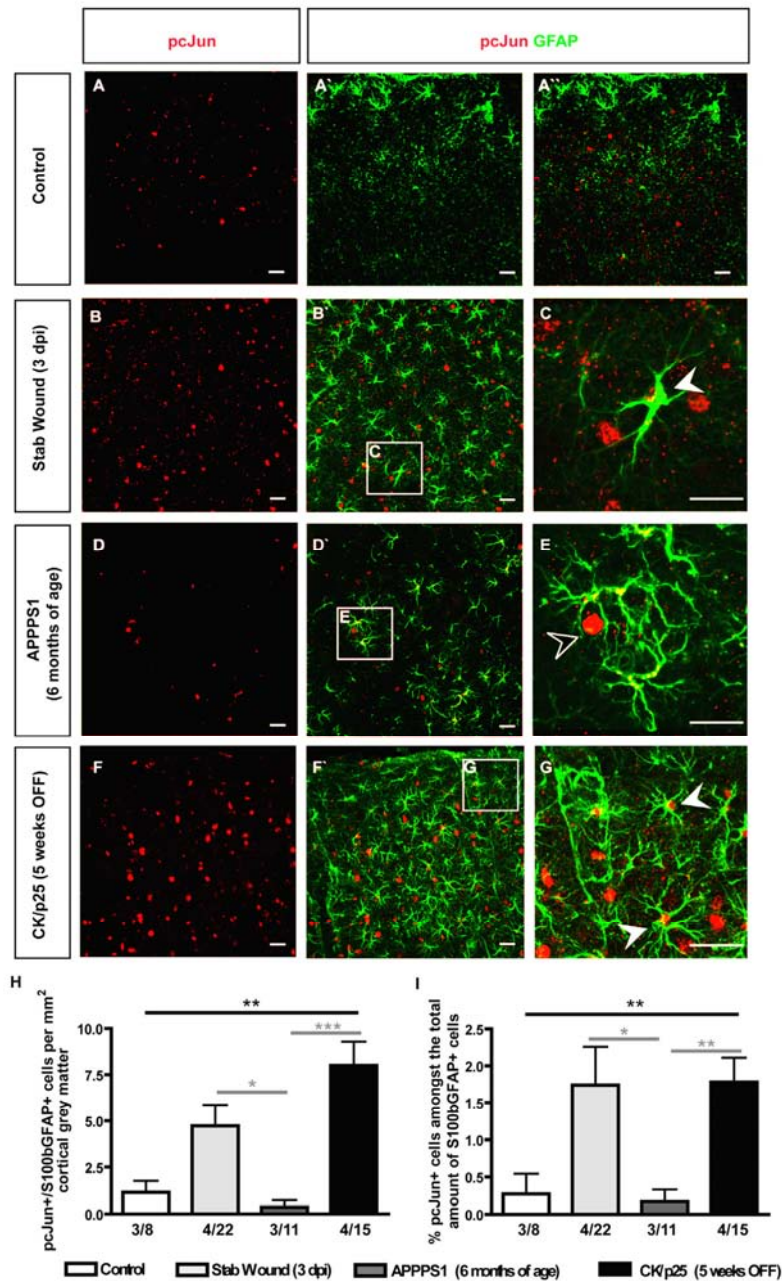
Figure 3- 12. pcJun Expression of Astrocytes in Different Lesion Paradigms.

Representative pictures of pcJun staining and co-staining of pcJun with GFAP-positive astrocytes in control (A), stab wounded (3 dpi) (B,C), APPPS1 at 6 months of age (D,E), and in CK/p25 mice 5 weeks after doxycycline withdrawal (F,G). A magnification of the overlay are shown in (C,E,G), respectively. The full arrowheads highlight double-positive cells, while the

dark arrowhead depict a single-positive cells. (H) reflects the quantification of the total number of pcJun/S100b and/or GFAP double-positive cells per mm^2 cortical grey matter. In (I) the percentage of astrocytes expressing pcJun are presented. The numbers underneath the columns indicate the number of animals as well as the number of slices quantified (n of animals/n of slices). Data are presented as mean per slices ±SEM. Scale bar: 20µm.
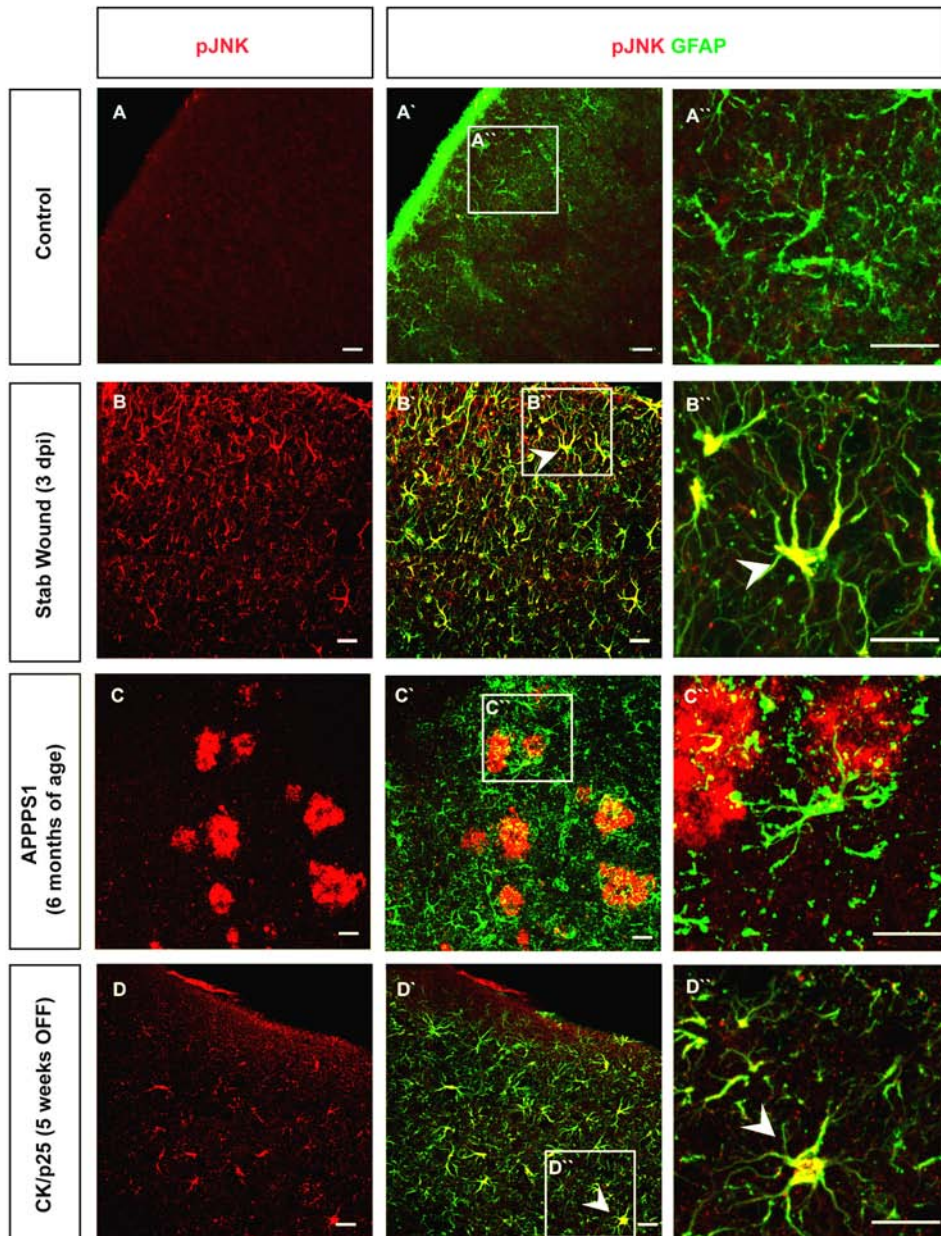
Figure 3- 13. Expression of pJNK in Different Lesion Paradigms.

Representative pictures of pJNK staining and co-staining of pJNK with GFAP-positive astrocytes in control (A), stab wounded (3 dpi) (B), APPPS1 at 6 months of age (C), and in CK/p25 mice 5 weeks after doxycycline withdrawal (D). Magnifications of the inlays (A`,B`,C`,D`) are shown in (A``,B``,C``,D``), respectively. Scale bar: 20µm.

3.1.12 Expression of Olig2 in Astrocytes in Different Lesion Paradigms

The transcription factor Olig2 is a further interesting candidate in regard to proliferation of astrocytes. Olig2 is expressed largely in the oligodendrocyte lineage, but also a subset of astrocytes expresses it[105,116,121]. After stab wound injury, astrocytes are known to up-regulate Olig2. Notably, when Olig2 expression was deleted after injury, astrocyte proliferation was reduced[116,382,383].

Double staining for Olig2 and S100b and/or GFAP, to label reactive and non-reactive astrocytes (Fig. 3- 14A-H) showed that the number of Olig2/S100bGFAP double-positive cells per mm^2 cortical grey matter was significantly increased 3 days after stab wound lesion as well as in 6 months old APPPS1 mice and CK/p25 mice in comparison to 6 months old control animals (Fig. 3- 14I). However, the number of double-positive upon stab wound injury (24.4±3 per mm^2) was increased compared to the other lesion paradigms tested. Moreover, the total number of double-positive cells per mm^2 was tendencially increased in APPPS1 mice (19.3±2.6 per mm^2) compared to CK/p25 mice (13.9±2.7 per mm^2). Investigation of the percentage of astrocytes expressing Olig2 in regard to all labelled astrocytes revealed that about 8.9±1 % in stab wounded expressed this transcription factor, being significantly more compared to controls (4.1±0.8 %) and CK/p25 mice (4.3±1 %) (Fig. 3- 14J). APPPS1 mice with 6.5±0.9 % of all astrocytes expressing Olig2 showed still an elevation compared to controls. This showed that Olig2 expression is decreased in CK/p25 mice compared to stab wound injury and APPPS1.

Therefore, it appears that different signalling cascades are present in the different AD-related mouse models, while in stab wounded animals both signalling candidates were present at an elevated level.
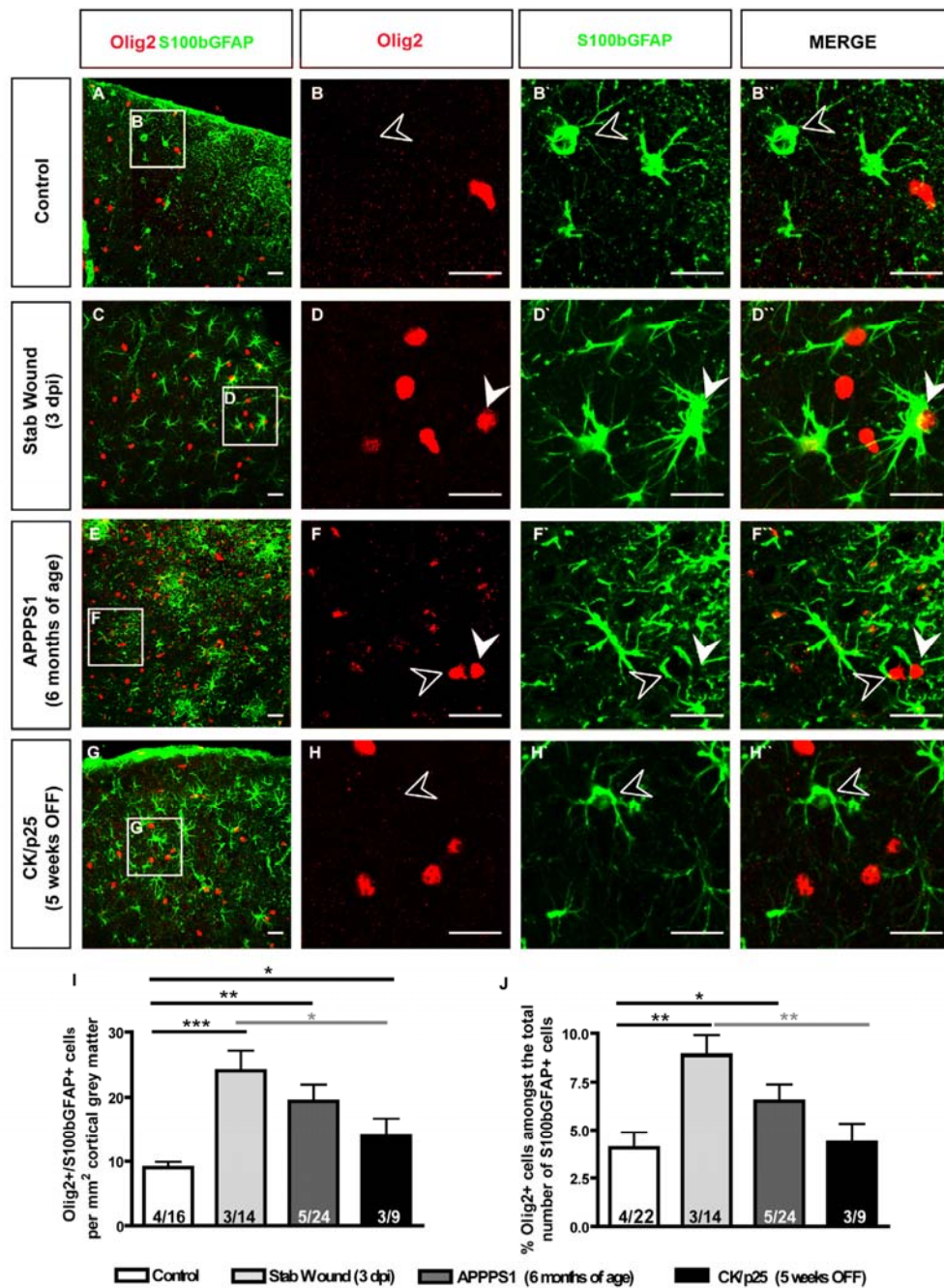
Figure 3- 14. Expression of Olig2 in Astrocytes after Different Lesion Paradigms.

Representative pictures of co-staining of Olig2 with S100b/GFAP-positive astrocytes in control (A,B), stab wounded (3 dpi) (C,D), APPPS1 at 6 months of age (E,F), and in CK/p25 mice 5 weeks after doxycycline withdrawal (G,H). Magnifications of the inlays in (A,C,E,G) are shown in (B,D,F,H), respectively. The filled arrowheads highlight double-positive cells, whereas the dark arrowheads point toward single-positive astrocytes. (I) reflects the quantification of the total number of Olig2/S100b GFAP double-positive cells per mm^2 cortical grey matter. The numbers within the columns indicate the number of animals as well as the number of slices quantified (n of animals/n of slices). Data are presented as mean per slices ±SEM. Scale bar: 20μm.

3.1.13 Increased Expression of Cyclin D1 in Astrocytes in Different Lesion Paradigms

Since astrocytes in APPPS1 and CK/p25 mice did not resume proliferation but up-regulated distinct signalling cascades involved in it, I aimed to understand if astrocytes in AD-related mouse models become activated sufficiently strong to re-enter at least early stages of the cell cycle. Astrocytes in the healy brain mostly are in the Gap 0 (Go) phase, which is a resting phase where cells stopped dividing. In accordance with that few astrocytes proliferate in the non-lesioned healthy grey matter[103,116]. After e.g. initial proliferative triggers, cells may re-enter the cell cycle by progressing into the gap 1 (G1) phase, in which they usually grow in size and prepare for DNA synthesis. One protein typically expressed at the end of the G1 phase is Cyclin D1, which is also involved in cell cycle progression into the DNA synthesis (S)-phase[384]. Notably, BrdU, which was used as a marker for proliferation in the previous experiments, incorporates into the DNA in S-phase[385]. After successful DNA replication, cells pass through another gap phase (Gap 2; G2) followed by the mitosis[386].

Therefore, I analyzed the expression of the protein cyclin D1 in astrocytes to understand if astrocytes may become activated enough to re-enter cell cycle. Quantification of the number of cyclin D1/S100b and/or GFAP double-positive cells showed a significant elevation in all lesion paradigms tested (Fig. 3- 15A-I). Interestingly, about 32.6 ± 2.9 % of all astrocytes expressed cyclin D1 upon stab wound injury, whereas in APPPS1 (16.3 ± 1.8 %) and CK/p25 mice (12.8 ± 1.8 %) their percentage was significantly less. Interestingly, however the percentage of cyclin D1-positive astrocytes was still elevated in the AD-related mouse models compared to control levels (5.1 ± 0.9 %; summarized in Fig. 3- 15I).

This showed that upon chronic plaque deposition and neuronal loss the number of astrocytes re-entering cell cycle increases, however most of these cells fail to perform S-phase. For example in APPPS1 mice 16.3 % of the astrocytes expressed cyclin D1 while only 2.5 % actually incoporated BrdU. On the contrary, upon stab wound injury 32.6 % of the astrocytes expressed cyclin D1 3 days after lesion and about 50 % of the astrocytes re-entered cell

cycle until 7 days after injury[103], which implicates that most of the cyclin D1+ astrocytes actually perform S-phase in this lesion paradigm.

Therefore, other factors may contribute to the different amounts of astrocyte proliferation observed upon stab wound, in APPPS1 and in CK/p25 mice. One such difference may be different ongoing inflammatory processes.
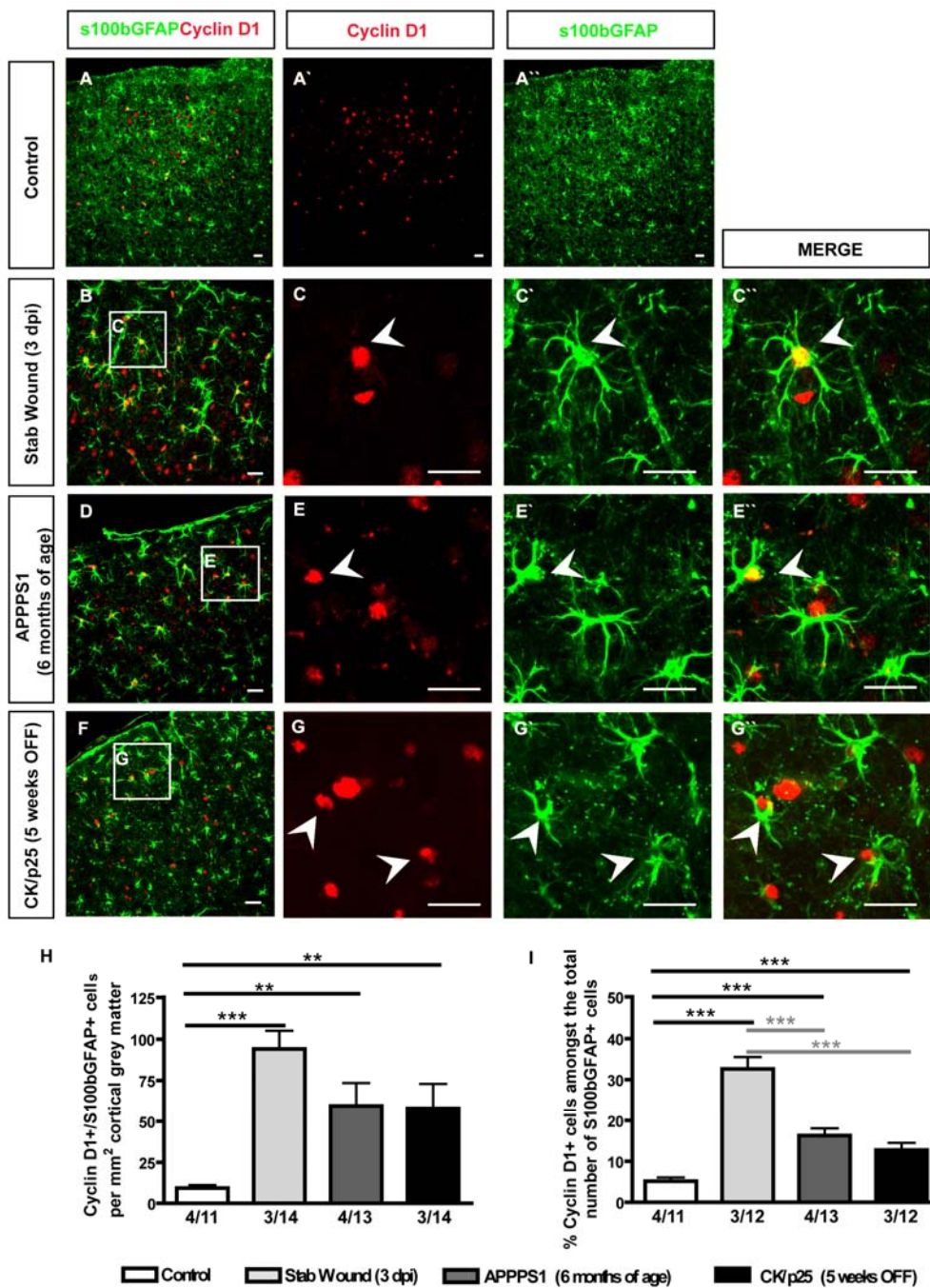
Figure 3- 15. Cyclin D1 Expression of Astrocytes in Different Lesion Paradigms,

Representative pictures of co-staining of cyclin D1 with S100b/GFAP-positive astrocytes in control (A), stab wounded (3 dpi) (B,C), APPPS1 at 6 months of age (D,E), and in CK/p25 mice 5 weeks after doxycycline withdrawal (F,G). Magnifications of the inlay in (B,D,F) are shown in (C,E,G), respectively. The white arrowheads highlight double-positive cells, while dark arrowheads point toward single-positive cells. (H) shows the quantification of the total number of cyclin D1/S100b and/or GFAP double-positive cells per mm^2 cortical grey matter. In (I) the percentage of astrocytes expressing cyclin D1 are presented. The numbers underneath the columns indicate the number of animals as well as the number of slices quantified (n of animals/n of slices). Data are presented as mean per slices ±SEM. Scale bar: 20µm.

3.1.14 Invasion of Blood-derived Cells in APPPS1 and CK/p25 Mice

Since upon stab wound injury, blood-derived immune cells participate in the inflammatory process, I investigated if such cells would invade the brain upon AD-related chronic plaque deposition or neuronal loss in CK/p25 mice. To examine this, I stained brain sections with CD45, which is a protein expressed at highest levels by blood-derived cells. However, as CD45 is also expressed by resident microglia and increases in expression in activated resident microglia, I co-stained CD45 with Iba1, expressed in non-activated and activated microglia. To ensure localization outside blood vessels, I took advantage of the β-dystroglycan antibody, which outlines blood vessels.

In control animals, high CD45-immunostaining was nearly absent with the exception of CD45-positive cells located within blood vessels (Fig. 3- 16A,B). In APPPS1 mice, resident Iba1-positive microglia up-regulated CD45 expression. In addition, Iba1-negative CD45-positive immune cells invaded the brain, since they localized away from blood vessels (Fig. 3- 16C,D). Similarly, in CK/p25 mice invading immune cells away from blood vessels were also present (Fig. 3- 16E,F). This indicates that, as observed in stab wound lesion, also in the AD-related mouse model blood-derived cells have the ability to enter the brain parenchyma. One reason for the presence of these cells within the brain parenchyma could be an opening of the blood brain barrier.
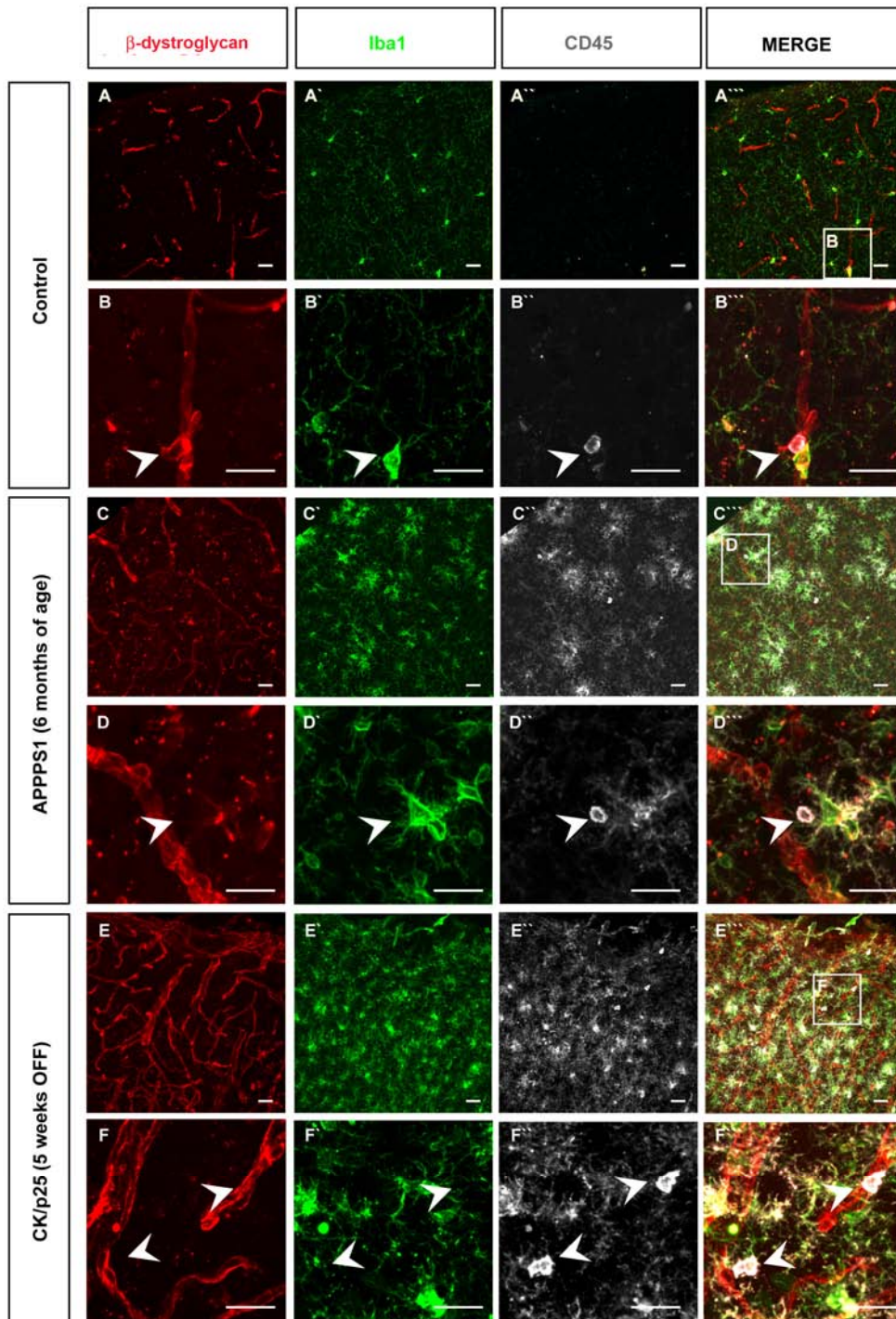
Figure 3- 16. CD45-positive Cells in the Cortical Grey Matter of APPPS1 and CK/p25 Mice.

Representative pictures of a triple-staining of β-dystroglycan for blood vessels, with Iba1 for microglia and CD45 for invading blood-derived immune cells. Lower magnifications of control in (A), APPPS1 in (C) and CK/p25 in (E). In (B) is the magnification for the inlay for control and in (D,E) for APPPS1 and CK/p25 mice, respectively. The arrowheads highlight single CD45-positive cells. Scale bar: 20μm.

3.1.15 Unchanged Blood Brain Barrier Integrity in APPPS1 and CK/p25 Mice

To test for the blood brain barrier integrity of APPPS1 and CK/p25 mice, I first performed a stab wound as a positive control in one hemisphere of these mice, as it is known that the blood brain barrier is ruptured in this lesion paradigm. Afterwards, a fluorescent coupled dextran of 3000 dalton (Da) was injected into the tail vein. As expected, stab wound lesion resulted in a spread of the fluorescent dye into the brain parenchyma in the AD-related mouse models. However, on the contralateral, non-lesioned side, the blood brain barrier integrity remained intact in APPPS1 and CK/p25 mice for molecules of a size of 3000 Da (Fig. 3- 17).

These data indicate a dramatic difference between acute stab wound (as well as MCAO) and the AD-related mouse models investigated. They further open the possibility that factors released from the blood may represent an essential trigger for astrocytes to proliferate and/or form neurospheres.

In addition to the differences observed in the astrocyte proliferation and neurosphere formation in different lesion paradigms, also differences in the reaction of NG2+ glia could be detected. These cells specifically reacted toward amyloid plaque deposition, whereas their reactivity was absent in CK/p25 mice. To understand the reaction of oligodendroglial cells over time upon chronic amyloid plaque deposition, I analyzed the APPPS1 mouse line in more detail[324]. These mice reflect certain clinical aspects of Alzheimer's disease (AD) like a progressive amyloid plaque deposition already present at 3 months of age in the cortical grey matter. However, tangle pathology and overt neuronal loss are absent in this mouse model, contrary to the human pathology[324,329]. As it has been pointed out before, human AD is normally accompanied with myelin diminutions [367,369,387,388] and focal demyelination[389]. Moreover, also white matter lesions are often associated with AD[390,391]. In the healthy brain, myelin insulates axons allowing the propagation of action potentials at high velocity. Disruption of the myelin sheaths upon AD, may therefore also contribute to cognitive impairment, since action potential conductance may become slower or completely disturbed.
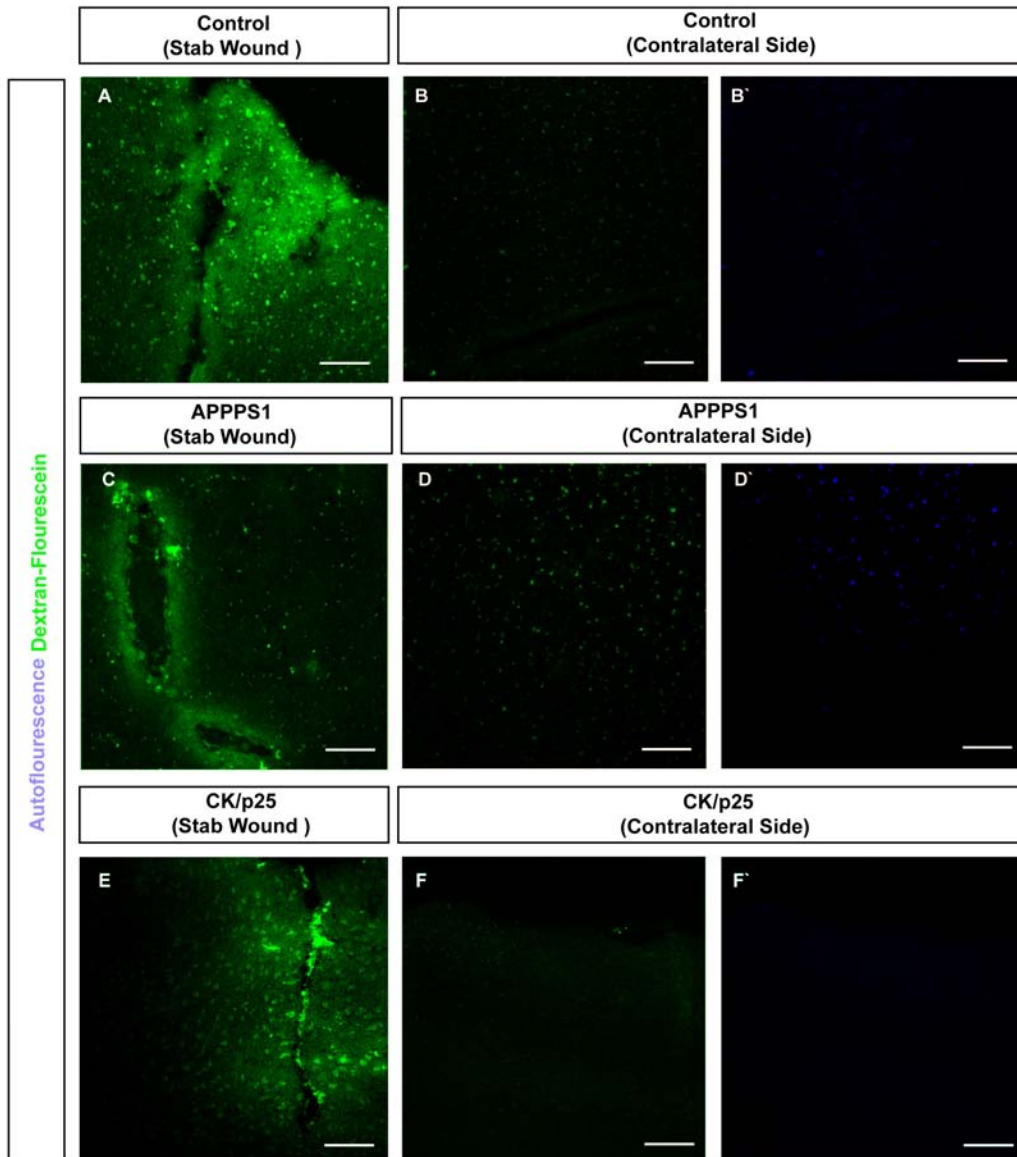
Figure 3- 17. Blood Brain Barrier Integrity in AD-related Mouse Models.

Depicted are the positive stab wound control of stab wounded control, APPPS1 and CK/p25 mice. The contralateral side was evaluated for the integrity of the blood brain barrier. Scale bar: 50 µm.

3.2   Reactivity of Oligodendrocyte Progenitors upon Chronic Amyloid Plaque Deposition

3.2.1   Focal Loss of Myelin in Plaque Core Areas

First, I carefully investigated to which extend these myelin diminutions and/or aberrations can be reproduced in APPPS1 mice resembling plaque deposition as the only feature of the human AD pathology. To analyze changes in the myelin in the aged APPPS1 mice, I stained brain sections of transgenic and control littermates at different ages (3, 6, 9 and 11 months) for the myelin associated glycoprotein (MAG), while plaques were labelled with the 6E10 antibody that detects both, human Aβ and the human APP. Additionally, I performed a Gallyas silver impregnation to label myelin in a quantitative and antigen independent manner. Interestingly, I observed focal demyelination in the plaque core areas of the cerebral grey as well as white matter with both staining techniques. This result is similar to the observations in humans or other mouse models of plaque deposition[389], and it shows that plaques alone are sufficient to induce demyelination, while neuronal loss and tangle pathology, as occurring in human pathology, is not necessary (Fig. 3- 18).
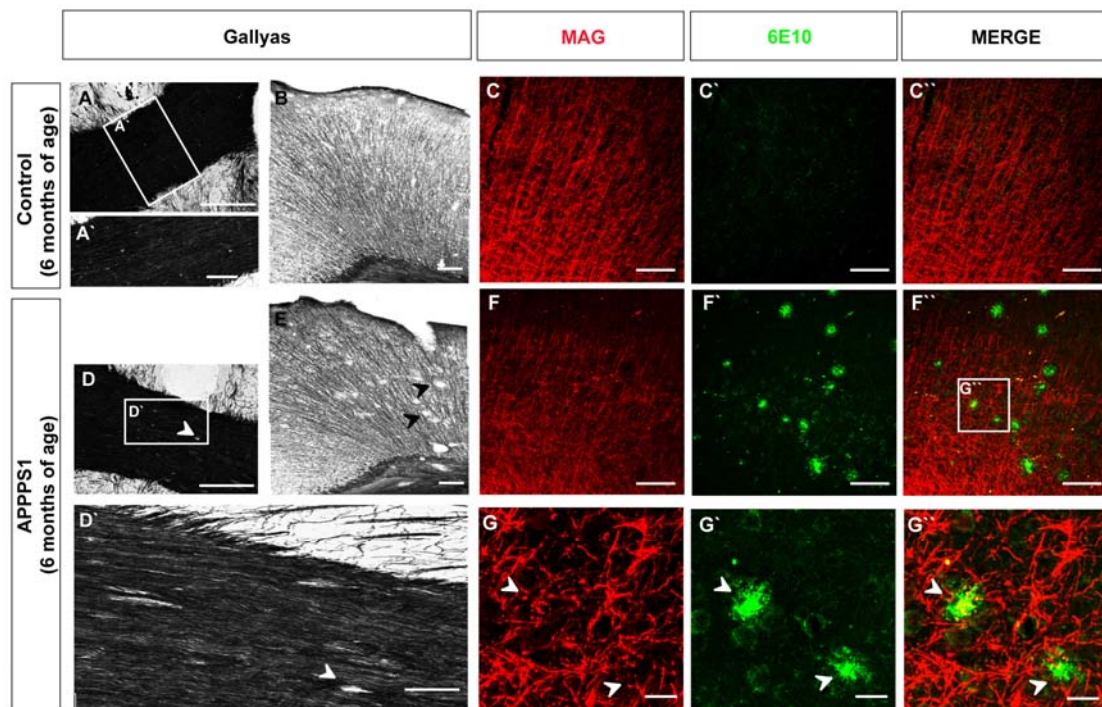
Figure 3- 18. Myelin in the Cortical Grey and White Matter.

Overview of the myelin by the Gallyas impregnation for myelin in the white and grey matter at 6 months of age in control and APPPS1 mice. The arrowheads indicate plaque core areas being devoid of myelin. Immunostainings of the cortical grey matter for MAG and 6E10 at the same age. The inlay depicts a magnification of a plaque core area devoid of MAG staining. Scale bar: 200 μm (in A, D) 100 μm (in A`, C, F) 50 μm (B, D`, E) and 20 μm in (G).

3.2.2 Analysis of Myelin Protein Amounts

To analyze the amount of myelin, I performed a western blot analysis on the cerebral cortex of control and APPPS1 mice with an antibody directed against the 2', 3'-cyclic nucleotide 3'-phosphodiesterase (CNPase), which was already shown to be expressed at reduced levels in human AD patients[388]. Notably, apart from the localization in the non-compact myelin, the CNPase protein is also expressed in mature oligodendrocytes. To have a precise readout, I examined the ratio between CNPase and NF70 protein to evaluate the amount of CNPase present per axons (Fig. 3- 19A). Interestingly, a significant decrease in the ratio could be detected in 6 months old APPPS1 mice compared to age matched controls (Fig. 3- 19B). As neuronal

loss can be excluded[329] the data indicate a decreased amount of CNPase present per axon in 6 months old APPPS1 mice. Surprisingly, at 9 months of age, controls and APPPS1 mice display equal CNPase/NF70 ratios (Fig. 3-19B). This result is suggestive of myelin repair mechanisms taking place between 6 and 9 months of age in APPPS1 mice. However, as this analysis only examined the total amount of myelin but not its integrity, I proceeded to perform electron microscopic analysis.
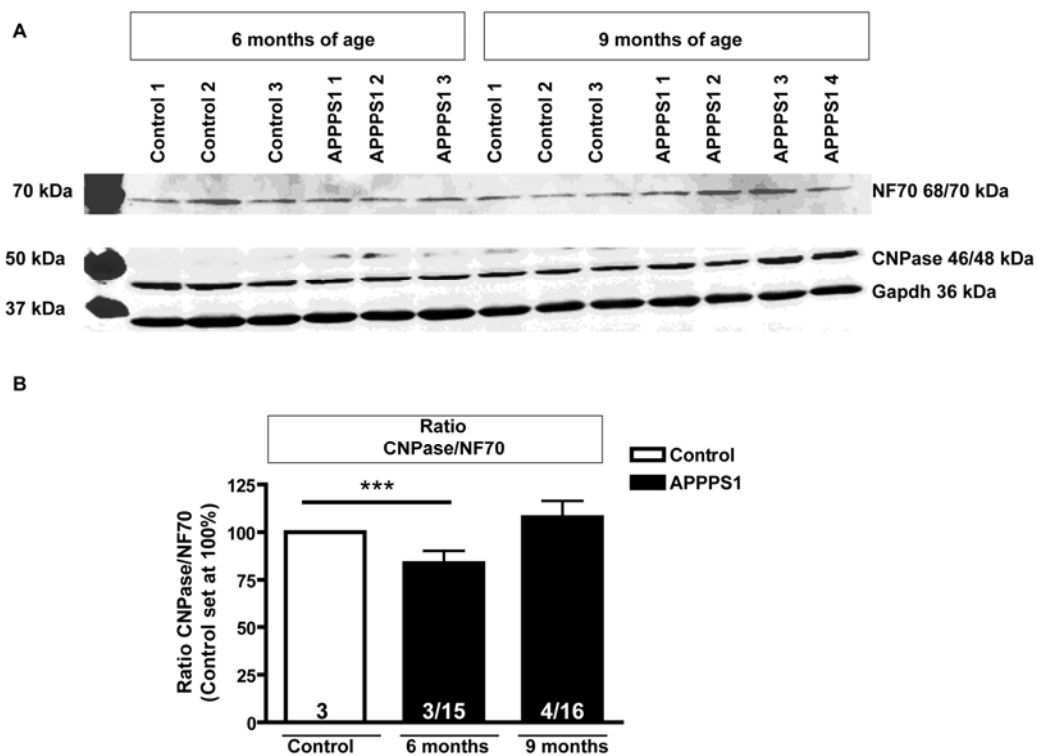
Figure 3- 19. Western Blot Analysis of CNPase and NF70 in the Cerebral Cortex.

To examine total protein amounts of NF70 and CNPase, western blot analysis was performed on cerebral grey and white matter of APPPS1 mice at different ages compared to age-matched controls. (A) is a representative picture taken from one western blot. As it is originally two-colored the single channels were adjusted first and then the colored blot was converted into greyscale picture. (B) is the ratio between the total pixels of CNPase divided through NF70, which shows a significant decrease specifically in 6 months old APPPS1 mice compared to age-matched controls. The numbers within the columns indicate the number of animals as well as the number of datapoints quantified (n of animals/n of datapoints). Data are presented as mean of all data points ±SEM for a minimum of 2 independent western blots.

3.2.3 Increase in Myelin Aberrations in APPPS1 Mice

To analyze the myelin integrity, I performed electron microscopy of the corti-cal grey (GM; Fig. 3- 20B-F; Fig. 3- 20A wild type control) and white matter (WM; Fig. 3- 20H-L; Fig. 3- 20G wild type control) of APPPS1 mice at differ-ent ages. Myelin aberrations were classified according to[392,393]:

a) An axon surrounded by two myelin sheaths, separated by a space (Fig. 3-20D, J),

b) Excess cytoplasm in the inner loop (Fig. 3- 20K),

c) Degenerated sheaths (Fig. 3- 20E),

d) Balooned myelin (Fig. 3- 20F,L)

e) Abnormal myelin outfoldings (Fig. 3- 20C,J) – these are areas of the internode where the myelin sheath protruded away from the axon surface or

f) Other myelin abnormalities (Fig. 3- 20B,H).

Interestingly, the compaction of the aberrant myelin looks normal without ob-vious irregularities (inlay Fig. 3- 20H). Myelin aberrations could be detected in APPPS1 mice in both cortical GM and WM, however the quantitative analysis was focused on the WM, since the GM has a much lower number of myeli-nating axons. The percentage of defects was counted per number of axons. At 6 months of age, APPPS1 mice revealed a significantly higher proportion of dysmyelinated axons compared to control littermates (Fig. 3- 20M). In con-trast, in 9 months old animals no significant difference in myelin aberrations was detectable indicating no further increase in myelin aberrations with age and plaque deposition in the APPPS1 mice. Most strikingly, these data fur-ther indicate a potential repair, regarding also the aberrations, taking place between 6 and 9 months of age in APPPS1 mice. Along with myelin aberra-tions in APPPS1 mice, also activated microglia that phagocytized myelin-like structures in the cortical grey and white matter were present (Fig. 3- 20N). Apart from differences between transgenic and control animals, interestingly, a significantly elevated number of myelin aberrations was observed in 9 months old control animals compared to control mice of 6 months of age (Fig. 3- 20N). This age-related increase in myelin aberrations has also been ob-served in rhesus monkeys[394] and was absent in APPPS1 mice, which had

reached the maximum of myelin aberrations already in 6 months of age. In summary, APPPS1 mice exhibited an increase in the disruption of myelin integrity at 6 months of age and then remained on a similar level, unlike in control mice, which showed no signs for a further increase in myelin aberrations until 6 months of age.

To exclude a developmental effect on myelin integrity in APPPS1 mice, where the mutations in APP and PS1 are overexpressed from late embryonic stages to early postnatal stages on. I also analyzed myelin formation and integrity in 20 days old animals (postnatal day 20, P20). This is the peak of myelination in the mouse. Neither the Gallyas silver impregnation that specifically stains myelin nor immunostaining with MAG revealed any obvious differences between control and APPPS1 mice (data not shown). Accordingly, also analysis of myelin integrity in the white matter at the ultrastructural level further confirmed no differences in myelin aberrations between control and APPPS1 mice at this age. The number of myelin aberrations was higher than at later stages. This is likely a result of the developmental myelination process since at p14 numerous myelin sheaths with a loosely built structure were shown to be present[395]. Even though the number of myelin sheaths increases continuously thereafter, at P28 (and as well at p21), the presence of both thick, compact and thin, loosely structured myelin sheaths, which were included in this quantification, are still present and suggestive for a still ongoing myelination[395]. Therefore, the myelin aberrations observed in 6 months old animals were not due to a developmental failure of myelination (Fig. 3-20M).

To investigate if early plaque deposition is sufficient to induce the myelin aberrations, I additionally analyzed animals at 3 months of age. Only few myelin aberrations were present at this time point (Fig. 3- 20M) in both, control and APPPS1 mice, indicating that the myelin aberrations are a rather late effect that appears secondary to the plaque formation.
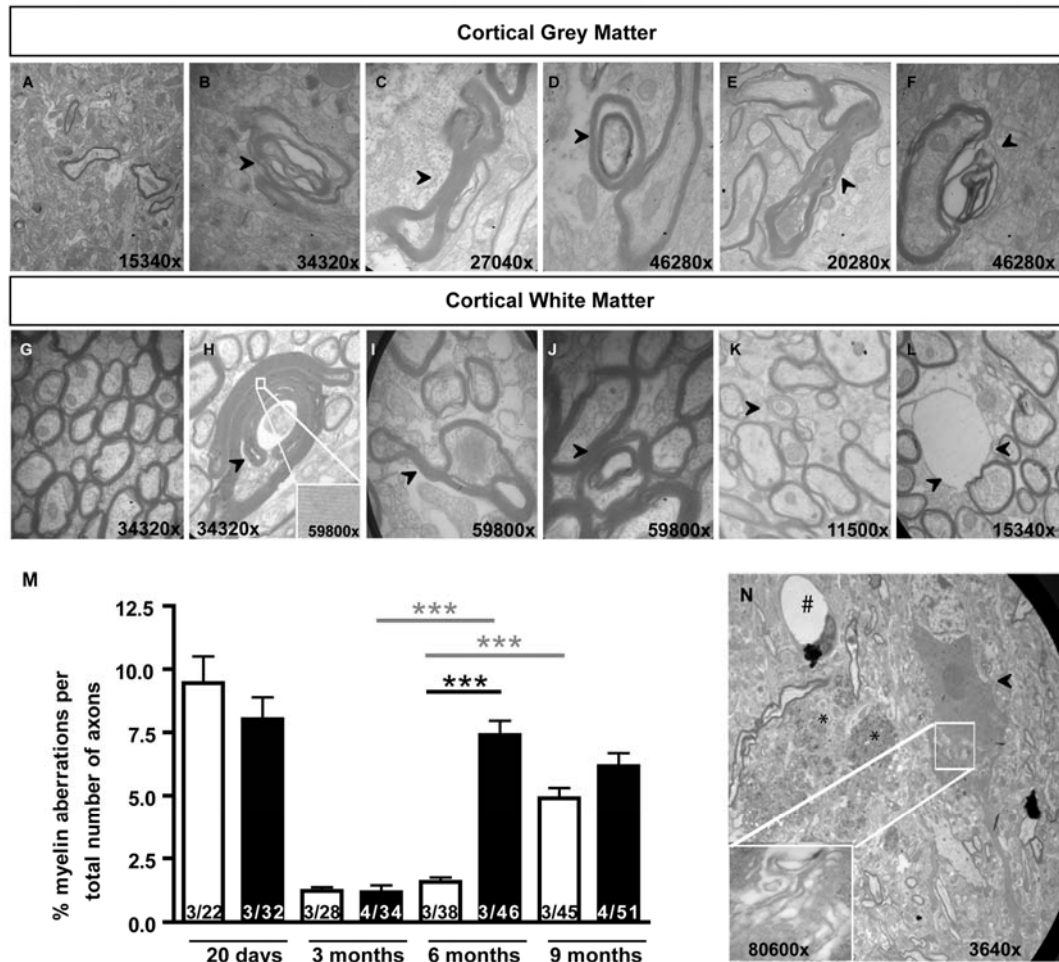
Figure 3- 20. Analysis of the Myelin Integrity in the Cortical Grey and White Matter.

(A) depicts a field of view of the cortical grey matter in control mice. (G) represents the cortical white matter of control animals. This transverse section contains closely packed myelinated nerve fibers with a range of sizes. Grey matter and white matter aberrations observed in APPPS1 mice are depicted in (B-F and G-L). Among them are such aberrations as an axon surrounded by two myelin sheaths, separated by a space (9D,J), balooned myelin (F,L) degenerated sheaths (E), excess cytoplasm in the inner loop (K) and abnormal myelin outfoldings (C,I) or other myelin abnormalities (B,H). The insert in (H) shows the normal myelin compaction. The quantification of myelin defects per axons is shown in (M) with a significant increase of myelin aberrations at 6 months of age in APPPS1 mice and in 9 months old control mice. (N) is an example of a microglia located in the grey matter phagocytozing myelin sheath-like structures. The according magnifications are indicated within the pictures. Arrowheads point toward aberrations while (#) indicates a blood vessel and (*) dystrophic neurites. (M). The numbers within the columns indicate the number of animals as well as the number of pictures quantified (n of animals/n of pictures). Data are presented as mean per pictures ±SEM.

3.2.4 Transient Increase in the Number of Olig2-positive Cells

At the age of 6 months, myelin integrity but not myelin amounts were significantly disturbed in APPPS1 mice. At this stage, plaques are spread all over the cortical grey matter (Fig. 3- 1A). Given the increase in the quantification of myelin aberrations specifically at 6 months of age, I aimed to study the effect on the cells of the oligodendrocyte lineage, because new remyelinating oligodendrocytes can be generated from oligodendrocyte progenitors (OPCs)[170,237]. As Olig2 is expressed throughout the oligodendrocyte lineage[115,396,397], it represents a valuable marker to test if cells of the oligodendrocyte lineage are reacting towards chronic plaque deposition. Furthermore, the number of Olig2-positive cells has been shown to increase in different lesion paradigms including APPPS1 mice[116]. Therefore, I quantified the number of Olig2-positive cells present in the cortical GM at different ages, namely 3, 6 and 11 months of age. No change in the number of Olig2+ cells was observed between control and APPPS1 mice at 3 months of age (Fig. 3- 21B). With increasing age and plaque deposition, at 6 months of age, the number of Olig2 positive cells was significantly increased in APPPS1 mice (Fig. 3- 21A,B). At 11 months of age the number of Olig2+ cells was still increased in APPPS1 mice compared to controls, however this was not significantly different anymore. This result was mostly due to an increase in Olig2+ cells in control animals. Interestingly, the increase in the number of Olig2-expressing cells may be correlated with an increase in myelin aberrations present in controls at 9 months of age, which may indicate some ongoing myelin repair mechanisms also in healthy aging mice. In addition, it can be concluded that the onset of amyloid plaque deposition precedes the increase of Olig2+ cell number with a transient elevation at 6 months of age in APPPS1 mice.

Since Olig2 is expressed in a variety of cell types and this composition can vary enormously between different lesion types[116], I assessed which cell types were responsible for the increase in number of Olig2+ cells in the grey matter of 6 months old APPPS1 mice. I costained Olig2 with antibodies directed against the chondroitin sulfate proteoglycan NG2 (NG2) to label OPCs, with glutathione S-transferase pi (GSTpi) for mature oligodendrocytes

and the calcium binding protein S100 b and/or the GFAP (S100bGFAP) to label astrocytes.

The number of S100bGFAP+/Olig2+ cells were about 20 cells per mm^2 and a significant increase was detectable between controls and APPPS1 mice, however they constituted only about 6 % of the total Olig2+ cells (Fig. 3- 14). Amongst the remaining cells there was an increase in the NG2/Olig2 double-positive cell population while the GSTpi/Olig2 double positive population was tendencially increased (Fig. 3- 21C).
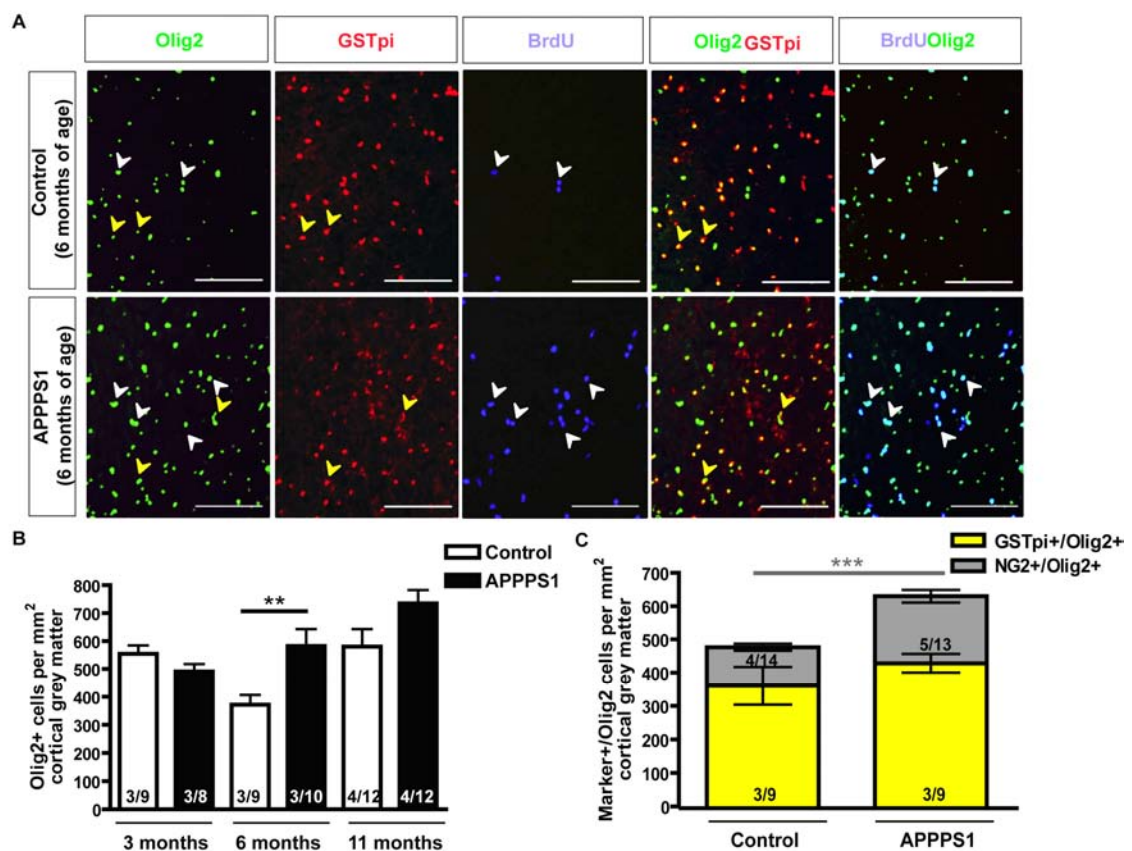
Figure 3- 21. Olig2+ Cells in the Cortical Grey Matter.

Staining for BrdU, GSTpi and Olig2 is depicted in (A) for control and APPPS1 mice at the age of 6 months. In (B) the number of Olig2-positive cells was quantified at different time points showing a transient increase of APPPS1 mice at 6 months of age. The histogram in (C) shows the composition of the Olig2+ cells at the age of 6 months. The numbers within the columns indicate the number of animals as well as the number of data points quantified (n of animals/n of slices). Data are presented as mean per slices ±SEM. Scale bar: 100 µm.

3.2.5 Proliferation Analysis of Olig2- positive Cells

The transient increase of Olig2+ cells in the cortical grey matter of 6 months old APPPS1 mice could be a result of an increase in the proliferation of these cells. To test this hypothesis, the animals received BrdU in the drinking water for 2 weeks. With this protocol all dividing cells including slow and fast proliferating cells as well as cells that have divided and became post mitotic within this labelling time period are detectable. I determined the number of Olig2/BrdU double-positive cells per mm^2 at different ages (3, 6 and 11 months), to see possible changes in proliferation upon chronic amyloidosis. At 3 months of age, the number of proliferating Olig2+ cells was comparable between control and APPPS1 mice (Fig. 3- 22). In contrast, a significant increase in the number of Olig2+/BrdU+ cells was observed in the cortical grey matter of APPPS1 mice at 6 as well as at 11 months of age compared to age matched controls (Fig. 3- 21A,Fig. 3- 22). Thus, the increase in the number of Olig2/BrdU double-positive cells per mm^2 is indeed the result of, at least in part, enhanced proliferation of these cells in APPPS1 mice.

The proliferative oligodendroglial reaction was delayed compared to plaque deposition and coincided with the increase in myelin aberrations. Most interestingly, the number of proliferating Olig2+ cells was still increased in APPPS1 mice at 11 months of age compared to control mice. As the number of myelin aberrations, detected with electron microscopy, did not further increase between 6 and 9 months old APPPS1 mice the proliferating Olig2+ cells may serve to generate an increased number of oligodendrocytes for repair. Conversly in controls, the number of BrdU/Olig2 double-positive cells decreased with age (between 3 and 9 months) which correlated to a significant increase in myelin aberrations in controls. These data indicate that with age myelin aberrations develop possibly due to a lack of new oligodendrocytes, which may hint to a decreased myelin repair capacity in normal ageing.
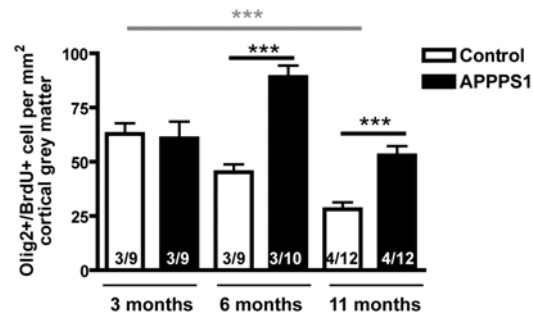
Figure 3- 22. Proliferation of Olig2+ Cells per mm^2.

Proliferation of Olig2-positive cells was investigated by the number of cells that incorporated BrdU, when BrdU was given into the drinking water for 2 weeks. Quantification of BrdU/Olig2 double-positive cells per mm^2 shows an elevation in APPPS1 mice at 6 and 11 months of age. The numbers within the columns indicate the number of animals as well as the number of slices quantified (n of animals/n of slices). Data are presented as mean per slices ±SEM.

Despite the significant increase in the number of Olig2/BrdU double-positive cells per mm^2 at 6 and 11 months of age in APPPS1 mice, I noted a simultaneously decreased percentage in proliferating Olig2+ cells amongst the total BrdU-incoorporating cells in APPPS1 mice (Fig. 3- 23A). In the healthy adult cortical grey matter mostly Olig2+ cells proliferated, which is in line with previous observations[103,105]. However, upon chronic amyloid plaque deposition other cell types, which normally did not divide, started to proliferate. This effect was already apparent at 3 months of age, when plaque deposition has just started.

Along this line, also age seemed to initiate proliferation of non-Olig2+ cells, since the percentage of Olig2-positive cells over the BrdU population decreased with age. Control as well as APPPS1 mice exhibited a significantly lower percentage of Olig2+ cells over the total BrdU population between 6 and 11 months of age (Fig. 3- 23A).

Even though Olig2+ cells mostly constituted to the proliferating cell population in control mice, these cells represented only a subpopulation of about 10-20 % of all Olig2+ cells. Also in APPPS1 mice only a subpopulation of Olig2+ cells resumed proliferation (Fig. 3- 23B). Therefore, I focused further on this dividing subpopulation of the Olig2+ cells of the oligodendrocyte lineage, which co-localizes with the chondroitin sulfate proteoglycan NG2[103,105].
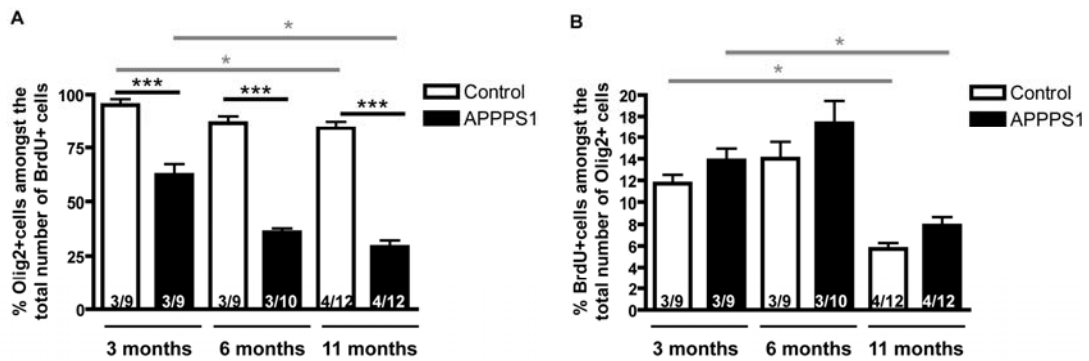
Figure 3- 23. Olig2+ Cell Percentage over the BrdU Pool and Total Proliferation of Olig2+ Cells.

(A) represents the percentage of Olig2+ cells over the total BrdU population at 3, 6 and 11 months of age in APPPS1 mice compared to control animals. With age the percentage decreased in control animals and upon chronic amyloidosis. (B) depicts the percentage of the proliferating Olig2+ cells over the total Olig2+ population at different time points in control and APPPS1 mice. With age, proliferation of these cells decreased in the control as well as in the condition of chronic amyloidosis. The numbers within the columns indicate the number of animals as well as the number of slices quantified (n of animals/n of slices). Data are presented as mean per slices ±SEM.

3.2.6 Increase in Proliferation of Oligodendrocyte Progenitors and Differentiation into Mature Oligodendrocytes in the Cortical Grey Matter

As I already observed a tendency of specifically NG2+ cells to be elevated in the Olig2+ cell composition and given the fact, that NG2+/Olig2+ cells are the most proliferative cell type in the healthy cortical grey matter[103,105,116], I aimed to investigate the increase of Olig2+/NG2+ cells in more detail. Therefore, 6 months old animals received BrdU for 2 weeks. Interestingly, the number of NG2+/BrdU+ cells was increased about 2-fold in the cortical grey matter of APPPS1 mice (Fig. 3- 24A,B). This reaction of NG2+ oligodendrocyte progenitor cells could be a response toward the focal loss of myelin and increasing plaque load in the grey matter. As OPCs have the ability to differentiate

further to become mature oligodendrocytes within the oligodendrocyte line-
age, I aimed to follow the differentiation of these cells as well. Therefore, I
applied BrdU for 2 weeks to the animals and then left them on normal water
for another 4 weeks, to be able to look for the maturation of the previously
dividing cells. Interestingly, I observed a significant 2-fold increase in the
generation of mature GSTpi+ oligodendrocytes in the APPPS1 mice (Fig. 3-
24C,D).

This increased maturation of oligodendrocyte progenitors may serve to repair
the focal demyelination or myelin aberrations observed in the grey matter.
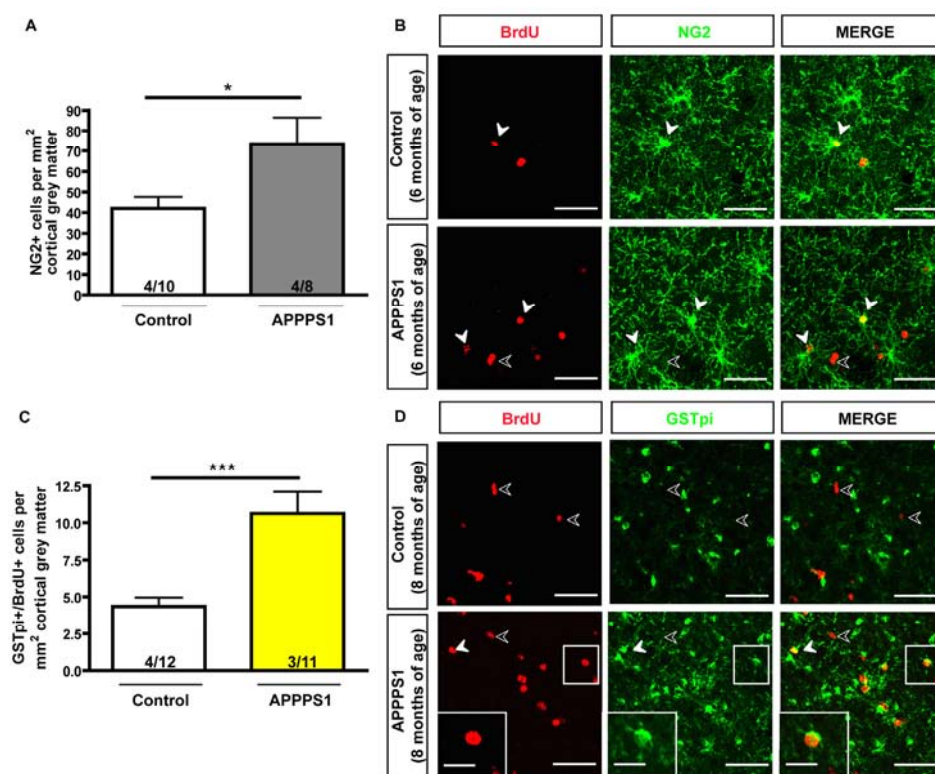
Figure 3- 24. Proliferation and Differentiation of Olidodendrocyte Progenitors in the Cortical
Grey Matter.

Proliferation and differentiation of grey matter cells was investigated by different BrdU pulses
(A) BrdU was applied for 2 weeks into the drinking water for studying proliferation or (B) it
was applied for 2 weeks followed by a 4 weeks differentiation period. This allowed following
the differentiation of the cells that previously incorporated BrdU. The identity BrdU-labelled
cells cells was characterized by NG2 as shown in (B) with representative immunostainings
for BrdU and NG2 and their overlay in 6 months old control mice and APPPS1 mice. In (C)
the quantification of GSTpi/BrdU double-positive cells per mm^2 is represented and examples
are shown in (D). The white arrowheads indicate double-positive cells, while the dark arrow-
heads point toward single positive cells.The inlay is a magnification of the according cell in

(D). The numbers within the columns indicate the number of animals as well as the number of slices quantified (n of animals/n of slices). Data are presented as mean per slices ±SEM. Scale bar: 50 µm and 20 µm for the inlay in (D).

3.2.7 Proliferation and Differentiation of Oligodendrocyte Progenitors in the Cortical White Matter

The above analysis showed an increased proliferation of oligodendrocyte progenitors and a subsequent increased generation of mature oligodendrocytes in the GM. Yet, quantitative analysis for the integrity of the myelin was performed in the cortical white matter and focal demyelination could also be observed in this particular brain region. However, cortical grey and white matter may respond differently. Therefore, I next examined the above described parameters in the WM. The proliferation of NG2-positive cells in the white matter of control mice that had incorporated BrdU (after 2 weeks) was 4 times higher in the WM than in the GM in control animals. To investigate differentiation of the proliferating NG2+ cells, I added a retaining period of 4 weeks to the 2 weeks BrdU labelling. The number of GSTpi/BrdU double-positive cells is also increased by 2.5-times in the WM compared to the GM of control mice. This underlines the strong differences in the density of proliferating or differentiating cells between GM and WM (Fig. 3- 24A,C;Fig. 3-25A,B).

To analyze if these cells would react similarly to the cells in the GM toward plaque deposition, I quantified the total number of NG2+/BrdU+ cells in the white matter of APPPS1 mice. Also in the WM, an increase of NG2+/BrdU+ cells per mm^2 could be observed in APPPS1 mice compared to control mice (Fig. 3- 25A). Subsequent analysis of the newly generated mature oligodendrocytes (BrdU+/GSTpi+ cells) in white matter of APPPS1 mice revealed a 2-fold increase comparable to what was observed in the grey matter (Fig. 3-25B,C).

Thus, myelin aberrations correlated to an elevation in proliferation of oligodendrocyte progenitors and a consequent increase in the differentiation into mature oligodendrocytes in both GM and WM. This could further explain

the stable number of myelin aberrations observed between 6 and 9 months old APPPS1 mice.
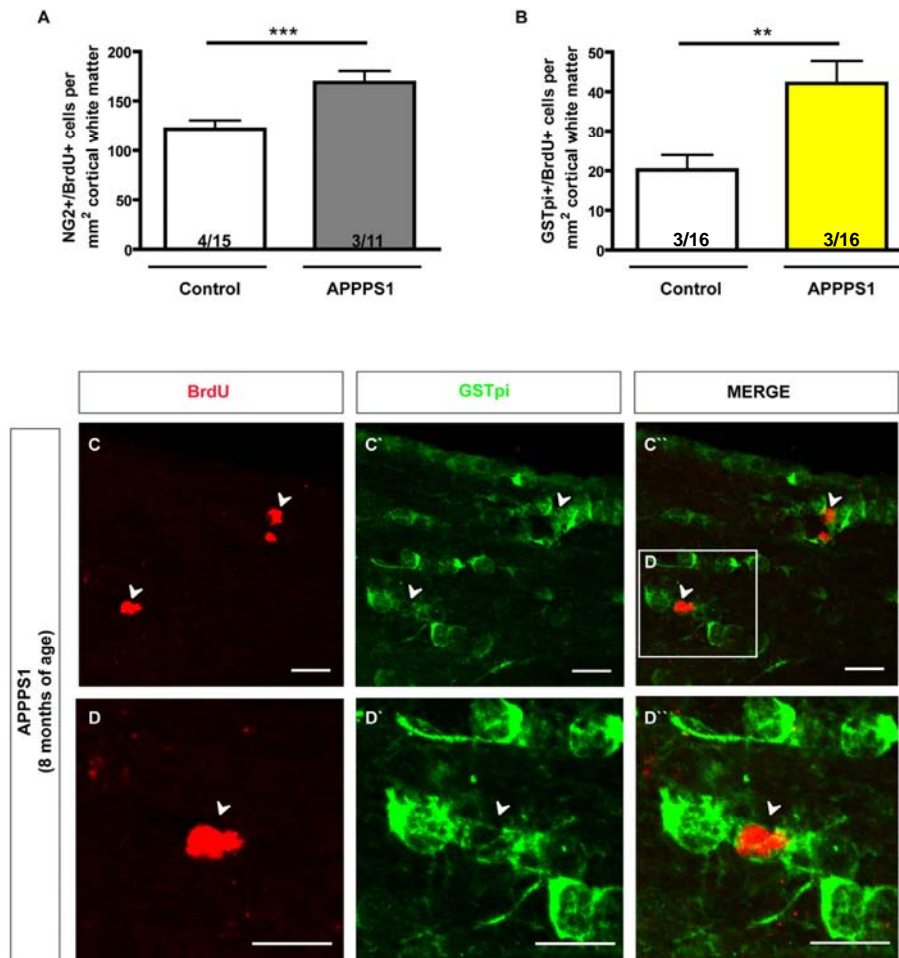
Figure 3- 25. Proliferation and Differentiation of Oligodendrocyte Progenitors in the White Matter.

Proliferation and differentiation of white matter cells was investigated by different BrdU pulses (A) 2weeks for studying proliferation and (B) 2 weeks followed by 4 weeks label retaining period. Retaining allows following the differentiation of the cells that previously incorporated BrdU. (A) depicts quantification of NG2+/BrdU+ double-positive cells per mm^2 (B) the differentiation of the oligodendrocyte progenitors investigated by staining for GSTpi/BrdU double-positive cells. (C) is a representative picture of a GSTpi/BrdU immunostaining, with the inlay (D) representing a magnification of a double-positive cell. The numbers within the columns indicate the number of animals as well as the number of slices quantified (n of animals/n of slices). Data are presented as mean per slices ±SEM. Scale bar: 20μm.

3.2.8 Olig2-positive Cells Do not Transdifferentiate into Astrocytes

From the data presented above it became clear that cells of the oligodendro-cyte lineage specifically react to amyloid plaque deposition. Yet, these cells may also generate astrocytes as observed upon e.g. cortical cryolesion[229]. Therefore, I asked the question if after such a chronic and persistent lesion paradigm as present in APPPS1 mice, Olig2-positive cells would also give rise to astrocytes.

To monitor cells of the oligodendrocyte lineage I utilized Olig2::CreER^{TM} x CAGGFP mice that express GFP specifically in Olig2-positive cells after in-duction with tamoxifen (Fig. 3- 26A)[105,115,398]. Mice were analyzed at different time points after induction at 5 months of age, namely 9, 30 and 90 days after induction. As you can see in Fig. 3- 26B,C already at 9 days after induction, mostly mature GSTpi-positive oligodendrocytes or NG2+ oligodendrocyte progenitors were recombined and thus expressed GFP. In line with previous reports, that find a small overlap of S100b expressing NG2+ cells[121], also a small fraction of S100b and/or GFAP-positive astrocytes could be visualized. However, there were no significant differences between control and APPPS1 mice observed at any time point tested. Therefore, Olig2+ cells did not react divert from but rather stayed within their lineage, the oligodendrocyte lineage, upon chronic amyloid plaque deposition. Notably, the increased maturation of OPCs into GSTpi+ cells was not observed with this approach, which is pos-sibly due to the specific Olig2+ cell population that is fate mapped, since about 20 % of all Olig2+ cells recombine (data not shown)[105].
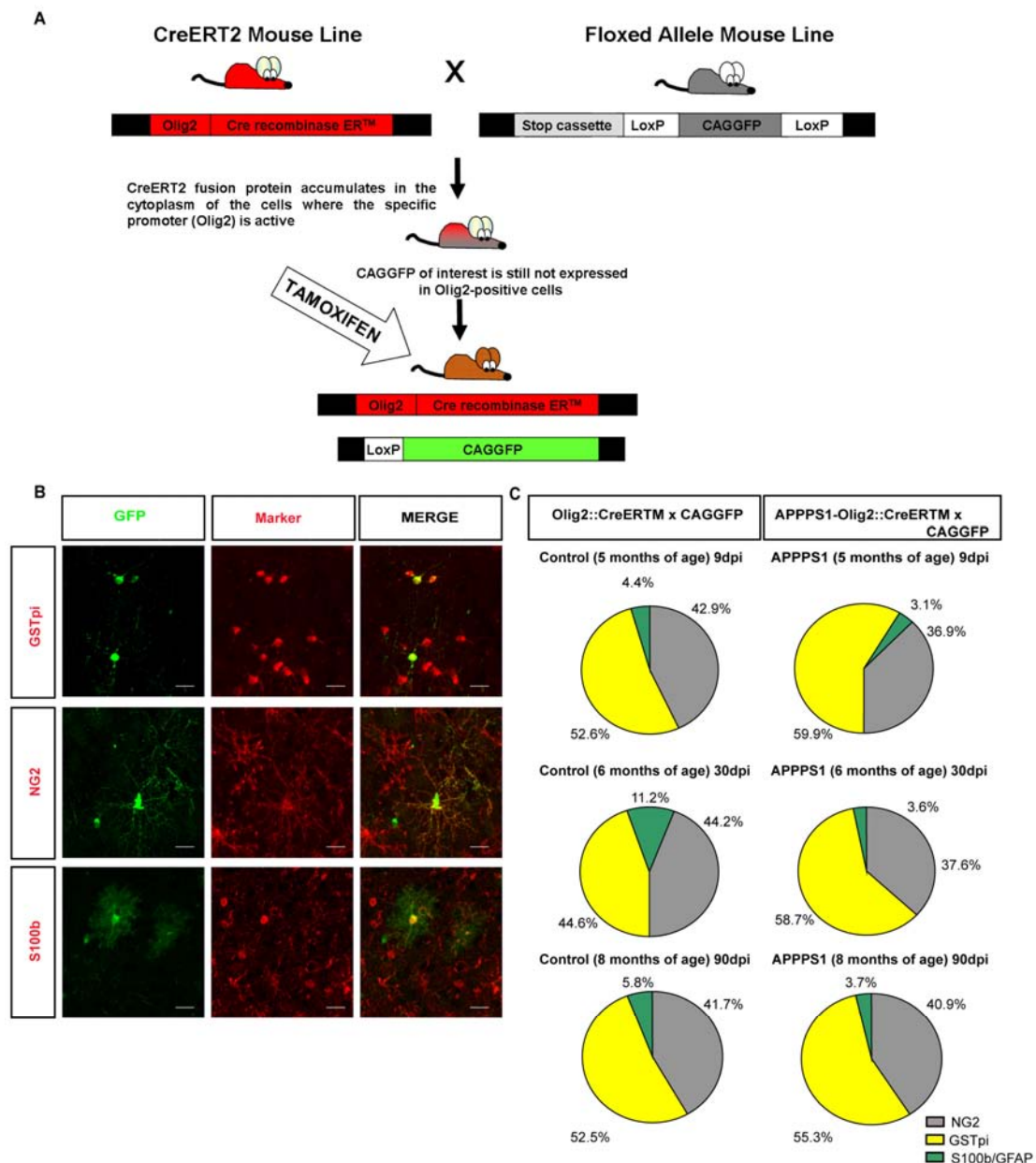
Figure 3- 26. Fatemapping of Olig2+ Cells in the Cortical Grey Matter.

(A) shows the schematic drawing of the generation of the mouse line. (B) are representative pictures of reporter (GFP) positive cells in APPPS1-Olig2::CreER[TM] x CAGGFP mice at 6 months of age, which are double-positive with different cell markers such as GSTpi, NG2 and S100b and/or GFAP. (C) quantification at different time points after recombination of reporter+ cells in the cortical grey matter are shown. No changes concerning the oligodendrocyte lineage can be detected between 9, 60 and 90 days after induction (dpi). n=4 NG2 and S100bGFAP staining controls 30 dpi and APPPS1 NG2 staining 90 dpi, n=5 APPPS1 S100bGFAP staining 90 dpi and n=3 for all other quantifications in (C). Data are presented as mean per animal normalized to 100 % ±SEM. Scale bar: 20µm.

3.2.9 Decrease in the Number of OLIG2+ cells in Human Alzheimer's Disease

The previous results indicated a specific response of cerebro-cortical grey matter oligodendrocyte progenitors and a subsequent increase in generation of mature oligodendrocytes in a chronic amyloid plaque deposition mouse model. Interestingly, the cells belonging to the oligodendrocyte lineage have not been investigated in human AD in detail so far. In order to examine whether a similar response of OLIG2+ cells that I observed in mice is also present in human AD pathology, I assessed the number of OLIG2-expressing cells in the grey and white matter of post mortem neurologically healthy human and AD tissue (8 subjects for each condition; for detailed information to the human material used look at table 6- 3 in material and methods). Since in the APPPS1 mouse model I mainly investigated the somatosensory cortex, I decided to also study this area in human material (Fig. 3- 27). Surprisingly and in contrast to the mouse data, I observed a significant decrease in the number of OLIG2+ cells in both GM (Fig. 3- 27A,C) and WM (Fig. 3- 27B,D) of AD patients. Since the sensory-motor cortex is not predominantly affected in human AD patients, I also quantified the number of Olig2+ cells in the Superior Temporal Gyrus (STG; Fig. 3- 27E,F) and Mid Frontal Gyrus (MFG; Fig. 3- 27G,H), regions known to be affected already early upon AD. Also in these cortical regions I detected a decrease in the number of OLIG2+ cells as observed in the sensory-motor cortex, except for the white matter of the MFG (Fig. 3- 27H). To further confirm that the observed overall reduction of OLIG2 expressing cells upon AD pathology are not due to neuronal and subsequential loss of oligodendrocytes, I quantified the percentage of OLIG2+ cells per DAPI+ cells in the human grey and white matter. The percentage of Olig2+ cells over DAPI was significantly reduced upon AD in SSC, STG and MFG. The only exception was the white matter of the MFG, where the percentage of OLIG2+/DAPI+ cells was similar between normal and AD cases (Fig. 3- 28).

In summary, these data indicate a loss of oligodendrocytes in different brain regions including both cortical grey and white matter upon human AD pathology.
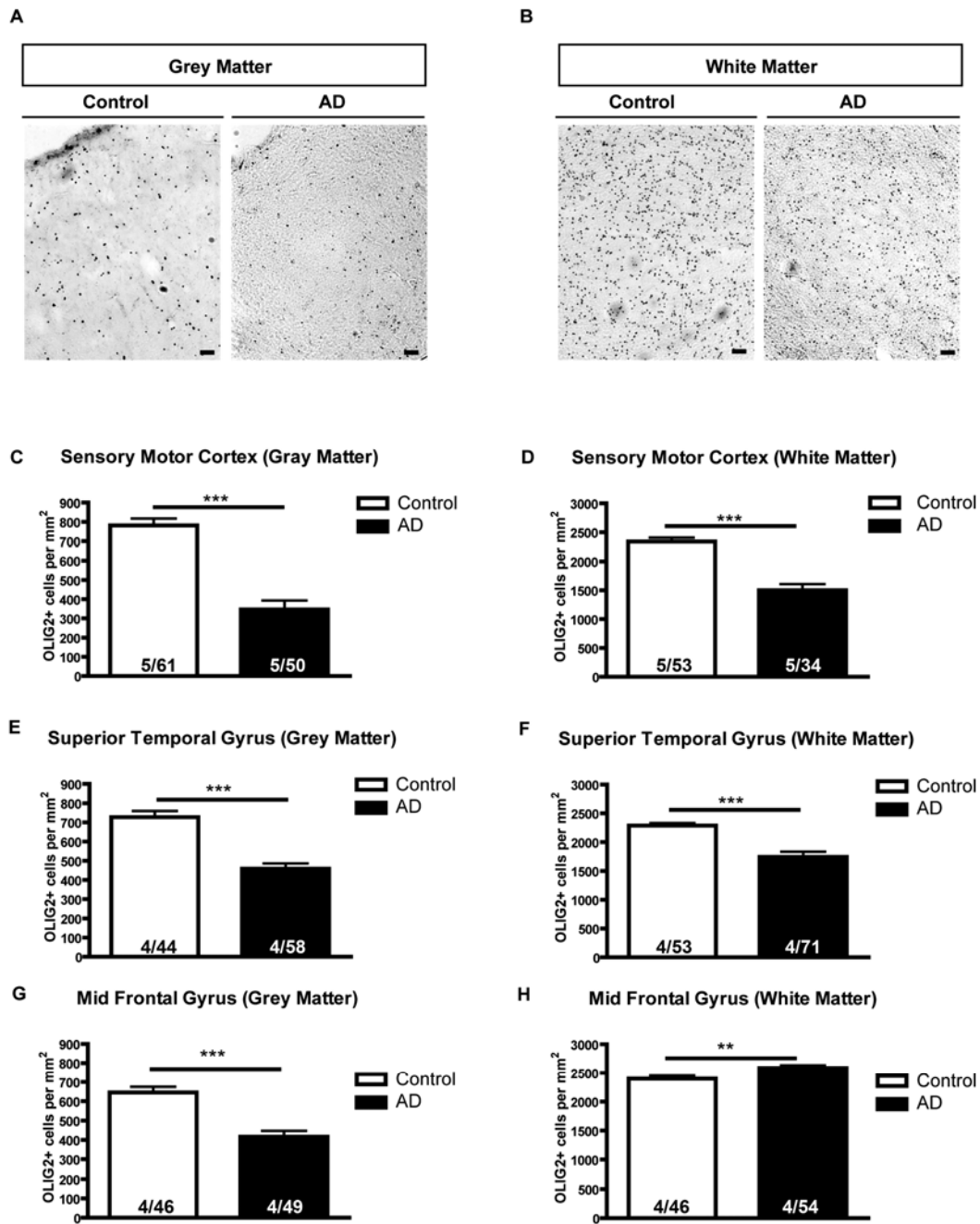
Figure 3- 27. OLIG2-positive Cells in Human Cortical Grey and White Matter.

(A,B) representative pictures of OLIG2+ cells in the cortical grey and white matter of healthy control patients and human AD patients. (C-H) histograms depicing the total number of OLIG2+ cells per mm^2 in different areas of the cortical grey and white matter of human control and AD patients. The numbers within the columns indicate the number of animals as well as the number of pictures quantified (n of patients/n of pictures). Data are represented per mean of spictures ±SEM. Scale bar: 100μm.
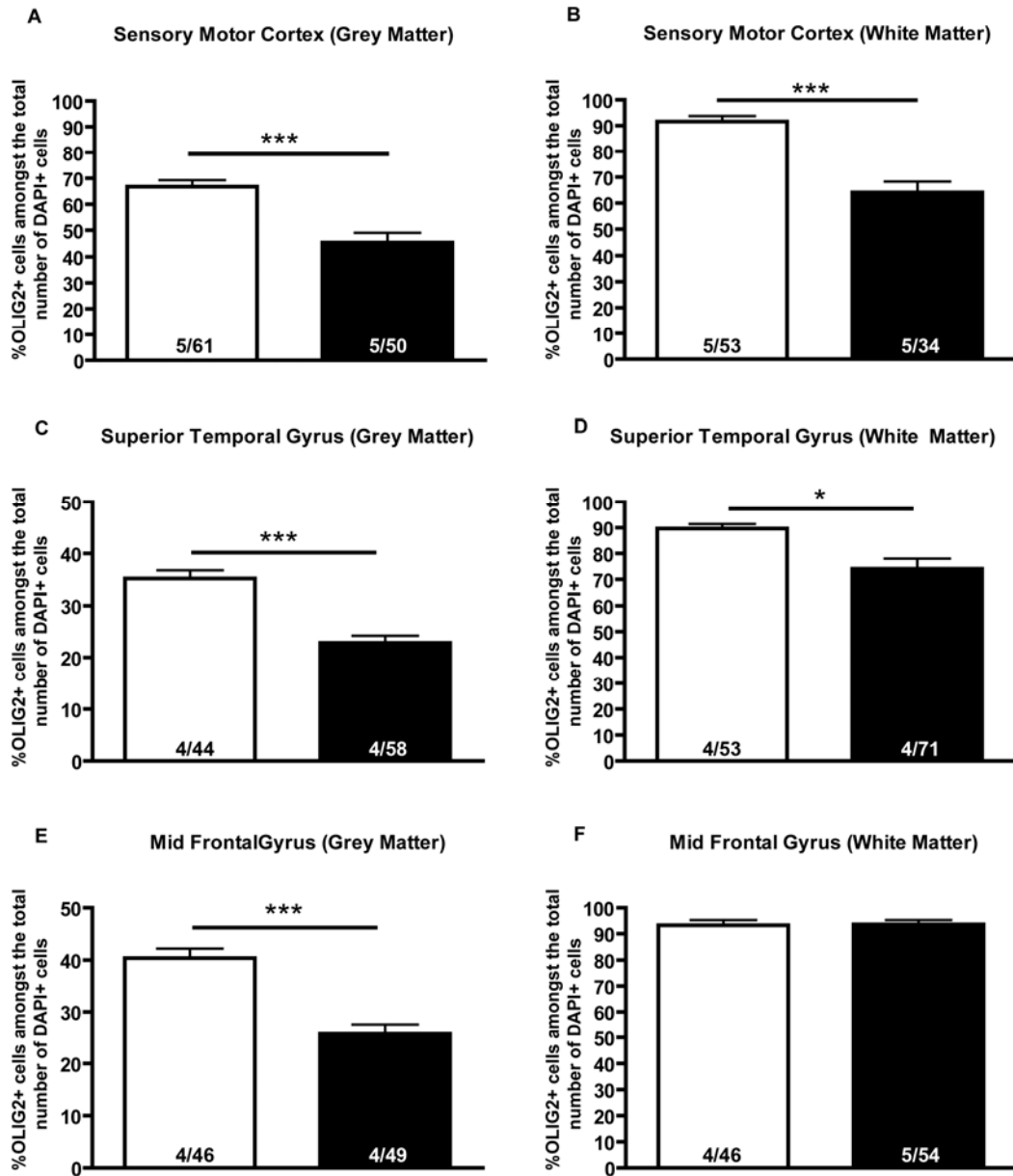
Figure 3- 28. Percentage of OLIG2-positive Cells Amongst the Total Number of DAPI-positive Cells.

(A,C,E) indicate the percentage of OLIG2+ cells over the total number of DAPI+ cells in different brain regions of the cortical grey matter. (B,D,F) indicate the percentage of OLIG2+ cells over the total number of DAPI+ cells in different brain regions of the cortical white matter. The numbers within the columns indicate the number of animals as well as the number of pictures quantified (n of patients/n of pictures). Data are represented per mean of pictures ±SEM.

4   Discussion

4.1   Reactive Gliosis in Different Lesion Paradigms

4.1.1   Differences in the Neurosphere Forming Capacity of Reactive Glia between Acute Injury and upon AD Pathology

Despite the strong glial reactivity, the neurosphere forming capacity of the lesioned cortical grey matter (GM) tissue is significantly lower in AD-related mouse models compared to large invasive injuries such as stab wound. Interestingly, this stem cell capacity *in vitro* is correlated to proliferation of cells after injury *in vivo*, which is higher in stab wound and lower in APPPS1 mice, with many neurospheres generated in the former and few in the latter (table 4- 1)[217]. Similarly in another invasive injury paradigm such as stroke, induced by an occlusion of the middle cerebral artery (MCAO), neurosphere formation is present to the same extent as observed in stab wound. Interestingly, this ability was accompanied as well by a similarly enhanced astrocyte proliferation[218,399]. In further support of this idea, in CK/p25 mice the failure of neurosphere formation also correlates with the absence of increased proliferation of macroglial cells (table 4- 1).

One possible explanation for the decreased number of neurospheres obtained from APPPS1 mice could be the age of the animals. APPPS1 mice were 6 months or older, while stab wound or MCAO were performed in 2 to 3 months old animals (data not shown). With age, proliferation is known to decrease in the neurogenic niches and cortical GM (Fig. 3- 4)[400]. In line with this suggestion, I also observe a decrease in the neurosphere forming capacity in 6 months old stab wound animals (data not shown). However, age does not explain the fact that no neuropheres are generated in CK/p25 mice, as they were 2-3 months old.

Another interesting feature which could play a role in the neurosphere forming capacity is the "*in vitro* senescence" present in astrocytes isolated from AD patients[401]. These cells can only undergo about 7 cell cycles in culture before proliferation decreases and finally stops. At late stages, astrocytes

start to express senescence markers, such as cyclin D1 and are prone to undergo apoptosis when they stop dividing[401]. Such an up-regulation of cyclin D1 in the absence of proliferation in astrocytes is also observed in the AD-related mouse models utilized in this study (Fig. 3- 15)[401]. Therefore, astrocytes may particularly lose their proliferative ability during aging or in mouse models reflecting certain aspects[402].

Besides the link between proliferation and neurosphere forming potential, it is unclear which cell type is giving rise to the neurospheres observed in APPPS1 mice. In principle, both postnatal cortical astroglia and NG2+ cells are able to generate multipotent and self-renewing neurospheres *in vitro*[403,404]. However after the second postnatal week, the potential of these cells located in the cortical GM is lost[217,403]. Recent rodent data reveal that after stab wound injury, adult GM astrocytes re-gain their developmental potential to generate self-renewing, multipotent neurospheres[103,217]. In contrast, other glial progenitors such as NG2$^+$ cells that actively proliferate as well in this lesion paradigm are not capable to do so[95,116,217]. In this study mouse models reflecting different injury paradigms are used. As glial cells may respond differently toward distinct lesion paradigms the neurosphere formation observed in APPPS1 mice may still be attributable to both, astroglia and NG2+ glia, since both cell types seem to harbour some developmental potential to generate neurospheres. One indication that also adult NG2+ cells harbour the potential to generate multipotent neurospheres arises from the fact that their formation is observed after isolation of unlesioned human adult cortical white matter[405].

Thus, in principle both cell types appear to be potent to generate neurospheres, I cannot exclude the possibility that also NG2+ glia may retain the ability to generate neurospheres after certain lesion conditions like chronic amyloidosis.

4.1.2 Striking Differences in the Glial Cell Proliferation in Response toward Different CNS Pathologies

As it has been pointed out above, the degree of astrocyte proliferation is strikingly different between acute invasive and non-invasive mouse models of AD pathology. Factors contributing to these differences in proliferation may be present at the cellular level or may be determined by the specific injury environment. All data obtained in this study are summarized in table 4-1.

Feature	Control	Stab Wound (3 dpi)	MCAO	APPPS1	CK/p25 (5 weeks OFF)
Expression of GFAP in Astrocytes	−	+	+ (a)	+	+
Expression of nestin in Astrocytes	−	+	+ (b)	+	+
Expression of DSD-1	−	+	n.d.	+	+
Expression of TNC	−	+	n.d. gene expression elevated (c)	+	+
Astrocyte Proliferation	−	+	+ (d)	+/−	−
Neurosphere Formation	−	+	+	+/−	−
Expression of pJNK in Astrocytes	−	+	n.d. pathway active (e,f)	−	+
Expression of pcJun in Astrocytes	−	+/−	n.d. pathway active (e,f)	−	+
Expression of Olig2 in Astrocytes	+	+++	++ (g)	++	+
Expression of Cyclin D1 in Astrocytes	+	+++	++ (h)	++	++
Invasion of Blood-dervied Immune Cells	−	++ (k)	++ (i)	+	+
Integrity of the Blood Brain Barrier	INTACT	OPEN	OPEN (j)	INTACT	INTACT

Table 4- 1. Overview over the Specific Features of Reactive Gliosis in Different Lesion Paradigms.

The table summarizes data obtained in this study. The AD-related mouse models used (APPPS1 and CK/p25) are compared to available data for acute invasive injuries such as stab wound and MCAO. Studies referred to are (a)[406]; (b)[218]; (c)[407]; (d)[399]; (e)[408]; (f)[409]; (g)[410]; (h)[411]; (i)[412]; (j)[187]; (k)[189]. The increased potential in forming neurospheres after stab wound and MCAO is indicated by the green background.

4.1.2.1   JNK/c-Jun pathway

The discrepancy in the astrocyte proliferation may be mediated by differently activated signalling cascades. One candidate represents the activation of the c-Jun N-terminal kinase (JNK). An increase in JNK phosphorylation has been demonstrated in reactive astrocytes in different injury paradigms such as epilepsy and demyelination[381,413]. Also my observations indicate an activation of the JNK after stab wound injury as well as in the AD-related mouse models (Figure 3- 13). The JNK is expressed in astrocytes after stab wound and in CK/p25 mice, while in APPPS1 mice only plaque-associated areas are immunostained. In support of the latter result, the JNK pathway has been shown to be active also in other plaque depositing mouse models of AD, such as the Tg2576 and Tg2576/PS1[P264L] mice[414,415] (table 4- 2). In accordance with my observations, both mouse models show an elevation of phosphorylated JNK expression mostly in plaque areas and in dystrophic neurons in the peri-plaque regions[414,415].

It has also been previously described that reactive astrocytes upon lesion show increased phosphorylation of a downstream target of JNK, namely c-Jun, an immediate early gene[416-418]. Phosphorylation of c-Jun (pcJun) is further implicated in the modification of astrocyte proliferation after demyelination[381]. In accordance with the activation of the JNK in GFAP-positive astrocytes upon stab wound and in CK/p25 mice, pcJun is detected in a small subset of reactive astrocytes in these lesion models (Fig. 3- 12). Other pcJun positive cells in this study, mostly detected in stab wounded and CK/p25 mice, likely comprise neurons, since pcJun is linked the induction of apoptosis after lesion[419,420]. However, not all pcJun positive neurons die, which indicates that pcJun expression may have broader and even protective functions in neurons after lesion[421]. The total amount of pcJun expression is accordingly higher in stab wound and CK/p25 mice (data not shown), with prominent neuronal death[189,331], while in APPPS1 mice the total number of pcJun-positive cells is lower correlated to the lack of cell death in this model[329]. These results are also in line with the results obtained in Tg2576 mice (table 4- 2), where expression of pcJun remains at control levels[415]. Interestingly, also in human AD pathology, pcJun positive neurons, which often carry paired helical filaments (PHF), can be identified[422]. In addition, pcJun-

positive GFAP+ astroglia as well as neurons, both located in the vicinity of plaques are present in the cortex, hippocampus and enthorinal cortex of AD patients[422]. This further supports the idea that tangle pathology as well as neuronal loss may be important triggers for pcJun expression in astrocytes.

4.1.2.2   Olig2

A transcription factor possibly involved in astrocyte proliferation after injury is the expression of the Olig2, a basic helix loop helix repressor, which is mostly expressed within the oligodendrocyte lineage[117]. However, also a small subset of astrocytes expresses it (Fig. 3- 14). Upon cortical stab wound lesion and in APPPS1 mice the number of Olig2 expressing cells is known to increase[105,116]. Olig2 is also up-regulated most prominently in astrocytes upon stab wound injury and in APPPS1 mice, which is in line with my own observations (Fig. 3- 14)[116]. Introduction of Olig2 via retroviruses into the lesion area of spinal cord-injured adult rats, results in massive proliferation of the transduced cells. However, only small subsets of these cells are astrocytes[423]. Also in human gliomas, Olig2 is strongly expressed, yet again mostly in cells of the oligodendrocyte lineage. One possible mechanism how Olig2 mediates its pro-proliferative function may be repression of p21, a tumor suppressor and inhibitor of stem cell proliferation[424]. Accordingly, repression of p21 would then lead to an increase in proliferation. Since Olig2 is frequently implicated in proliferation and tumor formation, it is likely that Olig2 is also involved in proliferation of astrocytes after injury. Indeed, genetic deletion of Olig2+ cells after cortical contusion injury, results in a reduced proliferation of astrocytes[382]. In line with this idea, Olig2+ astrocytes are highest after stab wound injury and lowest in CK/p25 mice, which is in accordance with the absence of astrocytes resuming proliferation in the latter mouse model (see Fig. 3- 11). Therefore the results indicate that only specific pathologies lead to a strong induction of Olig2 expression in astrocytes and the signals mediating this in astrocytes still need to be determined[383].

4.1.2.3   Cyclin D1

Astrocytes in AD pathology attempt to re-enter the cell cycle but fail to complete it. Along this line, I observe an increased number of reactive astrocytes in APPPS1 mice as well as CK/p25 mice that express cyclin D1. Expression of this protein, as a delayed early gene in the gap 1 (G1) phase of the cell cycle, is induced by e.g. growth factors and integrins[384,425,426]. D-type cyclines control the re-entry into DNA-synthesis (S)-phase, when the DNA is replicated, by regulating the phosphorylation status of the retinoblastoma protein[386,427,428]. Upon phosphorylation, the retinoblastoma protein releases the E2F transcription factor that then activates genes important for G1 to S phase transition. Cyclin D1 exerts its cell cycle-related functions by forming a holoenzyme with the cyclin dependend kinases (CDK) 4 and CDK6, however its expression has to be significantly downregulated for progression into S-phase[384,429]. The increase in expression of this protein indicates that astrocytes upon chronic plaque deposition (APPPS1) and heavy neuronal loss (CK/p25) become reactive and additionally attempt to re-enter cell cycle. Despite this increase in cyclin D1 expression, however, astrocytes do not incorporate BrdU to an extent observed upon stab wound injury[103,217]. Interestingly, after neurodegeneration in the retina, similar results are obtained. The Müllerglia in the retina fail to proliferate after a neurodegenerative insult but increase in the expression of cell cycle markers such as cyclin D1[430]. 3 days after stab wound injury, significantly more astrocytes express cyclin D1 compared to the AD-related mouse models. However, for proliferation to occur cyclin D1 expression has to be downregulated. At the time point where most proliferation of astrocytes is detectable upon stab wound (7 dpi) cyclin D1 expression is likely to be reduced compared to 3 dpi (Fig. 3- 15)[103].

However, cyclin D1 may also exert functions independent of CDK4 and CDK6, since different signalling pathways may converge on the cyclin D1 promoter. Interestingly, amongst such candidates are inflammatory signalling pathways e.g. the NF-κB (nuclear factor κB)/IKK (inhibitor of NF-κB) pathway or cytokines[431,432]. NF-κB resides in the cytoplasm in an inactive state due to the presence of members of the IκB family. Upon activation of this signalling pathway, IκB becomes phosphorylated and subsequently degraded. This allows the NFκB to translocate into the nucleus thereby activating or repress-

ing target genes[431,433]. NF-κB signalling is involved e.g. in the immune response toward injury, cell proliferation and cell death[433] and has been additionally implicated in the induction of cyclin D1 expression[434,435].

On the other hand, cytokines, which play an important role in the immune response, bind to cell surface receptors initiating signalling via the JAK-STAT pathway. The Janus activated kinase (JAK) e.g. upon binding to ligand-bound cytokine receptors, phosphorylates activators of transcription (STAT) transcription factors. Upon phosphorylation, STAT translocates into the nucleus[436]. Cytokines such as interleukin-3 or interleukin-6 are shown to stimulate the cyclin D1 promoter via STAT3 and STAT5 mediated signalling[432,437-439]. Since brain injury is accompanied by inflammation, cyclin D1 expression may be induced by inflammatory processes independently of a cell cycle function. However, one should keep in mind that so far most of the studies on that issue are conducted in other cell types. If such an inflammatory activation of cyclin D1 expression would also take place in astrocytes is not known yet.

4.1.2.4   Immune Response

The immune response taking place upon acute stab wound or MCAO injury may be different compared to the one taking place upon progressive amyloidosis (APPPS1) or induced neuronal loss (CK/p25). In general, the brain's immune response is mediated by astrocytes[440] and microglia which cooperate and influence each other[383,441]. In response to stimulation with cytokines, murine astrocytes up-regulate genes involved for example in innate immunity (e.g. IL-6, INF-β, IL-15, interferon-inducible GTPases), genes involved in adaptive immunity (e.g. MHC class I and II molecules) but also genes involved in signalling (NF-κB)[442]. Furthermore, other genes are down regulated such as CNTF (cilliary neurotrophic factor) as well as NT-3 (neurotrophin 3)[442]. This shows that astrocytes change their gene expression profile upon injury and it may be that different injury paradigms may lead to up- or down-regulation of distinct sets of genes. In support of this idea it has been shown that distinct astrocytes such as GM and WM astrocytes respond differently toward stroke[443,444]. One explanation for this may be that astrocytes repre-

sent a heterogenous cell population, since e.g. astrocytes cultured from different brain regions are diverse in their release of chemokines and cytokines or by the induction of the expression of nitric oxide (NO) synthase-2 (NOS-2)[445,446,447].

Also microglia produce numerous factors such as pro- and anti-inflammatory cytokines, growth factors and neurotrophins[252]. They furthermore rapidly migrate toward the lesion side[243], adopt an amoeboid shape and proliferate. Upon e.g. large invasive injuries or AD pathology they additionally acquire the ability to phagocytose and may produce reactive oxygen and nitrogen species[177,448].

A similar time course in microglial proliferation is observed upon stab wound and MCAO injury. At an early time point, 3 days after stab wound lesion, microglial cells constitute to most of the proliferating cells, whereas this reaction diminishes with time[103]. Similarly, upon MCAO in rats, activated microglia are observed 1 day after stroke and increase in number by day 2. Afterwards, this reaction subsides and resumes control levels around 14 days after MCAO[449,450]. In addition, peripheral leucocytes, including neutrophils, macrophages and T-cells invade into the lesioned area, thereby contributing together with the activated microglia to the increased production of cytokines including TNFα following ischemia[451]. However, certain immunomodulatory factors may react faster and more temporary, as it has been shown in acute traumatic spinal cord injury, where an increase of interleukin 1ß (IL1ß), interleukin 1α (IL1α) and tumor necrosis factor α (TNFα) transcripts are observed as early as 30 minutes after lesion. Other cytokines such as interleukin 6 (IL-6) and transforming growth factor-As (TGFAs) are also increased after spinal cord injury, however transcript up-regulation occurs later in time. 24 hours after spinal cord trauma the presence of these molecules starts to diminish, while simultaneously the number of microglia/macrophages increases[452]. Similar to stroke injury, after acute stab wound injury platelet-derived growth factor (PDGF) and TGFß are present early at the lesion side, since they are generated by platelet lyses[453,454]. The expression of TGFß is mostly present at the lesion side between 1 and 3 days after lesion. Thereafter, the TGFß protein expression decreases and becomes mostly located at the glial scar[454]. All the above described immunomodulators are expressed by infiltrat-

ing blood-derived immune cells but also by resident microglia and reactive astrocytes after lesion. Even though expression of e.g IL-6 and TGFß proteins can still be detected 12 to 14 days after lesion, the great inflammatory response toward the CNS insult endures relatively short in acute invasive injuries, which is in contrast to a more persistent chronic inflammatory response in AD pathology[453,455].

Aβ is a potent activator of microglial reactivity resulting in increased secretion of e.g. inflammatory cytokines, activated complement proteins, proteases and reactive oxygen species[456,457]. Microglia becoming reactive upon AD pathology are often associated with compact amyloid plaques, as also observed in different mouse models with plaque deposition[324,359,456] but also neurons with tangles or phosphorylated tau as well as aberrant neurites can be associated with reactive microglia[456]. Interestingly, the total numbers of microglial cells is well comparable between APPPS1 and CK/p25 mice. Furthermore, the proliferative response of microglial cells in CK/p25 mice with inducible neuronal cell death, follows a time course similar to acute invasive lesions, even though these changes were observed in longer periods of time. For example, at an early stage after onset of the pathology, microglia constitute about 60% of the total BrdU pool. At later stages of the pathology, the percentage adjusts to 50 % (Fig. 3- 11). This indicates an initial increase in microglial proliferation also in CK/p25 mice. In conclusion, regardless of the lesion paradigm microglial cells are one of the first cell types (together with NG2+ cells in APPPS1 mice) to increase in proliferation.

In addition to proliferation upon acute invasive injury, an invasion of blood-derived immune cells takes place, which may contribute to the immune response[458,459]. These infiltrating cells seem to exert important functions, since their ablation after spinal cord lesion impairs functional recovery[460]. Interestingly, such blood-derived cells are also detectable in APPPS1 and CK/p25 mice, however the density of these cells is rather low in comparison to acute injury paradigms (Fig. 3- 16). Since these cells together with microglia are a major source of TNFα[451], which also promotes astrocyte proliferation[461], this may be an additional candidate to mediate differences in proliferation between stab wound and AD-related mouse models.

The inflammatory response has been shown to exert both, beneficial effects as well as detrimental effects for the regenerative outcome after injury. For example, immediately after a stroke injury, the inflammatory process conveyed by microglia seems to be beneficial for neuronal survival, since ablation of proliferating microglia until 48-72 hours after stroke results in an increase in the size of the lesion and in the number of cells undergoing apoptosis[462]. Later in time, microglia may exert more detrimental effects on brain repair, as reduced microglial proliferation from 4 days after stroke on results in improved functional recovery after the insult[463]. Also in AD pathology, microglia may exert both beneficial as well as detrimental effects. For example, microglia migrate toward amyloid plaques and have the ability to phagocytose Aβ, thereby contributing to Aβ clearance. On the other hand, the increased expression of pro-inflammatory cytokines may enhance Aβ deposition[455]. Therefore it is believed that the immune response needs to balance beneficial versus detrimental effects and this balance seems to be of critical importance in terms of brain repair[456,464]. Interestingly, chronic inflammation may be a result of an imbalance of the presence of such inflammatory mediators, conveying the inflammatory response, and inflammatory regulators (include anti-inflammatory mediators), which down-regulate inflammation[456]. An imbalance of these different mediators upon aging[465] or chronic inflammatory stimulation may lead to an exacerbated pathology[456]. One observation supporting this suggestion is the observation that AD patients show a greater number of reactive microglia than non-demented patients bearing high amounts of plaques as well[456,466]. In addition to this possible imbalance of the inflammatory reaction, detrimental actions of activated microglia may predominate in AD pathology[455,467].

Therefore, microglia are activated in various pathologic conditions and may exert different functions depending on the specific CNS insult. Furthermore, they may release different sets of pro- and anti-inflammatory cytokines, growth factors and neurotrophins as well as different amounts of reactive oxygen and nitrogen species, which may also influence astrocyte and NG2+ cell reactivity differently.

4.1.2.5   Extracellular Matrix

In addition to the possible differences in the immune response upon different brain injuries, also other molecules present in the injury environment may support astrocyte and NG2+ cell proliferation in acute invasive injuries, whereas they may be less-supportive in AD-related mouse models. Along this line, the expression of the extracellular matrix proteoglycan DSD-1, which can be secreted from astrocytes, is increased in APPPS1 and CK/p25 mice[95,216] as detected with the 473HD antibody[50,468] (Fig. 3- 3, 3- 9)[92,93]. The 473 epitope recognizes the chondroitin sulfate proteoglycan (CSPG) phosphacan, which is expressed in the neurogenic niches of the healthy non-lesioned brain[48]. CSPGs have been shown to bind various growth factors that may promote cell division in the neurogenic niches as well as glial proliferation after lesion[47,95]. In addition to the DSD-1 proteoglycan also the extracellular matrix (ECM) glycoprotein tenascin C (TNC) is up-regulated and secreted from reactive astrocytes upon e.g. acute stab wound or laser lesion[95,216,469]. TNC is highly expressed by radial glial cells in the developing brain[470] and within the SVZ throughout postnatal and adult life contributing to the stem cell niche by e.g. modulating growth factor signalling[49,50]. In principle both of the above described molecules may be supportive for astrocyte proliferation but are obviously not sufficient as they are also up-regulated in APPPS1 and CK/p25 mice despite the lack of astrocyte proliferation. Notably, the extracellular matrix after lesion includes many more molecules than the DSD-1 and TNC, which may additionally influence the lesion environment and exert different effects on glial cells according to the different lesion conditions.

4.1.3 Upregulation of Intermediate Filaments

Another hallmark of reactive gliosis upon acute invasive brain injuries, like stab wound and stroke, includes the up-regulation of intermediate filaments such as GFAP and nestin[95,216,218,406]. Similar to the observations obtained from acute invasive injury, astrocytes up-regulate the intermediate filaments GFAP and nestin upon chronic plaque deposition (Fig. 3- 2; 3- 8; 3- 9). This

is in line with previous reports demonstrating that reactive astrocytes in an AD environment up-regulate GFAP and that they are mostly associated with focal plaques[324,344-346]. Furthermore, these reactive astrocytes in the vicinity of plaques become hyperthrophic, similar to the observations in APPPS1 mice (Fig. 3- 1)[348]. In addition to GFAP up-regulation, also increased expression levels for nestin have been observed upon human AD pathology and in neurodegeneration[471].

In contrast to APPPS1 mice, the CK/p25 mice do not show extracellular plaque deposition; however they show intraneuronal accumulation of Aβ, tau pathology and neuronal loss. Also these features were previously demonstrated to induce GFAP up-regulation which could in principle be due to either tau pathology or neuronal loss[331,336]. For example neurofibrillary tangle (NFT) pathology in mice leads to severely degenerated neurons as well as astrogliosis visualized with GFAP immunostaining[472].

In conclusion, on the one hand reactive gliosis upon AD pathologies shares many similarities with invasive injuries. On the other hand, certain aspects such as astrocyte proliferation, neurosphere formation are strikingly different comparing invasive and non-invasive injury paradigms.

4.1.4 Blood Brain Barrier Integrity

A very prominent difference observed in this study is the "open" versus "closed" blood brain barrier (up to a molecule size of 3000 Dalton) upon acute invasive and AD-related mouse models, respectively (Fig. 3- 17). Notably, this might be different in human AD pathology or in very old APPPS1 mice, since the blood brain barrier (BBB) has been suggested to be leaky[473,474]. Yet a possible leakiness is still is a matter of debate. A compromised blood brain barrier, however, is considered a feature of human AD pathology[475]. One difference of human AD pathology and APPPS1 (6 months of age) or CK/p25 mice (5 weeks OFF) is the presence of vascular amyloid deposits in human and its virtual absence (except for large pial vessels at late stages) in the mouse models[324,331,342]. Therefore, the absence of vascular

amyloid deposits within vessels may account for the unchanged blood brain barrier integrity in the AD-related mouse models I tested.

Given the rupture of the BBB upon acute invasive injuries, this can have dramatic influences on the specific lesion environment. For example, it is known that upon acute brain injury fibromeningal cells invade into the brain and take part in the generation of the glial scar[199,200]. In addition, factors that promote astrocyte and NG2+ cell proliferation as well as neurosphere forming capacity may be released from the blood entering the brain. Rupture of blood vessels and their astrocyte's contact may further trigger astrocyte proliferation upon large invasive injuries. Yet, the BBB and blood vessels remain intact in APPPS1 and CK/p25 mice and therefore this strong re-enforcement of proliferation may be missing. However, it should be noted that plaque deposition in APPPS1 mice is sufficient to elicit an increase in glial cell proliferation and neurophere forming capacity similar to age-matched stab wounded animals. However, it still needs to be elucidated what cell type generates these neurospheres and what are the factors leading to that response.

4.2   Reactivity of Cells of the Oligodendrocyte Lineage toward Chronic Plaque Deposition

4.2.1 Transient Increase in Disruption of Myelin Integrity in APPPS1 Mice

I could demonstrate that the percentage of myelin aberrations per axon upon chronic amyloid plaque deposition are significantly increased at the age of 6 months in APPPS1 mice, an age when in these mice plaque formation is already visible. In contrast to this observation, in another mouse model reflecting distinct aspects of human Alzheimer's disease, the 3xTg mice (table 4-2), myelin sheath aberrations are detectable even before plaque deposition starts[476]. One explanation for the discrepancy in the onset of myelin aberrations may be that 3xTg mice express mutations in APP, PS1 and tau, whereas APPPS1 mice specifically reflect the plaque pathology by overexpressing only APP and PS1 mutations (table 4- 2). Furthermore, in 3xTg mice the expression of the PS1 mutation starts prenatally[477], meaning that

the expression of the PS1 mutation starts earlier than in APPPS1 mice, where the PS1 mutation is postnatally expressed[324]. Above that, the different γ-secretase mutations of the two mouse models may also account for the discrepancy in the onset of myelin aberrations, since PS1 may be crucially involved in myelination. It has been shown that PS1 cleaves the insulin-like growth factor 1 (IGF-1) receptor[478] as well as the structurally homologous insulin receptor[479,480], which both are receptor tyrosine kinases. The corresponding ligand of these two receptors, IGF-1, is a strong promoter of myelination[480-483] as for example, knockout mice for IGF-1 show a marked reduction in the size of WM structures in brain and spinal cord[484]. As in the 3xTg mouse line the expression of the PS1 mutation starts before myelination onset, it could be that in these mice IGF-1 receptor is not efficiently cleaved by PS1. This may result in problems of IGF1-mediated signalling resulting in inefficient myelination. In accordance with this, APPPS1 mice do not show effects on myelination as examined at postnatal day 20 or 3 months of age, but rather on myelin integrity at later stages (6 months of age; Fig. 3- 20). However, the function of the PS1-mediated cleavage of the IGF1 receptor is not well known and it could be that different PS1 mutations differently affect IGF-1 receptor function[479].

Interestingly, also the ErbB4 signalling pathway is affected by the γ-secretase-mediated cleavage[480,485]. This pathway is known to be important for myelination in the peripheral nervous system (PNS) determined by *in vivo* studies[486,487]. For example, transgenic mice expressing a dominant-negative ErbB receptor in myelinating Schwann cells of the PNS have a delayed onset of myelination, thinner myelin, shorter internodal length and smaller axonal caliber in adulthood[487]. One signalling cascade involved in this phenotype is neuregulin-1 (NRG1) mediated via the ErbB receptors, which was similarly shown to be important for Schwann cell myelination in the peripheral nervous system (PNS)[488]. Similar to the NRG1 heterozygous mice, also BACE1 knock-out mice show severe hypomyelination in the PNS[489-491]. In the absence of BACE1, uncleaved full-length NRG1 accumulates resulting in this phenotype[489,490]. Therefore, it is possible that the cleavage of Erb can be mediated by both the γ-secretase and the β-secreatse, which may in principle affect myelination in the PNS. However, in the adult central nervous sys-

tem (CNS) the function of neuregulin-ErbB4 signalling seems conflictive, because ErbB4 knockout mice show no effect on myelination in the CNS[492]. On the other hand, a selective blocking of Erb signalling in oligodendrocytes is followed by hypomyelination, neuronal dendritic arborisation changes and interfered with dopaminergic neurotransmission[493]. Upon activation of Erb signalling the intracellular domain is released and translocates into the nucleus promoting the expression of the myelin basic protein (MBP) in oligodendrocytes[494]. Therefore, mutations or alterations in APP-related secretases may greatly influence myelin integrity[480].

Besides PS1, also overexpression of APP may affect myelination. The PDAPP mice[495], which overexpresses exclusively mutated APP under a mostly neuronal promotor (see table 4- 2), shows myelin loss by a reduction in the size of the corpus callosum, fornix and hippocampus. The length of the corpus callosum (CC) is reduced at the age of 40 days, as a result of an impaired WM development. No further change in the CC size can be detected until 21 months of age[496]. These morphological changes can be correlated to the gene dose of the mutant gene as homozygous animals have a greater reduction than heterozygous animals[497]. One difference between the mouse lines is again the onset of transgene expression prenatal in PDAPP and postnatal in APPPS1 mice[324,498]. In addition to the distinct onset of APP transgene expression in the two mouse lines, the overexpressed mutation is different (table 4- 2), which may distinctively affect myelination[324,495].

Apart from the possible involvement of APP mutations in myelin reductions, the APP-N-terminus has been recently shown to serve as an activator of the death receptor 6 (DR6). This receptor mediates axonal degeneration and neuronal loss via the activation of different caspases (caspase 3 and 6)[499]. Interestingly, another recent study demonstrates an involvement of DR6 also in the regulation of oligodendrocyte survival via caspase 3 activation. This study, however, does not observe any caspase 3 activation, when the oligodendrocytes are treated with the APP-N-terminus, which implies different effects of APP-N-terminus on the DR6 in different cell types[500]. Mutations in APP may still alter the activation of the DR6 in a way that affects survival of axons or myelin maintenance in different APP-mouse lines.

In summary, the above mentioned effects of different mutations were discussed in regard to myelination. Yet, in my study I could not detect myelination effects, but rather effects on myelin integrity. However, there is also evidence that oligodendrocyte cultures obtained from PSM146VKI (AD-associated PS1 mutation) mice show increased vulnerability towards different stressors such as glutamate and Aβ, which may in general account for changes in the observed myelin integrity[477,501-503]. Contrary to the PSM146VKI mouse line (table 4- 2), in APPPS1 mice the PS1-mutation is only neuronally expressed. However, also application of Aβ 42 to rat oligodendrocyte cultures reduces the survival of mature oligodendrocytes and even inhibits myelin sheath formation, while not affecting OPCs[504]. These results raise the possibility that the Aβ production could also result in death of oligodendrocyte progenitors thereby affecting myelin integrity APPPS1 mice. Therefore, specific APP as well as PS1 mutations may result in disturbances of both, myelin production and myelin integrity. Yet, also extracellular plaque deposition influences myelin, since focal demyelination can be observed in plaque core areas[389]. In conclusion, the myelin aberrations I observed in APPPS1 mice may be the result of mutant transgene overexpression as well as extracellular plaque deposition.

Mouse-line	Pro-moter	Start of Promotor Expres-sion	APP	PS1 Mutation	Tau	Onset of Plaque and Tau/Tangle Pathology
APPPS1 [324]	Thy1; neuronal	Postnatal	KM670/671NL (Swedish double-mutation)	L166P		**Plaques:** 2-3 months of age
La Ferla (3xTg) [505]	Thy1: Neuronal PS1: neuronal and glial (knock-in)	Postnatal: App, Tau Prenatal: PS1 (knock-in)	KM670/671NL (Swedish double-mutation)	M146V Knock-in[477]	P301L	**Plaques:** 6 months of age **Tangles:** 12-15 months of age
NFT-tg [472]	Tau promotor; neuronal	During de-velopment			K257T/ P301S	**Tangles:** 6 months of age
PDAPP [495]	PDGFß; mostly neuronal [506]	Prenatal: Aß produc-tion from embryonic E16 cul-tures	V4717F			**Plaques:** 6-9 months of age
PS1 M146VKI [477,503]	neuronal and glial (knock-in)	Prenatal (knock-in)		M146V Knock-in		No gross phenotype
Tg2576 [507]	Hamster Prion Protein (PrP); neuronal and glial	From E13.5 on[508]	KM670/671NL (Swedish double-mutation)			**Plaques:** 9-11 months of age
Tg2576/ PS1 [P264L] [507,509,510]	Hamster Prion Protein (PrP); neuronal and glial	From E13.5 on[508]	KM670/671NL (Swedish double-mutation)	P264L Knock-in		**Plaques:** 2-3 months of age

Table 4- 2. Overview on Different AD-Related Mouse Lines.

The characters indicate mutated amino acids: F = Phenylalanine; K= Lysine; L= Leucine; M = Methionine; N = Asparagine; P = Proline; S = Serine; V = Valine. The numbers refer to the location of the mutation.

4.2.2 Indications for Myelin Repair upon Chronic Plaque Deposition

Possibly as a reaction to the above observed aberrations, I reported an increase in the generation of mature oligodendrocytes and no further defects on myelin in APPPS1 mice compared to controls, respectively. This could hint toward some myelin repair mechanisms taking place in APPPS1 mice at this age. Remyelination is commonly observed after demyelination, where axons that lost their myelin, redistribute axonal sodium channels along the axon, formerly only located at the node of Ranvier[232]. This results in a non-saltatory and therefore slower conduction of action potentials. Upon remyelination, saltatory conduction is functionally re-acquired[233]. Yet, the remyelinated axons have thinner myelin sheaths with less compaction[511,512], which is most obvious for large diameter axons but not easy to detect for corpus callosal axons[170]. Therefore, when only morphology of myelin is taken into account, it is difficult to evaluate whether remyelination has taken place in the latter area in APPPS1 mice. However, there are some indications that myelin repair mechanisms might be ongoing.

In the spinal cord it has been shown that an increase of cells expressing the transcription factor Olig2 occurs in response to demyelination. A slower and delayed increase in the number of Olig2+ cells could be correlated to increasing age[237,513]. Also APPPS1 mice show an elevated number of Olig2-expressing cells in the GM at 6 months of age, when most myelin aberrations are observed. The majority of them belong to the oligodendrocyte lineage. At the latest time point tested (11 months of age) still a tendency toward an increase in the number of Olig2+ cells is detectable between control and APPPS1 mice. Furthermore, at 6 months of age, the increased number of Olig2-expressing cells in APPPS1 mice correlates to an enhanced Olig2+ cell proliferation, assessed by BrdU incorporation. At this time point, I could further attribute the increase in the number of Olig2+/BrdU+ cells to an increase in OPC proliferation. Strikingly, at 11 months of age, I still observe an increase in the number of proliferating Olig2/BrdU double-positive cells. Maybe this phenomenon indicates some ongoing myelin repair mechanisms still present at 11 months of age in APPPS1 mice, as these proliferating

Olig2/BrdU double-positive cells may serve as a reservoir for new myelinating oligodendrocytes.

Interestingly, the Olig2/BrdU double-positive cells are only a minority of all dividing cells in APPPS1 mice, whereas they are the majority in control mice. This is in line with previous observations in wildtype mice describing that Olig2+ cells represent the major cell population dividing outside the neurogenic niches[103,105]. In addition to this observation, the percentage of proliferating Olig2+ cells over the total Olig2 pool implies that only a subpopulation has the capacity to divide (Figure 3- 23)[105].

The major cell type mediating myelin repair upon demyelination of the cortical grey and WM are the Olig2+/NG2+ OPCs[237,514,515,103,170]. Upon demyelination these cells proliferate and are located around the lesion side, before differentiation into myelinating oligodendrocytes is observed[170,236-238]. Therefore, the increase in OPC proliferation and the consequent increase in the generation of mature oligodendrocytes upon chronic amyloid plaque deposition could hint to a remyelination attempt.

In line with this suggestion, the ratio of the myelin protein CNPase divided through the axonal marker NF70 is significantly decreased at 6 months of age in APPPS1 mice and it reaches control levels again at 9 months of age (Fig. 3- 19D). As axonal loss can be largely excluded[329], the decreased ratio indicates that less myelin is present per axon. As CNPase is additionally expressed in mature oligodendrocytes, the ratio indicates a transient decrease in rather both, myelin as well as mature oligodendrocytes at 6 months of age. Amyloidosis may inhibit the further differentiation of mature oligodendrocytes into myelinating oligodendrocytes, since Aβ application to oligodendorcyte cultures exhibits an effect on myelin formation, while leaving NG2+ cells unaffected. Dystrophic neurites as observed in plaque areas of the APPPS1 mice (Fig. 3- 20 and[323]), are usually rarely remyelinated[170].

However, not only demyelination stimuli can lead to an increased maturation of OPCs. For example, axonal degeneration without myelin pathology can also cause an increase in the proliferation of NG2+ OPCs[516]. Interestingly, activated microglia alone may mediate a response of NG2+ OPCs[517] and microglia are known to become reactive upon chronic plaque deposition[518]. Also after stab wound injury, an increase in NG2+ glia is detectable[103,105]. I

can therefore not exclude that the response of the NG2+ cells is only due to the myelin defects I observed in APPPS1 mice.

4.2.3 Heterogeneity of Cells of the Oligodendrocyte Lineage in the White and Grey Matter

OPC proliferation is significantly increased in the GM and WM of APPPS1 mice. However, GM and WM OPCs differ in their physiological properties[519] and WM OPCs display a higher rate of proliferation (see Fig. 3- 24; 3- 25). Previous fatemapping of Olig2+ cells revealed that WM OPCs are able give rise to myelinating oligodendrocytes in the adult healthy rodent brain. In contrast, few OPCs in the GM differentiate into mature oligodendrocytes and most do not progress to myelinating oligodendrocytes[105]. In another study, however, a greater proportion of proliferating GM NG2+ cells matures into GSTpi-positve oligodendrocytes, which is in line with my own observations (Fig. 3- 24)[103]. Notably, when the Olig2::CreER[TM] mouse is used, about 50 % of the recombined cells are proliferating, while in the healthy cortical GM only about 10 % of the Olig2+ cells proliferate (Fig. 3- 23)[105]. Therefore, Olig2::CreER[TM] supposedly labels the NG2+ cells with the highest levels of Olig2. Consistent with the role of Olig2 in proliferation as discussed above, NG2+ glia with the highest levels of Olig2 may proliferate most. These cells may then take longer to differentiate into mature oligodendrocytes[105].

Also my data indicate a greater number of NG2+/Olig2+ cells differentiating into mature oligodendrocytes in the GM compared to the white matter. In the WM an additional recruitment from the SVZ and RMS to the local OPCs may also explain the higher number of cells maturating observed in this brain region compared to the GM (Fig. 3- 24, Fig. 3- 25) [242,520]. However, also a possible migration of OPCs from the GM to the WM cannnot be excluded[105]. When I investigated the Olig2::CreER[TM] mouse line (Fig. 3- 26), however, I could observe no increase in the generation of mature oligodendrocytes in the cortical GM. This is likely due to the employment of a different reporter, since I observe already shortly after recombination of about 50 % GSTpi-positive cells in the cortical GM, while with the other reporter (Z/EG) about 80 % were NG2+[105].

In conclusion, both GM and WM OPC maturated more extensively into mature oligodendrocytes upon chronic plaque deposition, indicating some possibly ongoing myelin repair mechanisms present in this pathology.

4.2.4 Comparison of APPPS1 Mice to Human Aging and Human Alzheimer 's Disease

Myelin diminutions are frequently observed in AD tissue samples both in cortical GM and WM[367,369,387,388,520]. In APPPS1 mice, I observed a transient reduction in the ratio CNPase/NF70. While myelin is analyzed in post-mortem human samples, mice are analyzed at adult stages that do not represent the last period of a mouse's lifespan. However, these different time points may be of great importance for the obtained results, when taking into account that myelin amount and myelin integrity changes with age. For example in humans, myelination of the WM increases until mid-life (45 years of age) and then decreases, while myelin of the GM is constantly lost throughout life[521]. These damaged and lost sheaths may be constantly turned over[103,105,125,480]. Furthermore, ageing leads to deterioration of WM integrity[522-525], while also the efficiency of remyelination decreases with age[170]. Therefore upon AD, in addition to myelin reductions also exacerbated myelin breakdown is observed[520,526]. This suggests that even if myelin could be repaired at early stages, increasing age may confuse the issue of AD-associated myelin repair and may result in oligodendrocyte loss.

In support of this idea I observe less OLIG2+ cells in human AD patients in comparison to age-matched controls, while in APPPS1 mice (6 months of age) the number of Olig2+ cells is increased. However, in mice I cannot exclude that at later time points the number of Olig2+ cells would also decline, since the latest time point analyzed was 11 months of age. Indeed, in another AD mouse model, the Tg2579 mice (see table 4- 2) the number of Olig2+ cells is decreased at the age of 15-20 months[527].

Interestingly, studies in humans suggest that OPCs continue to divide in the adult as observed in mice[103,124]. These cells may serve as a potential source for new myelinating oligodendrocytes. However, the proliferation is known to

decrease with age and may also account for the decreased number of Olig2+ cells observed in this study[400].

Another explanation for the severity of the myelin reductions observed only in human pathology, could be the different evolutionary stati of the oligodendrocytes in humans and mice. Oligodendrocytes in humans are more complex and evolved later in time. Thus, these cells may respond different to pathologic insults such as Aβ accumulation. *In vitro* studies on rat oligodendrocytes already suggest a generally high toxicity of Aβ for oligodendrocytes[528,529]. Possibly, human oligodendrocytes or aged oligodendrocytes may be more vulnerable to Aβ toxicity than healthy or younger ones. Apart from the myelin aberrations focal demyelination is present in plaque core areas in the APPPS1 mouse models as well as in human AD[389].

Interestingly, similar to human aging, in the rodent model, I observe progressive deterioration of WM myelin integrity with age in control animals (Fig. 3-20). In contrast, APPPS1 mice show an increase in the number of effects already at the age between 3 and 6 months (Fig. 3- 20). One explanation for this result is that normal aging of myelin may be exacerbated upon amyloid plaque deposition, as it has been suggested for AD pathology[520,526].

In conclusion, myelin in mice is a vulnerable target upon chronic amyloid plaque deposition both, in terms of myelin aberrations at an early stage of the pathology and focal demyelination. APPPS1 mice additionally display possible endogenous repair mechanisms at early stages of the pathology. In human AD patients, on the contrary, a loss of oligodendrocytes manifests, indicating an inefficient or no myelin repair.

4.3   General Considerations

4.3.1   Differences between APPPS1 and CK/p25 mice

The proliferation of astrocytes and NG2+ glia as well as the neurosphere forming capacity is increased in APPPS1 mice compared to CK/p25 mice. Interestingly in APPPS1 mice, at 3 months of age, proliferation is mostly located around the plaques. Previous work showed that mostly astrocytes surrounding plaques are immunoreactive for acidic FGF[530,531] and basic FGF as well as FGF receptor 1 (FGFR-1) in human AD pathology[532,533]. Acidic and basic FGF are considered to represent strong mitogens and their presence may initiate proliferation of reactive astrocytes as well as NG2+ glia in APPPS1 mice[534], while CK/p25 mice that lack the hallmark of plaque deposition also lack increases in proliferation of these cells.

In addition to the differences in proliferation, astrocytes seem to initiate different signalling pathways upon different aspects of AD pathology. While in APPPS1 mice Olig2 is more prominently up-regulated in astrocytes compared to CK/p25 mice[116] (see also table 4- 2), pcJun expression in astrocytes seems to be a specific hallmark only present in CK/p25 mice. A possible explanation for these differences in astrocyte proliferation as well as astrocyte signalling between APPPS1 and CK/p25 mice is that neurons die via apoptosis in CK/p25 mice, whereas virtually no cell death is observed in APPPS1 mice[329]. However, cells in the vicinity of extracellular plaques in the latter mouse model eventually undergo necrosis. Thereby, mitogenic factors could possibly be released. For example, upon traumatic or ischemic pathologies, massive amounts of purine (ATP, ADP) and pyrimidine (UTP, UDP, UDP-sugars) nucleotides are released due to e.g. increased excitotoxic neurotransmission or liberation from dying cells[244]. Purines and pyrimidines exert their functions by e.g. activating the G-protein-coupled P2Y receptors on astrocytes, which results in up-regulation of GFAP and proliferation[535,536]. This mechanism may therefore be specifically involved in astrocyte signalling, and possibly glial proliferation in general, in APPPS1 mice, since CK/p25 mice show apoptotic cell death[331].

In addition to astrocyte proliferation another hallmark of severe astrogliosis is glial scar formation, which is observed upon stab wound injury as well as MCAO[187]. In plaque-depositing APPPS1 mice, astrocytes densely surround the plaques with their processes, thereby also possibly forming a glial-scar-like barrier between plaque and brain tissue[71,347]. Also I observed that astrocytes close to plaques polarize toward them (Fig. 3- 1). However, glial scar formation is absent in CK/p25 mice, even though severe neuronal death takes place. This may be due to the widespread occurrence of the neuronal loss. A further indication for this scenario is that astrocytes do not polarize and become extremely hyperthroph in CK/p25 mice (Fig. 3- 8).

Another difference between the AD-related mouse models is the increase in the proliferation of NG2+ OPCs specifically in the APPPS1 mice, but not in CK/p25 mice. OPCs are known to increase in proliferation upon various insults, however, this proliferative response is often attributed to demyelination[537,538]. Furthermore, OPCs have the ability to remyelinate demyelinated axons[237,242]. In support of this idea, focal demyelination is present in plaque core areas and myelin integrity is disturbed in APPPS1 mice (Fig. 3- 20; 3-18)[331,342,389]. Therefore, demyelination and aberrant myelin integrity may be the trigger for OPC proliferation specifically in APPPS1 mice. However, one should consider that also possible differences in the immune response between APPPS1 and CK/p25 mice may account for these discrepancies, since it has been shown that specific inflammatory stimuli can force NG2-glia proliferation[517]. However, in terms of microglial proliferation APPPS1 and CK/p25 mice show great similarities. In addition, in both of the AD-related mouse models some invading blood-derived immune cells are observed, which may contribute to the immune response (Fig. 3- 16).

This study provides evidence that astroglia and NG2-glia react distinctly toward different aspects of AD pathology. In general, it seems that extracellular plaque deposition triggers their reactivity more prominently than a combination of neuronal loss, tau pathology and intracellular amyloid accumulation. Furthermore, in APPPS1 mice, NG2+ glia may contribute to myelin repair and additionally astrocytes resume proliferation and reactive glia exhibit stem cell capacity *in vitro*. In CK/p25 mice, astrocytes fail to divide and also NG2+ glia do not react in terms of increases in cell proliferation. This further under-

lines that astrocytes and NG2-glia exert very different reactivity's and potentials depending on the specific injury. Therefore, the question arises what signalling pathways may be further involved in the reaction and proliferation of these two cell types?

4.3.2 Activation of Signalling Pathways Upon Injury

One interesting approach to identify such signalling pathways considers the different signalling pathways normally involved in stem cell signalling, since a hallmark of these cells is proliferation. Notably, many of these pathways are re-activated in glial cells after injury and therefore represent interesting candidates in identifying factors involved in glial cell proliferation and/or neurosphere formation[95]. Active signalling pathways of astroglia-like stem cells in the adult neurogenic zones include sonic hedgehog (Shh) and Wnt signalling[95,539-541]. In the cortical GM these pathways are present in a small subset of astrocytes. After lesion, Wnt signalling increases in astrocytes and its expression correlates to the newly (by proliferation) born cells[542,541,543]. Likewise, the mitogen sonic hedgehog is produced in reactive astrocytes after acute cortical cryoinjury inducing cell proliferation[544]. A synthesis and possible release of Shh and/or Wnt may explain the great proliferation of astrocytes also upon acute stab wound lesion. Furthermore, Amankulor et al. (2009) describes that specific inflammatory processes of macrophages seem to trigger Shh release of astrocytes, since ablation of these cells abrogates Shh expression [544]. As the inflammatory processes may be very different between acute and AD-related pathologies (as discussed above), these could also dramatically affect Shh signalling. Another interesting candidate pathway is growth factor signalling, which is also present at high levels in the stem cell niches. In the healthy non-lesioned cortical GM the basic fibroblast growth factor receptors (FGFRs)[95] are expressed at low levels by astrocytes[545-547]. After e.g. WM demyelination or focal brain injury an up-regulation in FGF expression in astrocytes is observed, possibly inducing the expression of FGF receptors[548,549]. The expression of another receptor for a different growth factor, the epidermal growth factor receptors (EGFRs), is absent in astrocytes

populating the healthy adult GM[550-553]. Yet, upon injury, astrocytes up-regulate the expression of EGFR, which may be important for astrocytes to become reactive[550,554,555].

In summary, astrocytes seem to up-regulate many signalling pathways, which are also active in adult neural stem cell niches. This may also explain the potential of reactive astrocytes to develop stem cell features after acute brain lesion[95]. Furthermore, all the above described signalling pathways may represent interesting candidates to test for in regard to their presence or absence in APPPS1 and CK/p25 mice, since astrocytes show different properties in these lesion paradigms.

However, also NG2+ cells increase in proliferation after injury and may also harbour the potential to generate neurospheres in APPPS1 mice. Similar to GM astrocytes, a small subset NG2+ cells expresses Wnt signalling-related molecules, while after lesion Wnt signalling increases and corresponds to cell proliferation[541]. Also FGFRs[95] are expressed by both, astrocytes and NG2+ cells[545-547] and after e.g. WM demyelination NG2+ glia up-regulate them, similar to astrocytes[548]. EGFR expression is absent in NG2+ cells in the healthy adult GM[550-553] and upon brain lesion it is not yet determined if NG2+ cells are able to express this receptor[547]. Furthermore, one study so far suggests that NG2+ glia seem not to be a source for the mitogen Shh, yet this has to be determined in more detail[544]. Thus, the signalling pathways of NG2+ glia after injury still need to be elucidated, but so far interesting candidate signalling pathways after injury such as in FGF and Wnt signalling show an overlap to astrocytes. Yet, different signalling molecules may affect astrocytes and NG2+ glia differently as they comprise distinct cell populations.

4.3.3 General Differences between Astrocytes and NG2-Positive Cells

One important difference between astrocytes and NG2+ glia may be that the developmental neuroepithelial cells first transform into radial glia, which then directly transform into astrocytes. Besides that these neuronal progenitors transform into adult neural stem cells as well as ependymal cells[35,40,68,547,556-560]. A subset of astrocytes is also generated from either subventricular or cor-

tical progenitors as well as NG2+ cells during development[70,129,561,562]. Conversely, an early neuroepithelial origin for NG2+ glia is not observed so far. There is evidence obtained from fatemapping of ventral radial glial cells indicating some direct transformation of these cells into into NG2+ cells[29]. In the dorsal telencephalon, however, NG2 glia are mostly generated from committed intermediate progenitors[29,40,100,547,563]. This indicates that NG2+ glia may divert from the astroglial cells, since the latter are directly derived from neural stem cells. However, as NG2+ cells also give rise to certain astrocyte subtypes may indicate some overlap between these two cell population.

The close relationship of adult parenchymal astrocytes with neural stem cells is further underlined by the shared expression of specific markers. Amongst them are e.g. the beta subunit of the calcium binding protein S100 (S100b), the excitatory amino acid transporter 2 (also known as GLT1) or the glutamine synthetase (GS)[74]. Furthermore, parenchymal astrocytes retain the expression of stem cell-related markers such as Sox2, Sox9 and Musashi, which are not expressed by NG2+ glia[399,547,564-568]. Other molecular features reminiscent of the stem cell niches are downregulated in parenchymal astrocytes (e.g. Tenascin C, nestin, DSD-1) but can be re-expressed after lesion[48,95,216].

In addition, the neurogenic potential of adult astroglia-like stem cells is well established[569,570], while the neurogenic potential of NG2+ glia remains debated. Some studies claim the generation of interneurons in the olfactory bulb from NG2+ cells located in the subventricular zone, which are fate mapped utilizing the 2',3'-cyclic nucleotide 3'-phosphodiesterase (CNPase) promoter[571,572], while fate mapping studies of NG2+ or Olig2+ glia do not reveal such neurogenic potential[69,70,105,121,129].

In the adult, a subset of NG2-glia expresses astrocytic proteins[121], while some astroglia-like stem cells in the adult subependymal zone were shown to express the Plateled Derived Growth Factor receptor alpha (PDGFRα)[573], which is most commonly expressed by NG2+ glia[125]. Yet another study does not confirm the co-expression of PDGFRα in GFAP+ neural stem cells[574]. Apart from the discrepancies concerning the PDGFRα expression, still some overlap in the expression of certain markers between these two cell types exists. Yet, despite this small overlap in expression of markers, in APPPS1

mice fate mapping of Olig2+ cells of the oligodendrocyte lineage shows that they do not overt the potential to transdifferentiate into astrocytes, as observed after cortical cryolesion[229,230]. These cells rather stay within their lineage upon chronic plaque deposition, which is in line with observations obtained from stab wounded animals[105,231] Therefore, the ability of NG2-glia to generate astrocytes seems to depend on the specific lesion paradigm or may be due to the transgenic mouse lines utilized.

One striking difference of these two cell populations in the adult healthy cortical GM is that astrocytes are quiescent[103,217] and may only resume proliferation after large invasive injury, while NG2+ glia continuously divide in the healthy brain and further increase in proliferation after e.g. acute stab wound injury and in APPPS1 mice but not in CK/p25 mice (Fig. 3- 5; 3- 11)[103,105]. This indicates that after lesion these cell types may be more similar, as they both respond with an increase in proliferation after injury. Interestingly, after acute stab wound lesion only astrocytes have the ability to give rise to multipotent neurospheres[217]. However, the generated neurospheres from APPPS1 mice may be derived from both astrocytes or NG2+ glia, which both hold a certain potential (see above).

This study provides evidence that astrocytes exert different potentials between acute invasive and AD-related pathologies. Furthermore, also different aspects of AD pathology influence the extent of astroglial cell reactivity. Further investigation of signalling cascades involved in the brain's reaction toward injury may give new ideas how to promote astrocyte proliferation also in APPPS1 and CK/p25 mice. In addition to that, another glial cell type, the NG2+ glia react only in the APPPS1 mice, while in CK/p25 mice this reaction does not take place. Upon AD pathology NG2+ glia seem to exert their functions while remaining in their lineage. However, signalling molecules that induce that response in APPPS1 mice may be important to be investigated with the aim to increase myelin repair mechanisms that seem to be ongoing upon extracellular plaque deposition. This is of special importance in light of the finding that in human AD oligodendrocytes are lost.

In summary, all data indicate dramatic differences between the glial cell reactivity toward different pathologies. In addition to that, the different glial cell types exert very distinct functions. The glial cell reactivity in such a complex pathological disease as AD is determined by different aspects of the pathology, which may induce different beneficial as well as detrimental glial cell responses.

5   Material

5.1   Equipment

Table 5- 1. List of Equipment:

Description	*Company*
Geldoc™ XR	BIO-RAD
Heat sealing device Vacuplus	Petra electrics
Incubator	Memmert
Incubator	Binder
Laminar flow	Bdk
Magnetic stirrer IKAMAG® RCT	Bachofer
Magnetic stirrer IKACOMBIMAG RET	Jahnke & Kunkel GmbH and CoKG IKA-Wok
Microscope Axiovert 40CFL (fluolamp HXP120: Kübler) (camera A640: Canon)	Zeiss
Microscope LSM700 (confocal microscope)	Zeiss
Microscope Fluo Olympus BX61 (fluorescence microscope)	Olympus
Microscope Leica MZ6 (light microscope)	Leica
Microwave	Privileg
Odyssey Scanner	LI-COR

Description	Company
Perfusion pump	Gilson
pH meter WTW	inoLab
Refrigerator	Privileg
Refrigerator	Liebherr
Semi-Dry Transfer Cell Trans-Blot® SD	BIO-RAD
Shaker IKA-Vibrax-VXR	Electronic
Shaker RM5 (rotary shaker)	Assistant
Shaker Duomax 1030	Heidolph
Shaker Vortemp56EVC	Uniequip
Spectral photometer Prim advanced	Secoman
Stereotactic apparatus	Stoelting
Thermocycler 3000	Biometra
Thermomixer comfort	Eppendorf
Ultrathorax Sonopuls	Bandelin
Vibratome VT1000S	Leica
Vortex-Genie	Bender & Hobein AG
Water bath	Haake
Water bath (cell culture)	**Memmert**

5.2   Consumables

Table 5- 2. List of Consumables:

Description	*Company*
Augen- und Nasensalbe	Bepanthen
BC assay reagent A	Uptima
BC assay reagent B	Uptima
Cell culture flask with filter lid	Greiner bio-one
Cellstar® (T25,T75, T175), PS red	CELLSTAR
Cell strainer	BD Falcon (70 µm)
Coverslips	Roth
Drill	Foredom
Filaments (Vicryl)	Ethicon
Filter/strainer 70 µm	BD Transduction Laboratory
Filter tips	Biosphere
Gloves	Diana Baronin von Schaezler
Gloves	NeoTouch
Gloves Nitra-Tex® (nitrile)	Ansell
Insulin needles, U-100, 1 ml	BD Micro Fine (PZN: 324870)
Microscope slides	Roth
Microscope slides Superfrost	Thermo Scientific
Pasteur pipettes (glass)	VWR
Parafilm PM-996	Parafilm

Description	Company
Reaction tubes for PCR	Eppendorf
Reaction tubes (0.5 ml; 1.5 ml; 2 ml)	Plastibrand
Reaction tubes safelock (1.5 ml; 2 ml)	Eppendorf
Reaction tube (15 ml; 20 ml)	Greiner
Serological pipettes (5 ml; 10 ml; 15 ml)	Sarstedt
Syringe (10 ml; 30 ml)	Braun
V-Lance^{TM} Knife, 19 Gauge	Alco © Surgical
Well-plate (24)	**Orange Scientific**

5.3   Chemicals

Table 5- 3. List of Chemicals:

Chemical	*Company*
Aceton	Roth
Acetic acid	Roth
Acetic acid anhydride	Sigma
Acrylamid 30 %	BioRad
Agarose	Serva
Ammonium nitrate	Sigma

Chemical	Company
Ammonium Persulfate (APS)	BioRad
Aprotinin	BioMol
Araldit Kit	Fluka
BCA Assay	Uptima Interchim
Bromphenol blue	Sigma
5-Bromo-2′-Deoxy-Uridine (BrdU)	Sigma
Cacodylic acid	Sigma
Calcium chloride dihydrate	Sigma
Citric acid monohydrate	Roth
Corn oil	Sigma
4′,6-diamidino-2-phenylindole, dilactate (DAPI)	Invitrogen
dNTPs	PeqLab
Dimethylarsinic acid sodium salt tri-hydrate	Merck
Edetate disodium	Sigma
Ethanol	Roth
Ethanol 70 %	Roth
Ethidiumbromid	Roth
Ethylene glycol	Sigma
Ethylenediamine-tetraacetic acid (EDTA)	Sigma
Formaldehyde (Formol)	Roth
Formamide	Roth

Chemical	Company
Glutaraldehyde 25 %	Serva
Glycerol	Sigma
Glycine	Sigma
Goat Serum	Gibco
Leupeptin	BioMol
Ketaminhydrochlorid (Ketavet) 100 mg/ml	Pfizer
Magnesium sulphate heptahydrate	Sigma
Magnesium sulphate hexahydrate	Merck
Methanol 20 %	Merck
2-Mercaptoethanol	Sigma
Mounting solution (AquaPolymount)	Polysciences
Mounting solution (DPX)	Fluka
0,9% NaCl solution (Saline)	Braun
Osmium tetroxide solution 4 %	Sigma
Paraformaldehyd	Sigma
PCR Reaction buffer 10 x	NEB
PCR Reaction buffer 10 x	Quiagen
Pefabloc	BioMol
Pepstatin	BioMol
2-Propanol (Isopropanol)	Roth
Proteinkinase K	Roth
Potassium chloride	Sigma
Potassium dihydrogen phosphate	Merck

Chemical	Company
Potassium phosphate	Sigma
Potassium hydroxide	Sigma
Potassium permanganate	Fluka
Potassium phosphate	Sigma
Pyridine	Sigma
Q- solution	Qiagen
Sucrose	Merck
Silicotungstic acid	Sigma
Silver nitrate	Sigma
Sodium acetate trihydrate	Roth
Sodium bicarbonate	Sigma
Sodium carbonate	Fluka
Sodium chloride	Sigma
Sodium citrate dehydrate	Sigma
Sodium dodecyl sulphate (SDS)	Sigma
di-Sodium hydrogen phosphate di-hydrate	Merck
Sodium hydroxide	Fluka
Sodium hydroxide pellets	Sigma
Sodium nitrite	Fluka
Sodium phosphate	Sigma
Sodium thiosulfate	Sigma
5-Sulfosalicylic acid dihydrate	Roth
Tamoxifen	Sigma

Chemical	Company
Taq Polymerase	NEB/ self-made
TEMED	BioRad
Triethanolamine Hydrochloride	Sigma
Triton X-100	Sigma
TRISbase	Sigma
TRISHCL	Sigma
Tween20	Sigma
Xylazinhydrochlorid (Rompun) 2%	Bayer
Xylene cyanole	**Sigma**

5.4   Buffers and Solutions

5.4.1 Mouse DNA Preparation

Tris- HCl 10mM for DNA (1l)

1.211 g	*TRISbase*
	ad 1l H$_2$Odd, pH 8.5

Lysis Buffer for Tail Biopsies

1 M	*NaCl*
1 M	TRISHCl pH 8.5
10 %	SDS
0.5 M	EDTA
10 mg/ml	Proteinase K
	(freshly added)
	ad H2Odd

10 x PCR Buffer (uni)

500 mM	*Potassium chloride*
100 mM	TRISHCl
	pH 8.7

dNTP Mix

2.5 mM	*each dATP, dTTP, dGTP, dCTP*
	in H$_2$Odd

50 x TAE

242 g	*TRISbase*
32.2 g	Edetate disodium
57.1 mg	Acetic acid (100 %)
	ad 1l H2Odd , pH 8.0

Ethidiumbromid

100 mg	*Ethidiumbromid*
2 ml	**H$_2$Odd**

4 x DNA Loading Buffer

20 ml	*100 % Glycerin*
1 ml	50 x TAE
200 µl	Bromphenol blue
500 µl	Xylene cyanol solution
	ad 50 ml H$_2$Odd

5.4.2 Electron Microscopy

Cacodylat Solution

0.2 M	*Cacodylate*
21.4 g	Dimethylarsinic acid sodium salt trihydrate
0.22 g	Calcium chloride de-hydrate
	ad 500 ml H$_2$Odd, pH 7.2

Karnovski Fixative for Perfusion

2.5 %	*Glutaraldehyde*
2 %	PFA
0.1 %	Cacodylate solution
	in H$_2$Odd

Storing Solution for Electron Microscopic Tissue Samples

4 %	*PFA*
2.5 %	Sucrose
	in H$_2$Odd

Washing Solution

0.1 %	*Cacodylate*
2 %	Sucrose
	in H$_2$Odd

Osmication Solution

2 %	*Osmium tetroxide solution*
0.002 %	Calcium chloride
2%	Sucrose
	in 0.2 % Cacodylate buffer

5.4.3 Western Blot

Lysis buffer for Tissue Samples

50 mM	*TrisHCl, pH 7.4*
1 %	TritonX 100
10 %	Glycerin
5 mM	EDTA

Protease Inhibitors:

4.2 µM	Leupeptin
100 nM	Aprotinin
5.8 µM	Pepstatin
1.7 mM	**Pefabloc**

20% Tween

50 ml	*Tween 20*
200 ml	**H_2Odd**

TBS Buffer (10 x)

12.1 g	*TRISbase*
87.8 g	Sodium chloride
	ad 1l H2Odd
	pH 8.0; autoclave

TBST Buffer (1 x)

100 ml	*TBS 10x*
10 ml	Tween20
	ad 1l H$_2$Odd

Electrophoresis Buffer (Elpho buffer)

30.3 g	*TRISbase*
144 g	Glycine
10 g	SDS
	ad 1l H$_2$Odd **pH 8.45**

APS (10%)

100 mg	*Ammonium Persulfate* **in 1 ml H$_2$Odd**

Stacking Gel Solution (4 % Acryalamid)

1.86 ml	*0.5M TrisHCl pH 6.8*
37.5	20% SDS
0.98 ml	Acrylamide
37.5 µl	10% APS
7.5 µl	TEMED
4.58 ml	**H$_2$Odd**

Running Gel Solution (12 % Acryalamid)

7,5 ml	*1,5M TrisHCl pH 8.8*
0,15 ml	20% SDS
12,0 ml	Acrylamide
0,15 ml	10% APS
0,02 ml	TEMED
10.2 ml	**H$_2$Odd**

Transfer Buffer

3.03 g	*TRISbase*
0.1 %	SDS
14.4 g	Glycine
20 %	Methanol
ad 1 l H$_2$Odd	

4x Loading Dye

2 ml	*1M TrisHCl pH 8.5*
8 ml	20 % SDS
5 ml	Glycerin
1.6 ml	β-Mercaptoethanol
50 mg	Bromphenol blue
3.4 ml	**H$_2$Odd**

5.5   Tissue Preparation for Immunohistochemistry

Anesthesia Solution

2.5 ml	*Saline*
1 ml	Ketamin
0.25 ml	**Rivapoun**

Prepare freshly.

Tamoxifen

40 mg/ml	*Tamoxifen*
10 %	Ethanol
in corn oil	

For preparation of the solution shake 3-4 h at 37 °C

BrdU – Drinking Water

1 mg/ml	*BrdU*
10 %	Saccharose
	in H$_2$O

20 % Paraformaldehyd (PFA) Stock

67 g	*di-Sodium hydrogen phosphate dihydrate in 800 ml H2Odd*
200 g	PFA
ca. 10 ml	Sodium hydroxide
	pass through paper filters
	ad 2 l H$_2$Odd, pH 7.4

4 % Paraformaldehyd

100ml	*PFA 20 %*
	ad 500 ml H$_2$Odd

10 x Phosphate Buffer 0.25M (400 ml)

5 N	*Hydrochloric acid (approximately 2 ml)*
15 g	NaOH
65 g	Sodium phosphate
	pH 7.2-7.4

30 % Saccharose Solution for Cryoprotection

15 g	*Sucrose*
	ad 50 ml 1 x PBS

Storing Solution for Free Floating Brain Tissue Sections

4 M	*Glycerol*
5.4 M	Ethylenglycol
25 mM	**Phosphate buffer pH 7.2-7.4**

5.6 Immuno-histochemistry/cytochemistry

10 x Phosphate Buffered Saline (PBS)

1.5 M	*Sodium chloride*
0.03 M	Potassium chloride
0.080 M	di-Sodium hydrogen phosphate dihydrate
0.010 M	Potassium dihydro-gen phosphate
	pH 7,5
	in 1l H$_2$Odd, pH 7.4

4 % Agarose Solution for Embedding of Vibratome Sections

4 %	*Agarose*
	in 1 x PBS

Blocking Solution for Brain Tissue Sections

0.5 %	*TritonX100*
10 %	goat or donkey se-rum
	in 1 x PBS

Blocking Solution (cells)

0.1 %	*TritonX100*
10 %	goat or donkey se-rum
	in 1 x PBS

Citric Acid Solution

2.1 g	*Citric acid monohydrate* **ad 1 l ddH$_2$O; pH 6**

4′,6-Diamidino-2-phenylindol (DAPI) Stock

10.9 mM	*DAPI, dilactate* **in H$_2$Odd**

Sodium Citrate Buffer 0,1 M

29.41 g	*sodium citrate* **ad 1l H$_2$Odd, pH 6.0**

Storing solution for Free Floating Brain Tissue Sections

4 M	*Glycerol*
5.4 M	Ethylenglycol
25 mM	**phosphate buffer pH 7.2-7.4**

5.7   Immunohistochemistry of Human Brain Tissue

Citric Acid Solution

10.5	*Citric acid monohydrate*
15.36	Sodium dihydrogen-phosphate
	ad 500 ml ddH$_2$O; pH 4.5

50 % Methanol Solution (10 ml)

5 ml	*Methanol*
333 µl	H_2O_2
4.66	**ddH$_2$O**

0.4 M PO_4 buffer

46 g	*Sodium dihydrogen-phosphate*
9.07 g	Sodium phosphat
	ad 1 l ddH$_2$O

DAB solution (25 ml)

12.5 mg	*DAB*
18.75 ml	H_2O_2
0.4 M PO$_4$ buffer	**6.25 ml**
250 µl	**H$_2$O$_2$ (1 %)**

Glycerin yelly for coating of glass slides

3 g	*Gelatin*
60 ml	dH_2O
	dissolve in beaker placed in waterbath
70 ml	**glycerin**
0.25 g	**phenol crystals**

Nickel/DAB Staining

0.4 ml	*Nickel-ammonium sulphate (1 %)*
10 ml	**DAB solution**
200 µl	**H$_2$O$_2$**
	incubate for about 10 min

5.8   Gallyas Impregnation for Myelin

Incubation Solution

1 g	*Ammonium nitrate*
1 g	Silver nitrate
	solve in 1 l H$_2$Odd
3 ml	**Sodium hydroxide (pH 7.4- 7.6)**

Physical Development Solution A

50 g	*Sodium carbonate*
	in 1 l H$_2$Odd

Physical Development Solution B

2 g	*Ammonium nitrate*
2 g	Silver nitrate
10 g	Silicotungstic acid
	in 1 l H$_2$Odd

Physical Development Solution C

2 g	*Ammonium nitrate*
2 g	Silver nitrate
10 g	Silicotungstic acid
7 ml	Formol (37 %)
	in 1 l H$_2$Odd

5.9   Cell Culture

5.9.1 Cell Culture Media and Components

Table 5- 4. List of Consumables and Media for Cell Culture:

Description	Company
B27	Gibco
basic fibroblast growth factor (FGF)	Gibco
Bovine serum albumin (BSA)	Sigma
DMEM/ F12 + GlutaMAX™	Gibco
DMEM/ F12	Gibco
D-Glucose (45%)	Sigma
Earle`s Balanced Salt Solution (EBSS)	Life Technologies
Hank's Balanced Salt Solution (HBSS)	Gibco
Hepes 1M	Gibco
Human epidermal growth factor (EGF)	Gibco
Hyaluronidase	Sigma
L-Glutamine 200mM	Gibco
Neurobasal A	Gibco
Penicillin/Streptomycin 100x	Gibco
poly-L-Lysine (PDL)	Sigma
Sucrose	Sigma
TripleLExpress	Gibco
Trypsin/ EDTA 0.05%	Gibco
Trypsin	**Sigma**

5.9.2 Solutions and Media

Solution 1 (HBSS-Glucose)

50 ml	*HBSS*
9 ml	D- Glucose
7.5 ml	Hepes (1 M)
	ad 0,5 l H$_2$Odd , pH 7.5

Dissociation Medium

10 ml	*Solution 1*
13,3 mg	Trypsin (Sigma)
7 mg	**Hyaluronidase**

Solution 2 (Sucrose-HBSS)

25 ml	*HBSS*
154 g	Sucrose
475 ml	H$_2$Odd,
	pH 7.5

Solution 3 (BSA-EBSS-Hepes)

20 g	*BSA*
10 ml	Hepes
490 ml	EBSS
	pH 7.5

Neurosphere Differentiation Medium

1 ml	*B27*
500 µl	Glutamate
500 µl	Hepes
48 ml	Neurobasal A
500 µl	**Penicillin/Streptomycin**

Neurosphere Medium

1 ml	*B27*
48 ml	DMEM/ F12
500 µl	Glutamate
8 mM	Hepes
100 units/ ml	Penicillin/ Streptomycin
10 µg/ ml	EGF
10 µg/ ml	**FGF**

6 Methods

6.1 Animals

6.1.1 Mouse Strains

All animal procedures were performed in accordance with the policies of the use of Animals and Humans in Neuroscience Research, revised and approved by the Society of Neuroscience and the state of Bavaria under licence number 55.2-1-54-2531-144-07 and 55.2.-1-54-2531-152-10.

The following mouse lines were used for experiments:

APPPS1, overexpresses the Swedish double mutation as well as a PS1 mutation under the neuronal promotor Thy1[316]

CAG-CAT-EGFP (refered to as **CAGGFP**) reporter mouse line, expressing the CMV-β-actin promoter and the loxP flanked chloramphenicol acetyl-transferase (CAT) gene upstream of the EGFP cassette[377]

CK/p25 mouse line, inducible overexpression (tetOFF) of the p25-GFP fusion protein under the control of the neuronal CAMKII promotor[323,364]

GLAST::CreERT2, expressing a Cre recombinase estrogen receptor fusion protein in the GLAST locus[378]

Olig2::CreER[TM] expresses a Cre recombinase estrogen receptor fusion protein in the Olig2 locus[115]

6.1.2 Genotyping

To maintain colonies of experimental mice, animals were tagged with numbered ear clips (0001-9999). Small tail biopsies of less than 0.5 mm length were taken to isolate the DNA. The tail pieces were transferred into a 1.5 ml

eppendorf tube and incubated in 500 µl lysis buffer, shaking at 55°C over night. After lysis, centrifugation at 10000 rpm for 5 minutes (min) resulted in sedimentation of tissue residues. The supernatant was transferred into a new 1.5 ml tube. Precipitation of DNA was achieved by addition of 0.5 ml isopropanol for 5 min and pelleted by centrifugation of 10 min for 10000 rpm. The supernatant was removed and the pellet was dried by turning the tube upside down for 1 hour (hr) at room temperature. Dissolving of the dried DNA was accomplished by addition of 200 µl 10 mM Tris buffer followed by 1-2 hrs shaking at 55 °C. The extracted DNA was kept at 4 °C until further processing. For PCRs 1-2 µl of DNA were mixed with 10 mM dNTPs in 30 µl reaction tubes. The final concentration of the primers was 10 pM in the reaction mix. The precise PCR conditions and reaction mixes are described in detail for each mouse line below. After the PCR, the reactions were mixed with loadingbuffer and loaded on a 2 % agarose gel (with 1 x TBS buffer), to detect the PCR products.

6.1.2.1   APPPS1

<u>APP-PCR</u>
Primer sequences:
APP (forward): GAA TTC CGA CAT GAC TCA GG
APP (reverse): GTT CTG CTG CAT CTT GGA CA
Reaction mix

2.5 µl	*10 x buffer (Quiagen)*
0.6 µl	dNTPs
0.5 µl	each Primer
0.3 µl	Taq Polymerase
19.1 µl	H$_2$O
1 µl	**DNA**

Cycling conditions (PCR program):

	95°C	4 min
34 x	95°C	45 sec
	58°C	45 sec
	72°C	45 sec
	72°C	5 min

Band size: about 270 basepairs

PS1-PCR

Primer sequences:

PS1 (forward) : CAG GTG CTA TAA GGT CAT CC

PS1 (reverse): ATC ACA GCC AAG ATG AGC CA

2.5 µl	*10x buffer (Quiagen)*
0.6 µl	dNTPs
0.5 µl	each Primer
1 µl	Taq Polymerase
18.4 µl	H_2O
1.5 µl	**DNA**

Cycling conditions (PCR program):

	94°C	5 min
35 x	94°C	45 sec
	58°C	45 sec
	72°C	45 sec
	72°C	10 min

Band size: about 270 basepairs

Due to cointegration of the APP and PS1 transgenes[316], for routine analysis genotyping for APP was performed. PS1 genotyping was conducted sporadically as an additional control.

6.1.2.2   CAGGFP (CAG-CAT-EGFP)

Primer sequences:

CAG-CAT-EGFP (forward) 5'-CTG CTA ACC ATG TTC ATG CC-3'
CAG-CAT-EGFP (reverse) 5'-GGT ACA TTG AGC AAC TGA CTG-3'

Reaction mix

2.5 µl	*10x buffer (uni)*
3.0 µl	Magnesium chloride (25mM)
0.5 µl	dNTPs
5 µl	Q-Solution (Qiagen)
1 µl	each Primer
0.5 µl	Taq Polymerase
10.5 µl	H$_2$O
1 µl	**DNA**

Cycling conditions (PCR program):

	94°C	5 min
29 x	94°C	30 sec
	55°C	30 sec
	72°C	1 min
	72°C	10 min

Band size: 350 basepairs

6.1.2.3   CK/p25

CK-PCR

Primer sequences:

tTA-JC6: 5'-GCT GCT TAA TGA GGT CGG-3'
tTa-HC6: 5'-CTC TGC ACC TTG GTG ATC-3'

Reaction mix:

2.5 µl	*PCR buffer (NEB)*
0.5 µl	dNTPs
1.8 µl	each Primer
0.4 µl	Taq Polymerase (NEB)
16 µl	H$_2$O
2 µl	**DNA**

Cycling conditions (PCR program):

	94°C	5 min
34 x	94°C	45 sec
	55°C	45 sec
	72°C	1 min
	72°C	1 min

Band size: 480 basepairs

ZEG-PCR for p25-GFP

Primer sequences:

ZEG (forward): 5'-TTC ACC TTG ATG CCG TTCT-3'

ZEG (reverse): 5'-GCC GCT ACC CCG ACC AC-3'

Reaction mix:

2.5 µl	*PCR buffer (uni)*
0.5 µl	*Magnesium chloride (25mM)*
0.5 µl	dNTPs
1 µl	each Primer
0.5 µl	Taq Polymerase
4 µl	Q- solution
14 µl	H_2O
1 µl	**DNA**

Cycling conditions (PCR program):

	94°C	5 min
34 x	94°C	45 sec
	55°C	45 sec
	72°C	1 min
	72°C	1 min

Band size: 400 basepairs

6.1.2.4   GLAST::CreERT2

The protocol for genotyping was adopted from Mori et al. [378]

Primer sequences:

Glast F8 (forward): 5'-GAG GCA CTT GGC TAG GCT CTG AGG A-3'

Glast R3 (reverse): 5'-GAG GAG ATC CTG ACC GAT CAG TTG G-3'

CER 1 (CreERT2 specific primer):

            5'-GGT GTA CGG TCA GTA AAT TGG ACA T-3'

Reaction mix:

2.5 µl	*10x buffer*
2.5 µl	Magnesium chloride (25mM)
0.5 µl	dNTPs
5 µl	Q-Solution (Qiagen)
1 µl	each Primer
0.5 µl	Taq Polymerase
9 µl	H_2O
2 µl	**DNA**

Cycling conditions (PCR program):

	94°C 2 min
35 x	94°C 20 sec
	55°C 20 sec
	72°C 30 sec
	72°C 5 min

Band size: wildtype 700 basepairs, Glast::CreERT2 recombinant: 400 base-

pairs

6.1.2.5   Olig2::CreER[TM]

The protocol for genotyping was adopted from[115].

Primer sequences:

Olig2 sense (forward)   5'-TCG AGA GCT TAG ATC ATC C-3'

Olig2 antisense (reverse)   5'-CAC CGC CGC CCA GTT TGT CC-3'

Olig2KICreER   5'-AGC ATT GCT GTC ACT GGG T-3'

Reaction mix

2.0 µl	*Magnesium chloride (25mM)*
2.5 µl	10 x buffer (uni)
0.6 µl	dNTPs
1 µl	each Primer
4 µl	Q-solution
0.5 µl	Taq Polymerase
11.4 µl	H$_2$O
1 µl	**DNA**

Cycling conditions (PCR program):

	94°C	9 sec
36 x	94°C	20 sec
	58°C	30 sec
	72°C	30 sec
	72°C	10 min

Band size: wildtype 247 basepairs, Olig2KICreER recombinant 367 base-pairs

6.1.3 Tamoxifen Administration

Tamoxifen was applied to mice which were older than 2 months of age either orally (p.o.; 3 times 250 µl) every second day or by intraperitonal injection daily 2 times for 5 consecutive days (100 µl; 1 mg per injection).

6.1.4 Doxycycline Administration

Doxycycline (0.05 %) was applied to CK/p25 mice via the drinking water containing 1.5 % succrose until 6 weeks of age. Mice received doxycyline prenatally through application of doxycycline water already to matings or later via the milk of the mother. Doxycycline is light sensitive, therefore, it was applied

in bottles impervious to light and was additionally exchanged 3 times a week. Doxycycline drinking water was finally exchanged with normal drinking water after 2 or 5 weeks, to achieve overexpression of p25-GFP.

6.1.5 BrdU Labelling

The DNA-base-analogue 5-Bromo-2′-deoxy-Uridine (BrdU) was applied to the animals for 1 or 2 weeks to the drinking water at a concentration of 1 mg/ml. 1 % sucrose was added and stirred for at least 1 hr at room temperature. Every 3rd day BrdU drinking water was exchanged and the bottles containing BrdU water were protected from light. The BrdU solution was stored in the fridge for maximal 1 week.

6.1.6 Anesthesia

To anesthetize the mice for perfusion an anesthesia solution was prepared. 1 ml ketamin (10 %) were mixed with 0.25 ml xylazine hydrochloride (2 %) and 2.5 ml saline (0.9 %). The injection of the anesthesia was performed intraperitoneally with an insulin syringe and the volume of the injection depended on the animal's weight, since 5 µl per 1 g were injected. Afterwards, the animals reflexes (e.g. eye blink reflex and the reflex after pinching the hindpaw) were checked until they disappeared. In case of an unsufficient anesthesia an additional amount of about 20 µl anesthesia solution was injected intraperitonally.

For stab wound injuries another anesthesia solution was prepared for intraperitoneal injection. 300µl of a mixture of 0.5 mg/kg Medetomidin with 5 mg/kg Midazolam and 0.05 mg/kg Fentanyl were injected. To wake animals up after the operation 250 µl of an antisedate were applied intraperitoneally (2.5 mg/kg antisedan with 0.5 mg/kg flumacenil and 1.2 mg/kg naloxone).

6.1.7 MCAO – A Mouse Model of Stroke

These mice were used and analyzed in collaboration with Dr. Christophe Heinrich and Steffen Tiedt from my lab and Prof. Dr. med. Martin Dichgans. The MCAO lesion was performed in the lab of Martin Dichgans.

The protocol was performed as described in Vosko et al. (2006). In short, mice were anesthetized by isoflurane inhalation. Initial anesthesia contained 5 % isoflurane (< 1 min) and 2 % isoflurane in a mixture of 70%/30% of N_2O/O_2 were used to maintain it. The body temperature was keept between 37 °C and 38 °C with a DC temperature regulation system (FHA, Bowdoin, USA). After successful anesthesia, a fiberoptic probe (Perimed, Järfäla, Sweden) was placed over the MCA territory + 2 mm posterior and + 6 mm lateral to bregma, while the regional cerebral blood flow (rCBF) was controlled with a laser Doppler flowmetry (Perimed, Järfäla, Sweden). Focal cerebral ischemia was induced by occlusion of the middle carotid artery (MCA). After ventral midline neck incision, the left common and external carotid arteries were ligated utilizing an intraluminal filament. The internal carotid artery (ICA) was temporarily clipped with a microvascular clip (Aesculap, Germany). A silicon-coated 8-0 nylon monofilament (Ethicon, Johnson & Johnson, Belgium) was gently advanced into the ICA until resistance was felt. Successful occlusion of the MCA reduced the rCBF baseline by > 70 %. After ischemic induction, laser Doppler probes were removed, and the mice returned to their cages, where they woke up. During the 1 to 2 hrs of ischemia, mice were placed in a cage in the incubator (Babytherm 4200, Drägerwerk AG Lübeck, Germany) to keep the body temperature stable. After 1-2 hrs the animals were anesthetized again and the filament was removed. Animal care and all experimental procedures were performed in accordance to the German and National Institutes of Health animal legislation guidelines and were approved by the local animal care and use committees[379].

6.1.8 Stab Wound Mouse Model

Another mouse model utilized in this study as an acute lesion paradigm is the stab wound. To perform a stab wound lesion, the animals were first anesthe-

tized with the opoid anaesthesia. After all reflexes disappeared the mice were placed in a sterotactic apparatus. The skin above the scull was cut with a razor blade and then turned in a way that the skull above the brain becomes accessible. A unilateral small hole located behind bregma but before lambda was then drilled with a dental drill through the skull, while leaving the meninges intact. Afterwards, the somatosensory cortical grey matter was scratched with a V-Lance[TM] knife. The scratch was 0.5 to 0.6 mm deep and 1 to 2 mm long and did not touch the white matter. After stab wound, the animals were removed from the stereotactic apparatus and the skin incision was stiched. Stab wound lesion results in a rapid onset of glial reaction, rupture of the blood brain barrier and cell death in the lesion area. These mice are used in collaboration with Dr. Swetlana Sirko in my lab.

6.2   Electron Microscopy

The animals were deeply anesthetized with ketamin/xylazine and perfused with the Karnovski-fixative (see solutions electron microscopy). The perfusion was performed with high pressure and 200 ml fixative were used per animal. Afterwards, the brains were dissected and post-fixed over night at 4 °C in the same fixative. Then, the brains were transferred into the storing solution and kept at 4 °C until further processing. Prior to cutting, brains were washed in washing solution over night at 4 °C. Coronal vibratome sections were then cut at the vibratome at a thickness of 500-600 μm. Small pices of the area of interest (grey matter and white matter including the corpus callosum) were carefully dissected using a razor blade. The following osmication was performed in the dark by adding the osmication solution for 2 hrs to the specimen in a small glass ware. Importantly, the incubation was conducted on a metal plate, which has been cooled down to -20°C before the experiment was started. Glutaraldehyd, which was used for the perfusion is a fixative to preserve structures, however it does not stabilize lipids, the major component of myelin, sufficiently. Therefore, osmium was needed for lipid stabilization. Osmium reacts as oxidant mainly with unsatured lipids thereby labelling lipid rich structures, such as myelin, since it renders the tissue black in its reduced state[575]. After osmication, sections were transferred to a 24-well-plate and

were washed in 0.1 M cacodylat for 20 min. A graded series of ethanol for hydration of the tissue samples followed. Every 20 minutes the sections were transferred into the next ethanol solution (70 %, 80 %, 90 %, 96 %, 100 %, and 100 %). Finally, sections were transferred again into glass vials to wash them in propylenoxide for 30 min. Incubation in a 1:1 mixture of araldid in propylenoxide was carried out over night at 4 °C thereafter. In the last step the sections were embedded in araldit epoxy using an araldit epoxy embedding kit (Fluka) according to the manufacturer's protocol. Polymerization of the araldid epoxy was achieved at 60 °C for 2 days. The araldit blocks were sent to the LMU Anatomy Institute for contrasting and cutting semi-and ultrathin sections. Semithin cross-sections of 0.5 µm in thickness were cut for light microscopy inspection, whereas ultrathin sections of 65-85 nm were cut for electron microscopy analysis. Grids were then analyzed at a transmission electron microscope belonging to the LMU Anatomy Institute.

6.2.1   Quantification of Myelin Integrity

Pictures were taken randomly in the white matter at 11440 x for quantification at the electron microscope. Analysis of the pictures took place by two independent persons, namely Dr. Leda Dimou and myself. Myelin aberrations were classified according to Peters et al. (2000) and Thurnherr et al. (2006):

a) An axon surrounded by two myelin sheaths, separated by a space

b) Excess cytoplasm in the inner loop

c) Degenerated sheaths

d) Balooned myelin

e) Abnormal myelin outfoldings– these are areas of the

   internode where the myelin sheath protruded away from the axon surface

or

f) Other myelin aberrations

6.3   Western Blot

6.3.1   Tissue Lysis

Brain tissue containing cortical grey and white matter as well as the hippo-campus was dissected in HBSS medium. Then the tissue pieces of interest were collected in a 1.5 ml eppendorf tube, immediately frozen in liquid nitrogen and stored at -80 °C until further processing. After defrosting at 4 °C, 500 µl of lyses buffer (solutions western blot) were added and then the mixture of tissue and buffer was transfered into a dounce tissue grinder. By moving the tight pestle up and down 10-15 times, the tissue was homogenisated. Then, the homogenat was transferred into a 1.5 ml eppendorf tube and pulse soni-ficated for 5 seconds at 10 % intensity. Afterwards, an incubation at 4 °C (on ice) for 15 minutes followed. Then the lysate was centrifuged at 4 °C and 10000 g for 15 min. The supernatant was collected and stored at -80 °C until further processing.

6.3.2   Gel Preparation

After mixing the ingredients needed for the adequate percentage of the run-ning gel (see solutions western blot) the solution was quickly poured into the gel casting form, while space for the stacking gel was left. The top of the run-ning gel layer was loaded with water saturated isopropanol to remove bub-bles. After the gel fully polymerized, isopropanol was washed out with aqua dest. and the freshly prepared stacking gel solution was added on top. Then a comb was placed in the stacking gel. After its polymerization the complete gel was transferred into the electrophoresis chamber, which was filled with 1 x Elpho buffer, and the comb was removed.

6.3.3 Sample Preparation

The amount of protein was measured using the BCA assay, a colorimetric assay, according to manufacturer's protocol. It is based on the so called Biuret reaction, where, under alkaline conditions, substances containing two or more peptide bonds form a purple complex with copper salts in the reagent. More specifically, it involves the reduction of Cu^2+ (copper) to Cu+ by peptide bonds of proteins. The BC Assay (bicinchoninic acid) chelates Cu+ ions with very high specificity to form a water soluble purple coloured complex.

The reagent B from the BC Assay kit was diluted 1:50 in reagent A, which results in a green solution. 10 µl lysate were mixed to 1 ml of the solution for 30 min at 37°C. As the protein standard, samples with different bovine serum albumin (BSA) amounts were also mixed with the solution. Afterwards, the absorption of the BSA standards, measured with a spectrometer, generated a standard curve, which was used to measure the concentration of the protein lysate samples. According to the protein amount, the probes were adjusted to an amount of 30 µg with aqua dest. After addition of the 4 x loading buffer, samples were boiled for 5 minutes at 95 °C, without shaking. Then the samples were transferred to 4 °C on ice for another 5 minutes before they were loaded in the gel. Then a voltage of 80 V was applied, until the samples traveled through the stacking gel. When the samples entered the running gel, the voltage was increased up to 120 V. In order for the proteins to migrate through the gel they are first negatively charged by exposure to the detergent sodium dodecyl sulfate (SDS). The amount of bound SDS is relative to the size of the protein, and the proteins have a similar charge to mass ratio. Therefore, they migrate according to their size and can be separated within the gel. Smaller proteins migrate faster than bigger ones. As the concentration of acrylamide determines the resolution of the gel, 12 % acrylamid were used for the running gel, to obtain a good resolution of lower molecular weight proteins.

6.3.4 Transfer

In order to make the proteins accessible to antibody detection, they are moved from the gel onto a membrane. An electric current is applied to the gel and the proteins migrate out of the gel onto the membrane. PVDF-membranes (Millipore) were incubated prior to the blotting for 10 min in methanol and then another 10 min in transfer buffer. For the "'semi-dry'" blotting method, membranes and filter papers (Whatman-3MMChromatography papers) were cut to the exact size of the gel. Also, the filter papers were kept in transfer buffer prior to the transfer. Now the following order was used to prepare for the transfer:

1. Anode
2. Filter paper
3. PVDF membrane
4. Gel
5. Filter paper
6. Kathode

The transfer was conducted for 40 min with constant voltage of 15V.

6.3.5 Signal Detection

Proteins of interest were visualized using immunostaining. Therefore, the membranes were blocked for 1 hour with 5 % milk powder in TBS. Then they were probed with the respective antibody over night at 4 °C. The antibodies used include: anti-CNPase (mouse, 1:1000, Sigma); anti-NF70 (mouse, 1:1000, Chemicon); For protein loading control, membranes were reprobed with mouse anti-Gapdh (Glyceraldehyde 3-phosphate dehydrogenase) antibody (mouse, 1:7500, abcam). The detection was performed with the Licor scanning system. The secondary antibodies were coupled to near infrared fluorescent dyes. Membranes were incubated with these secondary antibodies (1:15000 in TBST) for 2 hours at room temperature. Western blots were replicated at least 2 times for quantification. For quantification the Odyssey V3.0 software was employed to calculate the pixels of each band by substraction of the background signal. A minimum of 2 blots were performed for 1 tissue sample and 1 tissue sample equals 1 animal. Quantification was per-

formed for all obtained data points using the one sample t –test seperately for each column, where the hypothetical value was set at 100.

6.4 Test for Integrity of the Blood Brain Barrier

First the mice were anesthesized and then a stab wound was performed in one hemisphere, which served as a positive control. Afterwards, a flourescent dextran with a molecular size of 3000 Da (5mg/ml dissolved in saline) was injected into the tail vein. 15 minutes after the injection, animals were sacrificed by cervical dislocation. After the careful dissection of the brain, it was frozen on a metal plate which was located on dry ice. The brains were then stored at -20 °C until they were cut at a cryostat at a thickness of 16 µm. The slides containing sections of interest were then defrosted at room temperature, rinsed with 1 x PBS and fixed for 20 min with 4 % PFA. After an additional intensive washing step in 1 x PBS, the sections were dried and finally coversliped with AquaPolymount. The blood brain barrier integrity was analyzed using a microscope.

6.5   Immuno/cyto-histochemistry

6.5.1 Perfusion

Animals were deeply anethesised using ketamin/xylazine. Transcardial perfusion was first performed with 1 x PBS for approximately 3 minutes, followed by 4 % PFA for 25 minutes. After careful preparation of the brains, these were post-fixed in 4 % PFA for another 5 minutes and cryoprotected by incubation in 30 % succrose solution until the brains saturated (usually 12 hours at 4 °C). Brains were kept in this solution until free floating sections were made (maximal 5 days of storage). For vibratome sectioning the cryopotection-step was omitted. Rather the brains were kept in PBS until embedding in 4 % agarose solution until further processing.

6.5.2 Brain Sectioning

For free floating sections, brains were cut at the cryostat at a thickness of 30 µm. Vibratome sections on the contrary were cut at the vibratome at a thickness of 50 µm. Free floating as well as vibratome sections were stored at -20 °C in a 1.5 ml tube filled with 1 ml storing solution until immunohistochemistry.

6.5.3 Immunohistochemistry

Primary antibodies (for details see table 7- 1) were incubated with specimen overnight at 4 °C blocking solution. Afterwards, brain sections were washed 3 times with 1 x PBS. Incubation with the secondary antibody directed against the host of the primary antibody, was performed in blocking solution containing DAPI (1:1000) for 1 hour at room temperature. After careful rinsing in 1 x PBS, sections were placed by the use of brushes on glass slides and dried and embedded with Aqua Polymount. Stained sections were then analyzed either at the light or confocal microscope.

For BrdU and Olig2 staining a pretreatment to better access proteins or DNA in the cell nucleus was necessary. Before staining, the sections were transferred into 1 x sodium citrate buffer and kept shaking at 96 °C for 20 minutes. Afterwards, sections were rinsed carefully 3 times for 10 minutes in 1 x PBS until incubation with the primary antibody. Double-labelling was performed by staining first with the antibody not requiring pre-treatment. After a short fixation of the first staining 5-10 minutes in 4 % PFA, pre-treatment for BrdU or Olig2 was started. Other antibodies required an amplification using as a first secondary a biotinylated antibody and then an amplification with streptavidin488 or streptavidin594. Another method to amplify the signal from the biotynilated secondary antibody was achieved by using the Thyramid kit (Perkin Elmar Life Science). Some antibodies had a better and more specific signal when the subtype specific secondary was used. All special treatments are indicated in the primary antibody list.

Table 6- 1. List of Primary Antibodies (unless otherwise indicated for immu-
nohistochemistry):

Recognized Antigene	Host	Dilution	Special Treatment	Company (Order number)
473HD	Rat IgG	1:100	No Triton	Kindly provided by Andreas Faissner
6E10	Mouse IgG1	1:200		Millipore (MAB1560)
Amyloid beta (1-14)	Rabbit IgG	1:200		Acris (BP2185)
BrdU	Rat IgG2a	1:200	Boiling; evtl. biotinylated Secondary	Biozol (OPT0030)
βIIItubulin	Mouse IgG2b	1:200	subtype specific secondary	Sigma (T8600)
Activated Caspase 3	Rabbit IgG	1:100	Thyramid Kit	Promega (G7481)
Cux1	Rabbit IgG	1:100		Sigma (C5922)
GFAP	Mouse IgG1	1:1000		Sigma (G3898)
GFAP	Rabbit IgG	1:1000		DAKO (Z0334)
GFP	Chick IgG	1:500		Abcam (139070)
GSTpi	Mouse IgG1	1:500	subtype specific secondary	BD Bioscience (610718)
Iba1	Rabbit IgG	1:500		WAKO (01919741)
MAG	Mouse IgG	1:100		Millipore (ST1684)
Nestin	Mouse IgG1	1:100	subtype specific secondary	Millipore (MAB377)

NeuN	Mouse IgG1	1:100	subtype specific secondary	Millipore (AB5922)
NF70	Mouse IgG1	1:100	immunostaining	Millipore (MAB1615)
NG2	Rabbit	1:200		Chemicon (AB5320)
Olig2	Rabbit	1:500	boiling	Chemicon (AB9610)
S100b	Mouse IgG IgG1	1:500		Sigma (S2532)
S100b	Rabbit	1:100		Sigma (S2644)
TNC	Rabbit	1:100	No Trition	Kindly provided by Andreas Faissner

For Westernblot Signal Detection

CNPase	Mouse IgG1	1:1000	western blot	Sigma (C5922)
Gapdh	Mouse IgG	1:7500	western blot	Abcam (ab8245)
NF70	**Mouse IgG1**	**1:1000**	**western blot**	**Millipore (MAB1615)**

Table 6- 2. List of Secondary Antibodies:

Antibody	*Host*	*Label*	*Dilution*	*Company*
Anti-chick	Donkey	FITC	1:200	Dianova (106166003)
	Goat	Alexa488	1:500	Invitrogen (A11039)
Anti-rat	Donkey	Alexa488	1:500	Invitrogen (A21208)
		Alexa594	1:500	Invitrogen (A21209)
	Goat	Cy3	1:500	Dianova (112165167)

	Rabbit	biotinylated	1:200	Vector (BA-4001)
Anti-rabbit	Donkey	Alexa488	1:500	Invitrogen (A21206)
		Alexa594	1:500	Invitrogen (21207)
		Cy3	1:500	Dianova (711165152)
	Goat	Cy3	1:500	Dianova (111165144)
		biotinylated	1:200	Vector (BA-1000)
Anti-mouse IgG1	Goat	Alexa488	1:500	Invitrogen (A21121)
		Alexa594	1:500	Invitrogen (21125)
		biotinylated	1:200	Biozol (1070-08)
Anti-mouse IgG2b	Goat	TRITC	1:200	Biozol (1090-03
Anti-mouse IgG	Goat	Alexa488	1:500	Invitrogen (A11029)
		Cy3	1:500	Dianova (115165166)
		Cy5	1:500	Dianova (115176072)
	Donkey	Alexa594	1:500	Invitrogen (A-21203)
Streptavidin				
	Goat	Alexa647	1:500	Invitrogen (S21374)
		Alexa555	1:500	Invitrogen (S21381)
For Western Blot Signal Detection				
Anti-mouse	Goat	IRDye 500	1:15000	Li-Cor 926-68020
Anti-rabbit	Goat	IRDye 800	1:15000	Li-Cor 926-32211

6.5.4 Analysis of Immunostainings

Stainings were analyzed at the Zeiss LSM700 confocal microscope with optical sections of maximum 0.5-2 µm intervals. Pictures were taken with a z-stack between 6-8 µm. Afterwards, pictures were saved as tiffs. The area of interest was measured and cells were quantified using Image J. In sections quantified at the light microscope, cell numbers or overlays were counted flipping fast between channels, to verify them. Statistical analysis was performed with the Graph Pad Prism program. Quantification of immunolabelled cells was determined in sections from more than 3 animals and tested for normal distribution using then either the unpaired Student's t-test or Mann-Whitney test (* $p < 0.05$; ** $p < 0.01$; *** $p < 0.001$). Significant changes are indicated in the diagram bars.

6.6 Immunostaining of Human Brain Tissue

6.6.1 Brain Tissue

The analysis of human brain tissue samples were conducted in collaboration with Dr. Kristin Baer from the Institute of Neuroscience and Molecular Psychiatry, Swansea University. The human brain tissue for this study was obtained from the Neurological Foundation of New Zealand Human Brain Bank (Department of Anatomy with Radiology, University of Auckland). The University of Auckland Human Participants Ethics Committee approved the protocols used in this study, and all tissue was obtained with full consent of the families. Brain tissue was obtained from 8 neurologically normal cases, with no history of neurological disease and no evidence of neuropathology and from 8 Alzheimer's Disease cases. The average age was 73 years with an age range of 35-85 years. The cases had a post-mortem interval between 2

and 36 hrs after death (mean post-mortem interval 14.75 hrs) and included 8 female and 8 males.

Table 6- 3. Human Brain Tissue Samples:

Case	Age (years)	Sex	Postmortem Delay (hours)	Diagnosis
H123	78	f	7.5	Control - Rupt. Aortic aneurysm
H126	35	f	10	Control - Suicide - hanging
H136	75	m	13	Control - Rupt. Aorta, abdom. aneurysm
H137	77	m	12	Control - Coronary artherosclerosis
H150	78	m	11	Control - Rupt. Myocardial infarction
H191	77	m	20	Control
H192	65	f	24	Control
H193	71	m	23	Control
AZ32	75	f	3	Alzheimer's Dementia (mild)
AZ34	74	f	18	Alzheimer's Dementia (moderate-definite)
AZ52	68	f	36	Alzheimer's Dementia (severe)
AZ53	85	f	2	Alzheimer's Dementia (probable) – Bronchial pneumonia
AZ57	82	m	14.5	Alzheimer's Dementia (possible) – Bronchial pneumonia
AZ58	75	m	20	Alzheimer's Dementia (severe)
AZ59	83	m	15	Alzheimer's Dementia (mild) Cardiopulm collapse
AZ72	70	f	7	Alzheimer's Dementia

6.6.2 Immunohistochemical procedures

The following preparation was conducted as previously described[576] in the Department of Anatomy with Radiology, University of Auckland. The human brains were fixed by perfusion through the vertebral and internal carotid arteries, first with phosphate-buffered saline (PBS) with 1% sodium nitrite, followed by 15% formalin in 0.1M phosphate buffer, pH 7.4. After perfusion, blocks from the cerebral cortex were carefully dissected and kept in the same fixative for 24 hours. The tissue blocks were cryoprotected in 20% sucrose in 0.1 M phosphate buffer with 0.1% Sodium azide (Sigma) for 2-3 days, and then in 30% sucrose in 0.1 M phosphate buffer with 0.1% Sodium azide for a further 2-3 days. The blocks were sectioned on a freezing microtome at 50 µm and the sections stored in PBS with 0.1% sodium azide (PBS-azide) until use.

6.6.3 Single Immunoperoxidase Labelling

The following procedure was conducted in the Institute of Neuroscience and Molecular Psychiatry, Swansea University. Free-floating brain sections were transferred into 6-well tissue culture plates and washed in PBS containing 0.2% Triton-X (PBS-triton) and pretreated for antigen retrieval. Therefore, the sections were incubated overnight in 0.1 M sodium citrate buffer, pH 4.5, transferred into 10 ml of fresh sodium citrate buffer solution, microwaved in a 650 W microwave oven for 30 seconds and allowed to cool before washing (3 x 15 minutes) in PBS-triton. The sections were then incubated for 20 minutes in 50 % methanol and 1 % H_2O_2. After washing (3 x 15 minutes) in PBS-triton, the sections were incubated in the primary antibody (polyclonal rabbit anti-Olig2 antibody; 1:500; Santa Cruz (sc-48817)) for 2-3 days on a shaker at 4°C. Then the primary antibody was washed off (3 x 15 minutes, PBS-triton) and the sections incubated overnight in species-specific biotinylated secondary antibodies (diluted 1:500; sheep anti-rabbit; Chemicon, USA). Afterwards the secondary antibody was washed off (3 x 15 minutes, PBS-triton) and the sections were incubated for 4 hours at room temperature in ABC solution diluted at 1:250 (Vectastain). The sections were reacted in 0.05 % 3,3-diaminobenzidine tetrahydrochloride (DAB; Sigma) and 0.01% H_2O_2 in 0.1 M

phosphate buffer, pH 7.4, for 15-30 minutes to produce a brown reaction product. A nickel-intensified procedure was also used in which 0.4 % nickel ammonium sulphate was added to the DAB solution to produce a blue-black reaction product[577]. The sections were washed in PBS, mounted from gelatine solution onto glass slides, rinsed in distilled water, dehydrated, and coverslipped with DPX (BDH, Poole, UK). Control sections were routinely processed to determine nonspecific staining using the same immunohistochemical procedures detailed above except that the primary antibody was omitted from the procedure.

6.6.4 Analysis

Single immunoperoxidase labeled sections were examined by light microscopy using a Zeiss Axioscope. Digital images were captured and contrast optimised using ImageJ software (NIH) and quantitative observations were recorded. Statistical analysis was carried out using Excel and Minitab software.

Three independent rounds of staining were carried out, each time using one brain section from 3-5 healthy control brains and from 3-5 AD brains. Per brain section, using the 4x magnification, a minimum of 3 digital pictures was captured from the white matter and from the grey matter. The digital pictures were coded and the quantification (count of Olig2 immunoreactivity positive nuclei) was carried out using ImageJ software (NIH). The sections were analyzed with the Mann-Whitney test (* $p < 0.05$; ** $p < 0.01$; *** $p < 0.001$). Significant changes are indicated in the diagram bars.

6.7   Gallyas Silver Impregnation

First, the brain sections were mounted on superfrost microscopic glass slides. After drying, the sections were left for 5 minutes in aqua dest. Then an incubation of 30 minutes in pyridine (200 ml) mixed with acetic acid anhydrid (100 ml) followed. After washing for 10 minutes in aqua dest., including changing the water 2 times, the tissue specimen was incubated at 30 °C for

45-50 minutes in pre-warmed incubation solution (see material). The incubation solution was rinsed off for 3 x 5 minutes with acetic acid (0.5 %). For the physical development first 70 ml solution B and then 30 ml solution C were added slowly upon stirring to 100 ml solution A. Physical development took place in this solution for 3-15 minutes. Afterwards, the slides were washed 3 x 5 minutes with acetic acid (1 %). After a short wash in aqua dest., slides were then incubated for 5 minutes in sodium thiolsulfate (2 %). Finally, a washing step for 3 x 5 minutes in aqua dest. was conducted. After passing the slides through an increasing ethanol chain (70 %, 80 %, 90 %, 95 %, 100 % each solution 10 minutes) slides were incubated in xylol for 10 minutes and then coversliped with DPX mounting medium. The method for the gallyas silver impregnation is based on the principle that myelin can bind colloidal silver particles in a 0.1% ammonical silver nitrate solution of pH 7.5. The production of metallic silver by other tissue elements is suppressed by the sections pre-treated with 2:1 mixture of pyridine an d acetic anhydride for 30 minutes. The collodial silver particles bound in the myelin are enlarged to microscopic dimensions by a special physical developer[381,382].

6.8   Neurosphere Assay

6.8.1 Dissection

Mice were shortly euthanized by asphyxiation in CO_2 and then killed by cervical dislocation. The brain was removed and transferred into a petridish containing HBSS with 10 mM Hepes. As a postive control, the lateral wall of the lateral ventricle was isolated and kept in a 1.5 ml tube filled with 500 µl Solution 1 on ice until further processing. For detection of the stem cell capacity of reactive tissue a defined volume of the lesioned and non-lesioned areas of the acute injured cerebral cortex (Stab wound, MCAO) or the corresponding anatomical areas of APPPS1 and Ck/p25 mice were punched out using a "stanze" after removal of meninges. The remaining white matter was then carefully removed using forceps. The collected tissue was stored in a 1.5 ml tube containing 500 µl solution 1 on ice until further processing.

6.8.2 Preparation

After the dissection, the dissociation medium was freshly prepared and filter sterilized. The dissected tissue pieces were gently pipetted up and down with a blue pipette. Then, 500 µl of dissociation medium was added to the tube containing the dissected tissue as well as 500 µl of solution 1. The tubes were incubated for 20 minutes at 37 °C. Afterwards, the enzyme activity was stopped by adding 1 volume ice cold solution 3, meanwhile pipetting up and down again with a blue pipette tip. The pellet was re-suspended in 1 ml pre-warmed neurosphere medium. A centrifugation step of 5 minutes at 1500 rpm followed. The pellet was again re-suspended in 1 ml neurosphere medium. The suspension was carefully pipetted through a 70 µm filter on top of 8 ml ice-cold solution 2 in a 15 ml tube. Another centrifugation step at 2000 rpm for 20 minutes was performed. The pellet was re-suspended in 1 ml pre-warmed neurosphere medium. Cells were plated at a density of 3000 cells per 600 µl per well in a 24-well-plate. EGF as well as FGF was added in a concentration of 20 ng/ml. The number of neurospheres were counted after 2 weeks in culture using the microscope Axiovert 40CFL (Zeiss).

6.8.3 Passaging of Neurospheres

Neurospheres were collected in a 15 ml falcon tube and Trypsin-EDTA wa-sadded to a final concentration of 0.01 % (diluted 1:5). Then the tube was incubated for 3 minutes at 37 °C. After addition of an equal amount of solution 3 to stop the reaction a single cell suspension was generated from the neurospheres pipetting up and down. Centrifugation at 700-800 rpm for 5 min was used to pellet the cells. Then, the cells were re-suspended in pre-warmed neurosphere medium and plated at clonal density of 3000 cells per 600 µl (5 cells per 1 µl) medium per well in a 24-well-plate. The number of neuropheres was quantified after 7 days.

6.8.4 Differentiation of Neurospheres

First neurospheres were picked in a very small volume with a yellow pipette and carefully plated on poly-D-lysine (PDL) coated coverslips in a 24-well-plate in differentiation medium (without growth factors). Then the plate was kept for approximately 3 hours in the incubator at 37 °C. After the neurospheres have settled down, 1 ml fresh neurosphere medium, without growth factors was added. The next day the medium was changed and the differentiation medium was added. After 7-10 days the medium was removed and the neurospheres were fixed for 5 minutes with 4 % PFA.

Bibliography

1.   Altman, J. Autoradiographic and histological studies of postnatal neurogenesis. IV. Cell proliferation and migration in the anterior forebrain, with special reference to persisting neurogenesis in the olfactory bulb. *J Comp Neurol* **137**, 433-457 (1969).

2.   Altman, J. & Das, G.D. Autoradiographic and histological studies of postnatal neurogenesis. I. A longitudinal investigation of the kinetics, migration and transformation of cells incorporating tritiated thymidine in neonate rats, with special reference to postnatal neurogenesis in some brain regions. *J Comp Neurol* **126**, 337-389 (1966).

3.   Doetsch, F., Caille, I., Lim, D.A., Garcia-Verdugo, J.M. & Alvarez-Buylla, A. Subventricular zone astrocytes are neural stem cells in the adult mammalian brain. *Cell* **97**, 703-716 (1999).

4.   Seri, B., Garcia-Verdugo, J.M., McEwen, B.S. & Alvarez-Buylla, A. Astrocytes give rise to new neurons in the adult mammalian hippocampus. *J Neurosci* **21**, 7153-7160 (2001).

5.   Kriegstein, A. & Alvarez-Buylla, A. The Glial Nature of Embryonic and Adult Neural Stem Cells. *Annual Review of Neuroscience* **32**, 149-184 (2009).

6.   Ninkovic, J. & Gotz, M. Signaling in adult neurogenesis: from stem cell niche to neuronal networks. *Curr Opin Neurobiol* **17**, 338-344 (2007).

7.   Schleiden, M.J. Beiträge zur Phytogenesis. *Archiv für Anatomie, Physiologie und wissenschaftliche Medizin*, pp. 137-176 (1838).

8.   Schwann, T. *Mikroskopische Untersuchungen über die Übereinstimmung der Struktur und dem Wachstum der Tiere und Pflanzen.*, (Sanderschen Buchhandlung, Berlin, 1839).

9.   Schwann, T. & Schleiden, M.J. *Microscopical Researchers into the Accordance in the Structure and Growth of Animals and Plants.*, (Sydenham Society London, 1847).

10.   Virchow, R. Cellularpathologie. *Virchows Archiv für Pathologie und Anatomie und für klinische Medizin.* **8**, 3-39 (1855).

11.   Virchow, R. *Cellularpathologie und ihre Begründung auf Physiologische Gewebelehre*, (Verlag von August Hirschwald, Berlin, 1858).

12.   Somjen, G.G. Nervenkitt: notes on the history of the concept of neuroglia. *Glia* **1**, 2-9 (1988).

13.   Müller, H. Zur Histologie der Netzhaut. *Zeitschrift für Wissenschaftliche Zoologie* **3**, 234-237 (1851).

14.   Lenhossek, M.v. *Der feinere Bau des Nervensystems im Lichte neuster Forschung*, (Fischer's Medizinische Buchhandlung H. Kornfield, Herne/Berlin, 1893).

15.   Lenhossek, M.v. Zur Kenntnis der Neuroglia des menschlichen Rückenmarks *Verhandlungen der Anatomischen Gesellschaft* **5**, 193-221 (1891).

16.   Andriezen, W.L. The Neuroglia Elements in the Human Brain. *Br Med J* **2**, 227-230 (1893).

17.   del Rio-Hortega, P. The microglia. *Lancet* **1**, 1023-1026 (1939).

18.   Del Rio-Hortega, P. El 'tercer elemento' de los centros nerviosos. *Biol. Soc. Esp. Biol.* **9**, 69-129 (1919).

19.   Penfield, W. A method of staining oligodendroglia and microglia (combined method). *American Journal of Pathology* **4**, 153-157 (1928).

20.   Reyners, H., Gianfelici de Reyners, E. & Maisin, J.R. The beta astro-cyte: a newly recognized radiosensitive glial cell type in the cerebral cortex. *J Neurocytol* **11**, 967-983 (1982).

21.   Stallcup, W.B. The NG2 proteoglycan: past insights and future pros-pects. *J Neurocytol* **31**, 423-435 (2002).

22.   Levine, J.M., Beasley, L. & Stallcup, W.B. Localization of a neurecto-derm-associated cell surface antigen in the developing and adult rat. *Brain Res* **392**, 211-222 (1986).

23.   Berry, M., Hubbard, P. & Butt, A.M. Cytology and lineage of NG2-positive glia. *J Neurocytol* **31**, 457-467 (2002).

24.   Butt, A.M., Kiff, J., Hubbard, P. & Berry, M. Synantocytes: new func-tions for novel NG2 expressing glia. *J Neurocytol* **31**, 551-565 (2002).

25.   Guillery, R.W. Observations of synaptic structures: origins of the neu-ron doctrine and its current status. *Philos Trans R Soc Lond B Biol Sci* **360**, 1281-1307 (2005).

26.   Greene, N.D. & Copp, A.J. Development of the vertebrate central nervous system: formation of the neural tube. *Prenat Diagn* **29**, 303-311 (2009).

27.   Williams, B.P. & Price, J. Evidence for multiple precursor cell types in the embryonic rat cerebral cortex. *Neuron* **14**, 1181-1188 (1995).

28.   Noctor, S.C., Flint, A.C., Weissman, T.A., Dammerman, R.S. & Krieg-stein, A.R. Neurons derived from radial glial cells establish radial units in neocortex. *Nature* **409**, 714-720 (2001).

29.   Malatesta, P.*, et al.* Neuronal or glial progeny: regional differences in radial glia fate. *Neuron* **37**, 751-764 (2003).

30.   Rakic, P. Guidance of neurons migrating to the fetal monkey neocor-tex. *Brain Res* **33**, 471-476 (1971).

31.   Bentivoglio, M. & Mazzarello, P. The history of radial glia. *Brain Res Bull* **49**, 305-315 (1999).

32.   Aaku-Saraste, E., Oback, B., Hellwig, A. & Huttner, W.B. Neuroepithe-lial cells downregulate their plasma membrane polarity prior to neural tube closure and neurogenesis. *Mech Dev* **69**, 71-81 (1997).

33.   Hartfuss, E., Galli, R., Heins, N. & Gotz, M. Characterization of CNS precursor subtypes and radial glia. *Dev Biol* **229**, 15-30 (2001).

34.   Malatesta, P., Hartfuss, E. & Gotz, M. Isolation of radial glial cells by fluorescent-activated cell sorting reveals a neuronal lineage. *Devel-opment* **127**, 5253-5263 (2000).

35.   Noctor, S.C., Martinez-Cerdeno, V., Ivic, L. & Kriegstein, A.R. Cortical neurons arise in symmetric and asymmetric division zones and mi-grate through specific phases. *Nat Neurosci* **7**, 136-144 (2004).

36.   Rowitch, D.H. & Kriegstein, A.R. Developmental genetics of vertebrate glial-cell specification. *Nature* **468**, 214-222 (2010).

37.   Altman, J. Proliferation and migration of undifferentiated precursor cells in the rat during postnatal gliogenesis. *Exp Neurol* **16**, 263-278 (1966).

38.   McCarthy, M., Turnbull, D.H., Walsh, C.A. & Fishell, G. Telencephalic neural progenitors appear to be restricted to regional and glial fates before the onset of neurogenesis. *J Neurosci* **21**, 6772-6781 (2001).

39.   Walsh, C. & Reid, C. Cell lineage and patterns of migration in the de-veloping cortex. *Ciba Found Symp* **193**, 21-40; discussion 59-70 (1995).

40.   Pinto, L. & Gotz, M. Radial glial cell heterogeneity--the source of diverse progeny in the CNS. *Prog Neurobiol* **83**, 2-23 (2007).

41.   Brill, M.S*., et al.* Adult generation of glutamatergic olfactory bulb interneurons. *Nat Neurosci* **12**, 1524-1533 (2009).

42.   Beckervordersandforth, R*., et al.* In vivo fate mapping and expression analysis reveals molecular hallmarks of prospectively isolated adult neural stem cells. *Cell Stem Cell* **7**, 744-758 (2010).

43.   Mirzadeh, Z., Merkle, F.T., Soriano-Navarro, M., Garcia-Verdugo, J.M. & Alvarez-Buylla, A. Neural stem cells confer unique pinwheel architecture to the ventricular surface in neurogenic regions of the adult brain. *Cell Stem Cell* **3**, 265-278 (2008).

44.   Ortega-Perez, I., Murray, K. & Lledo, P.M. The how and why of adult neurogenesis. *J Mol Histol* **38**, 555-562 (2007).

45.   Tavazoie, M*., et al.* A specialized vascular niche for adult neural stem cells. *Cell Stem Cell* **3**, 279-288 (2008).

46.   Alvarez-Buylla, A. & Lim, D.A. For the long run: Maintaining germinal niches in the adult brain. *Neuron* **41**, 683-686 (2004).

47.   Deepa, S.S., Yamada, S., Zako, M., Goldberger, O. & Sugahara, K. Chondroitin sulfate chains on syndecan-1 and syndecan-4 from normal murine mammary gland epithelial cells are structurally and functionally distinct and cooperate with heparan sulfate chains to bind growth factors - A novel function to control binding of midkine, pleiotrophin, and basic fibroblast growth factor. *Journal of Biological Chemistry* **279**, 37368-37376 (2004).

48.   Sirko, S., von Holst, A., Wizenmann, A., Gotz, M. & Faissner, A. Chondroitin sulfate glycosaminoglycans control proliferation, radial glia cell differentiation and neurogenesis in neural stem/progenitor cells. *Development* **134**, 2727-2738 (2007).

49.   Garcion, E., Halilagic, A., Faissner, A. & ffrench-Constant, C. Generation of an environmental niche for neural stem cell development by the extracellular matrix molecule tenascin C. *Development* **131**, 3423-3432 (2004).

50.   Gates, M.A*., et al.* Cell and Molecular Analysis of the Developing and Adult-Mouse Subventricular Zone of the Cerebral Hemispheres. *Journal of Comparative Neurology* **361**, 249-266 (1995).

51.   Reynolds, B.A., Tetzlaff, W. & Weiss, S. A multipotent EGF-responsive striatal embryonic progenitor cell produces neurons and astrocytes. *J Neurosci* **12**, 4565-4574 (1992).

52.   Reynolds, B.A. & Weiss, S. Generation of neurons and astrocytes from isolated cells of the adult mammalian central nervous system. *Science* **255**, 1707-1710 (1992).

53.   Berninger, B., Guillemot, F. & Gotz, M. Directing neurotransmitter identity of neurones derived from expanded adult neural stem cells. *Eur J Neurosci* **25**, 2581-2590 (2007).

54.   Seidenfaden, R., Desoeuvre, A., Bosio, A., Virard, I. & Cremer, H. Glial conversion of SVZ-derived committed neuronal precursors after ectopic grafting into the adult brain. *Mol Cell Neurosci* **32**, 187-198 (2006).

55.   Arvidsson, A., Collin, T., Kirik, D., Kokaia, Z. & Lindvall, O. Neuronal replacement from endogenous precursors in the adult brain after stroke. *Nat Med* **8**, 963-970 (2002).

56.   Parent, J.M., Vexler, Z.S., Gong, C., Derugin, N. & Ferriero, D.M. Rat
       forebrain neurogenesis and striatal neuron replacement after focal
       stroke. *Ann Neurol* **52**, 802-813 (2002).
57.   Jin, K.L., Wang, X.M., Xie, L., Mao, X.O. & Greenberg, D.A. Trans-
       genic ablation of doublecortin-expressing cells suppresses adult neu-
       rogenesis and worsens stroke outcome in mice. *Proceedings of the
       National Academy of Sciences of the United States of America* **107**,
       7993-7998 (2010).
58.   Chen, J.H., Magavi, S.S.P. & Macklis, J.D. Neurogenesis of cortico-
       spinal motor neurons extending spinal projections in adult mice. *Pro-
       ceedings of the National Academy of Sciences of the United States of
       America* **101**, 16357-16362 (2004).
59.   Azevedo, F.A.C.*, et al.* Equal Numbers of Neuronal and Nonneuronal
       Cells Make the Human Brain an Isometrically Scaled-Up Primate
       Brain. *Journal of Comparative Neurology* **513**, 532-541 (2009).
60.   Pelvig, D.P., Pakkenberg, H., Regeur, L., Oster, S. & Pakkenberg, B.
       Neocortical glial cell numbers in Alzheimer's disease. *Dementia and
       Geriatric Cognitive Disorders* **16**, 212-219 (2003).
61.   Pakkenberg, B., Pelvig, D.P., Pakkenberg, H. & Stark, A.K. Neocorti-
       cal glial cell numbers in human brains. *Neurobiology of Aging* **29**,
       1754-1762 (2008).
62.   Allen, N.J. & Barres, B.A. NEUROSCIENCE Glia - more than just
       brain glue. *Nature* **457**, 675-677 (2009).
63.   Pfrieger, F.W. & Barres, B.A. What the Flys Glia Tell the Flys Brain.
       Cell **83**, 671-674 (1995).
64.   Nedergaard, M., Ransom, B. & Goldman, S.A. New roles for astro-
       cytes: Redefining the functional architecture of the brain. *Trends in
       Neurosciences* **26**, 523-530 (2003).
65.   Sulston, J.E., Schierenberg, E., White, J.G. & Thomson, J.N. The Em-
       bryonic-Cell Lineage of the Nematode Caenorhabditis-Elegans. *De-
       velopmental Biology* **100**, 64-119 (1983).
66.   Tramontin, A.D., Garcia-Verdugo, J.M., Lim, D.A. & Alvarez-Buylla, A.
       Postnatal development of radial glia and the ventricular zone (VZ): a
       continuum of the neural stem cell compartment. *Cereb Cortex* **13**, 580-
       587 (2003).
67.   Merkle, F.T. & Alvarez-Buylla, A. Neural stem cells in mammalian de-
       velopment. *Curr Opin Cell Biol* **18**, 704-709 (2006).
68.   Voigt, T. Development of glial cells in the cerebral wall of ferrets: direct
       tracing of their transformation from radial glia into astrocytes. *J Comp
       Neurol* **289**, 74-88 (1989).
69.   Zhu, X.Q., Komitova, M., Bergles, D. & Nishiyama, A. NG2-expressing
       cells differentiate into both oligodendrocytes and astrocytes. *Neuron
       Glia Biology* **2**, S46-S47 (2007).
70.   Zhu, X.Q., Bergles, D.E. & Nishiyama, A. NG2 cells generate both oli-
       godendrocytes and gray matter astrocytes. *Development* **135**, 145-
       157 (2008).
71.   Sofroniew, M.V. & Vinters, H.V. Astrocytes: biology and pathology.
       Acta Neuropathol **119**, 7-35 (2010).
72.   Ogata, K. & Kosaka, T. Structural and quantitative analysis of astro-
       cytes in the mouse hippocampus. *Neuroscience* **113**, 221-233 (2002).

73.   Halassa, M.M., Fellin, T., Takano, H., Dong, J.H. & Haydon, P.G. Synaptic islands defined by the territory of a single astrocyte. *J Neurosci* **27**, 6473-6477 (2007).

74.   Seifert, G., Schilling, K. & Steinhauser, C. Astrocyte dysfunction in neurological disorders: a molecular perspective. *Nat Rev Neurosci* **7**, 194-206 (2006).

75.   Heneka, M.T., Rodriguez, J.J. & Verkhratsky, A. Neuroglia in neurodegeneration. *Brain Res Rev* **63**, 189-211 (2010).

76.   Halassa, M.M., Fellin, T. & Haydon, P.G. The tripartite synapse: roles for gliotransmission in health and disease. *Trends Mol Med* **13**, 54-63 (2007).

77.   Perea, G., Navarrete, M. & Araque, A. Tripartite synapses: astrocytes process and control synaptic information. *Trends Neurosci* **32**, 421-431 (2009).

78.   Verkhratsky, A. & Kettenmann, H. Calcium signalling in glial cells. *Trends Neurosci* **19**, 346-352 (1996).

79.   Verkhratsky, A., Orkand, R.K. & Kettenmann, H. Glial calcium: homeostasis and signaling function. *Physiol Rev* **78**, 99-141 (1998).

80.   Bezzi, P.*, et al.* Astrocytes contain a vesicular compartment that is competent for regulated exocytosis of glutamate. *Nat Neurosci* **7**, 613-620 (2004).

81.   Rossi, D.J., Oshima, T. & Attwell, D. Glutamate release in severe brain ischaemia is mainly by reversed uptake. *Nature* **403**, 316-321 (2000).

82.   Nieweg, K., Schaller, H. & Pfrieger, F.W. Marked differences in cholesterol synthesis between neurons and glial cells from postnatal rats. *J Neurochem* **109**, 125-134 (2009).

83.   Pfrieger, F.W. Roles of glial cells in synapse development. *Cell Mol Life Sci* **66**, 2037-2047 (2009).

84.   Christopherson, K.S.*, et al.* Thrombospondins are astrocyte-secreted proteins that promote CNS synaptogenesis. *Cell* **120**, 421-433 (2005).

85.   Rajdev, S. & Reynolds, I.J. Glutamate-induced intracellular calcium changes and neurotoxicity in cortical neurons in vitro: effect of chemical ischemia. *Neuroscience* **62**, 667-679 (1994).

86.   Iadecola, C. & Nedergaard, M. Glial regulation of the cerebral microvasculature. *Nat Neurosci* **10**, 1369-1376 (2007).

87.   Koehler, R.C., Roman, R.J. & Harder, D.R. Astrocytes and the regulation of cerebral blood flow. *Trends Neurosci* **32**, 160-169 (2009).

88.   Abbott, N.J., Ronnback, L. & Hansson, E. Astrocyte-endothelial interactions at the blood-brain barrier. *Nat Rev Neurosci* **7**, 41-53 (2006).

89.   Ballabh, P., Braun, A. & Nedergaard, M. The blood-brain barrier: an overview: structure, regulation, and clinical implications. *Neurobiol Dis* **16**, 1-13 (2004).

90.   Blanchette, M. & Fortin, D. Blood-brain barrier disruption in the treatment of brain tumors. *Methods Mol Biol* **686**, 447-463 (2011).

91.   Benarroch, E.E. Glycogen metabolism: metabolic coupling between astrocytes and neurons. *Neurology* **74**, 919-923 (2010).

92.   Oshima, R.G. Intermediate filaments: A historical perspective. *Experimental Cell Research* **313**, 1981-1994 (2007).

93.   Ninkovic, J., Mori, T. & Gotz, M. Distinct modes of neuron addition in adult mouse neurogenesis. *J Neurosci* **27**, 10906-10911 (2007).

94.   Imura, T., Nakano, I., Kornblum, H.I. & Sofroniew, M.V. Phenotypic and functional heterogeneity of GFAP-expressing cells in vitro: differential expression of LeX/CD15 by GFAP-expressing multipotent neural stem cells and non-neurogenic astrocytes. *Glia* **53**, 277-293 (2006).

95.   Robel, S., Berninger, B. & Gotz, M. The stem cell potential of glia: lessons from reactive gliosis. *Nat Rev Neurosci* **12**, 88-104 (2011).

96.   Kessaris, N.*, et al.* Competing waves of oligodendrocytes in the forebrain and postnatal elimination of an embryonic lineage. *Nat Neurosci* **9**, 173-179 (2006).

97.   Levine, J.M. & Stallcup, W.B. Plasticity of Developing Cerebellar Cells-Invitro Studied with Antibodies against the Ng2 Antigen. *Journal of Neuroscience* **7**, 2721-2731 (1987).

98.   Stallcup, W.B. & Beasley, L. Bipotential Glial Precursor Cells of the Optic-Nerve Express the Ng2 Proteoglycan. *Journal of Neuroscience* **7**, 2737-2744 (1987).

99.   Nishiyama, A. & Stallcup, W.B. A glial population identified in vivo by antibodies to NG2 proteoglycan and PDGF alpha receptor. *Journal of Neurochemistry* **66**, S85-S85 (1996).

100. Nishiyama, A., Lin, X.H., Giese, N., Heldin, C.H. & Stallcup, W.B. Co-localization of NG2 proteoglycan and PDGF alpha-receptor on O2A progenitor cells in the developing rat brain. *Journal of Neuroscience Research* **43**, 299-314 (1996).

101. Komitova, M., Zhu, X., Serwanski, D.R. & Nishiyama, A. NG2 cells are distinct from neurogenic cells in the postnatal mouse subventricular zone. *J Comp Neurol* **512**, 702-716 (2009).

102. Trotter, J., Karram, K. & Nishiyama, A. NG2 cells: Properties, progeny and origin. *Brain Research Reviews* **63**, 72-82 (2010).

103. Simon, C., Gotz, M. & Dimou, L. Progenitors in the adult cerebral cortex: Cell cycle properties and regulation by physiological stimuli and injury. *Glia* (2011).

104. Horner, P.J.*, et al.* Proliferation and differentiation of progenitor cells throughout the intact adult rat spinal cord. *Journal of Neuroscience* **20**, 2218-2228 (2000).

105. Dimou, L., Simon, C., Kirchhoff, F., Takebayashi, H. & Gotz, M. Progeny of Olig2-expressing progenitors in the gray and white matter of the adult mouse cerebral cortex. *J Neurosci* **28**, 10434-10442 (2008).

106. Tansey, F.A. & Cammer, W. A Pi-Form of Glutathione-S-Transferase Is a Myelin-Associated and Oligodendrocyte-Associated Enzyme in Mouse-Brain. *Journal of Neurochemistry* **57**, 95-102 (1991).

107. Demerens, C.*, et al.* Induction of myelination in the central nervous system by electrical activity. *Proceedings of the National Academy of Sciences of the United States of America* **93**, 9887-9892 (1996).

108. Brady, S.T.*, et al.* Formation of compact myelin is required for maturation of the axonal cytoskeleton. *Journal of Neuroscience* **19**, 7278-7288 (1999).

109. Sanchez, I., Hassinger, L., Paskevich, P.A., Shine, H.D. & Nixon, R.A. Oligodendroglia regulate the regional expansion of axon caliber and local accumulation of neurofilaments during development independently of myelin formation. *Journal of Neuroscience* **16**, 5095-5105 (1996).

110.   Sanchez, I., *et al.* Local control of neurofilament accumulation during radial growth of myelinating axons in vivo: Selective role of site-specific phosphorylation. *Journal of Cell Biology* **151**, 1013-1024 (2000).

111.   Wilkins, A., Majed, H., Layfield, R., Compston, A. & Chandran, S. Oligodendrocytes promote neuronal survival and axonal length by distinct intracellular mechanisms: A novel role for oligodendrocyte-derived glial cell line-derived neurotrophic factor. *Journal of Neuroscience* **23**, 4967-4974 (2003).

112.   Du, Y.Z. & Dreyfus, C.F. Oligodendrocytes as providers of growth factors. *Journal of Neuroscience Research* **68**, 647-654 (2002).

113.   Ligon, K.L., *et al.* Development of NG2 neural progenitor cells requires Olig gene function. *Proceedings of the National Academy of Sciences of the United States of America* **103**, 7853-7858 (2006).

114.   Anderson, D.J., Choi, G. & Zhou, Q. Olig genes and the genetic logic of CNS neural cell fate determination. *Clinical Neuroscience Research* **2**, 17-28 (2002).

115.   Takebayashi, H., Nabeshima, Y., Yoshida, S., Chisaka, O. & Ikenaka, K. The basic helix-loop-helix factor olig2 is essential for the development of motoneuron and oligodendrocyte lineages. *Curr Biol* **12**, 1157-1163 (2002).

116.   Buffo, A., *et al.* Expression pattern of the transcription factor Olig2 in response to brain injuries: implications for neuronal repair. *Proc Natl Acad Sci U S A* **102**, 18183-18188 (2005).

117.   Nishiyama, A., Komitova, M., Suzuki, R. & Zhu, X.Q. Polydendrocytes (NG2 cells): multifunctional cells with lineage plasticity. *Nature Reviews Neuroscience* **10**, 9-22 (2009).

118.   Nishiyama, A., Chang, A.S. & Trapp, B.D. NG2+glial cells: A novel glial cell population in the adult brain. *Journal of Neuropathology and Experimental Neurology* **58**, 1113-1124 (1999).

119.   Dawson, M.R.L., Levine, J.M. & Reynolds, R. NG2-Expressing cells in the central nervous system: Are they oligodendroglial progenitors? *Journal of Neuroscience Research* **61**, 471-479 (2000).

120.   Butt, A.M., Hamilton, N., Hubbard, P., Pugh, M. & Ibrahim, M. Synantocytes: the fifth element. *J Anat* **207**, 695-706 (2005).

121.   Karram, K., *et al.* NG2-expressing cells in the nervous system revealed by the NG2-EYFP-knockin mouse. *Genesis* **46**, 743-757 (2008).

122.   Ge, W.P., Zhou, W., Luo, Q.M., Jan, L.Y. & Jan, Y.N. Dividing glial cells maintain differentiated properties including complex morphology and functional synapses. *Proceedings of the National Academy of Sciences of the United States of America* **106**, 328-333 (2009).

123.   Richardson, W.D., Psachoulia, K., Jamen, F. & Young, K.M. Cell cycle dynamics of NG2 cells in the postnatal and ageing brain. *Neuron Glia Biology* **5**, 57-67 (2009).

124.   Geha, S., *et al.* NG2+/Olig2+ cells are the major cycle-related cell population of the adult human normal brain. *Brain Pathol* **20**, 399-411 (2010).

125.   Rivers, L.E., *et al.* PDGFRA/NG2 glia generate myelinating oligodendrocytes and piriform projection neurons in adult mice. *Nature Neuroscience* **11**, 1392-1401 (2008).

126. Franklin, R.J.M., Bayley, S.A., Milner, R., Ffrenchconstant, C. & Blakemore, W.F. Differentiation of the O-2a Progenitor-Cell Line Cg-4 into Oligodendrocytes and Astrocytes Following Transplantation into Glia-Deficient Areas of Cns White-Matter. *Glia* **13**, 39-44 (1995).

127. Windrem, M.*, et al.* Fetal and adult human oligodendrocyte progenitor cells effectively myelinate dysmyelinated brain (vol 10, pg 93, 2004). *Nature Medicine* **10**, 209-209 (2004).

128. Zhu, X.Q.*, et al.* Age-dependent fate and lineage restriction of single NG2 cells. *Development* **138**, 745-753 (2011).

129. Zhu, X.Q., Hill, R.A. & Nishiyama, A. NG2 cells generate oligodendro-cytes and gray matter astrocytes in the spinal cord. *Neuron Glia Biology* **4**, 19-26 (2008).

130. Belachew, S.*, et al.* Postnatal NG2 proteoglycan-expressing progeni-tor cells are intrinsically multipotent and generate functional neurons. *Journal of Cell Biology* **161**, 169-186 (2003).

131. Richardson, W.D.*, et al.* PDGFRA/NG2 glia generate myelinating oli-godendrocytes and piriform projection neurons in adult mice. *Nature Neuroscience* **11**, 1392-1401 (2008).

132. Guo, F.*, et al.* Pyramidal neurons are generated from oligodendroglial progenitor cells in adult piriform cortex. *J Neurosci* **30**, 12036-12049 (2010).

133. Kang, S.H., Fukaya, M., Yang, J.K., Rothstein, J.D. & Bergles, D.E. NG2+ CNS glial progenitors remain committed to the oligodendrocyte lineage in postnatal life and following neurodegeneration. *Neuron* **68**, 668-681 (2010).

134. Kukley, M., Capetillo-Zarate, E. & Dietrich, D. Vesicular glutamate re-lease from axons in white matter. *Nature Neuroscience* **10**, 311-320 (2007).

135. Ziskin, J.L., Nishiyama, A., Rubio, M., Fukaya, M. & Bergles, D.E. Ve-sicular release of glutamate from unmyelinated axons in white matter. *Nature Neuroscience* **10**, 321-330 (2007).

136. Bergles, D.E., Roberts, J.D.B., Somogyi, P. & Jahr, C.E. Glutamater-gic synapses on oligodendrocyte precursor cells in the hippocampus. *Nature* **405**, 187-191 (2000).

137. Butt, A.M.*, et al.* Cells expressing the NG2 antigen contact nodes of Ranvier in adult CNS white matter. *Glia* **26**, 84-91 (1999).

138. Ong, W.Y. & Levine, J.M. A light and electron microscopic study of NG2 chondroitin sulfate proteoglycan-positive oligodendrocyte precur-sor cells in the normal and kainate-lesioned rat hippocampus. *Neuro-science* **92**, 83-95 (1999).

139. Lin, S.C. & Bergles, D.E. Synaptic signaling between GABAergic in-terneurons and oligodendrocyte precursor cells in the hippocampus. *Nature Neuroscience* **7**, 24-32 (2004).

140. Karadottir, R., Cavelier, P., Bergersen, L.H. & Attwell, D. NMDA recep-tors are expressed in oligodendrocytes and activated in ischaemia. *Nature* **438**, 1162-1166 (2005).

141. Karadottir, R., Hamilton, N.B., Bakiri, Y. & Attwell, D. Spiking and non-spiking classes of oligodendrocyte precursor glia in CNS white matter (vol 11, pg 450, 2008). *Nature Neuroscience* **11**, 851-851 (2008).

142. Yuan, X.Q., Eisen, A.M., McBain, C.J. & Gallo, V. A role for glutamate and its receptors in the regulation of oligodendrocyte development in cerebellar tissue slices. *Development* **125**, 2901-2914 (1998).

143. Wang, C.*, et al.* Functional N-methyl-D-aspartate receptors in O-2A glial precursor cells: A critical role in regulating polysialic acid-neural cell adhesion molecule expression and cell migration. *Journal of Cell Biology* **135**, 1565-1581 (1996).

144. Gallo, V., Etxeberria, A., Mangin, J.M. & Aguirre, A. Adult-born SVZ progenitors receive transient synapses during remyelination in corpus callosum. *Nature Neuroscience* **13**, 287-289 (2010).

145. Etxeberria, A., Mangin, J.M., Aguirre, A. & Gallo, V. Adult-born SVZ progenitors receive transient synapses during remyelination in corpus callosum. *Nat Neurosci* **13**, 287-289 (2010).

146. Hartline, D.K. & Colman, D.R. Rapid conduction and the evolution of giant axons and myelinated fibers. *Current Biology* **17**, R29-R35 (2007).

147. Jahn, O., Tenzer, S. & Werner, H.B. Myelin Proteomics: Molecular Anatomy of an Insulating Sheath. *Molecular Neurobiology* **40**, 55-72 (2009).

148. Poliak, S. & Peles, E. The local differentiation of myelinated axons at nodes of Ranvier. *Nature Reviews Neuroscience* **4**, 968-980 (2003).

149. Ranvier, L. (ed.) *Leçons sur l'histologie du système nerveux*, (Savy, Paris, 1878).

150. Stampfli, R. [Current-voltage characteristics of the sensitive membranes of individual nodes of Ranvier and their dependence on ion concentration]. *Helv Physiol Pharmacol Acta* **16**, 127-145 (1958).

151. Tasaki, I. & Bak, A.F. Current-voltage relations of single nodes of Ranvier as examined by voltage-clamp technique. *J Neurophysiol* **21**, 124-137 (1958).

152. Lappe-Siefke, C.*, et al.* Disruption of Cnp1 uncouples oligodendroglial functions in axonal support and myelination. *Nature Genetics* **33**, 366-374 (2003).

153. Griffiths, I.*, et al.* Axonal swellings and degeneration in mice lacking the major proteolipid of myelin. *Science* **280**, 1610-1613 (1998).

154. Kursula, P. Structural properties of proteins specific to the myelin sheath. *Amino Acids* **34**, 175-185 (2008).

155. Eng, L.F., Chao, F.C., Gerstl, B., Pratt, D. & Tavaststjerna, M.G. The maturation of human white matter myelin. Fractionation of the myelin membrane proteins. *Biochemistry* **7**, 4455-4465 (1968).

156. Norton, W.T. & Poduslo, S.E. Myelination in Rat-Brain - Changes in Myelin Composition during Brain Maturation. *Journal of Neurochemistry* **21**, 759-773 (1973).

157. Bird, T.D., Farrell, D.F. & Sumi, S.M. Brain Lipid-Composition of Shiverer Mouse - (Genetic Defect in Myelin Development). *Journal of Neurochemistry* **31**, 387-& (1978).

158. Chernoff, G.F. Shiverer - an Autosomal Recessive Mutant Mouse with Myelin Deficiency. *Journal of Heredity* **72**, 128-128 (1981).

159. Dupouey, P.*, et al.* Immunochemical Studies of Myelin Basic-Protein in Shiverer Mouse Devoid of Major Dense Line of Myelin. *Neuroscience Letters* **12**, 113-118 (1979).

160. Galiano, M.R.*, et al.* Myelin basic protein functions as a microtubule stabilizing protein in differentiated oligodendrocytes. *Journal of Neuroscience Research* **84**, 534-541 (2006).

161. Dyer, C.A., Philibotte, T.M., Billingsgagliardi, S. & Wolf, M.K. Cytoskeleton in Myelin-Basic-Protein-Deficient Shiverer Oligodendrocytes. *Developmental Neuroscience* **17**, 53-62 (1995).

162. Boggs, J.M. Myelin basic protein: a multifunctional protein. *Cellular and Molecular Life Sciences* **63**, 1945-1961 (2006).

163. Klugmann, M.*, et al.* Assembly of CNS myelin in the absence of proteolipid protein. *Neuron* **18**, 59-70 (1997).

164. Sternberger, N.H., Quarles, R.H., Itoyama, Y. & Webster, H.D. Myelin-Associated Glycoprotein Demonstrated Immunocytochemically in Myelin and Myelin-Forming Cells of Developing Rat. *Proceedings of the National Academy of Sciences of the United States of America* **76**, 1510-1514 (1979).

165. Bartsch, U., Kirchhoff, F. & Schachner, M. Immunohistological Localization of the Adhesion Molecules L1, N-Cam, and Mag in the Developing and Adult Optic-Nerve of Mice. *Journal of Comparative Neurology* **284**, 451-462 (1989).

166. Kumar, S., Yin, X.H., Trapp, B.D., Paulaitis, M.E. & Hoh, J.H. Role of long-range repulsive forces in organizing axonal neurofilament distributions: Evidence from mice deficient in myelin-associated glycoprotein. *Journal of Neuroscience Research* **68**, 681-690 (2002).

167. Liu, B.P., Fournier, A., GrandPre, T. & Strittmatter, S.M. Myelin-associated glycoprotein as a functional ligand for the Nogo-66 receptor. *Science* **297**, 1190-1193 (2002).

168. Domeniconi, M.*, et al.* Myelin-associated glycoprotein interacts with the Nogo66 receptor to inhibit neurite outgrowth. *Neuron* **35**, 283-290 (2002).

169. Matthews, M.A. An Electron Microscopic Study of Relationship between Axon Diameter and Initiation of Myelin Production in Peripheral Nervous System. *Anatomical Record* **161**, 337-& (1968).

170. Franklin, R.J.M. & Ffrench-Constant, C. Remyelination in the CNS: from biology to therapy. *Nature Reviews Neuroscience* **9**, 839-855 (2008).

171. Uzman, L.L. & Rumley, M.K. Changes in the Composition of the Developing Mouse Brain during Early Myelination. *Journal of Neurochemistry* **3**, 170-& (1958).

172. Hess, D.C.*, et al.* Hematopoietic origin of microglial and perivascular cells in brain. *Exp Neurol* **186**, 134-144 (2004).

173. Vallieres, L. & Sawchenko, P.E. Bone marrow-derived cells that populate the adult mouse brain preserve their hematopoietic identity. *J Neurosci* **23**, 5197-5207 (2003).

174. McKercher, S.R.*, et al.* Targeted disruption of the PU.1 gene results in multiple hematopoietic abnormalities. *Embo Journal* **15**, 5647-5658 (1996).

175. Rezaie, P., Corbisiero, V. & Male, D. Transient expression of MIDC-8 in the normal mouse brain. *Neurosci Lett* **377**, 189-194 (2005).

176. Chan, W.Y., Kohsaka, S. & Rezaie, P. The origin and cell lineage of microglia: new concepts. *Brain Res Rev* **53**, 344-354 (2007).

177. Ransohoff, R.M. & Cardona, A.E. The myeloid cells of the central nervous system parenchyma. *Nature* **468**, 253-262 (2010).
178. Nimmerjahn, A., Kirchhoff, F. & Helmchen, F. Resting microglial cells are highly dynamic surveillants of brain parenchyma in vivo. *Science* **308**, 1314-1318 (2005).
179. Davalos, D*., et al.* ATP mediates rapid microglial response to local brain injury in vivo. *Nature Neuroscience* **8**, 752-758 (2005).
180. Ajami, B., Bennett, J.L., Krieger, C., Tetzlaff, W. & Rossi, F.M.V. Local self-renewal can sustain CNS microglia maintenance and function throughout adult life. *Nature Neuroscience* **10**, 1538-1543 (2007).
181. Priller, J*., et al.* Targeting gene-modified hematopoietic cells to the central nervous system: use of green fluorescent protein uncovers microglial engraftment. *Nat Med* **7**, 1356-1361 (2001).
182. Kennedy, D.W. & Abkowitz, J.L. Kinetics of central nervous system microglial and macrophage engraftment: analysis using a transgenic bone marrow transplantation model. *Blood* **90**, 986-993 (1997).
183. Simard, A.R. & Rivest, S. Bone marrow stem cells have the ability to populate the entire central nervous system into fully differentiated parenchymal microglia. *FASEB J* **18**, 998-1000 (2004).
184. Fawcett, J.W. & Asher, R.A. The glial scar and central nervous system repair. *Brain Research Bulletin* **49**, 377-391 (1999).
185. Rolls, A., Shechter, R. & Schwartz, M. NEURON - GLIA INTERACTIONS - OPINION The bright side of the glial scar in CNS repair. *Nature Reviews Neuroscience* **10**, 235-U291 (2009).
186. Silver, J. & Miller, J.H. Regeneration beyond the glial scar. *Nat Rev Neurosci* **5**, 146-156 (2004).
187. Sofroniew, M.V. Molecular dissection of reactive astrogliosis and glial scar formation. *Trends Neurosci* **32**, 638-647 (2009).
188. Goritz, C*., et al.* A pericyte origin of spinal cord scar tissue. *Science* **333**, 238-242 (2011).
189. Persson, L. Cellular reactions to small cerebral stab wounds in the rat frontal lobe. An ultrastructural study. *Virchows Arch B Cell Pathol* **22**, 21-37 (1976).
190. Back, T., Hemmen, T. & Schuler, O.G. Lesion evolution in cerebral ischemia. *J Neurol* **251**, 388-397 (2004).
191. Belayev, L., Zhao, W., Busto, R. & Ginsberg, M.D. Transient middle cerebral artery occlusion by intraluminal suture: I. Three-dimensional autoradiographic image-analysis of local cerebral glucose metabolism-blood flow interrelationships during ischemia and early recirculation. *J Cereb Blood Flow Metab* **17**, 1266-1280 (1997).
192. Doyle, K.P., Simon, R.P. & Stenzel-Poore, M.P. Mechanisms of ischemic brain damage. *Neuropharmacology* **55**, 310-318 (2008).
193. Pekny, M. & Nilsson, M. Astrocyte activation and reactive gliosis. *Glia* **50**, 427-434 (2005).
194. Airey, D.C., Lu, L. & Williams, R.W. Genetic control of the mouse cerebellum: Identification of quantitative trait loci modulating size and architecture. *Journal of Neuroscience* **21**, 5099-5109 (2001).
195. Dang, C*., et al.* The allen brain atlas: Delivering neuroscience to the web on a genome wide scale. *Data Integration in the Life Sciences, Proceedings* **4544**, 17-26 (2007).

196. Ridet, J.L., Malhotra, S.K., Privat, A. & Gage, F.H. Reactive astrocytes: cellular and molecular cues to biological function. *Trends in Neurosciences* **20**, 570-577 (1997).

197. Stichel, C.C. & Muller, H.W. The CNS lesion scar: new vistas on an old regeneration barrier. *Cell and Tissue Research* **294**, 1-9 (1998).

198. Loy, D.N.*, et al.* Temporal progression of angiogenesis and basal lamina deposition after contusive spinal cord injury in the adult rat. *Journal of Comparative Neurology* **445**, 308-324 (2002).

199. Herrmann, J.E.*, et al.* STAT3 is a critical regulator of astrogliosis and scar formation after spinal cord injury. *J Neurosci* **28**, 7231-7243 (2008).

200. Bundesen, L.Q., Scheel, T.A., Bregman, B.S. & Kromer, L.F. Ephrin-B2 and EphB2 regulation of astrocyte-meningeal fibroblast interactions in response to spinal cord lesions in adult rats. *J Neurosci* **23**, 7789-7800 (2003).

201. Rossi, D.J., Brady, J.D. & Mohr, C. Astrocyte metabolism and signaling during brain ischemia. *Nat Neurosci* **10**, 1377-1386 (2007).

202. Hamby, M.E., Hewett, J.A. & Hewett, S.J. TGF-beta1 potentiates astrocytic nitric oxide production by expanding the population of astrocytes that express NOS-2. *Glia* **54**, 566-577 (2006).

203. Brambilla, R.*, et al.* Inhibition of astroglial nuclear factor kappaB reduces inflammation and improves functional recovery after spinal cord injury. *J Exp Med* **202**, 145-156 (2005).

204. Brambilla, R.*, et al.* Transgenic inhibition of astroglial NF-kappa B leads to increased axonal sparing and sprouting following spinal cord injury. *J Neurochem* **110**, 765-778 (2009).

205. Bush, T.G.*, et al.* Leukocyte infiltration, neuronal degeneration, and neurite outgrowth after ablation of scar-forming, reactive astrocytes in adult transgenic mice. *Neuron* **23**, 297-308 (1999).

206. Wilhelmsson, U.*, et al.* Absence of glial fibrillary acidic protein and vimentin prevents hypertrophy of astrocytic processes and improves post-traumatic regeneration. *J Neurosci* **24**, 5016-5021 (2004).

207. Li, L.*, et al.* Protective role of reactive astrocytes in brain ischemia. *J Cereb Blood Flow Metab* **28**, 468-481 (2008).

208. Faulkner, J.R.*, et al.* Reactive astrocytes protect tissue and preserve function after spinal cord injury. *J Neurosci* **24**, 2143-2155 (2004).

209. Chen, Y.*, et al.* Astrocytes protect neurons from nitric oxide toxicity by a glutathione-dependent mechanism. *J Neurochem* **77**, 1601-1610 (2001).

210. Shih, A.Y.*, et al.* Coordinate regulation of glutathione biosynthesis and release by Nrf2-expressing glia potently protects neurons from oxidative stress. *J Neurosci* **23**, 3394-3406 (2003).

211. Rothstein, J.D.*, et al.* Knockout of glutamate transporters reveals a major role for astroglial transport in excitotoxicity and clearance of glutamate. *Neuron* **16**, 675-686 (1996).

212. Brown, A.M. & Ransom, B.R. Astrocyte glycogen and brain energy metabolism. *Glia* **55**, 1263-1271 (2007).

213. Eddleston, M. & Mucke, L. Molecular profile of reactive astrocytes--implications for their role in neurologic disease. *Neuroscience* **54**, 15-36 (1993).

214. John, G.R., Lee, S.C. & Brosnan, C.F. Cytokines: powerful regulators of glial cell activation. *Neuroscientist* **9**, 10-22 (2003).

215. Dobbertin, A*., et al.* Regulation of RPTPbeta/phosphacan expression and glycosaminoglycan epitopes in injured brain and cytokine-treated glia. *Mol Cell Neurosci* **24**, 951-971 (2003).

216. Sirko, S*., et al.* Focal laser-lesions activate an endogenous population of neural stem/progenitor cells in the adult visual cortex. *Brain* **132**, 2252-2264 (2009).

217. Buffo, A*., et al.* Origin and progeny of reactive gliosis: A source of multipotent cells in the injured brain. *Proc Natl Acad Sci U S A* **105**, 3581-3586 (2008).

218. Nakagomi, T*., et al.* Isolation and characterization of neural stem/progenitor cells from post-stroke cerebral cortex in mice. *European Journal of Neuroscience* **29**, 1842-1852 (2009).

219. Nishiyama, A., Yu, M., Drazba, J.A. & Tuohy, V.K. Normal and reactive NG2+ glial cells are distinct from resting and activated microglia. *Journal of Neuroscience Research* **48**, 299-312 (1997).

220. Keirstead, H.S., Levine, J.M. & Blakemore, W.F. Response of the oligodendrocyte progenitor cell population (defined by NG2 labelling) to demyelination of the adult spinal cord. *Glia* **22**, 161-170 (1998).

221. Levine, J.M. Increased Expression of the Ng2 Chondroitin-Sulfate Proteoglycan after Brain Injury. *Journal of Neuroscience* **14**, 4716-4730 (1994).

222. Jones, L.L., Yamaguchi, Y., Stallcup, W.B. & Tuszynski, M.H. NG2 is a major chondroitin sulfate proteoglycan produced after spinal cord injury and is expressed by macrophages and oligodendrocyte progenitors. *Journal of Neuroscience* **22**, 2792-2803 (2002).

223. Hampton, D.W., Rhodes, K.E., Zhao, C., Franklin, R.J.M. & Fawcett, J.W. The responses of oligodendrocyte precursor cells, astrocytes and microglia to a cortical stab injury, in the brain. *Neuroscience* **127**, 813-820 (2004).

224. Ughrin, Y.M., Chen, Z.J. & Levine, J.M. Multiple regions of the NG2 proteoglycan inhibit neurite growth and induce growth cone collapse. *Journal of Neuroscience* **23**, 175-186 (2003).

225. Dou, C.L. & Levine, J.M. Inhibition of Neurite Growth by the Ng2 Chondroitin Sulfate Proteoglycan. *Journal of Neuroscience* **14**, 7616-7628 (1994).

226. Tan, A.M., Colletti, M., Rorai, A.T., Skene, J.H.P. & Levine, J.M. Antibodies against the NG2 proteoglycan promote the regeneration of sensory Axons within the dorsal columns of the spinal cord. *Journal of Neuroscience* **26**, 4729-4739 (2006).

227. de Castro, R., Tajrishi, R., Claros, J. & Stallcup, W.B. Differential responses of spinal axons to transection: influence of the NG2 proteoglycan. *Experimental Neurology* **192**, 299-309 (2005).

228. Yang, Z.S*., et al.* NG2 glial cells provide a favorable substrate for growing axons. *Journal of Neuroscience* **26**, 3829-3839 (2006).

229. Tatsumi, K*., et al.* Genetic fate mapping of Olig2 progenitors in the injured adult cerebral cortex reveals preferential differentiation into astrocytes. *J Neurosci Res* **86**, 3494-3502 (2008).

230. Doucette, J.R., Jiao, R.B. & Nazarali, A.J. Age-Related and Cuprizone-Induced Changes in Myelin and Transcription Factor Gene Ex-

pression and in Oligodendrocyte Cell Densities in the Rostral Corpus Callosum of Mice. *Cellular and Molecular Neurobiology* **30**, 607-629 (2010).

231. Nishiyama, A., Komitova, M., Serwanski, D.R. & Lu, Q.R. NG2 Cells Are Not a Major Source of Reactive Astrocytes After Neocortical Stab Wound Injury. *Glia* **59**, 800-809 (2011).

232. Felts, P.A., Baker, T.A. & Smith, K.J. Conduction in segmentally demyelinated mammalian central axons. *Journal of Neuroscience* **17**, 7267-7277 (1997).

233. Smith, K.J., Blakemore, W.F. & Mcdonald, W.I. Central Remyelination Restores Secure Conduction. *Nature* **280**, 395-396 (1979).

234. Blakemore, W.F. Pattern of Remyelination in Cns. *Nature* **249**, 577-578 (1974).

235. Ludwin, S.K. & Maitland, M. Long-Term Remyelination Fails to Reconstitute Normal Thickness of Central Myelin Sheaths. *Journal of the Neurological Sciences* **64**, 193-198 (1984).

236. Watanabe, M., Toyama, Y. & Nishiyama, A. Differentiation of proliferated NG2-positive glial progenitor cells in a remyelinating lesion. *Journal of Neuroscience Research* **69**, 826-836 (2002).

237. Fancy, S.P., Zhao, C. & Franklin, R.J. Increased expression of Nkx2.2 and Olig2 identifies reactive oligodendrocyte progenitor cells responding to demyelination in the adult CNS. *Mol Cell Neurosci* **27**, 247-254 (2004).

238. Levine, J.M. & Reynolds, R. Activation and proliferation of endogenous oligodendrocyte precursor cells during ethidium bromide-induced demyelination. *Experimental Neurology* **160**, 333-347 (1999).

239. Menn, B.*, et al.* Origin of oligodendrocytes in the subventricular zone of the adult brain. *Journal of Neuroscience* **26**, 7907-7918 (2006).

240. Jablonska, B.*, et al.* Chordin-induced lineage plasticity of adult SVZ neuroblasts after demyelination. *Nat Neurosci* **13**, 541-550 (2010).

241. Aguirre, A., Dupree, J.L., Mangin, J.M. & Gallo, V. A functional role for EGFR signaling in myelination and remyelination. *Nat Neurosci* **10**, 990-1002 (2007).

242. Nait-Oumesmar, B.*, et al.* Progenitor cells of the adult mouse subventricular zone proliferate, migrate and differentiate into oligodendrocytes after demyelination. *Eur J Neurosci* **11**, 4357-4366 (1999).

243. Haynes, S.E.*, et al.* The P2Y(12) receptor regulates microglial activation by extracellular nucleotides. *Nature Neuroscience* **9**, 1512-1519 (2006).

244. Melani, A.*, et al.* ATP extracellular concentrations are increased in the rat striatum during in vivo ischemia. *Neurochemistry International* **47**, 442-448 (2005).

245. Dibaj, P.*, et al.* In Vivo imaging reveals distinct inflammatory activity of CNS microglia versus PNS macrophages in a mouse model for ALS. *PLoS One* **6**, e17910 (2011).

246. D'Ambrosi, N.*, et al.* The proinflammatory action of microglial P2 receptors is enhanced in SOD1 models for amyotrophic lateral sclerosis. *J Immunol* **183**, 4648-4656 (2009).

247. Almer, G., Vukosavic, S., Romero, N. & Przedborski, S. Inducible nitric oxide synthase up-regulation in a transgenic mouse model of familial amyotrophic lateral sclerosis. *J Neurochem* **72**, 2415-2425 (1999).

248. Streit, W.J., Graeber, M.B. & Kreutzberg, G.W. Functional plasticity of microglia: a review. *Glia* **1**, 301-307 (1988).

249. Kettenmann, H., Hanisch, U.K., Noda, M. & Verkhratsky, A. Physiology of microglia. *Physiol Rev* **91**, 461-553 (2011).

250. Davis, E.J., Foster, T.D. & Thomas, W.E. Cellular forms and functions of brain microglia. *Brain Res Bull* **34**, 73-78 (1994).

251. Streit, W.J., Walter, S.A. & Pennell, N.A. Reactive microgliosis. *Prog Neurobiol* **57**, 563-581 (1999).

252. Tambuyzer, B.R., Ponsaerts, P. & Nouwen, E.J. Microglia: gatekeepers of central nervous system immunology. *J Leukoc Biol* **85**, 352-370 (2009).

253. Lindvall, O. & Kokaia, Z. Stem cells in human neurodegenerative disorders--time for clinical translation? *J Clin Invest* **120**, 29-40 (2010).

254. Small, G.W*., et al.* Diagnosis and treatment of Alzheimer disease and related disorders. Consensus statement of the American Association for Geriatric Psychiatry, the Alzheimer's Association, and the American Geriatrics Society. *JAMA* **278**, 1363-1371 (1997).

255. Vijay Chandra, R.P., Ramanan Laxminarayan, Caroline Tanner, Bala Manyam, Sandanand Rajkumar, Donald Silberberg, Carol Brayne, Jeffrey Chow, Susan Herman, Fleur Hourihan, Scott Kasner, Luis Morillo, Adesola Ogunniyi, William Theodore and Zhen-Xin Zhang. Neurological Disorders. in *Disease Control Priorities in Developing Countries* (ed. Jamison DT, B.J., Measham AR, et al., editors) (World Bank, Washington (DC), 2006).

256. Hebert, L.E*., et al.* Age-specific incidence of Alzheimer's disease in a community population. *JAMA* **273**, 1354-1359 (1995).

257. Hebert, L.E., Scherr, P.A., Bienias, J.L., Bennett, D.A. & Evans, D.A. Alzheimer disease in the US population: prevalence estimates using the 2000 census. *Arch Neurol* **60**, 1119-1122 (2003).

258. Hebert, L.E., Scherr, P.A., Bienias, J.L., Bennett, D.A. & Evans, D.A. State-specific projections through 2025 of Alzheimer disease prevalence. *Neurology* **62**, 1645 (2004).

259. Castellani, R.J., Rolston, R.K. & Smith, M.A. Alzheimer Disease. *Dm Disease-a-Month* **56**, 484-546 (2010).

260. Hoyer, S. Age as Risk Factor for Sporadic Dementia of the Alzheimer-Type. *Aging Clock* **719**, 248-256 (1994).

261. Farrer, L.A*., et al.* Effects of age, sex, and ethnicity on the association between apolipoprotein E genotype and Alzheimer disease. A meta-analysis. APOE and Alzheimer Disease Meta Analysis Consortium. *JAMA* **278**, 1349-1356 (1997).

262. Strittmatter, W.J*., et al.* Apolipoprotein E: high-avidity binding to beta-amyloid and increased frequency of type 4 allele in late-onset familial Alzheimer disease. *Proc Natl Acad Sci U S A* **90**, 1977-1981 (1993).

263. Blennow, K., de Leon, M.J. & Zetterberg, H. Alzheimer's disease. *Lancet* **368**, 387-403 (2006).

264. Reisberg, B., Ferris, S.H., de Leon, M.J. & Crook, T. The Global Deterioration Scale for assessment of primary degenerative dementia. *Am J Psychiatry* **139**, 1136-1139 (1982).

265. Reisberg, B., Ferris, S.H., de Leon, M.J. & Crook, T. Global Deterioration Scale (GDS). *Psychopharmacol Bull* **24**, 661-663 (1988).

266. Reisberg, B. Functional assessment staging (FAST). *Psychopharma-col Bull* **24**, 653-659 (1988).

267. Sclan, S.G. & Reisberg, B. Functional assessment staging (FAST) in Alzheimer's disease: reliability, validity, and ordinality. *Int Psychoge-riatr* **4 Suppl 1**, 55-69 (1992).

268. Reisberg, B., Ferris, S. H., Anand, R., de Leon, M. J., Schneck, M. K., Buttinger, C. and Borenstein, J. . Functional Staging of Dementia of the Alzheimer Type. Vol. 435 481–483 (Annals of the New York Academy of Sciences, New York, 1984).

269. Reisberg, B.*, et al.* Evidence and mechanisms of retrogenesis in Alzheimer's and other dementias: management and treatment import. *Am J Alzheimers Dis Other Demen* **17**, 202-212 (2002).

270. Alzheimer, A. Ueber eine eigenartige Erkrankung der Hirnrinde. *Allgemeine Zeitschrift fur Psychiatrie und psychisch-gerichtliche Medizin* **64**, 146-148 (1907).

271. Braak, H. & Braak, E. Frequency of stages of Alzheimer-related lesions in different age categories. *Neurobiol Aging* **18**, 351-357 (1997).

272. Kang, J.*, et al.* The precursor of Alzheimer's disease amyloid A4 protein resembles a cell-surface receptor. *Nature* **325**, 733-736 (1987).

273. Haass, C.*, et al.* Amyloid beta-peptide is produced by cultured cells during normal metabolism. *Nature* **359**, 322-325 (1992).

274. Soba, P.*, et al.* Homo- and heterodimerization of APP family members promotes intercellular adhesion. *EMBO J* **24**, 3624-3634 (2005).

275. Moya, K.L., Benowitz, L.I., Schneider, G.E. & Allinquant, B. The amyloid precursor protein is developmentally regulated and correlated with synaptogenesis. *Dev Biol* **161**, 597-603 (1994).

276. Allinquant, B.*, et al.* Downregulation of amyloid precursor protein inhibits neurite outgrowth in vitro. *J Cell Biol* **128**, 919-927 (1995).

277. Hung, A.Y., Koo, E.H., Haass, C. & Selkoe, D.J. Increased expression of beta-amyloid precursor protein during neuronal differentiation is not accompanied by secretory cleavage. *Proc Natl Acad Sci U S A* **89**, 9439-9443 (1992).

278. Ciallella, J.R.*, et al.* Changes in expression of amyloid precursor protein and interleukin-1beta after experimental traumatic brain injury in rats. *J Neurotrauma* **19**, 1555-1567 (2002).

279. Hussain, I.*, et al.* Identification of a novel aspartic protease (Asp 2) as beta-secretase. *Mol Cell Neurosci* **14**, 419-427 (1999).

280. Yan, R.*, et al.* Membrane-anchored aspartyl protease with Alzheimer's disease beta-secretase activity. *Nature* **402**, 533-537 (1999).

281. Vassar, R.*, et al.* Beta-secretase cleavage of Alzheimer's amyloid precursor protein by the transmembrane aspartic protease BACE. *Science* **286**, 735-741 (1999).

282. Steiner, H., Fluhrer, R. & Haass, C. Intramembrane proteolysis by gamma-secretase. *J Biol Chem* **283**, 29627-29631 (2008).

283. Edbauer, D.*, et al.* Reconstitution of gamma-secretase activity. *Nat Cell Biol* **5**, 486-488 (2003).

284. Suzuki, N.*, et al.* An increased percentage of long amyloid beta protein secreted by familial amyloid beta protein precursor (beta APP717) mutants. *Science* **264**, 1336-1340 (1994).

285. Guntert, A., Dobeli, H. & Bohrmann, B. High sensitivity analysis of amyloid-beta peptide composition in amyloid deposits from human and PS2APP mouse brain. *Neuroscience* **143**, 461-475 (2006).

286. Tsai, J., Grutzendler, J., Duff, K. & Gan, W.B. Fibrillar amyloid deposition leads to local synaptic abnormalities and breakage of neuronal branches. *Nat Neurosci* **7**, 1181-1183 (2004).

287. Shepherd, C.E., Gregory, G.C., Vickers, J.C. & Halliday, G.M. Novel 'inflammatory plaque' pathology in presenilin-1 Alzheimer's disease. *Neuropathol Appl Neurobiol* **31**, 503-511 (2005).

288. Yamaguchi, H., Nakazato, Y., Shoji, M., Takatama, M. & Hirai, S. Ultrastructure of diffuse plaques in senile dementia of the Alzheimer type: comparison with primitive plaques. *Acta Neuropathol* **82**, 13-20 (1991).

289. Mann, D.M.*, et al.* Cases of Alzheimer's disease due to deletion of exon 9 of the presenilin-1 gene show an unusual but characteristic beta-amyloid pathology known as 'cotton wool' plaques. *Neuropathol Appl Neurobiol* **27**, 189-196 (2001).

290. Geula, C., Nagykery, N., Nicholas, A. & Wu, C.K. Cholinergic neuronal and axonal abnormalities are present early in aging and in Alzheimer disease. *J Neuropathol Exp Neurol* **67**, 309-318 (2008).

291. Grudzien, A.*, et al.* Locus coeruleus neurofibrillary degeneration in aging, mild cognitive impairment and early Alzheimer's disease. *Neurobiol Aging* **28**, 327-335 (2007).

292. Braak, H. & Braak, E. Development of Alzheimer-related neurofibrillary changes in the neocortex inversely recapitulates cortical myelogenesis. *Acta Neuropathol* **92**, 197-201 (1996).

293. Lindwall, G. & Cole, R.D. Phosphorylation affects the ability of tau protein to promote microtubule assembly. *J Biol Chem* **259**, 5301-5305 (1984).

294. Weingarten, M.D., Lockwood, A.H., Hwo, S.Y. & Kirschner, M.W. A protein factor essential for microtubule assembly. *Proc Natl Acad Sci U S A* **72**, 1858-1862 (1975).

295. Drubin, D.G. & Kirschner, M.W. Tau protein function in living cells. *J Cell Biol* **103**, 2739-2746 (1986).

296. Alonso, A.C., Zaidi, T., Grundke-Iqbal, I. & Iqbal, K. Role of abnormally phosphorylated tau in the breakdown of microtubules in Alzheimer disease. *Proc Natl Acad Sci U S A* **91**, 5562-5566 (1994).

297. Iqbal, K., Zaidi, T., Bancher, C. & Grundke-Iqbal, I. Alzheimer paired helical filaments. Restoration of the biological activity by dephosphorylation. *FEBS Lett* **349**, 104-108 (1994).

298. Alonso, A., Zaidi, T., Novak, M., Grundke-Iqbal, I. & Iqbal, K. Hyperphosphorylation induces self-assembly of tau into tangles of paired helical filaments/straight filaments. *Proc Natl Acad Sci U S A* **98**, 6923-6928 (2001).

299. Iqbal, K.*, et al.* Tau pathology in Alzheimer disease and other tauopathies. *Biochim Biophys Acta* **1739**, 198-210 (2005).

300. Chun, W. & Johnson, G.V. The role of tau phosphorylation and cleavage in neuronal cell death. *Front Biosci* **12**, 733-756 (2007).

301. Mann, D.M., Marcyniuk, B., Yates, P.O., Neary, D. & Snowden, J.S. The progression of the pathological changes of Alzheimer's disease in

frontal and temporal neocortex examined both at biopsy and at autopsy. *Neuropathol Appl Neurobiol* **14**, 177-195 (1988).

302. Mountjoy, C.Q., Roth, M., Evans, N.J. & Evans, H.M. Cortical neuronal counts in normal elderly controls and demented patients. *Neurobiol Aging* **4**, 1-11 (1983).

303. Gomez-Isla, T.*, et al.* Profound loss of layer II entorhinal cortex neurons occurs in very mild Alzheimer's disease. *J Neurosci* **16**, 4491-4500 (1996).

304. West, M.J., Coleman, P.D., Flood, D.G. & Troncoso, J.C. Differences in the pattern of hippocampal neuronal loss in normal ageing and Alzheimer's disease. *Lancet* **344**, 769-772 (1994).

305. Gomez-Isla, T.*, et al.* Neuronal loss correlates with but exceeds neurofibrillary tangles in Alzheimer's disease. *Ann Neurol* **41**, 17-24 (1997).

306. Masliah, E., Terry, R.D., DeTeresa, R.M. & Hansen, L.A. Immunohistochemical quantification of the synapse-related protein synaptophysin in Alzheimer disease. *Neurosci Lett* **103**, 234-239 (1989).

307. Masliah, E., Terry, R.D., Alford, M., DeTeresa, R. & Hansen, L.A. Cortical and subcortical patterns of synaptophysinlike immunoreactivity in Alzheimer's disease. *Am J Pathol* **138**, 235-246 (1991).

308. Scheff, S.W. & Price, D.A. Synapse loss in the temporal lobe in Alzheimer's disease. *Ann Neurol* **33**, 190-199 (1993).

309. Terry, R.D.*, et al.* Physical basis of cognitive alterations in Alzheimer's disease: synapse loss is the major correlate of cognitive impairment. *Ann Neurol* **30**, 572-580 (1991).

310. Perry, R.H., Irving, D., Blessed, G., Fairbairn, A. & Perry, E.K. Senile dementia of Lewy body type. A clinically and neuropathologically distinct form of Lewy body dementia in the elderly. *J Neurol Sci* **95**, 119-139 (1990).

311. Scheuner, D.*, et al.* Secreted amyloid beta-protein similar to that in the senile plaques of Alzheimer's disease is increased in vivo by the presenilin 1 and 2 and APP mutations linked to familial Alzheimer's disease. *Nat Med* **2**, 864-870 (1996).

312. Pimplikar, S.W. Reassessing the amyloid cascade hypothesis of Alzheimer's disease. *Int J Biochem Cell Biol* **41**, 1261-1268 (2009).

313. Bentahir, M.*, et al.* Presenilin clinical mutations can affect gamma-secretase activity by different mechanisms. *J Neurochem* **96**, 732-742 (2006).

314. Deng, Y.*, et al.* Deletion of presenilin 1 hydrophilic loop sequence leads to impaired gamma-secretase activity and exacerbated amyloid pathology. *J Neurosci* **26**, 3845-3854 (2006).

315. Qiu, W.Q.*, et al.* Insulin-degrading enzyme regulates extracellular levels of amyloid beta-protein by degradation. *J Biol Chem* **273**, 32730-32738 (1998).

316. Selkoe, D.J. The molecular pathology of Alzheimer's disease. *Neuron* **6**, 487-498 (1991).

317. Matthews, F.E.*, et al.* Epidemiological pathology of dementia: attributable-risks at death in the Medical Research Council Cognitive Function and Ageing Study. *PLoS Med* **6**, e1000180 (2009).

318. Davis, D.G., Schmitt, F.A., Wekstein, D.R. & Markesbery, W.R. Alzheimer neuropathologic alterations in aged cognitively normal subjects. *J Neuropathol Exp Neurol* **58**, 376-388 (1999).

319. Savva, G.M.*, et al.* Age, neuropathology, and dementia. *N Engl J Med* **360**, 2302-2309 (2009).

320. Edison, P.*, et al.* Amyloid, hypometabolism, and cognition in Alzheimer disease: an [11C]PIB and [18F]FDG PET study. *Neurology* **68**, 501-508 (2007).

321. Lue, L.F.*, et al.* Soluble amyloid beta peptide concentration as a predictor of synaptic change in Alzheimer's disease. *Am J Pathol* **155**, 853-862 (1999).

322. McLean, C.A.*, et al.* Soluble pool of Abeta amyloid as a determinant of severity of neurodegeneration in Alzheimer's disease. *Ann Neurol* **46**, 860-866 (1999).

323. Radde, R., Duma, C., Goedert, M. & Jucker, M. The value of incomplete mouse models of Alzheimer's disease. *Eur J Nucl Med Mol Imaging* **35 Suppl 1**, S70-74 (2008).

324. Radde, R.*, et al.* Abeta42-driven cerebral amyloidosis in transgenic mice reveals early and robust pathology. *EMBO Rep* **7**, 940-946 (2006).

325. Mullan, M.*, et al.* A pathogenic mutation for probable Alzheimer's disease in the APP gene at the N-terminus of beta-amyloid. *Nat Genet* **1**, 345-347 (1992).

326. Miravalle, L.*, et al.* Genetic mutations associated with presenile dementia. *Neurobiology of Aging* **23**, S322-S322 (2002).

327. Moehlmann, T.*, et al.* Presenilin-1 mutations of leucine 166 equally affect the generation of the Notch and APP intracellular domains independent of their effect on Abeta 42 production. *Proc Natl Acad Sci U S A* **99**, 8025-8030 (2002).

328. Hefendehl, J.K.*, et al.* Long-term in vivo imaging of beta-amyloid plaque appearance and growth in a mouse model of cerebral beta-amyloidosis. *J Neurosci* **31**, 624-629 (2011).

329. Rupp, N.J., Wegenast-Braun, B.M., Radde, R., Calhoun, M.E. & Jucker, M. Early onset amyloid lesions lead to severe neuritic abnormalities and local, but not global neuron loss in APPPS1 transgenic mice. *Neurobiol Aging* (2010).

330. Mayford, M.*, et al.* Control of memory formation through regulated expression of a CaMKII transgene. *Science* **274**, 1678-1683 (1996).

331. Cruz, J.C., Tseng, H.C., Goldman, J.A., Shih, H. & Tsai, L.H. Aberrant Cdk5 activation by p25 triggers pathological events leading to neurodegeneration and neurofibrillary tangles. *Neuron* **40**, 471-483 (2003).

332. Kusakawa, G.*, et al.* Calpain-dependent proteolytic cleavage of the p35 cyclin-dependent kinase 5 activator to p25. *J Biol Chem* **275**, 17166-17172 (2000).

333. Nath, R.*, et al.* Processing of cdk5 activator p35 to its truncated form (p25) by calpain in acutely injured neuronal cells. *Biochem Biophys Res Commun* **274**, 16-21 (2000).

334. Lee, M.S.*, et al.* Neurotoxicity induces cleavage of p35 to p25 by calpain. *Nature* **405**, 360-364 (2000).

335. Tsai, L.H., Delalle, I., Caviness, V.S., Jr., Chae, T. & Harlow, E. p35 is a neural-specific regulatory subunit of cyclin-dependent kinase 5. *Nature* **371**, 419-423 (1994).

336. Cruz, J.C. & Tsai, L.H. Cdk5 deregulation in the pathogenesis of Alzheimer's disease. *Trends Mol Med* **10**, 452-458 (2004).

337. Baumann, K., Mandelkow, E.M., Biernat, J., Piwnica-Worms, H. & Mandelkow, E. Abnormal Alzheimer-like phosphorylation of tau-protein by cyclin-dependent kinases cdk2 and cdk5. *FEBS Lett* **336**, 417-424 (1993).

338. Paudel, H.K., Lew, J., Ali, Z. & Wang, J.H. Brain proline-directed protein kinase phosphorylates tau on sites that are abnormally phosphorylated in tau associated with Alzheimer's paired helical filaments. *J Biol Chem* **268**, 23512-23518 (1993).

339. Lee, K.Y.*, et al.* Elevated neuronal Cdc2-like kinase activity in the Alzheimer disease brain. *Neurosci Res* **34**, 21-29 (1999).

340. Patrick, G.N.*, et al.* Conversion of p35 to p25 deregulates Cdk5 activity and promotes neurodegeneration. *Nature* **402**, 615-622 (1999).

341. Swatton, J.E.*, et al.* Increased MAP kinase activity in Alzheimer's and Down syndrome but not in schizophrenia human brain. *Eur J Neurosci* **19**, 2711-2719 (2004).

342. Cruz, J.C.*, et al.* p25/cyclin-dependent kinase 5 induces production and intraneuronal accumulation of amyloid beta in vivo. *J Neurosci* **26**, 10536-10541 (2006).

343. Fischer, A., Sananbenesi, F., Pang, P.T., Lu, B. & Tsai, L.H. Opposing roles of transient and prolonged expression of p25 in synaptic plasticity and hippocampus-dependent memory. *Neuron* **48**, 825-838 (2005).

344. Eng, L.F. & Ghirnikar, R.S. GFAP and astrogliosis. *Brain Pathol* **4**, 229-237 (1994).

345. Ruan, L.F., Kang, Z.J., Pei, G. & Le, Y.Y. Amyloid Deposition and Inflammation in APPswe/PS1dE9 Mouse Model of Alzheimer's Disease. *Current Alzheimer Research* **6**, 531-540 (2009).

346. Wharton, S.B.*, et al.* Population Variation in Glial Fibrillary Acidic Protein Levels in Brain Ageing: Relationship to Alzheimer-Type Pathology and Dementia. *Dementia and Geriatric Cognitive Disorders* **27**, 465-473 (2009).

347. Itagaki, S., McGeer, P.L., Akiyama, H., Zhu, S. & Selkoe, D. Relationship of microglia and astrocytes to amyloid deposits of Alzheimer disease. *J Neuroimmunol* **24**, 173-182 (1989).

348. Olabarria, M., Noristani, H.N., Verkhratsky, A. & Rodriguez, J.J. Concomitant astroglial atrophy and astrogliosis in a triple transgenic animal model of Alzheimer's disease. *Glia* **58**, 831-838 (2010).

349. Abramov, A.Y., Canevari, L. & Duchen, M.R. Changes in intracellular calcium and glutathione in astrocytes as the primary mechanism of amyloid neurotoxicity. *J Neurosci* **23**, 5088-5095 (2003).

350. Tian, G., Kong, Q., Lai, L., Ray-Chaudhury, A. & Lin, C.L. Increased expression of cholesterol 24S-hydroxylase results in disruption of glial glutamate transporter EAAT2 association with lipid rafts: a potential role in Alzheimer's disease. *J Neurochem* **113**, 978-989 (2010).

351. Li, S., Mallory, M., Alford, M., Tanaka, S. & Masliah, E. Glutamate transporter alterations in Alzheimer disease are possibly associated

with abnormal APP expression. *J Neuropathol Exp Neurol* **56**, 901-911 (1997).

352. Rodriguez, J.J., Olabarria, M., Chvatal, A. & Verkhratsky, A. Astroglia in dementia and Alzheimer's disease. *Cell Death Differ* **16**, 378-385 (2009).

353. Christie, R.H.*, et al.* Growth arrest of individual senile plaques in a model of Alzheimer's disease observed by in vivo multiphoton microscopy. *Journal of Neuroscience* **21**, 858-864 (2001).

354. Thal, D.R.*, et al.* Progression of neurofibrillary changes and PHF-tau in end-stage Alzheimer's disease is different from plaque and cortical microglial pathology. *Neurobiology of Aging* **19**, 517-525 (1998).

355. Wyss-Coray, T.*, et al.* Adult mouse astrocytes degrade amyloid-beta in vitro and in situ. *Nat Med* **9**, 453-457 (2003).

356. Nagele, R.G., D'Andrea, M.R., Lee, H., Venkataraman, V. & Wang, H.Y. Astrocytes accumulate A beta 42 and give rise to astrocytic amyloid plaques in Alzheimer disease brains. *Brain Res* **971**, 197-209 (2003).

357. Nagele, R.G., Wegiel, J., Venkataraman, V., Imaki, H. & Wang, K.C. Contribution of glial cells to the development of amyloid plaques in Alzheimer's disease. *Neurobiol Aging* **25**, 663-674 (2004).

358. Allaman, I.*, et al.* Amyloid-beta aggregates cause alterations of astrocytic metabolic phenotype: impact on neuronal viability. *J Neurosci* **30**, 3326-3338 (2010).

359. Apelt, J., Ach, K. & Schliebs, R. Aging-related down-regulation of neprilysin, a putative beta-amyloid-degrading enzyme, in transgenic Tg2576 Alzheimer-like mouse brain is accompanied by an astroglial upregulation in the vicinity of beta-amyloid plaques. *Neurosci Lett* **339**, 183-186 (2003).

360. Iwata, N.*, et al.* Metabolic regulation of brain Abeta by neprilysin. *Science* **292**, 1550-1552 (2001).

361. Yan, P.*, et al.* Matrix metalloproteinase-9 degrades amyloid-beta fibrils in vitro and compact plaques in situ. *Journal of Biological Chemistry* **281**, 24566-24574 (2006).

362. Xu, Q.*, et al.* Profile and regulation of apolipoprotein E (ApoE) expression in the CNS in mice with targeting of green fluorescent protein gene to the ApoE locus. *J Neurosci* **26**, 4985-4994 (2006).

363. Lahiri, D.K., Sambamurti, K. & Bennett, D.A. Apolipoprotein gene and its interaction with the environmentally driven risk factors: molecular, genetic and epidemiological studies of Alzheimer's disease. *Neurobiol Aging* **25**, 651-660 (2004).

364. Namba, Y., Tomonaga, M., Kawasaki, H., Otomo, E. & Ikeda, K. Apolipoprotein E immunoreactivity in cerebral amyloid deposits and neurofibrillary tangles in Alzheimer's disease and kuru plaque amyloid in Creutzfeldt-Jakob disease. *Brain Res* **541**, 163-166 (1991).

365. Koistinaho, M.*, et al.* Apolipoprotein E promotes astrocyte colocalization and degradation of deposited amyloid-beta peptides. *Nat Med* **10**, 719-726 (2004).

366. Bartzokis, G.*, et al.* Age-related changes in frontal and temporal lobe volumes in men - A magnetic resonance imaging study. *Archives of General Psychiatry* **58**, 461-465 (2001).

367. Hampel, H*., et al.* Corpus callosum atrophy is a possible indicator of region- and cell type-specific neuronal degeneration in Alzheimer disease: a magnetic resonance imaging analysis. *Arch Neurol* **55**, 193-198 (1998).

368. Lassmann, H*., et al.* Cell death in Alzheimer's disease evaluated by DNA fragmentation in situ. *Acta Neuropathol* **89**, 35-41 (1995).

369. Svennerholm, L. & Gottfries, C.G. Membrane lipids, selectively diminished in Alzheimer brains, suggest synapse loss as a primary event in early-onset form (type I) and demyelination in late-onset form (type II). *J Neurochem* **62**, 1039-1047 (1994).

370. Lee, C.Y. & Landreth, G.E. The role of microglia in amyloid clearance from the AD brain. *J Neural Transm* **117**, 949-960 (2010).

371. Koenigsknecht-Talboo, J. & Landreth, G.E. Microglial phagocytosis induced by fibrillar beta-amyloid and IgGs are differentially regulated by proinflammatory cytokines. *J Neurosci* **25**, 8240-8249 (2005).

372. Morgan, D. Immunotherapy for Alzheimer's disease. *J Intern Med* **269**, 54-63 (2011).

373. Mendez, I*., et al.* Dopamine neurons implanted into people with Parkinson's disease survive without pathology for 14 years. *Nat Med* **14**, 507-509 (2008).

374. Li, J.Y*., et al.* Lewy bodies in grafted neurons in subjects with Parkinson's disease suggest host-to-graft disease propagation. *Nat Med* **14**, 501-503 (2008).

375. Kordower, J.H., Chu, Y., Hauser, R.A., Freeman, T.B. & Olanow, C.W. Lewy body-like pathology in long-term embryonic nigral transplants in Parkinson's disease. *Nat Med* **14**, 504-506 (2008).

376. Berninger, B*., et al.* Functional properties of neurons derived from in vitro reprogrammed postnatal astroglia. *J Neurosci* **27**, 8654-8664 (2007).

377. Heinrich, C*., et al.* Directing astroglia from the cerebral cortex into subtype specific functional neurons. *PLoS Biol* **8**, e1000373 (2010).

378. Heins, N*., et al.* Glial cells generate neurons: the role of the transcription factor Pax6. *Nat Neurosci* **5**, 308-315 (2002).

379. Petito, C.K*., et al.* DNA fragmentation follows delayed neuronal death in CA1 neurons exposed to transient global ischemia in the rat. *J Cereb Blood Flow Metab* **17**, 967-976 (1997).

380. Li, Y., Chopp, M., Powers, C. & Jiang, N. Apoptosis and protein expression after focal cerebral ischemia in rat. *Brain Res* **765**, 301-312 (1997).

381. Gadea, A., Schinelli, S. & Gallo, V. Endothelin-1 regulates astrocyte proliferation and reactive gliosis via a JNK/c-Jun signaling pathway. *Journal of Neuroscience* **28**, 2394-2408 (2008).

382. Chen, Y*., et al.* The Basic Helix-Loop-Helix Transcription Factor Olig2 Is Critical for Reactive Astrocyte Proliferation after Cortical Injury. *Journal of Neuroscience* **28**, 10983-10989 (2008).

383. Buffo, A., Rolando, C. & Ceruti, S. Astrocytes in the damaged brain: Molecular and cellular insights into their reactive response and healing potential. *Biochemical Pharmacology* **79**, 77-89 (2010).

384. Baldin, V., Lukas, J., Marcote, M.J., Pagano, M. & Draetta, G. Cyclin D1 Is a Nuclear-Protein Required for Cell-Cycle Progression in G(1). *Genes & Development* **7**, 812-821 (1993).

385. Taupin, P. BrdU immunohistochemistry for studying adult neurogenesis: paradigms, pitfalls, limitations, and validation. *Brain Res Rev* **53**, 198-214 (2007).

386. Giacinti, C. & Giordano, A. RB and cell cycle progression. *Oncogene* **25**, 5220-5227 (2006).

387. Vlkolinsky, R., Cairns, N., Fountoulakis, M. & Lubec, G. Decreased brain levels of 2',3'-cyclic nucleotide-3'-phosphodiesterase in Down syndrome and Alzheimer's disease. *Neurobiol Aging* **22**, 547-553 (2001).

388. Roher, A.E.*, et al.* Increased A beta peptides and reduced cholesterol and myelin proteins characterize white matter degeneration in Alzheimer's disease. *Biochemistry* **41**, 11080-11090 (2002).

389. Mitew, S.*, et al.* Focal demyelination in Alzheimer's disease and transgenic mouse models. *Acta Neuropathol* **119**, 567-577 (2010).

390. Prins, N.D.*, et al.* Cerebral white matter lesions and the risk of dementia. *Arch Neurol* **61**, 1531-1534 (2004).

391. Vermeer, S.E.*, et al.* Silent brain infarcts and the risk of dementia and cognitive decline. *N Engl J Med* **348**, 1215-1222 (2003).

392. Peters, A., Moss, M.B. & Sethares, C. Effects of aging on myelinated nerve fibers in monkey primary visual cortex. *Journal of Comparative Neurology* **419**, 364-376 (2000).

393. Thurnherr, T.*, et al.* Cdc42 and Rac1 signaling are both required for and act synergistically in the correct formation of myelin sheaths in the CNS. *Journal of Neuroscience* **26**, 10110-10119 (2006).

394. Bowley, M.P., Cabral, H., Rosene, D.L. & Peters, A. Age changes in myelinated nerve fibers of the cingulate bundle and corpus callosum in the rhesus monkey. *J Comp Neurol* **518**, 3046-3064 (2010).

395. Vincze, A., Mazlo, M., Seress, L., Komoly, S. & Abraham, H. A correlative light and electron microscopic study of postnatal myelination in the murine corpus callosum. *Int J Dev Neurosci* **26**, 575-584 (2008).

396. Reeves, S.A., Lin, T., Xiang, Z.M., Cui, L.B. & Stallcup, W. New mouse oligodendrocyte precursor (mOP) cells for studies on oligodendrocyte maturation and function. *Journal of Neuroscience Methods* **157**, 187-194 (2006).

397. Fu, H.*, et al.* Dual origin of spinal oligodendrocyte progenitors and evidence for the cooperative role of Olig2 and Nkx2.2 in the control of oligodendrocyte differentiation. *Development* **129**, 681-693 (2002).

398. Nakamura, T., Colbert, M.C. & Robbins, J. Neural crest cells retain multipotential characteristics in the developing valves and label the cardiac conduction system. *Circ Res* **98**, 1547-1554 (2006).

399. Oki, K.*, et al.* Musashi1 as a marker of reactive astrocytes after transient focal brain ischemia. *Neuroscience Research* **66**, 390-395 (2010).

400. Lazarov, O., Mattson, M.P., Peterson, D.A., Pimplikar, S.W. & van Praag, H. When neurogenesis encounters aging and disease. *Trends in Neurosciences* **33**, 569-579 (2010).

401. Blasko, I.*, et al.* How chronic inflammation can affect the brain and support the development of Alzheimer's disease in old age: the role of microglia and astrocytes. *Aging Cell* **3**, 169-176 (2004).

402. Pertusa, M., Garcia-Matas, S., Rodriguez-Farre, E., Sanfeliu, C. & Cristofol, R. Astrocytes aged in vitro show a decreased neuroprotective capacity. *J Neurochem* **101**, 794-805 (2007).

403. Laywell, E.D., Rakic, P., Kukekov, V.G., Holland, E.C. & Steindler, D.A. Identification of a multipotent astrocytic stem cell in the immature and adult mouse brain. *Proceedings of the National Academy of Sciences of the United States of America* **97**, 13883-13888 (2000).

404. Belachew, S.*, et al.* Postnatal NG2 proteoglycan-expressing progenitor cells are intrinsically multipotent and generate functional neurons. *J Cell Biol* **161**, 169-186 (2003).

405. Nunes, M.C.*, et al.* Identification and isolation of multipotential neural progenitor cells from the subcortical white matter of the adult human brain. *Nat Med* **9**, 439-447 (2003).

406. Li, Y., Chopp, M., Zhang, Z.G., Zhang, R.L. & Garcia, J.H. Expression of Gfap in Areas of Focal Cerebral-Ischemia Accompanies Neuronal Expression of Hsp-72. *Neurology* **43**, A366-A366 (1993).

407. Lu, A.G.*, et al.* Genomics of the periinfarction cortex after focal cerebral ischemia. *Journal of Cerebral Blood Flow and Metabolism* **23**, 786-810 (2003).

408. Vogel, J.*, et al.* Infarct volume after transient middle cerebral artery occlusion (MCAo) can be reduced by attenuation but not by inactivation of c-Jun action. *Brain Research* **1151**, 12-19 (2007).

409. Dong, Y.*, et al.* Ischemia activates JNK/c-Jun/AP-1 pathway to upregulate 14-3-3gamma in astrocyte. *Journal of Neurochemistry* **109 Suppl 1**, 182-188 (2009).

410. Gertz, K.*, et al.* Modulation of fate determinants Olig2 and Pax6 in resident Glia evokes spiking neurons receiving synaptic input after mild brain ischemia. *Journal of Cerebral Blood Flow and Metabolism* **29**, S548-S548 (2009).

411. Kato, H., Takahashi, A. & Itoyama, Y. Cell cycle protein expression in proliferating microglia and astrocytes following transient global cerebral ischemia in the rat. *Brain Research Bulletin* **60**, 215-221 (2003).

412. Yamasaki, Y.*, et al.* Transient increase of cytokine-induced neutrophil chemoattractant, a member of the interleukin-8 family, in ischemic brain areas after focal ischemia in rats. *Stroke* **26**, 318-322; discussion 322-313 (1995).

413. Cole-Edwards, K.K., Musto, A.E. & Bazan, N.G. c-Jun N-terminal kinase activation responses induced by hippocampal kindling are mediated by reactive astrocytes. *J Neurosci* **26**, 8295-8304 (2006).

414. Braithwaite, S.P.*, et al.* Inhibition of c-Jun kinase provides neuroprotection in a model of Alzheimer's disease. *Neurobiology of Disease* **39**, 311-317 (2010).

415. Puig, B.*, et al.* Expression of stress-activated kinases c-Jun N-terminal kinase (SAPK/JNK-P) and p38 kinase (p38-P), and tau hyperphosphorylation in neurites surrounding beta A plaques in APP Tg2576 mice. *Neuropathology and Applied Neurobiology* **30**, 491-502 (2004).

416. Hashimoto, K.*, et al.* Long-term activation of c-Fos and c-Jun in optic nerve head astrocytes in experimental ocular hypertension in monkeys and after exposure to elevated pressure in vitro. *Brain Res* **1054**, 103-115 (2005).

417. Lee, S*., et al.* CpG oligodeoxynucleotides induce expression of proin-flammatory cytokines and chemokines in astrocytes: the role of c-Jun N-terminal kinase in CpG ODN-mediated NF-kappaB activation. *J Neuroimmunol* **153**, 50-63 (2004).

418. Nakagawa, T. & Schwartz, J.P. Gene expression profiles of reactive astrocytes in dopamine-depleted striatum. *Brain Pathol* **14**, 275-280 (2004).

419. Gillardon, F., Spranger, M., Tiesler, C. & Hossmann, K.A. Expression of cell death-associated phospho-c-Jun and p53-activated gene 608 in hippocampal CA1 neurons following global ischemia. *Molecular Brain Research* **73**, 138-143 (1999).

420. Oo, T.F., Henchcliffe, C., James, D. & Burke, R.E. Expression of c-fos, c-jun, and c-jun N-terminal kinase (JNK) in a developmental model of induced apoptotic death in neurons of the substantia nigra. *Journal of Neurochemistry* **72**, 557-564 (1999).

421. Raivich, G. c-Jun Expression, activation and function in neural cell death, inflammation and repair. *Journal of Neurochemistry* **107**, 898-906 (2008).

422. Anderson, A.J., Cummings, B.J. & Cotman, C.W. Increased immuno-reactivity for Jun- and Fos-related proteins in Alzheimer's disease: as-sociation with pathology. *Exp Neurol* **125**, 286-295 (1994).

423. Kim, H.M*., et al.* Differential and Cooperative Actions of Olig1 and Olig2 Transcription Factors on Immature Proliferating Cells After Con-tusive Spinal Cord Injury. *Glia* **59**, 1094-1106 (2011).

424. Ligon, K.L*., et al.* Olig2-regulated lineage-restricted pathway controls replication competence in neural stem cells and malignant glioma. *Neuron* **53**, 503-517 (2007).

425. Diehl, J.A. Cycling to cancer with cyclin D1. *Cancer Biology & Therapy* **1**, 226-231 (2002).

426. Walker, J.L. & Assoian, R.K. Integrin-dependent signal transduction regulating cyclin D1 expression and G1 phase cell cycle progression. *Cancer and Metastasis Reviews* **24**, 383-393 (2005).

427. Sherr, C.J., Kato, J., Quelle, D.E., Matsuoka, M. & Roussel, M.F. D-Type Cyclins and Their Cyclin-Dependent Kinases - G(1) Phase Inte-grators of the Mitogenic Response. *Cold Spring Harbor Symposia on Quantitative Biology* **59**, 11-19 (1994).

428. Sherr, C.J., Matsuoka, M., Kato, J., Roussel, M.F. & Quelle, D.E. Posi-tive and Negative Regulation of D-Type Cyclin-Dependent Kinases during G1 Progression. *Journal of Cellular Biochemistry*, 6-6 (1995).

429. Weinberg, R.A. The Retinoblastoma Protein and Cell-Cycle Control. *Cell* **81**, 323-330 (1995).

430. Joly, S., Pernet, V., Samardzija, M. & Grimm, C. Pax6-positive muller glia cells express cell cycle markers but do not proliferate after photo-receptor injury in the mouse retina. *Glia* **59**, 1033-1046 (2011).

431. Witzel, I.I., Koh, L.F. & Perkins, N.D. Regulation of cyclin D1 gene ex-pression. *Biochemical Society Transactions* **38**, 217-222 (2010).

432. Klein, E.A. & Assoian, R.K. Transcriptional regulation of the cyclin D1 gene at a glance. *Journal of Cell Science* **121**, 3853-3857 (2008).

433. Perkins, N.D. Integrating cell-signalling pathways with NF-kappa B and IKK function. *Nature Reviews Molecular Cell Biology* **8**, 49-62 (2007).

434.   Guttridge, D.C., Albanese, C., Reuther, J.Y., Pestell, R.G. & Baldwin, A.S. NF-kappa B controls cell growth and differentiation through transcriptional regulation of cyclin D1. *Molecular and Cellular Biology* **19**, 5785-5799 (1999).

435.   Joyce, D.*, et al.* Integration of Rac-dependent regulation of cyclin D1 transcription through a nuclear factor-kappa B-dependent pathway. *Journal of Biological Chemistry* **274**, 25245-25249 (1999).

436.   Murray, P.J. The JAK-STAT signaling pathway: Input and output intergration. *Journal of Immunology* **178**, 2623-2629 (2007).

437.   Matsumura, I.*, et al.* Transcriptional regulation of the cyclin D1 promoter by STAT5: its involvement in cytokine-dependent growth of hematopoietic cells. *Embo Journal* **18**, 1367-1377 (1999).

438.   Leslie, K.*, et al.* Cyclin D1 is transcriptionally regulated by and required for transformation by activated signal transducer and activator of transcription 3. *Cancer Research* **66**, 2544-2552 (2006).

439.   Gu, J.H.*, et al.* Blockage of the STAT3 signaling pathway with a decoy oligonucleotide suppresses growth of human malignant glioma cells. *Journal of Neuro-Oncology* **89**, 9-17 (2008).

440.   Hauwel, M.*, et al.* Innate (inherent) control of brain infection, brain inflammation and brain repair: the role of microglia, astrocytes, "protective" glial stem cells and stromal ependymal cells. *Brain Research Reviews* **48**, 220-233 (2005).

441.   Becher, B., Prat, A. & Antel, J.P. Brain-immune connection: Immune-regulatory properties of CNS-resident cells. *Glia* **29**, 293-304 (2000).

442.   Falsig, J., Porzgen, P., Lotharius, J. & Leist, M. Specific modulation of astrocyte inflammation by inhibition of mixed lineage kinases with CEP-1347. *J Immunol* **173**, 2762-2770 (2004).

443.   Lukaszevicz, A.C.*, et al.* High sensitivity of protoplasmic cortical astroglia to focal ischemia. *J Cereb Blood Flow Metab* **22**, 289-298 (2002).

444.   Shannon, C., Salter, M. & Fern, R. GFP imaging of live astrocytes: regional differences in the effects of ischaemia upon astrocytes. *J Anat* **210**, 684-692 (2007).

445.   Morga, E., Faber, C. & Heuschling, P. Regional heterogeneity of the astroglial immunoreactive phenotype: effect of lipopolysaccharide. *J Neurosci Res* **57**, 941-952 (1999).

446.   Fitting, S.*, et al.* Regional heterogeneity and diversity in cytokine and chemokine production by astroglia: differential responses to HIV-1 Tat, gp120, and morphine revealed by multiplex analysis. *J Proteome Res* **9**, 1795-1804 (2010).

447.   Hamby, M.E., Gragnolati, A.R., Hewett, S.J. & Hewett, J.A. TGF beta 1 and TNF alpha potentiate nitric oxide production in astrocyte cultures by recruiting distinct subpopulations of cells to express NOS-2. *Neurochem Int* **52**, 962-971 (2008).

448.   Ransohoff, R.M. & Perry, V.H. Microglial physiology: unique stimuli, specialized responses. *Annu Rev Immunol* **27**, 119-145 (2009).

449.   Morioka, T., Kalehua, A.N. & Streit, W.J. Characterization of Microglial Reaction after Middle Cerebral-Artery Occlusion in Rat-Brain. *Journal of Comparative Neurology* **327**, 123-132 (1993).

450.   Napoli, I. & Neumann, H. Microglial Clearance Function in Health and Disease. *Neuroscience* **158**, 1030-1038 (2009).

451. Finsen, B.*, et al.* Microglia Protect Neurons against Ischemia by Synthesis of Tumor Necrosis Factor. *Journal of Neuroscience* **29**, 1319-1330 (2009).

452. Rice, T., Larsen, J., Rivest, S. & Yong, V.W. Characterization of the early neuroinflammation after spinal cord injury in mice. *Journal of Neuropathology and Experimental Neurology* **66**, 184-195 (2007).

453. Ghirnikar, R.S., Lee, Y.L. & Eng, L.F. Inflammation in traumatic brain injury: Role of cytokines and chemokines. *Neurochemical Research* **23**, 329-340 (1998).

454. Logan, A., Frautschy, S.A., Gonzalez, A.M., Sporn, M.B. & Baird, A. Enhanced Expression of Transforming Growth-Factor Beta-1 in the Rat-Brain after a Localized Cerebral Injury. *Brain Research* **587**, 216-225 (1992).

455. Badoer, E. Microglia: Activation in acute and chronic inflammatory states and in response to cardiovascular dysfunction. *International Journal of Biochemistry & Cell Biology* **42**, 1580-1585 (2010).

456. Lue, L.F., Kuo, Y.M., Beach, T. & Walker, D.G. Microglia Activation and Anti-inflammatory Regulation in Alzheimer's Disease. *Molecular Neurobiology* **41**, 115-128 (2010).

457. Walker, D.G., Link, J., Lue, L.F., Dalsing-Hernandez, J.E. & Boyes, B.E. Gene expression changes by amyloid beta peptide-stimulated human postmortem brain microglia identify activation of multiple inflammatory processes (vol 79, pg 596, 2006). *Journal of Leukocyte Biology* **80**, 448-448 (2006).

458. Preston, E., Webster, J. & Small, D. Characteristics of sustained blood-brain barrier opening and tissue injury in a model for focal trauma in the rat. *J Neurotraum* **18**, 83-92 (2001).

459. Schnell, L., Fearn, S., Klassen, H., Schwab, M.E. & Perry, V.H. Acute inflammatory responses to mechanical lesions in the CNS: differences between brain and spinal cord. *Eur J Neurosci* **11**, 3648-3658 (1999).

460. Shechter, R.*, et al.* Infiltrating Blood-Derived Macrophages Are Vital Cells Playing an Anti-inflammatory Role in Recovery from Spinal Cord Injury in Mice. *Plos Medicine* **6**, - (2009).

461. Cui, M., Huang, Y.L., Tian, C.H., Zhao, Y. & Zheng, J.L. FOXO3a Inhibits TNF-alpha- and IL-1 beta-Induced Astrocyte Proliferation: Implication for Reactive Astrogliosis. *Glia* **59**, 641-654 (2011).

462. Lalancette-Hebert, M., Gowing, G., Simard, A., Weng, Y.C. & Kriz, J. Selective ablation of proliferating microglial cells exacerbates ischemic injury in the brain. *Journal of Neuroscience* **27**, 2596-2605 (2007).

463. Liu, Z.Y.*, et al.* Chronic treatment with minocycline preserves adult new neurons and reduces functional impairment after focal cerebral ischemia. *Stroke* **38**, 146-152 (2007).

464. Griffiths, M., Neal, J.W. & Gasque, P. Innate immunity and protective neuroinflammation: New emphasis on the role of neuroimmune regulatory proteins. *Neuroinflammation in Neuronal Death and Repair* **82**, 29-55 (2007).

465. Ye, S.M. & Johnson, R.W. An age-related decline in interleukin-10 may contribute to the increased expression of interleukin-6 in brain of aged mice. *Neuroimmunomodulation* **9**, 183-192 (2001).

466. Lue, L.F., Brachova, L., Civin, W.H. & Rogers, J. Inflammation, A beta deposition, and neurofibrillary tangle formation as correlates of Alz-

heimer's disease neurodegeneration. *Journal of Neuropathology and Experimental Neurology* **55**, 1083-1088 (1996).

467. Schlachetzki, J.C.M. & Hull, M. Microglial Activation in Alzheimer's Disease. *Current Alzheimer Research* **6**, 554-563 (2009).

468. Faissner, A.*, et al.* Isolation of a neural chondroitin sulfate proteoglycan with neurite outgrowth promoting properties. *Journal of Cell Biology* **126**, 783-799 (1994).

469. Laywell, E.D.*, et al.* Enhanced Expression of the Developmentally Regulated Extracellular-Matrix Molecule Tenascin Following Adult Brain Injury. *Proceedings of the National Academy of Sciences of the United States of America* **89**, 2634-2638 (1992).

470. Gotz, M., Stoykova, A. & Gruss, P. Pax6 controls radial glia differentiation in the cerebral cortex. *Neuron* **21**, 1031-1044 (1998).

471. Lu, G.*, et al.* bcl2, bax, and nestin in the brains of patients with neurodegeneration and those of normal aging. *Journal of Molecular Neuroscience* **27**, 167-174 (2005).

472. Rosenmann, H.*, et al.* A novel transgenic mouse expressing double mutant tau driven by its natural promoter exhibits tauopathy characteristics. *Experimental Neurology* **212**, 71-84 (2008).

473. Inoue, S. & Kisilevsky, R. Beta-amyloid fibrils of Alzheimer's disease: pathologically altered, basement membrane-associated microfibrils? *Ital J Anat Embryol* **106**, 93-102 (2001).

474. Ryu, J.K. & McLarnon, J.G. A leaky blood-brain barrier, fibrinogen infiltration and microglial reactivity in inflamed Alzheimer's disease brain. *J Cell Mol Med* **13**, 2911-2925 (2009).

475. Bell, R.D. & Zlokovic, B.V. Neurovascular mechanisms and blood-brain barrier disorder in Alzheimer's disease. *Acta Neuropathol* **118**, 103-113 (2009).

476. Desai, M.K.*, et al.* Triple-transgenic Alzheimer's disease mice exhibit region-specific abnormalities in brain myelination patterns prior to appearance of amyloid and tau pathology. *Glia* **57**, 54-65 (2009).

477. Guo, Q.*, et al.* Increased vulnerability of hippocampal neurons from presenilin-1 mutant knock-in mice to amyloid beta-peptide toxicity: central roles of superoxide production and caspase activation. *J Neurochem* **72**, 1019-1029 (1999).

478. Kasuga, K., Kaneko, H., Nishizawa, M., Onodera, O. & Ikeuchi, T. Generation of intracellular domain of insulin receptor tyrosine kinase by gamma-secretase. *Biochemical and Biophysical Research Communications* **360**, 90-96 (2007).

479. McElroy, B., Powell, J.C. & McCarthy, J.V. The insulin-like growth factor 1 (IGF-1) receptor is a substrate for gamma-secretase-mediated intramembrane proteolysis. *Biochemical and Biophysical Research Communications* **358**, 1136-1141 (2007).

480. Bartzokis, G. Alzheimer's disease as homeostatic responses to age-related myelin breakdown. *Neurobiology of Aging* **32**, 1341-1371 (2011).

481. Carson, M.J., Behringer, R.R., Brinster, R.L. & Mcmorris, F.A. Insulin-Like Growth Factor-I Increases Brain Growth and Central-Nervous-System Myelination in Transgenic Mice. *Neuron* **10**, 729-740 (1993).

482. Goddard, D.R., Berry, M. & Butt, A.M. In vivo actions of fibroblast growth factor-2 and insulin-like growth factor-I on oligodendrocyte de-

velopment and myelination in the central nervous system. *Journal of Neuroscience Research* **57**, 74-85 (1999).

483. Mason, J.L., Ye, P., Suzuki, K., D'Ercole, A.J. & Matsushima, G.K. Insulin-like growth factor-1 inhibits mature oligodendrocyte apoptosis during primary demyelination. *Journal of Neuroscience* **20**, 5703-5708 (2000).

484. Beck, K.D., Powellbraxton, L., Widmer, H.R., Valverde, J. & Hefti, F. Igf1 Gene Disruption Results in Reduced Brain Size, Cns Hypomyelination, and Loss of Hippocampal Granule and Striatal Parvalbumin-Containing Neurons. *Neuron* **14**, 717-730 (1995).

485. Lee, H.J.*, et al.* Presenilin-dependent gamma-secretase-like intramembrane cleavage of ErbB4. *Journal of Biological Chemistry* **277**, 6318-6323 (2002).

486. Garratt, A.N., Voiculescu, O., Topilko, P., Charnay, P. & Birchmeier, C. A dual role of erbB2 in myelination and in expansion of the Schwann cell precursor pool. *Journal of Cell Biology* **148**, 1035-1046 (2000).

487. Chen, S.*, et al.* Neuregulin 1-erbB signaling is necessary for normal myelination and sensory function. *Journal of Neuroscience* **26**, 3079-3086 (2006).

488. Birchmeier, C. & Nave, K.A. Neuregulin-1, a key axonal signal that drives Schwann cell growth and differentiation. *Glia* **56**, 1491-1497 (2008).

489. Willem, M.*, et al.* Control of peripheral nerve myelination by the beta-secretase BACE1. *Science* **314**, 664-666 (2006).

490. Hu, X.*, et al.* Bace1 modulates myelination in the central and peripheral nervous system. *Nat Neurosci* **9**, 1520-1525 (2006).

491. Michailov, G.V.*, et al.* Axonal neuregulin-1 regulates myelin sheath thickness. *Science* **304**, 700-703 (2004).

492. Brinkmann, B.G.*, et al.* Neuregulin-1/ErbB signaling serves distinct functions in myelination of the peripheral and central nervous system. *Neuron* **59**, 581-595 (2008).

493. Roy, K.*, et al.* Loss of erbB signaling in oligodendrocytes alters myelin and dopaminergic function, a potential mechanism for neuropsychiatric disorders. *Proceedings of the National Academy of Sciences of the United States of America* **104**, 8131-8136 (2007).

494. Lai, C. & Feng, L.Y. Implication of gamma-secretase in neuregulin-induced maturation of oligodendrocytes. *Biochemical and Biophysical Research Communications* **314**, 535-542 (2004).

495. Games, D.*, et al.* Alzheimer-Type Neuropathology in Transgenic Mice Overexpressing V717f Beta-Amyloid Precursor Protein. *Nature* **373**, 523-527 (1995).

496. Redwine, J.M.*, et al.* Dentate gyrus volume is reduced before onset of plaque formation in PDAPP mice: a magnetic resonance microscopy and stereologic analysis. *Proc Natl Acad Sci U S A* **100**, 1381-1386 (2003).

497. Valla, J., Schneider, L.E., Gonzalez-Lima, F. & Reiman, E.M. Nonprogressive transgene-related callosal and hippocampal changes in PDAPP mice. *Neuroreport* **17**, 829-832 (2006).

498. Games, D.*, et al.* Alzheimer-type neuropathology in transgenic mice overexpressing V717F beta-amyloid precursor protein. *Nature* **373**, 523-527 (1995).

499. Nikolaev, A., McLaughlin, T., O'Leary, D.D.M. & Tessier-Lavigne, M. APP binds DR6 to trigger axon pruning and neuron death via distinct caspases. *Nature* **457**, 981-U981 (2009).

500. Mi, S.*, et al.* Death receptor 6 negatively regulates oligodendrocyte survival, maturation and myelination. *Nat Med* **17**, 816-821 (2011).

501. Pak, K., Chan, S.L. & Mattson, M.P. Presenilin-1 mutation sensitizes oligodendrocytes to glutamate and amyloid toxicities, and exacerbates white matter damage and memory impairment in mice. *Neuromolecular Medicine* **3**, 53-64 (2003).

502. Pak, K.J., Chan, S.L. & Mattson, M.P. Homocysteine and folate deficiency sensitize oligodendrocytes to the cell death-promoting effects of a presenilin-1 mutation and amyloid beta-peptide. *Neuromolecular Medicine* **3**, 119-127 (2003).

503. Guo, Q.*, et al.* Increased vulnerability of hippocampal neurons to excitotoxic necrosis in presenilin-1 mutant knock-in mice. *Nat Med* **5**, 101-106 (1999).

504. Horiuchi, M.*, et al.* Amyloid beta1-42 oligomer inhibits myelin sheet formation in vitro. *Neurobiol Aging* (2010).

505. Oddo, S.*, et al.* Triple-transgenic model of Alzheimer's disease with plaques and tangles: intracellular Abeta and synaptic dysfunction. *Neuron* **39**, 409-421 (2003).

506. Sasahara, M.*, et al.* Pdgf B-Chain in Neurons of the Central-Nervous-System, Posterior Pituitary, and in a Transgenic Model. *Cell* **64**, 217-227 (1991).

507. Hsiao, K.*, et al.* Correlative memory deficits, Abeta elevation, and amyloid plaques in transgenic mice. *Science* **274**, 99-102 (1996).

508. Manson, J.*, et al.* The prion protein gene: a role in mouse embryogenesis? *Development* **115**, 117-122 (1992).

509. Flood, D.G.*, et al.* FAD mutant PS-1 gene-targeted mice: Increased A beta 42 and A beta deposition without APP overproduction. *Neurobiology of Aging* **23**, 335-348 (2002).

510. Holcomb, L.*, et al.* Accelerated Alzheimer-type phenotype in transgenic mice carrying both mutant amyloid precursor protein and presenilin 1 transgenes. *Nature Medicine* **4**, 97-100 (1998).

511. Blakemore, W.F. Pattern of remyelination in the CNS. *Nature* **249**, 577-578 (1974).

512. Prineas, J.W., Barnard, R.O., Kwon, E.E., Sharer, L.R. & Cho, E.S. Multiple sclerosis: remyelination of nascent lesions. *Ann Neurol* **33**, 137-151 (1993).

513. Talbott, J.F.*, et al.* Endogenous Nkx2.2+/Olig2+ oligodendrocyte precursor cells fail to remyelinate the demyelinated adult rat spinal cord in the absence of astrocytes. *Exp Neurol* **192**, 11-24 (2005).

514. Islam, M.S., Tatsumi, K., Okuda, H., Shiosaka, S. & Wanaka, A. Olig2-expressing progenitor cells preferentially differentiate into oligodendrocytes in cuprizone-induced demyelinated lesions. *Neurochem Int* **54**, 192-198 (2009).

515. Merkler, D., Ernsting, T., Kerschensteiner, M., Bruck, W. & Stadelmann, C. A new focal EAE model of cortical demyelination: multiple

sclerosis-like lesions with rapid resolution of inflammation and extensive remyelination. *Brain* **129**, 1972-1983 (2006).

516. Nielsen, H.H., Ladeby, R., Drojdahl, N., Peterson, A.C. & Finsen, B. Axonal degeneration stimulates the formation of NG2+ cells and oligodendrocytes in the mouse. *Glia* **54**, 105-115 (2006).

517. Glezer, I., Lapointe, A. & Rivest, S. Innate immunity triggers oligodendrocyte progenitor reactivity and confines damages to brain injuries. *Faseb J* **20**, 750-752 (2006).

518. Bolmont, T*., et al.* Dynamics of the Microglial/Amyloid Interaction Indicate a Role in Plaque Maintenance
10.1523/JNEUROSCI.4814-07.2008. *J. Neurosci.* **28**, 4283-4292 (2008).

519. Chittajallu, R., Aguirre, A. & Gallo, V. NG2-positive cells in the mouse white and grey matter display distinct physiological properties. *J Physiol* **561**, 109-122 (2004).

520. Bartzokis, G*., et al.* White matter structural integrity in healthy aging adults and patients with Alzheimer disease: a magnetic resonance imaging study. *Arch Neurol* **60**, 393-398 (2003).

521. Bartzokis, G*., et al.* Age-related changes in frontal and temporal lobe volumes in men: a magnetic resonance imaging study. *Arch Gen Psychiatry* **58**, 461-465 (2001).

522. Meier-Ruge, W., Ulrich, J., Bruhlmann, M. & Meier, E. Age-related white matter atrophy in the human brain. *Ann N Y Acad Sci* **673**, 260-269 (1992).

523. Peters, A. & Sethares, C. Aging and the myelinated fibers in prefrontal cortex and corpus callosum of the monkey. *J Comp Neurol* **442**, 277-291 (2002).

524. Peters, A., Sethares, C. & Killiany, R.J. Effects of age on the thickness of myelin sheaths in monkey primary visual cortex. *J Comp Neurol* **435**, 241-248 (2001).

525. Tang, Y., Nyengaard, J.R., Pakkenberg, B. & Gundersen, H.J. Age-induced white matter changes in the human brain: a stereological investigation. *Neurobiol Aging* **18**, 609-615 (1997).

526. Stricker, N.H*., et al.* Decreased white matter integrity in late-myelinating fiber pathways in Alzheimer's disease supports retrogenesis. *Neuroimage* **45**, 10-16 (2009).

527. Uchida, Y., Nakano, S., Gomi, F. & Takahashi, H. Differential regulation of basic helix-loop-helix factors Mash1 and Olig2 by beta-amyloid accelerates both differentiation and death of cultured neural stem/progenitor cells. *J Biol Chem* **282**, 19700-19709 (2007).

528. Roth, A.D., Ramirez, G., Alarcon, R. & Von Bernhardi, R. Oligodendrocytes damage in Alzheimer's disease: beta amyloid toxicity and inflammation. *Biol Res* **38**, 381-387 (2005).

529. Xu, J*., et al.* Amyloid-beta peptides are cytotoxic to oligodendrocytes. *J Neurosci* **21**, RC118 (2001).

530. Nakamura, S*., et al.* Fibroblast growth factor (FGF)-9 immunoreactivity in senile plaques. *Brain Res* **814**, 222-225 (1998).

531. Tooyama, I. [Fibroblast growth factors (FGFs) in neurodegenerative disorders]. *Rinsho Shinkeigaku* **33**, 1270-1274 (1993).

532. Gomez-Pinilla, F., Cummings, B.J. & Cotman, C.W. Induction of basic fibroblast growth factor in Alzheimer's disease pathology. *Neuroreport* **1**, 211-214 (1990).

533. Takami, K.*, et al.* Fibroblast growth factor receptor-1 expression in the cortex and hippocampus in Alzheimer's disease. *Brain Res* **802**, 89-97 (1998).

534. Itoh, N. Hormone-like (endocrine) Fgfs: their evolutionary history and roles in development, metabolism, and disease. *Cell Tissue Res* **342**, 1-11 (2010).

535. Franke, H., Krugel, U. & Illes, P. P2 receptor-mediated proliferative effects on astrocytes in vivo. *Glia* **28**, 190-200 (1999).

536. Franke, H., Krugel, U., Schmidt, R., Grosche, J. & Illes, P. P2 receptors and astrogliosis in vivo. *Naunyn-Schmiedebergs Archives of Pharmacology* **363**, R33-R33 (2001).

537. Franklin, R.J. & Ffrench-Constant, C. Remyelination in the CNS: from biology to therapy. *Nat Rev Neurosci* **9**, 839-855 (2008).

538. Redwine, J.M. & Armstrong, R.C. In vivo proliferation of oligodendrocyte progenitors expressing PDGF alpha R during early remyelination. *J Neurobiol* **37**, 413-428 (1998).

539. Shimogori, T., VanSant, J., Paik, E. & Grove, E.A. Members of the Wnt, Fz, and Frp gene families expressed in postnatal mouse cerebral cortex. *Journal of Comparative Neurology* **473**, 496-510 (2004).

540. Han, Y.G.*, et al.* Hedgehog signaling and primary cilia are required for the formation of adult neural stem cells. *Nature Neuroscience* **11**, 277-284 (2008).

541. White, B.D.*, et al.* beta-Catenin Signaling Increases in Proliferating NG2+Progenitors and Astrocytes during Post-Traumatic Gliogenesis in the Adult Brain. *Stem Cells* **28**, 297-307 (2010).

542. White, B.D.*, et al.* Beta-catenin signaling increases in proliferating NG2+ progenitors and astrocytes during post-traumatic gliogenesis in the adult brain. *Stem Cells* **28**, 297-307 (2010).

543. Garcia, A.D.R., Petrova, R., Eng, L. & Joyner, A.L. Sonic Hedgehog Regulates Discrete Populations of Astrocytes in the Adult Mouse Forebrain. *Journal of Neuroscience* **30**, 13597-13608 (2010).

544. Amankulor, N.M.*, et al.* Sonic Hedgehog Pathway Activation Is Induced by Acute Brain Injury and Regulated by Injury-Related Inflammation. *Journal of Neuroscience* **29**, 10299-10308 (2009).

545. Redwine, J.M., Blinder, K.L. & Armstrong, R.C. In situ expression of fibroblast growth factor receptors by oligodendrocyte progenitors and oligodendrocytes in adult mouse central nervous system. *Journal of Neuroscience Research* **50**, 229-237 (1997).

546. Chadashvili, T. & Peterson, D.A. Cytoarchitecture of fibroblast growth factor receptor 2 (FGFR-2) immunoreactivity in astrocytes of neurogenic and non-neurogenic regions of the young adult and aged rat brain. *Journal of Comparative Neurology* **498**, 1-15 (2006).

547. Boda, E. & Buffo, A. Glial cells in non-germinal territories: insights into their stern/progenitor properties in the intact and injured nervous tissue. *Archives Italiennes De Biologie* **148**, 119-136 (2010).

548. Messersmith, D.J., Murtie, J.C., Le, T.Q., Frost, E.E. & Armstrong, R.C. Fibroblast growth factor 2 (FGF2) and FGF receptor expression in an experimental demyelinating disease with extensive remyelination. *Journal of Neuroscience Research* **62**, 241-256 (2000).

549. Finklestein, S.P.*, et al.* Increased Basic Fibroblast Growth-Factor (Bfgf) Immunoreactivity at the Site of Focal Brain Wounds. *Brain Research* **460**, 253-259 (1988).

550. Liu, B., Chen, H.Y., Johns, T.G. & Neufeld, A.H. Epidermal growth factor receptor activation: An upstream signal for transition of quiescent astrocytes into reactive astrocytes after neural injury. *Journal of Neuroscience* **26**, 7532-7540 (2006).

551. Aguirre, A., Rizvi, T.A., Ratner, N. & Gallo, V. Overexpression of the epidermal growth factor receptor confers migratory properties to non-migratory postnatal neural progenitors. *Journal of Neuroscience* **25**, 11092-11106 (2005).

552. Fox, I.J. & Kornblum, H.I. Developmental profile of ErbB receptors in murine central nervous system: Implications for functional interactions. *Journal of Neuroscience Research* **79**, 584-597 (2005).

553. Gomez-Pinilla, F., Knauer, D.J. & Nieto-Sampedro, M. Epidermal growth factor receptor immunoreactivity in rat brain. Development and cellular localization. *Brain Res* **438**, 385-390 (1988).

554. Codeluppi, S.*, et al.* The Rheb-mTOR Pathway Is Upregulated in Reactive Astrocytes of the Injured Spinal Cord. *Journal of Neuroscience* **29**, 1093-1104 (2009).

555. Nieto-Sampedro, M., Gomez-Pinilla, F., Knauer, D.J. & Broderick, J.T. Epidermal growth factor receptor immunoreactivity in rat brain astrocytes. Response to injury. *Neurosci Lett* **91**, 276-282 (1988).

556. Merkle, F.T., Mirzadeh, Z. & Alvarez-Buylla, A. Mosaic organization of neural stem cells in the adult brain. *Science* **317**, 381-384 (2007).

557. Merkle, F.T., Tramontin, A.D., Garcia-Verdugo, J.M. & Alvarez-Buylla, A. Radial glia give rise to adult neural stem cells in the subventricular zone. *Proceedings of the National Academy of Sciences of the United States of America* **101**, 17528-17532 (2004).

558. Ventura, R.E. & Goldman, J.E. Dorsal radial glia generate olfactory bulb interneurons in the postnatal murine brain. *Journal of Neuroscience* **27**, 4297-4302 (2007).

559. Spassky, N. Ependymal differentiation of neural stem cells. *Neuron Glia Biology* **2**, S27-S27 (2007).

560. Spassky, N.*, et al.* Adult ependymal cells are postmitotic and are derived from radial glial cells during embryogenesis. *Journal of Neuroscience* **25**, 10-18 (2005).

561. Burns, K.A., Murphy, B., Danzer, S.C. & Kuan, C.Y. Developmental and Post-Injury Cortical Gliogenesis: A Genetic Fate-Mapping Study with Nestin-CreER Mice. *Glia* **57**, 1115-1129 (2009).

562. Costa, M.R., Bucholz, O., Schroeder, T. & Gotz, M. Late Origin of Glia-Restricted Progenitors in the Developing Mouse Cerebral Cortex. *Cerebral Cortex* **19**, I135-I143 (2009).

563. Levison, S.W. & Goldman, J.E. Both Oligodendrocytes and Astrocytes Develop from Progenitors in the Subventricular Zone of Postnatal Rat Forebrain. *Neuron* **10**, 201-212 (1993).

564. Sakakibara, S. & Okano, H. Expression of neural RNA-binding proteins in the postnatal CNS: Implications of their roles in neuronal and glial cell development. *Journal of Neuroscience* **17**, 8300-8312 (1997).

565. Pevny, L.H. & Nicolis, S.K. Sox2 roles in neural stem cells. *International Journal of Biochemistry & Cell Biology* **42**, 421-424 (2010).

566.   Schultz, P.G.*, et al.* Inhibition of histone deacetylase activity induces developmental plasticity in oligodendrocyte precursor cells. *Proceedings of the National Academy of Sciences of the United States of America* **104**, 14982-14987 (2007).

567.   Komitova, M. & Eriksson, P.S. Sox-2 is expressed by neural progenitors and astroglia in the adult rat brain. *Neuroscience Letters* **369**, 24-27 (2004).

568.   Wegner, M. & Stolt, C.C. From stem cells to neurons and glia: a Sox-ist's view of neural development. *Trends in Neurosciences* **28**, 583-588 (2005).

569.   Mori, T., Buffo, A. & Gotz, M. The novel roles of glial cells revisited: the contribution of radial glia and astrocytes to neurogenesis. *Curr Top Dev Biol* **69**, 67-99 (2005).

570.   Mori, T.*, et al.* Inducible gene deletion in astroglia and radial glia--a valuable tool for functional and lineage analysis. *Glia* **54**, 21-34 (2006).

571.   Aguirre, A. & Gallo, V. Postnatal neurogenesis and gliogenesis in the olfactory bulb from NG2-expressing progenitors of the subventricular zone. *Journal of Neuroscience* **24**, 10530-10541 (2004).

572.   Aguirre, A.A., Chittajallu, R., Belachew, S. & Gallo, V. NG2-expressing cells in the subventricular zone are type C-like cells and contribute to interneuron generation in the postnatal hippocampus. *Journal of Cell Biology* **165**, 575-589 (2004).

573.   Jackson, E.L.*, et al.* PDGFR alpha-positive B cells are neural stem cells in the adult SVZ that form glioma-like growths in response to increased PDGF signaling. *Neuron* **51**, 187-199 (2006).

574.   Chojnacki, A., Mak, G. & Weiss, S. PDGFRalpha expression distinguishes GFAP-expressing neural stem cells from PDGF-responsive neural precursors in the adult periventricular area. *J Neurosci* **31**, 9503-9512 (2011).

575.   Bozolla, J.J. & Russel, L.D. Electron Microscopy: principles and techniques for biologists. (ed. Inc., J.a.B.P.) (Tom Walker, London, 1999).

576.   Waldvogel, H.J., Curtis, M.A., Baer, K., Rees, M.I. & Faull, R.L. Immunohistochemical staining of post-mortem adult human brain sections. *Nat Protoc* **1**, 2719-2732 (2006).

577.   Adams, J.C. Heavy metal intensification of DAB-based HRP reaction product. *J Histochem Cytochem* **29**, 775 (1981).

Acknowledgments

First and foremost I would like to thank Magdalena Götz for the opportunity to conduct the PhD project and for her great support during my time in the lab. Her enthusiasm and the insightful discussions were always very encouraging. I learned a lot not only about science, scientific discussions or how to present data in a straight forward way but also how one should manage/organize ideas or things with many people involved. I am really happy to have her as a mentor.

Many thanks also for all the support and advice of Leda Dimou, who above many other things showed me how one should organize data sets in the most accurate way. I highly appreciated her as a mentor as well.

I would also like to warmly thank Lana for the help with the neurosphere cultures but also for her support and discussions. I am also deeply grateful that Corinna critically read my thesis.

I would further like to thank Annalisa Buffo for the opportunity to start my PhD work in Turin. I learned many techniques and worked on very interesting projects there. The discussions were always very encouraging and I am glad she was also a member of my Thesis Committee.

Furthermore, I would like to thank Kristin Baer for giving me the exciting opportunity to work with human brain tissue at the University of Swansea. I really enjoyed my stays there. In addition, I would like to also thank Mark Rees for providing the laboratory in Swansea. Finally, I would like to thank the Neurological Foundation of New Zealand for donating the post-mortem human brain tissue as well as Jenny Price for help with the statistical analysis.

Thanks also go to Prof. Dr. Bernd Sutor for last minute statistical help and numerous interesting insights into electrophysiologic techniques.

In regard to supervision I would also like to thank Prof. Brandt, who was a member of my Thesis Committee Meeting and for the great discussions in this regard.

Furthermore, I would like to thank of course also Gabi, Tatjana, Ines, Detlef, Simone, Rebecca, Andrea, Angelika, Arif for sharing their technical expertise and Lana for sharing her organizational expertise! They were always there to support me and often took the time for trouble shooting.

I am also grateful that all the animal caretakers especially Susi, Petra, Darko and Moni helped me to manage my mouse lines.

Thanks to all my great office-mates for sharing enjoyable and pleasant working hours as well as many laughers which includes Steffi, Sophia, Monika, Steffen, Basti, Christiane, Hilde. Many thanks also to Felipe for support with the westerns, Sergio, Ronny and Aditi for the "N", and also Francesca, Christophe, Steffen, Benedikt, Matteo, Alex, Giacomo, Christoph, Melle, Marisa, Elisa as well as the Helmholz-people for interesting discussions, help of any kind and creating a pleasant environment.

Last but not least, I would like to thank my family for all the "northern german" mental support and for believing in me. Thank you for that continous encouragement!

And the very last thanks are for "den besten Tennisspieler der Welt". Thank you for making me laugh not only on the tennis court, sharing the experience of doing a PhD and for all the support in this regard an beyond.

Eidestattliche Erklärung

Ich erkläre hiermit, dass ich diese Dissertation selbstständig ohne Hilfe Dritter und ohne Benutzung anderer als der angegebenen Quellen und Hilfsmittel verfasst habe. Alle den benutzten Quellen wörtlich oder sinngemäß entnommenen Stellen sind als solche einzeln kenntlich gemacht.

Ich bin mir bewusst, dass eine falsche Erklärung rechtliche Folgen haben wird.

_____

Ort, Datum, Unterschrift

Publications

Parts of this PhD thesis will be published in:

Gwendolyn Behrendt, Kristin Baer, Annalisa Buffo, Magdalena Götz, Leda Dimou. "Myelin aberrations and oligodendrocyte repair in a mouse model of amyloid plaque deposition". *In preparation.*

Gwendolyn Behrendt, Swetlana Sirko, Pratibha Tripathi, Marcos Costa, Christophe Heinrich, Steffen Tiedt, Dilek Colak, Martin Dichgans, Isabel Rebekka Fischer, Christian Haass, Li-Huei Tsai, André Fischer, Kay Grobe, Leda Dimou and Magdalena Götz. "The stem cell response of reactive glia: differential regulation by sonic hedgehog in distinct injury paradigms." *Submitted.*